Culinary fluid mechanics and other currents in food science

Arnold J. T. M. Mathijssen,[1,*] Maciej Lisicki,[2,†] Vivek N. Prakash,[3,‡] and Endre J. L. Mossige[4,§]

[1] *Department of Physics & Astronomy, University of Pennsylvania, 209 South 33rd Street, Philadelphia, PA 19104, USA*
[2] *Institute of Theoretical Physics, Faculty of Physics, University of Warsaw, Pasteura 5, 02-093 Warsaw, Poland*
[3] *Departments of Physics, Biology, Marine Biology and Ecology, University of Miami, 1320 Campo Sano Ave, Coral Gables, FL 33146, USA*
[4] *Department of Physics, University of Oslo (UiO), Sem Saelands vei 24, 0371 Oslo, Norway*

(Dated: January 31, 2022)

Innovations in fluid mechanics have refined food since ancient history, while creativity in cooking inspires science in return. Here, we review how recent advances in hydrodynamics are changing food science, and we highlight how the surprising phenomena that arise in the kitchen lead to discoveries and technologies across the disciplines, including rheology, soft matter, biophysics and molecular gastronomy. This review is structured like a menu, where each course highlights different aspects of culinary fluid mechanics. Our main themes include multiphase flows, complex fluids, thermal convection, hydrodynamic instabilities, viscous flows, granular matter, porous media, percolation, chaotic advection, interfacial phenomena, and turbulence. For every topic, we first provide an introduction accessible to food professionals and scientists in neighbouring fields. We then assess the state-of-the-art knowledge, the open problems, and likely directions for future research. New gastronomic ideas grow rapidly as the scientific recipes keep improving too.

CONTENTS

I. Introduction 2

II. Kitchen Sink Fundamentals 3
A. Eureka! 4
B. Navier-Stokes equations 4
C. Drinking from a straw: Hagen–Poiseuille flow 5
D. Onset of turbulence: Reynolds number 5
E. Bernoulli principle 5
F. Pendant drop: Surface tension 6
G. Wetting and capillary action 7
H. From jets to drops: Plateau-Rayleigh instability 7
I. Hydraulic jumps in the kitchen sink 8
J. How to cook a satellite dish 9
K. Washing and drying hands, skincare 9

III. Drinks & Cocktails: Multiphase Flows 10
A. Layered cocktails 10
1. Inverted Fountains 10
2. Internal Waves 11
3. Kelvin–Helmholtz Instability 11
4. Rayleigh-Taylor instability 12
B. Tears of wine 12
C. Whisky tasting 13
D. Marangoni cocktails 14
E. Bubbly drinks 15
F. Foams 16
G. Ouzo effect 18

IV. Soup Starter: Complex Fluids 19
A. Food rheology 19
1. Linear viscoelasticity 20
2. Non-linear viscoelasticity 21
B. Mixing up a sauce 23
C. Suspensions 23
D. Emulsions 24
E. Cheerios effect: capillary floating 25

V. Hot Main Course: Thermal Effects 25
A. Feel the heat: energy transfer 25
B. Levitating drops: Leidenfrost effect 26
C. Heating and Boiling: Rayleigh-Bénard convection 27
D. Layered latte: double-diffusive convection 27
E. Tenderloin: moisture migration 28
F. Flames, vapors, fire and smoke 29
G. Melting and freezing 29
H. Non-stick coatings 30

VI. Honey Dessert: Viscous Flows 30
A. Flows at low Reynolds number 30
B. Fundamental solution of Stokes flow 31
C. Coffee grains in free fall 32
D. Slender body theory 33
E. Lubrication theory 33
F. Pot stuck to stove top: Stefan adhesion 34
G. Viscous gravity currents 34
Making the perfect crêpe 34
H. Viscous fingering 35
I. Microbial fluid mechanics 35
J. Microfluidics for improved food safety 35
K. Ice creams 36

* amaths@upenn.edu
† mklis@fuw.edu.pl
‡ vprakash@miami.edu
§ endre.mossige@gmail.com

VII. Coffee: Granular Matter & Porous Media 36
A. Granular flows and avalanches 36
B. Hoppers: grains flowing through an orifice 37
C. Brazil nut effect 38
D. Brewing coffee: porous media flows 38
E. Coffee ring effect 40

VIII. Tempest in a Teacup: Non-linear Flows, Turbulence and Mixing 41
A. Tea leaf paradox 41
B. Secondary flows 42
C. Turbulent jets emanating from tea kettles 42
D. Sound generation by kitchen flows 42
E. Making macarons: chaotic advection 44
F. Sweetening tea with honey: mixing at low Re and high Pe 45

IX. Washing the dishes: Interfacial flows 45
A. Greasy galleys smooth the waves 45
B. Splashing and sloshing 46
C. Dishwashing and soap film dynamics 46
D. Ripples and waves 47
E. Rinsing flows: thin film instabilities 48
F. Dynamics of falling and rising drops 48
1. Immiscible drops 48
2. Miscible drops 49

X. Discussion 50
A. Summary 50
B. Learning from kitchen experiments 50
C. Curiosity-driven research 52
D. Conclusion 52

Acknowledgements 52

References 53

I. INTRODUCTION

The origins of fluid mechanics trace back to ancient water technologies [Fig. 1a], which supplied our earliest civilizations with reliable food sources [1]. Subsequently, as soon as the water flows, surprising phenomena emerge beyond number. This naturally sparked the interest of the first inventors, since the kitchen can serve as a laboratory [2] that is accessible to people of different backgrounds, ages, and interests. As such, the scullery is a source of curiosity that has driven innovations throughout history [3]. The problems that emerge while cooking have led to creative solutions, which have not only improved food science but also led to breakthroughs in modern engineering, medicine, and the natural sciences. In turn, fundamental research has improved gastronomy, and thus the cycle continues. Hence, science and cooking are intrinsically connected across people and time.

Today, numerous chefs have written extensive cookbooks from a scientific perspective. Well acclaimed is the work on molecular gastronomy [4], which turned into a scientific discipline, as reviewed by Barham *et al.* [5]. Another recent movement, known for using advanced equipment including centrifuges and blow torches, is called modernist cuisine [6]. With its striking photography, sometimes tricked, it also connects science with art in the field of fine dining [7]. The book by McGee [8] is particularly influential too: Celebrity chef Heston Blumenthal stated it is "the book that has had the greatest single impact on my cooking", and then he wrote eight books himself. Another excellent cookbook containing various experiments and scientific diagrams was written by López-Alt [9]. One of the first people to approach cooking systematically, a century earlier, was the 'king of chefs and chef of kings' Escoffier [10], whose 943-page culinary guide still remains a golden standard in haute cuisine [11].

In the scientific community, a wave of excitement hit when Kurti and Kurti [12] solicited recipes or essays on cooking from the members of the Royal Society. Science can improve cooking, but they also showed that food can lead to better science, a notion that was not taken very seriously at the time. Later, in her essay 'food for thought', Dame Athene Donald FRS pleads that the scientific challenges are as exciting in food as in any more conventional area. They should not be overlooked or, worse, sneered at [13]. Her early vision sparked scientists to regard food as an interdisciplinary research topic. Food science now spans across many fields, including materials science [e.g. 14], food chemistry and physical chemistry [e.g. 15], nutrition genetics [e.g. 16], food engineering [e.g. 17], food microbiology [e.g. 18], food rheology [e.g. 19], soft condensed matter [e.g. 20–22] and biophysics [e.g. 23, 24].

However, to the best of our knowledge, and despite the overwhelming number of surprising hydrodynamic effects that emerge in the kitchen, there is no comprehensive review of fluid mechanics in gastronomy and food science. Therefore, we aim to address this topic here in a manner that first provides a broad overview and then highlights the frontier of modern research. As such, we aim to connect the following communities:

First, for chefs and gastronomy professionals, fluid mechanics can make or break their culinary creations. Hydrodynamic instabilities can ruin a layered cocktail [§III A], while the Leidenfrost effect helps with searing your steak [§V B], and baristas learn about percolation to perfect their coffee [§VII D]. We will discuss these examples here, and quite a few more. Indeed, throughout this Review we aim to connect the science with food applications. We also point out some common mistakes in cooking and think of new ideas for recipes.

Second, for food scientists, it is important to unravel hydrodynamic effects in order to develop better food processing technologies [25]. For example, microfluidic techniques are now extensively used for edible foam generation and emulsification [26, 27], but also bioactive compound extraction and the design of novel food microstructures [28]. More generally, fluid mechanics de-

scribes the transport of mass, momentum and energy, which is to be optimised in food processing [29] and food preservation [30, 31]. We will highlight a number of unexpected flow phenomena, and their relation with food science technologies.

Third, from the perspective of medicine and nutrition professionals, flow physics has led to novel health care solutions and provided insights on the physiology of digestion [32]. For example, flow devices can detect food-borne pathogens or toxins [33], which is essential for food safety [34] and food quality control [35]. Similar technologies can equally be used for *in vitro* fertilization for agricultural animal breeding, or other applications in animal health monitoring, vaccination and therapeutics [36]. Moreover, using next-generation DNA and protein sequencing with nanopore technology [37], the field of foodomics could help with improving human nutrition [16]. In this article we will reflect on more of these food health innovations.

Fourth, for engineers and natural scientists, kitchen flows have led to breakthrough discoveries, and continue doing so. To name a few here, Agnes Pockels established the modern discipline of surface science after her observations of soap films while washing the dishes [§IX C], and Pyotr Kapitza discovered the roll wave instability while under house arrest [§IX E]. Most universities and labs were closed during the COVID-19 pandemic, which again lead to an unasked-for wave of kitchen science [38]. Moreover, culinary flows have given rise to engineering applications in completely different fields. The piston-and-cylinder steam engine was inspired by Papin's pressure cooker [§II A], and inkjet printers rely on capillary breakups observed in the sink [§II H]. Indeed, because of the low activation barrier, the kitchen is a hotspot for curiosity-driven research where new ideas arise.

Not least, for science education, the kitchen can serve as an exceptional classroom [39–41] or indeed a lab [2]. Being a natural gateway to learning about fluid mechanics, food science demonstrations equally connect to numerous other disciplines. Examples include teaching oceanography [42], chemistry education [43, 44], geology [45], soft matter physics [46], and the science of cooking for non-science majors [47]. Recently, based on their successful edX and Harvard University course, Brenner *et al.* [48] connected haute cuisine with soft matter science. Indeed, a lot of science awaits to be discovered during our daily meals.

This Review is structured like a menu: We begin with washing our hands in §II about kitchen sink fundamentals, where we provide a brief introduction to fluid mechanics that is accessible to scientists across the disciplines. Then we are ready to pour ourselves a cocktail, which we discuss in §III concerning multiphase flows. The first course might be a consommé, so in §IV we focus on complex fluids and food rheology. The main course is often hot, so we review thermal effects in cooking in §V. Tempted by dessert with honey and ice cream, we consider Stokesian flows in §VI. We then brew a coffee after the lavish meal, the thought of which sparks interest in granular flows and porous media, as discussed in §VII. Pouring another cup of tea, we discuss different aspects of non-linear flows and turbulence in §VIII. Once the meal comes to an end, it is time to wash the dishes, which brings our attention to interfacial flows in §IX. We conclude the Review with an extensive discussion in §X.

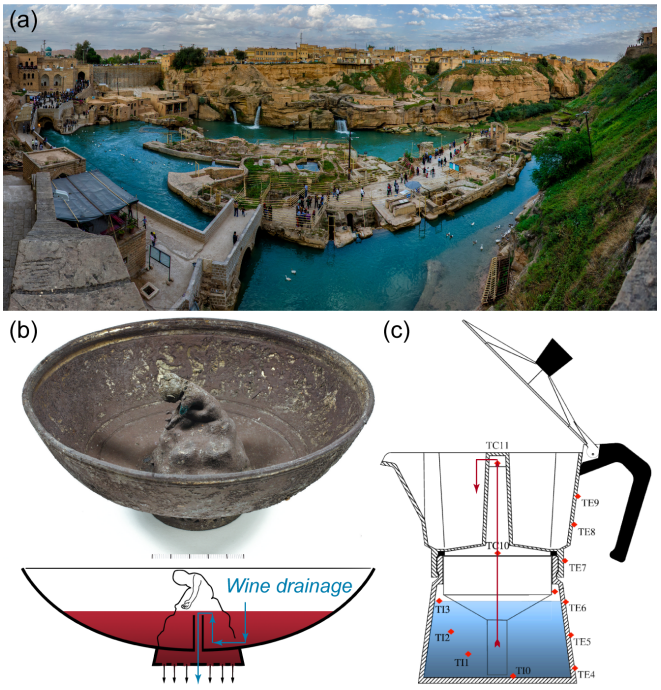

FIG. 1. Hidden channels. **(a)** The Shushtar Historical Hydraulic System in Iran, listed by UNESCO as 'a masterpiece of creative genius'. This irrigation system, dating back to the 5th century B.C., features canals, tunnels, dams, and water mills, which all work in unison. Image by Iman Yari, licenced under CC BY-SA 4.0. **(b)** The first discovered specimen of a Tantalus bowl (Pythagorean cup) from the late Roman period, catalogue no. 9 of the Vinkovci treasure. This silver-gilt bowl empties itself when filled above a critical level by a hidden siphon, soaking a greedy drinker in wine. Image credit: Damir Doračić, Archaeological Museum in Zagreb, from Vulić *et al.* [49]. **(c)** The moka pot, a traditional stove-top coffee maker, where the boiling water percolates through the coffee by following the red arrows. From Navarini *et al.* [50].

II. KITCHEN SINK FUNDAMENTALS

We begin this Review by introducing the basics of fluid mechanics in the context of food science. Flow experts may choose to skip this section, or to refresh their memory while enjoying the various anecdotes. Starting with surprising aspects of hydrostatics, we quickly transition to the hydrodynamics of wine aeration, hydraulic jumps and satellite dishes, to name a few. Some of these concepts are not as simple as appearance makes believe. In the words of Drazin [3],

A child can ask in an hour more questions about fluid dynamics than a Nobel prize winner can answer in a lifetime.

As things get harder in the later sections, we will often refer back to these kitchen sink fundamentals.

A. Eureka!

In his work "On Floating Bodies", Archimedes of Syracuse (c.287–c.212 BC) described the principles of hydrostatics. The buoyancy force on an immersed object equals the weight of the fluid it displaces. For a cube of volume L^3, aligned with gravity, this force is just the pressure difference between the top and bottom surfaces, $\rho g L \hat{\boldsymbol{z}}$, times the area of this surface, L^2, where ρ is the fluid density and $\boldsymbol{g} = -g\hat{\boldsymbol{z}}$ is gravity. More generally, we can integrate the pressure $p(z) = p_{\text{atm}} + \rho g z$ over the surface S of an object of any shape, which gives the buoyancy force

$$\boldsymbol{F}_b = \int_S -p \, d\boldsymbol{S} = -\int_V \rho \boldsymbol{g} \, dV = -\rho \boldsymbol{g} V_{\text{disp}}, \qquad (1)$$

where we used the divergence theorem. Since Greece is a sea-faring nation, Archimedes' principle is important to describe the stability of ships: If the center of gravity is above the metacentre (which is related to the centre of buoyancy of the displaced water), the boat will topple [51, 52]. Try floating a cup upside-down in the kitchen sink. Another classic experiment is throwing a stone out of a boat (upright cup). Does the water level rise? Buoyancy is also essential in heat convection [53], as described in §V C.

The concept of pressure became more established because the works of Evangelista Torricelli (1608-1647), often credited as the inventor of the barometer, and Blaise Pascal (1623-1662). Pascal's law states that a pressure change at any point in an enclosed fluid at rest is transmitted undiminished throughout the fluid [54]. This principle lies at the heart of many applications with siphons and 'communicating vessels' including water towers, modern plumbing and water gauges.

While hydrostatics may seem simple compared to hydrodynamics, it can still be rather counter-intuitive. For example, gravity can readily be defied when turning a glass of water up-side down, aided with a special trick [55]. One of the 'oldest pranks in history' is the Pythagoras cup, also known as the Tantalus bowl, which is a drinking vessel with a hidden siphon [Fig. 1b]. While described in ancient literature, the first specimen of a Tantalus bowl was discovered only very recently, in the Vinkovci treasure [49]. It functions normally when filled moderately, but if the liquid level rises above a critical height the bowl will drain its entire contents. Therefore, the bowl concretises a "Tantalean punishment", taking away pleasure from to those who get too greedy! The same siphon method is used in modern washing machines, certain toilet flushing systems, and anti-colic baby bottles [56]. Another example of non-intuitive hydrostatics is Heron's fountain, attributed to Heron of Alexandria (c.10-c.70 AD). It can spout water higher than its reservoirs without pump, so it appears to be a perpetual motion machine, but in the end it is just very clever hydraulics. Furthermore, in his treatise on pneumatics, Heron describes a total of 78 different inventions and discoveries made by himself and earlier ancient philosophers [57].

The use of pressure in the kitchen expanded with the invention of the steam digester by Denis Papin (1647-1713). His improved designs included a stream-release valve to prevent the machine from exploding, an essential feature in all modern pressure cookers, and coffee makers like the moka pot [see §VII D, Fig. 1c]. Besides kitchen appliances, the steam digester was the forerunner of the autoclave to disinfect medical instruments, and the piston-and-cylinder steam engine. Pascal's principle also underpins the hydraulic press, a force amplifier capable of uprooting trees, invented by Joseph Bramah (1748-1814). Bramah invented and improved many other culinary technologies during the Industrial Revolution, including high-pressure public water mains and the beer engine [58].

B. Navier-Stokes equations

Moving on from hydrostatics, we shift our attention to fluids in motion, which are described by the famous equations named after Claude-Louis Navier (1785-1836) and George Gabriel Stokes (1819-1903). For most simple liquids that are approximately incompressible, like water, the Navier-Stokes equations can be written as

$$\rho \frac{D\boldsymbol{u}}{Dt} = -\boldsymbol{\nabla} p + \mu \nabla^2 \boldsymbol{u} + \boldsymbol{f}, \qquad (2a)$$

$$0 = \boldsymbol{\nabla} \cdot \boldsymbol{u}. \qquad (2b)$$

Here $\boldsymbol{u}(\boldsymbol{x}, t)$ is the flow velocity at position $\boldsymbol{x}$ and time t, and $p(\boldsymbol{x}, t)$ is the pressure field, ρ is the fluid density, μ is the dynamic viscosity, $\nu = \mu/\rho$ is the kinematic viscosity, $\boldsymbol{f}$ is a body force (usually gravity) acting on the fluid, and the operator $D/Dt = \partial/\partial t + (\boldsymbol{u} \cdot \boldsymbol{\nabla})$ is the material derivative. Physically, Eq. (2a) stems from the conservation of momentum, essentially Newton's second law applied to an infinitesimal fluid parcel, and Eq. (2b) describes the conservation of mass.

Today, over 200 years after their formulation, the Navier-Stokes equations have still not been solved in general. This is mainly due to the non-linearity of the convective term, $(\boldsymbol{u} \cdot \boldsymbol{\nabla})\boldsymbol{u}$. Even basic properties of their solutions have never been proved, particularly the 'existence and smoothness problem'. One of the seven Millennium Prizes of $1 million can be earned with a correct solution [59]. Having said that, in specific cases, solutions to the Navier-Stokes equations can in fact be found analytically.

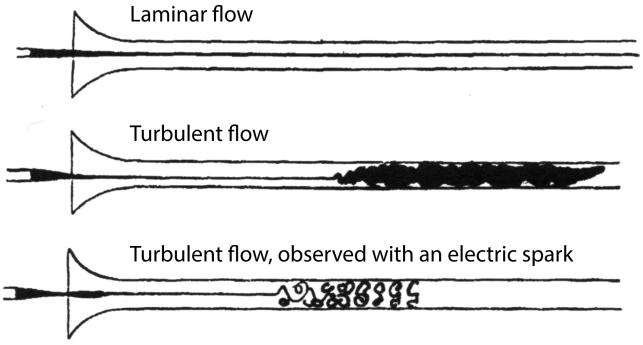

FIG. 2. Original drawings by Reynolds [66], showing laminar pipe flow, turbulent flow, and turbulent flow observed by the light of an electric spark.

C. Drinking from a straw: Hagen–Poiseuille flow

One example where an exact solution is known is the flow of drinking through a straw. This current is driven by a difference in pressure, Δp, where we consider a cylindrical tube of radius R and length L with negligible gravity. The volumetric flow rate (the flux) going through the tube is described by the Hagen–Poiseuille equation,

$$Q = \pi R^4 \Delta p/(8\mu L). \tag{3}$$

The expression was first deduced experimentally, independently by Gotthilf Hagen (1797-1884) and Jean Poiseuille (1797-1869), and soon after it was confirmed theoretically [60]. Perhaps the best-known theory [61] was derived by Sir George Stokes (1819-1903) in 1845, but he did not publish it until 1880, supposedly because he was not certain about the validity of the "no-slip" boundary condition of vanishing velocity at the walls [60]. Stokes also derived the exact flow velocity $\boldsymbol{u}$ everywhere in the pipe. Starting from the Navier-Stokes equations (2) in cylindrical coordinates (ρ, θ, z), assuming that the flow is steady, axisymmetric, and that the radial and azimuthal components of the velocity are zero, one finds the parabolic flow profile,

$$u_z = -\Delta p(R^2 - \rho^2)/(4\mu L), \tag{4}$$

which, as expected, is strongest at the center line. The consequences of the Hagen–Poiseuille equation (3) can be substantial: It is 16 times harder to drink through a straw that is 2 times thinner, to achieve the same flux. This fourth-power scaling is even more problematic for microscopic flow channels, in the field of microfluidics [see [62–65] and also §VI J]. For large pipes or fast flows, conversely, the flow is no longer laminar so the hydraulic resistance also increases. This is what we discuss next, in §II D.

D. Onset of turbulence: Reynolds number

Following the work by Reynolds [66], the transition from laminar to turbulent flow can be observed directly in the kitchen sink. When the tap is opened a little, the flow is laminar and follows parallel streamlines. The water column is clear and can be used as an optical lens. Opening the tap further, the image begins to fluctuate. Then bubbles appear and begin to jump around vigorously, blurring the water. When the tap is opened all the way, the column turns completely opaque and white (due to entrainment of air bubbles causing Mie scattering, which is roughly independent of the wavelength of light, as opposed to Rayleigh scattering that turns the sky blue). This transition from laminar (ordered) to turbulent (disordered) flow [Fig. 2] depends on the relative magnitude of fluid inertia to viscous dissipation in the fluid as described by the Reynolds number,

$$\mathrm{Re} \equiv \frac{\text{Inertial forces}}{\text{Viscous forces}} = \frac{\rho U_0 L_0}{\mu}. \tag{5}$$

The critical Reynolds, Re_c, number can be measured directly from this faucet experiment: The characteristic length scale L_0 is often chosen to be the diameter of the faucet nozzle, $d \sim 1\,\mathrm{cm}$, and the velocity scale U_0 can be determined easily by holding a cup under the faucet at the onset of turbulence [67]. One should find a volumetric flow rate of $Q \sim 1.8\,\mathrm{cm}^3/\mathrm{s}$, which corresponds to $\mathrm{Re}_c \approx 2300$ in pipe flow [68, 69].

Interestingly, one can also determine the diameter of the valve inside the faucet. Without seeing it, the onset of turbulence can still be heard, as a hissing sound. Using the same relation as before, $\mathrm{Re} = 4Q/(\nu\pi d)$, with Re known, we can find the critical Q at which the sound emerges, and thus compute the valve diameter. Because the valve is usually smaller than the nozzle, this happens at a lower flow rate. In medicine, this listening technique called auscultation [70] can be used to detect narrowing of blood vessels, sounds referred to as bruit or vascular murmurs [71–73] and, similarly, obstructions of the airways in respiratory conditions [74–76]. In §VIII D we will talk more about hydrodynamic sound generation.

E. Bernoulli principle

In his book "Hydrodynamica", Bernoulli (1700-1782) found that pressure decreases when the flow speed increases. More generally, Bernoulli's principle is a statement about the conservation of energy along a streamline. The Swiss mathematician Leonhard Euler (1707-1783) used this principle to derive the modern form of the Bernoulli equation,

$$\tfrac{1}{2}u^2 + \Psi + w = \text{constant along a streamline}, \tag{6}$$

where $\Psi = gz$ is the potential force due to gravity, w is the enthalpy of the fluid per unit mass, and where it is

FIG. 3. Wine aeration. **(a)** Oxygen injection using the Venturi effect: The wine moves down into a narrow funnel by gravity. In the funnel the liquid accelerates, which lowers the pressure compared to the surrounding atmosphere, as described by the Bernoulli principle [Eq. (6)]. Hence, air bubbles are drawn in, which aerate the wine. **(b)** Wine decanter: By pouring and swirling the liquid around, ripples form that mix in oxygen efficiently. (a,b) From Vintorio Wine Accessories, with permission.

assumed that the flow is steady and that friction due to viscosity is negligible. For an incompressible fluid this is $w = p/\rho$, which is often appropriate for water. For a compressible fluid additional information is required about its thermodynamic energy [54].

Despite its apparent simplicity, the Bernoulli principle is a powerful tool in many applications. On the one hand, it can be used to compute flow rates by measuring a pressure difference, for example to determine the speed of an aircraft with a Pitot tube [77]. On the other hand, it can be used to compute pressure differences by measuring flow rates, for example to determine the pressure distribution around a plane wing (airfoil) and thus the lift force [77]. Together with the principle of mass conservation, the Bernoulli equation also explains the "Venturi effect", the decrease in pressure in a pipe constriction. This effect is utilized in Venturi gauges to measure the flow rate through pipes; in the kitchen, it is exploited in wine aerators [Fig. 3a], where the low pressure is used to draw in air bubbles. The mixing with air can improve wine flavour [78, 79], which was already known to Louis Pasteur, who famously wrote *"C'est l'oxygène qui fait le vin"* [80], or "It's the oxygen that makes the wine". The Venturi effect is also used in gas stoves and grills, where inspirators mix air and flammable gas. Read more about the use of fire in the kitchen in §V F. Finally, the Bernoulli effect can be used to make food grippers, for instance to handle sliced fruits and vegetables [81, 82].

F. Pendant drop: Surface tension

The Bernoulli and Navier-Stokes equations describe the motion of fluids, but they don't say much about the interesting phenomena that occur at interfaces: How can droplets hang upside-down from a tap? Water molecules are attracted to each other by cohesion forces, particularly by hydrogen bonds [83, 84]. This cohesion leads to a surface tension, γ, a force per unit length, which acts as if there was a taut elastic sheet covering the liquid interface [85]. Indeed, surface tension acts to minimise the surface area, so free droplets tend to be spherical. This inward force is balanced by a higher pressure inside the droplet. The pressure difference across the water-air interface, called the Laplace pressure, is given by the Young-Laplace equation,

$$\Delta p = -\gamma H, \tag{7}$$

where H is the mean curvature of the interface. For spherical droplets of radius R, we have $H = 2/R$. The expression is named after Thomas Young (1773-1829) and Pierre-Simon Laplace (1749-1827).

In the kitchen, the surface tension of water-air interfaces can be measured with a dripping tap experiment: A drop of radius R hanging from a faucet balances surface tension ($F_\gamma \sim 2\pi R\gamma$) with the force of gravity ($F_g = \frac{4}{3}\pi R^3 \Delta\rho g$). Therefore, the pendant drop will fall if it grows larger than $R^* \sim \lambda_c$, the capillary length

$$\lambda_c = \sqrt{\gamma/(\Delta\rho g)}. \tag{8}$$

Then, by measuring this critical droplet radius, the surface tension can be estimated using the known values for gravity G and the density difference $\Delta\rho$ between water and air. For a more accurate result, one can measure the weight of an ensemble of (say) a hundred drops and take the exact shape of the nozzle and the pendant drop into account [86]. For water-air interfaces, we then find the surface tension $\gamma \approx 0.07$ N/m. This value (double-O-seven) is easy to remember because the non-dimensional parameter that characterises the importance of gravity compared to surface tension is called the Bond number,

$$\mathrm{Bo} \equiv \frac{\text{Gravitational forces}}{\text{Capillary forces}} = \frac{\Delta\rho g L_0^2}{\gamma} = \left(\frac{L_0}{\lambda_c}\right)^2, \tag{9}$$

named, however, after an English physicist Wilfrid Noel Bond (1897-1937). Here, L_0 is a characteristic length scale such as the drop radius R. Note that the Bond number is also called the Eötvös number (Eo). Surface tension can lead to a vast number of counter-intuitive phenomena, and new effects are still discovered every day. This is particularly important for nanotechnology and miniaturization in microfluidics, where the Bond numbers are inevitably small. Also in microgravity experiments the effects of surface tension are amplified [87], as highlighted by wringing out a wet cloth in the International Space Station [88]. An alternative simple method, accessible for students, is to use a smartphone camera to measure the shape of a hanging droplet [89].

G. Wetting and capillary action

Besides cohesion forces that lead to surface tension, liquid molecules are also subject to adhesion forces, when they are attracted to other molecules [83]. This can be observed directly when looking at a droplet sitting on a surface [84]. The line where the liquid, gas and the solid meet is called the contact line or the triple line. The contact angle, θ_c, is defined as the angle between the liquid-gas interface and the surface. If the surface is hydrophilic (attracts the water), the droplet spreads out and wets the surface [90], leading to a small contact angle of $0 \leq \theta_c < 90°$. But if the adhesion forces are weak such as on waxed surfaces (hydrophobic surface) the cohesion forces can keep the drop together, leading to a large contact angle of $90° < \theta_c \leq 180°$. The equilibrium contact angle is found by minimising the total free energy, for example using calculus of variations. This leads to the Young equation,

$$\cos\theta_c = \frac{\gamma_{\mathrm{SG}} - \gamma_{\mathrm{SL}}}{\gamma_{\mathrm{LG}}}, \tag{10}$$

where the interfacial energies γ_{ij} encode the relative strengths of the cohesion and adhesion forces between the three phases $i, j \in$ (Liquid, Gas, Solid). Note, without subscript we imply $\gamma = \gamma_{\mathrm{LG}}$, and the gas phase is sometimes also called the vapour phase. This equation may be improved by accounting for advanced effects like interface curvature and contact line dynamics [91, 92].

The degree to which a drop will wet a substrate can be estimated with the spreading parameter [84], given by

$$S = \gamma_{\mathrm{SG}} - (\gamma_{\mathrm{LG}} + \gamma_{\mathrm{SL}})\,. \tag{11}$$

When $S > 0$, the drop spreads indefinitely towards a zero equilibrium contact angle, as is the case of silicone oil spreading on water. When $S < 0$, the drop instead forms a finite puddle, as when a drop of cooking oil is placed on a bath of water in a simple kitchen experiment. Due to its weight, the drop deforms the water surface. The amount of distortion depends on the relative magnitude of buoyancy to surface tension forces, as characterized by the Bond number [Eq. (9)].

Capillary action. Leonardo da Vinci (1452-1519) first recorded that liquids tend to flow spontaneously into confined spaces, an effect now called capillary action [84]. When dipping a narrow glass tube or a straw into water, the liquid will rise up until it reaches a constant height h. The narrower the capillary, the more the liquid ascends. This is somewhat unexpected because the Hagen–Poiseuille equation (3) suggests that the flow rate should decrease for smaller tube radii, if the pressure difference were constant. Moreover, the flow even moves against the hydrostatic pressure imposed by gravity. This effect is also explained by intermolecular adhesion and cohesion forces.

The height to which the water rises in a capillary can be calculated by balancing the hydrostatic pressure, $\Delta p_g = \rho g h$, with the Laplace pressure as in Eq. (7). If the capillary is cylindrical with inner radius R_i, and the meniscus has a spherical shape, its radius of curvature is $R = R_i/\cos\theta_c$ in terms of the contact angle. Combining these ingredients yields Jurin's law [93],

$$h = 2\gamma_{\mathrm{LG}}\cos\theta_c/(\rho g R_i). \tag{12}$$

For a typical glass microchannel of $R_i = 50\mu$m, the water can rise up to ~ 30cm and much more for thinner tubes. Hence, capillary action has many applications [84]. For example, if you like growing your own basil, plants use capillarity for transporting water from the soil to their leaves, together with other mechanisms including osmosis and evaporation [94, 95].

Conversely, if the contact angle $\theta_c > 90°$ for hydrophobic surfaces, h turns negative in Jurin's law [Eq. (12)] so liquid is expelled. Then one can observe dewetting, the process of a liquid spontaneously retracting from a surface [96–98]. Consequently, thin liquid films are metastable or unstable on these surfaces, as it breaks up into droplets. Therefore, dewetting is often not desirable in industrial applications because it can peel off protective coatings or paint [99], and inhibit lubrication in machinery [see §VI E]. Dewetting is also important in solid-state physics because it can damage thin solid films. This effect can also be turned into an advantage for making photonic devices and for catalyzing the growth of nanotubes and nanowires [100]. An exemplary fine-dining accessory exploiting the effects of surface tension is the 'floral pipette' [101], which presents a novel means of serving small volumes of fluid in an elegant fashion.

H. From jets to drops: Plateau-Rayleigh instability

Dripping kitchen taps offer a direct example of an important hydrodynamic instability: When a vertical stream of water leaves a worn tap, it narrows down because it is stretched by gravity. Once the liquid cylinder is sufficiently thin, we observe its breakdown into droplets before hitting the sink [Fig. 4a]. Plateau [102] was the first one to describe it systematically, which then enticed Lord Rayleigh [103] to provide a theoretical description and a stability analysis of an inviscid jet. He showed that a cylindrical fluid column is unstable to disturbances whose wavelengths λ exceed the circumference of the cylinder. The most unstable mode for a jet of radius R has the wave number $k = 2\pi/\lambda \approx 0.697R$ and from the growth rate of this mode, a typical jet breakup time can be estimated as $\tau_b \sim 3\sqrt{\rho R^3/\gamma}$, which in a kitchen sink is typically a fraction of a second. Kitchen jets exhibit also cross-sectional shape oscillations attributed to capillary waves which can easily be seen in home-made experiments [104]. By measuring these variations of jet eccentricity, occurring at a frequency proportional to τ_b^{-1}, one can measure the surface tension [105].

The physics and stability of liquid jets are fundamentally important for a number of applications, as reviewed

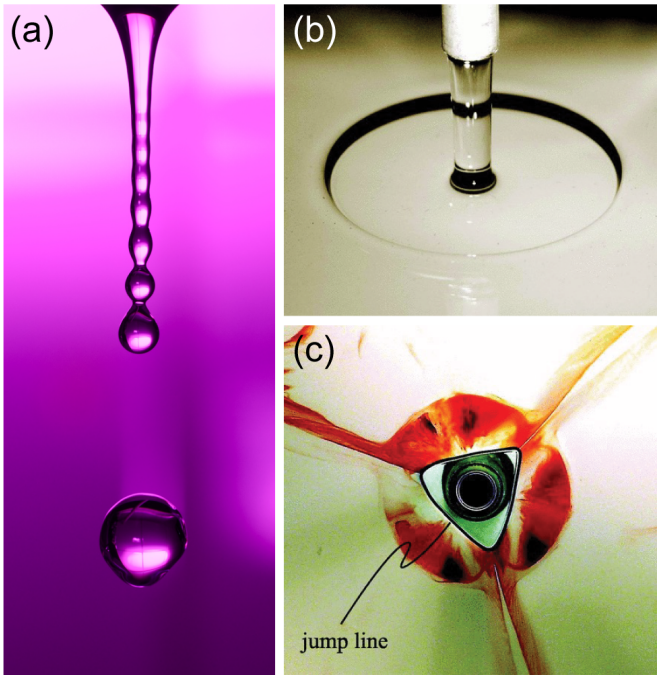

FIG. 4. Jets in the kitchen sink. **(a)** Example of the Rayleigh-Plateau instability, where a thin jet from a faucet breaks into droplets. Image by Niklas Morberg, licenced under CC BY-NC 2.0. **(b)** A circular hydraulic jump forms when a thicker liquid jet impinges on a planar surface. **(c)** A triangular hydraulic jump, seen from below through a glass plate. The impinging jet is the black center region, the jump line is the black line surrounding it, and an additional roller vortex is marked with a red dye. (b,c) From Martens *et al.* [112].

by Eggers and Villermaux [106]. The break-up of jets has some universal features, which result in a number of self-similar solutions. The scale invariance is manifested both in the conical shape of the tip of a French baguette, and in a bimodal distribution of droplets produced, independently of the initial conditions, in the pinch-off process. The latter is an important technological problem in ink-jet printing [107, 108]. In microfluidic systems, the surface-tension assisted breakup is also used to create mono-disperse droplets [109], and drinking (lapping) mammals including cats and dogs may adjust their jaw-closing times to the pinch-off dynamics to maximise water intake [110]. Citrus fruits can eject high-speed microjects from bursting oil gland reservoirs, up to 5000 g-forces, comparable to the acceleration of a bullet leaving a rifle [111].

I. Hydraulic jumps in the kitchen sink

When a thicker water jet (that does not break up) impinges on the kitchen sink, it will first spread out in a thin disk at high velocity. Surprisingly, at some distance from its origin, the thickness of the film suddenly increases; a hydraulic jump is formed [Fig. 4b]. Again, Leonardo da Vinci was the first known to study hydraulic jumps [113], and Lord Rayleigh [114] first described it mathematically. He postulated that a balance between inertia and gravity forces lead to the jump. In other words, a jump is expected when the Froude number,

$$\mathrm{Fr} \equiv \frac{\text{Inertial forces}}{\text{Gravitational forces}} = \frac{U_0}{\sqrt{gL_0}}, \tag{13}$$

transitions through unity, since the flow in the thin film continually loses momentum as is spreads out radially. Here, U_0 is the velocity at the free surface of the film, g is gravity, and L_0 is the film thickness. Rayleigh did not include effects of surface tension [§II F] in his analysis. However, he wrote that "On the smallest scale surface-tension doubtless plays a considerable part, but this may be minimised by increasing the stream, and correspondingly the depth of the water over the plate, so far as may be convenient". Watson [115] included effects of viscosity in his description of circular jumps, and two years later, in 1966, Olsson and Turkdogan [116] performed complementary experiments to validate Watson's theory and hypothesized that surface tension contributed to the loss of kinetic energy at the jump. Bush and Aristoff [117] expanded Watson's theory by exploring the role of surface tension on the formation of circular hydraulic jumps, and Mathur *et al.* [118] found surface tension to dominate over gravity for films on the micrometer scale. However, all of the above-mentioned authors regarded capillary pressures (due to surface tension, see Eq. (7)) as being negligible compared to hydrostatic pressures (due to gravity) on the scale of kitchen sink hydraulic jumps. Bhagat *et al.* [119] observed that when a strong jet impinges on a planar surface, the radius of the disk (inner region before the jump) is independent on the orientation of the surface. They concluded that gravity is not causing the hydraulic jump when the film is sufficiently thin, as it is when produced by a strong jet. Instead, a capillary pressure competes with the transport of momentum, and this balance is characterised by the Weber number,

$$\mathrm{We} \equiv \frac{\text{Inertial forces}}{\text{Cohesion forces}} = \frac{\rho U_0^2 L_0}{\gamma}, \tag{14}$$

where γ denotes surface tension and ρ denotes the density of the impinging liquid. For weaker jets, however, gravity can no longer be neglected. By balancing the energy at the jump and adopting the approach by Watson [115] by assuming a boundary layer flow inside the film, Bhagat *et al.* [119] found the following more general criterion for a circular jump to occur:

$$\mathrm{We}^{-1} + \mathrm{Fr}^{-2} = 1, \tag{15}$$

where the first term is associated with capillary waves and the second is associated with gravity waves.

As we have seen, the rich physics characterizing circular hydraulic jumps has attracted researchers for centuries, and the degree to which surface tension controls

these jumps remains an active research topic. Duchesne *et al.* [120] and Bohr and Scheichl [121] consider a static control volume and argue that surface tension has a negligible influence as it is fully contained in the Laplace pressure, while Bhagat and Linden [122] come to a different conclusion by an energy-based analysis. Another aspect of hydraulic jumps concerns the influence of different surface coatings on the jump radius and shape, and Walker *et al.* [123] showed that when a water jet impinges on a shear thinning liquid [see §IV A], the radius becomes time dependent. Later, the same group used viscoelastic liquids to enhance the degree of particle removal through inducing normal stresses that 'lift' the particles away from the substrate [124, 125]. Finally, it is also possible to create polygonal jumps, either by leveraging hydrodynamic instabilities in viscous liquids [112, 126–129], as displayed in Fig. 4c, or by utilizing micro-patterned surfaces [130].

J. How to cook a satellite dish

The importance of parabolas to focus light rays was already known since classical antiquity: Diocles described it in his book *On Burning Mirrors*, and legend has it that Archimedes of Syracuse (c.287–c.212 BC) used these to burn down the Roman fleet [131]. The latter is probably fictional, but Archimedes did write that the surface of a rotating liquid forms a paraboloid [Ibid]. At hydrostatic equilibrium, the gravitational force on a fluid element is balanced by the centripetal force and buoyancy [Fig. 5a], such that the liquid height profile is given by

$$h(\rho) - h(0) = \omega^2\rho^2/(2g), \tag{16}$$

where ρ is the radial distance from the rotation axis, ω is the angular velocity, and the corresponding focal distance is $f = g/2\omega^2$. Liquid-mirror telescopes use exactly this concept: the Large Zenith Telescope [Fig. 5b] is made of a 6-meter pool of rotating liquid mercury [132]. Note, the earliest known functional reflecting telescope by Isaac Newton (1642–1727) used a spherical mirror because paraboloids are hard to fabricate [133]. For modern large telescopes, the parabolic mirror is sometimes made by spinning molten glass in a rotating furnace. You can try to do this yourself in the kitchen, by melting some wax (or gelatin) and letting it cool on a record turntable. Once it has solidified you could even coat it with reflective paint. Parabolic reflectors are also widely used in solar cookers and various renewable energy technologies [134].

Equation (16) holds under the assumptions that the whole fluids rotates as a rigid body and that there is no local rotation of neighbouring fluid elements. Then the flow is called irrotational [135]. In closed containers, one must also account for surface tension and potential dewetting when the bottom becomes dry in the middle of the vessel [136]. For higher rotation speeds, however, this static description is no longer valid as the flow becomes

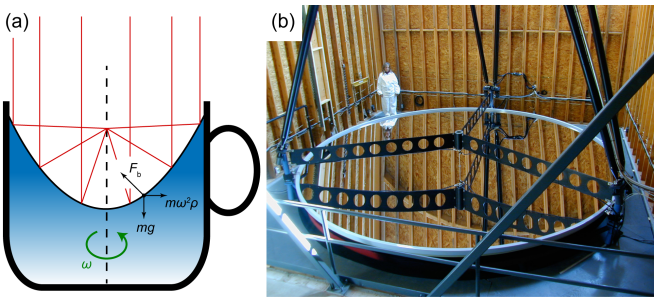

FIG. 5. Liquid mirrors. **(a)** Diagram of a rotating liquid that forms a parabolic reflector by the principle of hydrostatic equilibrium. The black arrows denote the force balance between gravity, rotation and buoyancy. **(b)** The Large Zenith Telescope uses this principle. It was one of the largest optical telescopes in the world. Diameter: 6.0 m, rotation period: 8.5 s, mercury thickness: 1.2 mm, accessible area of sky: 64.2 deg^2. Person for scale. From Hickson *et al.* [132].

rotational. In fact, this transition is also highlighted by a symmetry breaking, leading to the formation of polygonal rotating structures [137, 138] before all symmetry is lost in turbulence at even higher rotation speeds.

This local rotation of fluid elements is quantified by the fluid vorticity [135], defined as $\boldsymbol{\omega} = \nabla \times \boldsymbol{u}$. The Navier-Stokes equation (2) for an incompressible fluid ($\nabla \cdot \boldsymbol{u} = 0$) can be recast upon taking a curl of both sides, giving

$$\frac{D\boldsymbol{\omega}}{Dt} = (\boldsymbol{\omega} \cdot \nabla)\boldsymbol{u} + \nu\nabla^2\boldsymbol{\omega}. \tag{17}$$

Here the first term of the right-hand side accounts for the stretching or tilting of vorticity due to the flow gradients, while the last term describes the diffusion of vorticity in the fluid. Vortices formed across all scales, from atmospheric to molecular processes, are described by their velocity or vorticity distribution. The simplest models assume an axisymmetric velocity field in which the fluid circles around the vortex axis. However, the flow field in most practical cases is more complex, as secondary flows arise due to this circling motion. We describe them in more detail in §VIII B where we discuss how stirring the tea may impact the dynamics of submerged tea leaves. Secondary flows in the vertical direction arise also in bathtub or sink vortices [139].

K. Washing and drying hands, skincare

In Shakespeare's Scottish play, Lady Macbeth repeatedly washes her hands 'for a quarter of an hour' to cleanse away her murderous guilty conscience. At the start of the COVID-19 pandemic, her troubled soliloquy was used to satirise WHO posters that offer personal hygiene instructions in public restrooms [140]. Jokes aside, washing hands with soap is "a modest measure with big effects" to combat pathogen dispersal [141], which is of particular importance for the food industry [142]. Also coronaviruses can be cleaned off the skin with soap, or with

hand sanitisers that contain sufficiently high concentrations of agents such as ethanol or isopropanol [143–145]. Dancer [146] also reminds us that besides our hands, we should not forget to clean the surfaces that we touch, following the legacy of Florence Nightingale (1820-1910), often called the founder of modern nursing. Despite the importance of proper sanitation, its hydrodynamics is not so well explored. Mittal *et al.* [147] recently wrote "Amazingly, despite the 170+ year history of hand washing in medical hygiene [148], we were unable to find a single published research article on the flow physics of hand washing." There is of course a large body of literature about micelle formation and multi-phase flows [§III], foaming [see §III F] and the physics of micro-organisms [§VI I], but connecting this network of knowledge in the context of personal hygiene is only just starting.

Motivated by this gap in the literature and without access to a lab due to current stay-at-home orders, Hammond [149] conducted a theoretical assessment of hand washing. Using a lubrication approximation, he came a long way in describing how and when a virus particle is released from our hands when we rub them together. Hammond found that the rubbing speed needs to exceed a certain value set by the depth of the surface undulations of the skin, which in his model are represented by sinusoidal waves. Surprisingly, he found that multiple rubbing cycles are needed to remove a particle. More generally, the study of washing biological surfaces could widen our understanding of hydrodynamic interactions between particles, rough surfaces and fluid flows, with important implications in the food industry, for example. A natural extension of this work is to include viscoelastic effects, which might more realistically represent the material properties of the soap film. Moreover, two recent review papers that discuss the biological physics and soft matter aspects of COVID-19 were written by Poon *et al.* [144] and Bar-On *et al.* [145].

After washing our hands, it is essential to dry them properly [142, 150]. When we use a towel, the water gets pulled into the fabric by capillary action [see §II G]. This only works well if the towel is more hydrophilic (water-loving) than the surface of our hands. Paper and cotton cloth are especially hydrophilic, aided further by the large surface area of the fibres. Another method is to dry hands by evaporation. Whereas evaporation has been studied extensively on idealised surfaces [see §VII E], not so much is known about wetting and evaporation on soft materials like the skin [151, 152]. An ongoing debate is whether the dispersal of viruses and bacteria can be stopped more efficiently by warm air dryers, or jet dryers, which on the one hand may avoid having to touch surfaces but on the other hand could cause pathogen aerosolization [147, 153–155], which is especially problematic in food processing plants [156].

A common medical condition that comes with washing and drying hands frequently is xeroderma, or dry skin [157]. This can lead to symptoms including itching, scaling, fissure, or wrinkling [158, 159]. These problems can often be alleviated with moisturisers or emollients, but in more severe cases an effective treatment requires understanding the underlying biophysical mechanisms [160]. Liquid transport has been studied in the networked microchannels of the skin surface [161], as well as the physics of stratum corneum lipid membranes [162], and more generally soft interfacial materials [163]. Connecting the disciplines of physics and medicine will become increasingly important in future research.

III. DRINKS & COCKTAILS: MULTIPHASE FLOWS

After washing our hands, it is time to start dinner with a beverage of choice. In this section we review a wealth of hydrodynamic phenomena that emerge in these drinks, such as shock waves in the tears of wine, effervescence in Champagne, or 'awakening the serpent' during whisky tasking. These multi-phase flows [164, 165] have seen rapid scientific advances recently, and they are applied extensively in industrial processes. Perfect to contemplate while waiting for the main course to arrive, or to impress at a cocktail party.

A. Layered cocktails

A classic example of a culinary multi-phase fluid is a layered cocktail [Fig. 6a]. For instance, an Irish flag cocktail is made by first pouring crème de menthe, then a layer of Irish cream, topped off with orange liqueur. This beverage is called stably stratified, because each layer is less dense than the one below it. Multiple coloured layers can be formed using a density chart for the different liquid ingredients, also called a specific gravity chart [166]. Stratification is essential for life on Earth, both in the atmosphere [167], where sharp cloud layers can be observed, and in the ocean [168], where water layers can be characterised by large gradients in density (pycnocline), but also gradients in temperature (thermocline) or salinity (halocline), immediately impacting environmental stratified flows [169] and more generally geophysical fluid mechanics [170].

1. *Inverted Fountains*

The cocktail layers will separate readily if the ingredients are immiscible, such as, say, lemon water and rose oil. However, if the liquids are miscible, it is recommended to pour the layers slowly (ideally along the side of the glass with the help of a spoon) because otherwise the layers will mix. We can understand this turbulent and miscible mixing process as an 'inverted fountain' [171, 172], where the lighter fluid is forced down into the heaver fluid, opposed by buoyancy [173]. The

(inverted) height of the fountain, z_f, and thus the mixing volume, depends strongly on the Reynolds number [Eq. (5)], where U_0 is the pouring velocity and L_0 is the radius of the injected jet, but also the densimetric Froude number, where g in Eq. (13) is replaced by $|g'|$, the reduced gravity due to buoyancy, given by

$$g' = g(\rho_i - \rho_a)/\rho_a, \tag{18}$$

in terms of ρ_i and ρ_a, the densities of the injected and the ambient fluid. Conventionally, g' is negative for inverted fountains. For large Froude numbers, Turner [171] showed that the fountain height is given by

$$z_f \approx 2.46 L_0 \mathrm{Fr}. \tag{19}$$

This classical result predicts a linear relation, which agrees well with modern experiments. Note that different scaling laws have been derived for weaker fountains with a smaller Froude number, as reviewed by Hunt and Burridge [172].

Note, we already mentioned the Froude number in the context of hydraulic jumps [§II I]. Interestingly, it turns out that hydraulic jumps also occur in layered miscible fluids, as described by Wood and Simpson [174]. Recently, new models and experiments were developed to describe such internal hydraulic jumps, which do not rely on the Boussinesq approximation and account for entrainment effect as shear increases [175–179].

2. *Internal Waves*

Once the cocktail layers are established, more interesting flow phenomena can be observed. When the glass is slightly disturbed, internal waves can be seen, which are gravity waves (not to be confused with the gravitational waves in general relativity) that propagate inside the fluid instead of on its surface [181, 182]. Specifically, they are called interfacial (internal) waves when they propagate horizontally along an interface characterised by a density gradient, $d\rho/dz < 0$. Consider a fluid parcel in a continuously stratified fluid, with a smooth density profile $\rho(z)$, that is in hydrostatic equilibrium at z_0. If the parcel of density $\rho_0 = \rho(z_0)$ is displaced a vertical distance $\Delta z = z - z_0$ where the surrounding fluid has a different density $\rho(z_0 + \Delta z)$, it will feel a gravitational restoring force [Eq. (1)]. To first order, that leads to simple harmonic motion [183] with an oscillation frequency called the Brunt–Väisälä frequency,

$$f = \frac{1}{2\pi}\sqrt{-\frac{g}{\rho_0}\frac{d\rho}{dz}}. \tag{20}$$

These internal oscillations are typically slow compared to surface waves at the liquid-air interface, because the density gradient between the liquid layers is much smaller [see §IX D]. Internal waves are common in oceanography [184] and atmospheric science [170], where they lead for example to rippled clouds or lenticular clouds [185].

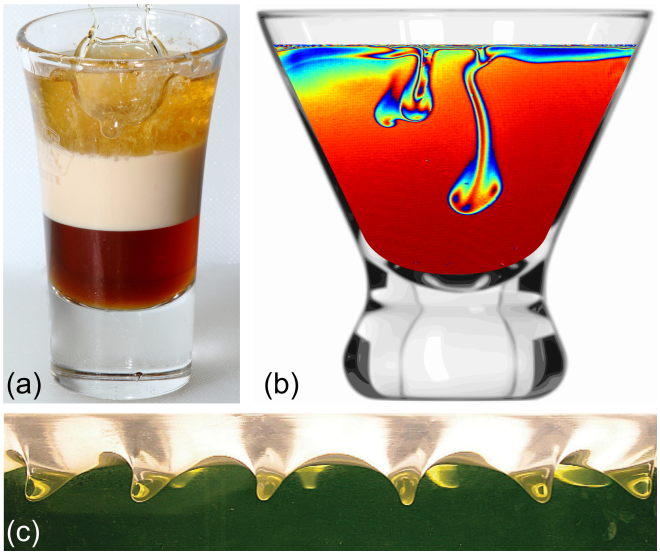

FIG. 6. Multi-phase cocktails. **(a)** B-52 shot made by layering Kahlua, Bailey's Irish Cream and Grand Marnier, with a splash on top. Image from J. D. Baskin on Flickr, licenced under CC BY 2.0. **(b)** Evaporation-induced Rayleigh-Taylor instability. Colours indicate the ethanol concentration, from blue (low) to red (high), measured with Mach–Zehnder interferometery. Image courtesy of Sam Dehaeck. **(c)** Kelvin-Helmholtz instability waves formed at an oscillated water-oil interface. From Yoshikawa and Wesfreid [180].

3. *Kelvin–Helmholtz Instability*

Fluctus clouds look like breaking ocean waves in the sky. They are caused by the Kelvin–Helmholtz (KH) instability [186, 187], when two fluid layers move alongside each other. Indeed, the same can be observed when a layered cocktail is sheared. By rotating the glass, a velocity gradient $\partial u/\partial z$ is created between the stratified layers. This shear is especially pronounced if the liquid spins up by friction with the bottom wall instead of the side walls [see §VIII A]. The velocity gradient drives the KH instability, while it is opposed by buoyancy, quantified by the density gradient $\partial\rho/\partial z$. The ratio of these two forces is encoded by a dimensionless quantity named the (densimetric) Richardson number,

$$\mathrm{Ri} \equiv \frac{\text{Buoyancy forces}}{\text{Shear forces}} = \frac{g'}{\rho}\frac{\partial\rho/\partial z}{(\partial u/\partial z)^2}. \tag{21}$$

The fluid layers are unstable when the shear is large enough, when $\mathrm{Ri} \lesssim 1$, depending on the system configuration. In a setup resembling our cocktail, the instability was characterised recently in a spin-up rotating cylindrical vessel by Yan *et al.* [188], and in an oscillatory cylindrical setup by Yoshikawa and Wesfreid [180], as shown in Fig. 6c. Naturally, the KH instability will cause the stratified layers to mix with one another, as reviewed by Peltier and Caulfield [189], or cause emulsion formation if the layers are immiscible [§IV D]. If the layers are immiscible, surface tension will stabilise the short

wavelength instability on top of buoyancy, which strongly affects emulsion formation [190, 191]. Therefore, the KH instability is important for many processes in industry and food science. Think about making mayonnaise with a blender, for example. From a fundamental point of view, understanding these flows is intrinsically connected with the heart of theoretical physics: symmetries. Only recently, Qin *et al.* [192] described that the KH instability results from parity-time symmetry breaking. Moreover, the Kelvin-Helmholtz instability also features in the magnetohydrodynamics of the sun [193], ocean mixing [170], relativistic fluids [194] and superfluids [195].

4. *Rayleigh-Taylor instability*

Until now we have discussed stably stratified cocktails. Yet, when a heavier fluid sits on top of a lighter fluid, the latter pushes into the former by gravity, so the mechanical equilibrium is unstable. Any small perturbation will lead to a familiar pattern of finger-like structures with a mushroom cap, as seen in Fig. 6b. This phenomenon is explained by the Rayleigh-Taylor (RT) instability, which was first discovered by Lord Rayleigh [196], and later described mathematically by Taylor [197] together with systematic experiments by Lewis [198]. Many developments followed, and Chandrasekhar [199] extended the theoretical description in his famous book. Like the KH instability, the RT instability is relevant across the disciplines, from the astrophysics of supernovae [200, 201] to numerous technological applications [187].

The RT instability arises because the system seeks to minimise its overall potential energy. Its onset is primarily governed by the Atwood number,

$$\mathrm{At} = \frac{\rho_h - \rho_l}{\rho_h + \rho_l}, \tag{22}$$

the non-dimensional difference between the densities of the heavier and the lighter fluid, ρ_h and ρ_l. We think this number is named after George Atwood FRS (1745-1807), who also invented the Atwood machine, but we struggled with finding the original source. To describe the RT instability more generally, one must account for the fluid viscosities and surface tension [202], and potential effects due to fluid compressibility [203]. Moreover, the dynamics depend strongly on the initial conditions: They begin with linear growth from perturbations, which transitions to a non-linear growth phase involving characteristic structures of rising 'plumes' and falling 'spikes'. Subsequently, these plumes and spikes interact with each other through merging and competition, and roll up into vortices. The final stages are characterized by turbulent mixing [see §VIII].

In the words of Benjamin [40], the RT instability is a fascinating gateway to the study of fluid dynamics. It can readily be observed in kitchen experiments, but it also occurs spontaneously without us even noticing

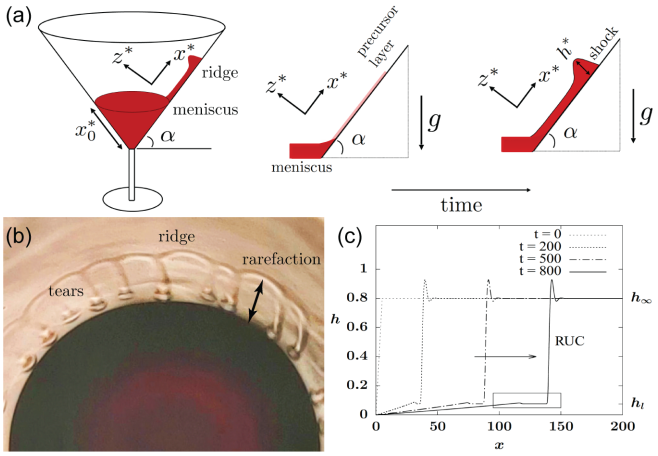

FIG. 7. Shock waves in tears of wine. **(a)** Schematic of a conical-shaped glass of inclination angle α, showing a one-dimensional thin wine film traveling up an inclined flat glass surface. The film height h^* is exaggerated for clarity. **(b)** Experiment using 18% ABV port wine and $\alpha = 65°$. Swirling the wine around the glass creates a front that forms out of the meniscus. The draining film advances up the glass and destabilises into wine tears. **(c)** The formation of a reverse-undercompressive (RUC) shock. (a-c) From Dukler *et al.* [207].

[Fig. 6b]: In a well-mixed (non-layered) cocktail, the alcohol evaporates faster than water. Hence, at the air interface, a water-rich layer develops that is denser than the bulk mixture, which gives rise to the RT instability [204]. The plumes of such 'evaporating cocktails' are observed using a Mach–Zehnder interferometer. By demodulating the fringe patterns using a Fourier transform method [205], it is possible to compute the refractive index field, and hence the local ethanol concentration. Evaporation-induced Rayleigh-Taylor instabilities also occur in polymer solutions [206], so your cocktail need not necessarily be alcoholic.

Interestingly, the RT instability is often inseparable from the Kelvin-Helmholtz instability. RT flows create velocity gradients that trigger KH billows, while KH flows create density inversions that trigger RT fingers. Moreover, the RT instability is closely related to the Richtmyer–Meshkov (RM) instability, when two fluids of different density are impulsively accelerated [201], and to the Rayleigh-Bénard convection, where an instability occurs due to heating a single liquid from below or cooling it from above, which we describe in more detail in §V C.

B. Tears of wine

One of the most surprising phenomena in multi-phase flows is the Marangoni effect, named after Marangoni [208]. You may have seen this effect already in the kitchen, when a droplet of dish soap falls into a bowl of water sprinkled with pepper: Within the blink of an

eye, the pepper moves to the edges by an outward flow along the liquid-air interface. Another striking example is adding food colouring drops to a bowl of milk, where poking it with a soap-covered cotton bud generates beautiful flow patterns (try it!). These Marangoni flows arise because the surfactant molecules in the soap lower the surface surface tension [209], leading to a difference in surface tension along the interface, of $\Delta\gamma = f\gamma$, where the factor $f \sim 10^{-1}$ for most soaps. Consequently, the water without soap pulls more strongly on the water with soap, generating a current from regions of lower to higher surface tensions. The flow strength can be estimated roughly as $u \approx \Delta\gamma/\mu$, so even small fractions f give rise to fairly strong flows, using $\gamma \sim 0.07\,\mathrm{N/m}$ and viscosity $\mu \sim 0.9\,\mathrm{mPa\,s}$ for water. Of course, more detailed calculations must take other influences into account, including solubility, surface contamination and system geometry [209–213]. The ratio between advective and diffusive transport over a characteristic length scale L_0 is given by the Marangoni number,

$$\mathrm{Ma} \equiv \frac{\text{Advective transport rate}}{\text{Diffusive transport rate}} = \frac{\Delta\gamma L_0}{\mu D}, \qquad (23)$$

where D is the diffusivity of the surfactants or any additive that changes the surface tension.

Fortunately, the Marangoni effect does not only occur with soap, but also with edible ingredients. In fact, the phenomenon was first identified by James Thomson (1822-1892) in the characteristic "tears" or "legs" of wine [214], and indeed other alcoholic drinks including liquors and whisky [see §III C]. These tears are formed because the alcohol is more volatile than water, and it has a lower surface tension [215]. To see this, pour yourself a glass of wine. In the thin meniscus that the wine forms with the glass surface, the alcohol evaporates faster than the water, so the surface tension here is higher than in the bulk. The wine is then pulled up the meniscus, forming a thin film that starts climbing up along the side of the glass. After a few seconds, the film forms a ridge approximately 1 cm above the meniscus. This ridge becomes unstable under its own weight as more wine climbs up, so it collapses into "tears" that fall down towards the meniscus. Large tears can fall back into the bulk, but small tears can also be pulled up again by the continuously climbing film that replenishes the ridge. This can cause the tears to bounce up and down, especially at the meniscus. The effects is beautifully imaged using the Schlieren or shadow projection techniques [216].

So far, so good. But the mechanism by which the droplets form and collapse is more complex. As the wine film climbs to its terminal height, when the Marangoni stresses are balanced by gravity, this transient stationary state is subject to various hydrodynamic instabilities [217–219]. Besides alcohol concentrations differences, the evaporation also induces temperature gradients that lead to additional Marangoni stresses [220]. The ridge instability that triggers the formation of wine tears was also studied and analysed with a Plateau-Rayleigh-Taylor theory [221]. Yet, the dynamic formation of the ridge itself is still not well understood.

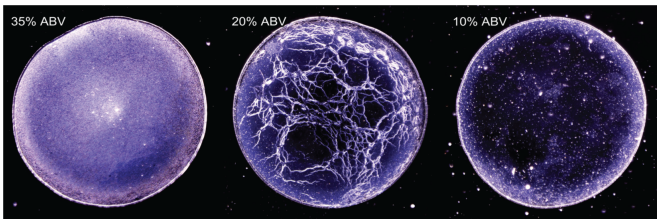

FIG. 8. Whiskey webs. Different patterns emerge after letting whiskey droplets of different alcohol percentages evaporate on a glass surface. At 35 % ABV **(left)**, the deposits are evenly distributed, while at 10 % ABV **(right)**, the deposits are distributed preferentially near the rim of the drop. At intermediate (20 % ABV) concentration **(middle)**, the deposits form complex 'whiskey web' patterns. From Williams *et al.* [224].

Until now we have discussed a wine film that spontaneously climbs up a dry wine glass, but it is common practice among connoisseurs to swirl the wine around. This often creates a wet coating film much higher than the terminal climbing height, which can give rise to rather different behaviours. Dukler *et al.* [207] showed that such swirled films can feature a 'shock wave' that climbs out of the meniscus [Fig. 7], again driven by Marangoni stresses due to evaporation. This wave can be observed as a ridge that propagates upwards, where the wine film above the shock front is thicker than below it. Specifically, the dynamics can be described as a reverse undercompressive (RUC) shock. This type of shock wave is unstable: Small inhomogeneities in the wine film are amplified into thick drops, which then fall down as tears. As described previously for rising films driven by thermal gradients [222, 223], different shock morphologies can occur in other circumstances. This is of great scientific and technical interest, including dip-coating and painting applications. Moreover, it would be interesting if people's dining experience could be improved by developing a new dish that uses the shock wave as a surprise effect.

C. Whisky tasting

When we taste whisky or whiskey, we use all of our senses [225]. Note: the spelling whiskey is common in Ireland and the United States, while the term whisky is common for produce from the UK and most other countries. While complete volumes have been written about the art of whisky tasting, see e.g. [226], we would like to highlight some of its hydrodynamic aspects, which are clearly visible. That is, a good deal of information may be gained by assessing the appearance and dynamics of spirits [227, 228]. The following tests can give clues about the whisky quality and vintage before any smelling or tasting.

As a first examination, it is customary to inspect the

tears that we described in §III B. This gives an indication of the whisky's alcohol content, its viscosity and its surface tension, which in turn depend on the exact chemical composition. When the tears run down slowly, with thick legs, it indicates that it will give more texture in the mouth [229]. Conversely, if the legs are thin and run quickly, the whisky is likely to be younger and of a lighter body. This is because the texture changes during the aging process, as viscous natural oils and other compounds are released from the wooden casks [230], which inevitably also influence the whisky colour. The rheological and thermophysical properties are also affected by storage and temperature [231]. However, it would be wrong to claim that a whisky with more pronounced tears is automatically sweeter or better in quality, since the tear formation is a purely physical phenomenon. Indeed, the tears vanish when the glass is covered, since the evaporation-induced Marangoni stresses disappear.

A second experiment is the 'beading' test [227, 232, 233]. When a whisky bottle is shaken vigorously, a foam can appear on the liquid interface if the alcohol concentration is higher than approximately 50% alcohol by volume (ABV). The beading is not necessarily more pronounced at higher concentrations, but it is not observed below a certain percentage. Beading can also say something about the age of the whisky: The bubbles tend to last longer in older vintages because the compounds released from the wooden casks can stabilise the foam. Read more about foam stability in §III F.

A third inspection method is called whisky viscimetry [229, 234]. When adding a little water to the whisky, small vortices called 'viscimetric whirls' appear when the liquids of different viscosities mix with one another. Connoisseurs sometimes refer to this phenomenon as 'awakening the serpent' [234]. These vortices only last for a few seconds, but again they tell us something about the texture of the whisky. The more persistent the whirls, the thicker the mouthfeel and the higher the alcohol concentration. To the best of our knowledge, this effect has not been quantified systematically in the scientific literature.

Depending on the distillation method, spirits reach an initial strength of $\sim 70\%$ ABV (pot still) or even higher (column still). Most whiskies are then diluted down to $\sim 60\%$ ABV prior to storage in casks. After maturation, they are often mixed with more water to $\sim 40\%$ ABV, the minimum in most countries. There are several reasons for this dilution: First, it can enhance the flavour because many of the taste-carrying molecules, such as guaiacol, are thermodynamically driven up to the liquid-air interface at low ethanol concentrations [235]. Second, the ethanol concentration influences the sensory perception [225, 236], where lower strengths are more palatable by most consumers. Third, besides enhancing the flavour of spirits, dilution can lead to a better mouthfeel. At 20 °C, the viscosity of pure ethanol and water is $\mu_1 \approx 1.2\,\mathrm{mPa\,s}$ and $\mu_2 \approx 1\,\mathrm{mPa\,s}$, respectively, but the viscosity of an ethanol-water mixture features a maximum of $\mu_{12} \approx 3\,\mathrm{mPa\,s}$ at 40-50% ABV [237]. This surprising non-linear effect of binary mixture viscosities is described in more detail in §IV B.

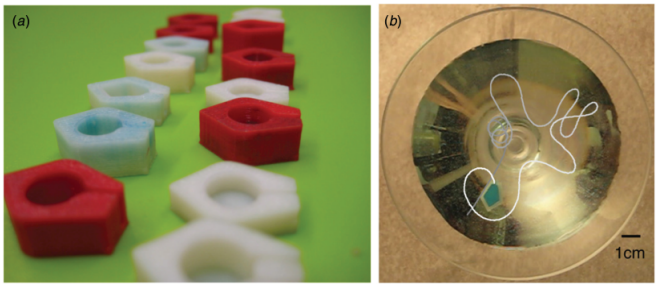

FIG. 9. Marangoni-stress powered cocktail boats. **(a)** A fleet of cocktail boats with different designs. The fuel (any liquor) is stored in the central cavity. The thin slit at the rear slowly releases the fuel into the glass, which establishes a surface tension gradient that drives the boat forward. **(b)** Trajectory in a cocktail glass. This boat is $\sim 1.5\,\mathrm{cm}$ long and fueled by Bacardi 151 (75% ABV). (a,b) From Burton *et al.* [101].

Remarkably, diluting your drink can also help with distinguishing whether it is whisky or whiskey: An evaporating bourbon droplet of 40% ABV tends to leave a uniform surface deposition [Fig. 8], while a diluted droplet at 20% ABV leaves distinctive patterns called whiskey webs [224, 238, 239]. Apparently, Scotch whisky and other distillates do not feature these web patterns and they are unique across different samples of American whiskey, so they could act like fingerprints. Indeed, the flavour profile results from the intricate chemical composition, which also affect the web patterns through the interplay of bulk chemistry with surfactants and polymers. Similarly, the webs do not form in droplets below 10% ABV, where instead the coffee-ring effect is observed [see §VII E]. In general, this rich variety of surface depositions results from a combination of intrinsic (chemical composition) and extrinsic factors (temperature, humidity) that lead to an interplay of Marangoni flows and macromolecular surface adsorbtion. The non-uniform residues are often undesired in many industrial applications including 3D printing, so whisky experiments could help us with understanding and controlling uniform coatings [240]. Drying drop technologies may also be used for wine and hard drinks quality control [241].

D. Marangoni cocktails

Another well-known demonstration of the Marangoni effect is the 'soap boat' [242, 243]. These boats propel themselves in the kitchen sink by releasing surfactant molecules from the back: The surface tension of water is then higher at the front, so the boat is effectively pulled forwards. The same effect is also used by water-walking insects as a quick escape mechanism [244]. However, this propulsion is short lived when using soap as fuel in a closed geometry, because the interface becomes saturated

with surfactants. A prolonged motion can be achieved by using other commonly available fuels [245]. Moreover, continuously moving boats can be made with camphor, a volatile surfactant that evaporates before the interface can saturate, allowing for persistent propulsion [246].

Recently, this technology was extended to create alcohol-powered 'cocktail boats' that move around in your glass [101, 247]. We depict them in Fig. 9. A typical commercial spirit can provide a surface tension difference up to $\Delta\gamma \sim 50$mN/m compared to pure water, but sugar and other cocktail ingredients tend to reduce this value somewhat. By collaborating with chefs, various materials were tested to make the boats edible. Gelatin boats were found to be capable of sustained motion and suitable for a wide range of flavourings, but they are susceptible to dissolving and sticking to the glass walls. Wax boats performed the best, with speeds up to 11cm/s and travel times up to 2 minutes, but unfortunately they are not well digestible [248]. It would be interesting if future research could improve or discover new edible materials.

Marangoni propulsion does not only lend itself to appetizing divertissements. The same mechanism can be used to create microscopic swimming droplets [249], which can be used as cargo carriers that move deep inside complex flow networks [250]. Recently, Dietrich *et al.* [251] developed very fast Marangoni surfers that can swim over ten thousand body lengths per second, and Timm *et al.* [252] developed Marangoni surfers that can be remotely controlled. More generally, similar *phoretic* effects [253], where interfacial flows are driven by gradients in concentration, electric fields, temperature etc., can be exploited to make a broad range of self-propelled colloids that are of extraordinary interest to understand collective dynamics and emergent phenomena out of equilibrium [254–260]. The same mechanisms are also at play in active emulsions [261], the transport of molecules in biological systems [262, 263], and the fragmentation of binary mixtures into many tiny droplets, a process called Marangoni bursting [264].

E. Bubbly drinks

Go ahead and pour yourself some nice sparkling wine into a glass, and observe the beautiful sight of rising bubbles and their effervescence [Fig. 10(a)]. Champagne and sparkling wines are supersaturated with dissolved CO_2 gas, which, along with ethanol, is a product of the wine fermentation process [265]. When the bottle is uncorked, there is a continuous release of this dissolved CO_2 gas in the form of bubbles. Hence, this physicochemical system provides a great opportunity to study several fundamental fluid mechanics phenomena involving bubbles: their nucleation, rise, and bursting dynamics, which in turn affect the taste of carbonated drinks [265–271].

Before savoring the wine or bubbles, you need to first open the cork of the bottle. We are all familiar with the curious "pop" sound, and of course the dangers of uncontrolled corks flying out! This uncorking process is also accompanied by the formation of a small fog cloud just above the bottle opening. It has been shown recently that uncorking champagne creates supersonic CO_2 freezing jets [272]. What is the underlying physical principle behind these interesting phenomena? It turns out that there is a sudden gas expansion when the bottle is uncorked (pressure drop from about 5 atm to 1 atm). This leads to a sudden drop in the temperature (about 90 °C), resulting in condensation of water vapor in the form of a fog cloud.

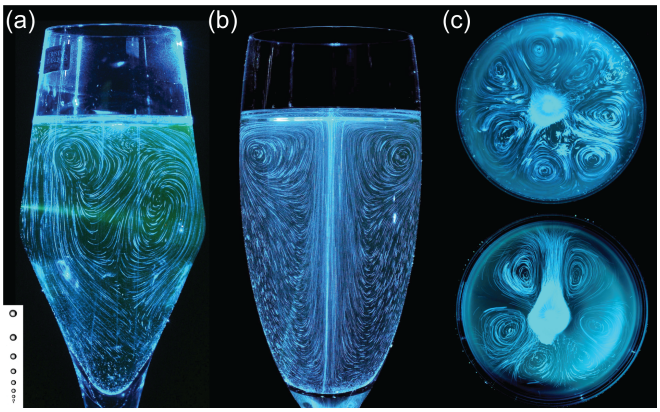

FIG. 10. Laser tomography of champagne glasses. **(a)** Natural, random effervescence in an untreated glass. Inset: Growth of bubbles as they rise. **(b)** Stabilized eddies in a surface-treated glass. (a,b) Courtesy of Gérard Liger-Belair. **(c)** Counter-rotating convection cells self-organise at the air-champagne interface. From Beaumont *et al.* [275].

The sudden temperature drop also leads to a drop in the CO_2 partial pressure above the champagne surface. Hence, the dissolved CO_2 in the champagne is no longer in equilibrium with its partial pressure in the vapor phase. In fact, just after the uncorking, it turns out that the champagne is supersaturated with CO_2. As described by Lubetkin and Blackwell [273], this is quantified by the supersaturation ratio,

$$S = (c_L/c_0) - 1, \tag{24}$$

where c_L is the CO_2 concentration in bulk liquid and c_0 is the equilibrium CO_2 concentration corresponding to partial pressure of CO_2 of 1 atm. Just after uncorking, $c_L/c_0 \approx 5$, so $S \approx 4$, and the champagne must degas in order to achieve stable thermodynamic equilibrium. The gas loss occurs through two mechanisms, by diffusion through the liquid surface (invisible to us), and by the vigorous bubbling (effervescence) that we can readily observe and also hear [274] [see §VIII D].

How do these bubbles form in the first place? The bubbles do not just pop out of nothing, the CO_2-dissolved gas molecules need to cluster and push their way to overcome attraction forces that hold together the liquid molecules. Hence, the bubble formation process is controlled by a nucleation energy barrier [276]. As described by Jones

et al. [277], the critical radius of curvature r^* that is necessary for gas pockets to overcome this barrier is

$$r^* \approx 2\gamma/(p_{\rm atm} S), \tag{25}$$

where the surface tension of champagne is $\gamma \approx 50\,\mathrm{mN/m}$, the atmospheric pressure is $p_{\rm atm} \approx 10^5\,\mathrm{Pa}$, and $S \approx 4$ at the time of uncorking. Using these values, we find that this critical radius r^* for bubble formation is very small (about $0.25\,\mu\mathrm{m}$).

The pleasing effervescence (bubbling) that we observe in champagne can arise from either natural or artificial sources [265, 278], as shown in Fig. 10(a,b). Natural effervescence refers to bubbling from a glass which has not received any specific surface treatment. When champagne is poured into a glass, a majority of bubble nucleation sites are found on small ($100\,\mu\mathrm{m}$ long) hollow, cylindrical fibre structures which contain trapped gas cavities (lumen). Another source of natural effervescence are gas pockets trapped in tartrate crystals precipitated on the glass wall. Hence, natural effervescence can vary significantly depending on how the glasses are cleaned, dried, and stored. On the other hand, artificial effervescence refers to bubbling from a glass surface where precise imperfections have been engraved by the glass manufacturer. The typical imperfections introduced on the glass are micro-scale scratches to produce a specific pattern, which give rise to bubbling phenomena that are markedly different from natural effervescence [265].

The bubble release mechanism from a fibre's lumen has been well studied [265]. After a champagne bottle is uncorked, the supersaturation of CO_2 implies that these CO_2 molecules will escape to the vapor phase using every available gas/liquid interface. The trapped tiny air pockets on fibre lumens offer gas/liquid interfaces to the dissolved CO_2 molecules enabling them to cross the interface to gas pockets. The CO_2 gas pockets grow in size, and when it reaches the fibre tip, it is ejected as a bubble. However, a portion of the gas packet is left trapped behind in the lumen, and the bubble ejection cycle continues until the dissolved CO_2 supply is depleted.

After the bubbles form in the trapped gas pockets on the glass, they rise towards the liquid surface due to their buoyancy and also grow in size since they absorb the dissolved CO_2 molecules. The repetitive production of bubbles from the nucleation sites has been captured in a model by Liger-Belair *et al.* [279], and it has been found that the bubble radius R increases linearly with time t as:

$$R(t) = R_0 + kt, \tag{26}$$

where R_0 is the initial bubble radius, $k = dR/dt$ is the growth rate. Bubble rise experiments conducted with champagne and sparkling wines revealed k values around $400\,\mu\mathrm{m/s}$ and experiments in beer revealed growth rates of around $150\,\mu\mathrm{m/s}$, indicating that the physicochemical properties of the liquids influenced the bubble growth rate [279].

According to wine tasters, the smaller the bubbles, the better the sparkling wine. Hence, plenty of attention has been focused on modeling the average size of the rising bubbles [Fig. 10(a), inset], which is a resultant of their growth rate and velocity of ascent. As discussed in detail by Liger-Belair *et al.* [280], the average bubble radius is

$$R \approx 2.7 \times 10^{-3} T^{5/9} \left(\frac{1}{\rho g}\right)^{2/9} \left(\frac{c_L - k_H p_{\rm atm}}{p_{\rm atm}}\right)^{1/3} h^{1/3}, \tag{27}$$

where T is the liquid temperature, ρ is the liquid density, g is gravity, k_H is Henry's law constant and h is the distance travelled by the bubble from the nucleation site. It is interesting to note that so many factors can influence the average bubble size, which is typically in the sub-millimeter length-scale in bubbly drinks. The bubble size in beer is significantly smaller than in champagne, and the reason for this is that the amount of dissolved CO_2 in champagne is about two times higher.

In addition to the visual beauty and fascination, the bubbles actually play an important role in the drink – the bubbles have been shown to generate large-scale time-varying convection currents and eddies inside the glass [265, 275, 281–283], often with surprising self-organised flow patterns [Fig. 10(b,c)]. Since they cause a continuous mixing of the liquid, bubbles are thought to play a key role in the flavor and aromatic gas release from the wine-air interface. These release rates are dependent on the fluid velocity field close to the surface, which is in turn significantly influenced by the ascending bubbles. As the bubbles collapse at the air interface, they radiate a multitude of tiny droplets into aerosols [284], which evaporate and release a distinct olfactory fingerprint [285].

In future, we can look forward to several innovations in bubbly drinks, where numerous factors must be taken into consideration – different types of glass shapes, natural versus artificial effervescence, engraving conditions, kinetics of flavor and CO_2 release under various conditions, and sensory analysis.

F. Foams

Bubbles (mentioned in the preceding section §III E) can burst when they reach the surface, but there is a finite lifetime associated with this process [265]. Thus, when the bubble production rate is very fast, greatly exceeding the surface bursting time-scales – then the bubbles start accumulating on the surface to create layers of bubbles called "foams" [Fig. 11] [286–289]. In many beers, these foams last long since they tend to be stabilized by proteins – they add to the visual appeal and provide a creamy texture enhancing the mouthfeel [Fig. 11a]. However, in champagne, the foam is more fragile and less stable due to the lack of proteins. Foams are formed in many other fizzy drinks and also in specially prepared coffees such as cappuccino. In cappuccino, the foam layer lasts for a long time since it is stabilized by milk pro-

teins. These observations naturally bring up questions on the mechanisms behind the formation, stability, age and drainage of foams – we will discuss these aspects below.

A foam is essentially a dispersion of gas in liquid, and gas bubbles tightly occupy most of the volume. The liquid phase in the form of films and junctions is continuous unlike the gas phase. Foams are also characterized by the presence of surface-active molecules called surfactants, which stabilise the bubbles at the interfaces of gas and liquid [290] (the same type of molecule can also stabilise an oil/water interface in an emulsion [see §IV D]). Since foams consist of significant quantities of gas, being hence less dense than the liquid it contains, which is why a foam floats on the surface of the liquid. Another interesting property of foam is the large surface area per unit volume, since the foam contains a large number of interfaces. Hence, foams enhance the possibilities for molecular transfer and find applications in foods for flavor enhancement (e.g. chocolate or spices) and also reduce the need for high sugar or salt content [286]. Foams also have special mechanical properties – they exhibit both solid-like and liquid-like behavior [291]. If the deformation is not too high, foams can show weak visco-elastic solid properties and can return to its original shape. However, if the foam is subjected to a high deformation, it can behave like a visco-plastic solid that can be sculpted. Foams can flow like liquids and seep through pores and cavities, so they can be poured into containers and tubes of various shapes. The foam's viscous resistance increases less quickly with flow rate compared to a normal fluid enabling it to reduce frictional losses, hence foams behave as a 'yield stress fluid' [see §IV A] with intermittent flow via avalanche-like topological bubble rearrangements [292]. Hence, given their unique properties, in addition to the food industry, foams find applications in many other areas of science and technology – e.g. cosmetics [293], cleaning, reducing pollution, surface treatment, fire-fighting, army, and building materials [286].

We will now examine the physical properties that allow a foam to exist in equilibrium. There are four relevant length-scales to consider: (i) the meter scale, where the foam appears to be a soft and opaque solid, (ii) the millimeter scale, where individual bubbles can be distinguished in the foam, (iii) the micron scale, which reveals liquid distribution between bubbles, and (iv) the nanometer scale, where molecules (e.g. soap molecules) at the interfaces (air/water) are relevant. The physics of foams is hence a very broad subject covering so many length-scales [286], and here we will only touch upon a few aspects.

At the scale of the gas/liquid interface, the surface tension [§II F] and the Young-Laplace law, Eq. (7), determine the shape of the interface. An interface is flat if geometric constraints allow it, while the surface of an interface that is completely surrounded by some fluid becomes spherical. The pressure being higher on the concave side, tries to curve the shape while surface tension tries to flatten the surface.

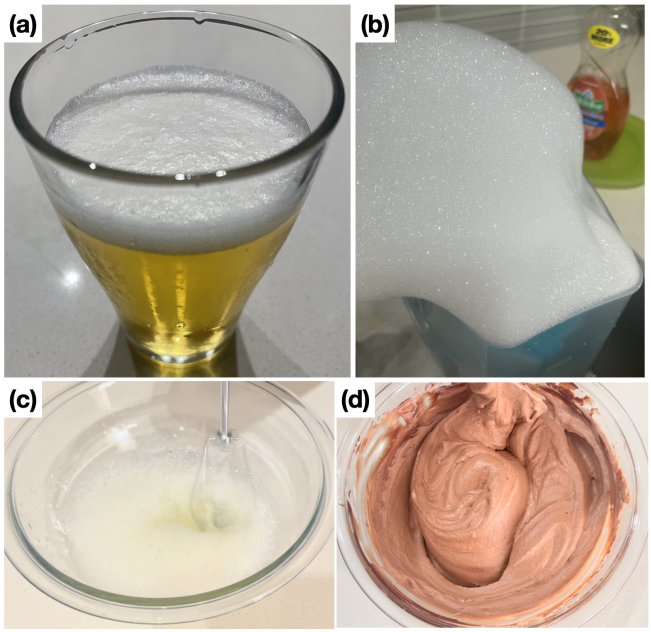

FIG. 11. Examples of foams in the kitchen: **(a)** Beer, **(b)**Dish washing, **(c)** Egg beating, and **(d)** Chocolate mousse.

Foams are prepared using additives that chemically consist of a polar head and a tail with a long carbon chain. The head is hydrophilic and the tail is hydrophobic [see §II G]. The combination of these properties results in an *amphiphilic* molecule (water-loving and fat-loving). Such a molecule, when dissolved in water, tends to absorb at the air/water interface. This forms a monolayer, which greatly affects the interfacial surface tension properties. Hence, these molecules are called surface-active molecules or *surfactants*. In our everyday experience, there are several examples where we find many small bubbles that burst quickly (few seconds), e.g. in sparkling wine or champagne. Here, the small volume of gas in the bubble encloses a thin film which is unstable due to van der Waals forces, and hence breaks. However, the presence of surfactants such as a dishwashing liquid carry a small charge giving rise to an electrostatic repulsion, which cancels out the van der Waals forces and stabilises the thin film – helping the foam last for a longer period [Fig. 11].

A bubble is essentially a small volume of gas enclosed by a film of water. The bubble assumes the smallest possible surface area to contain the gas, which typically results in a spherical shape for an isolated bubble. The pressure inside most foam bubbles is only slightly greater than the atmospheric pressure and is not sufficient to compress the gas appreciably, so the volume of gas can be considered to be fixed. If the bubble has a large size, then the interface becomes deformed and is no longer spherical under external forces such as gravity [294]. When two bubbles come in contact, they share an interface and hence change shape to reduce the total interfacial

area, and can no longer remain spherical. In general, when a group of bubbles come together to form a foam, the conservation of volumes and minimization of area leads to some simple laws for bubble shape, also known as *Plateau's laws*, first formulated by Plateau [102], and rigorously proved by Almgren and Taylor [295].

Plateau's laws are based on an 'ideal foam' model, which makes the following assumptions: (i) The foam is very dry: i.e. the liquid volume is assumed to be negligible compared to the total foam volume, (ii) The foam is at mechanical equilibrium: it is at rest since all forces within foam are balanced, in a local energy minimum, (iii) The foam energy is proportional to the surface area of its bubbles, and (iv) The foam is incompressible. The following are the three *Plateau's laws*: (I) Equilibrium of faces: The films are smooth, and mean curvature is determined by the Young-Laplace law [Eq. (7)]. (II) Equilibrium of edges: Along the edges, the films always meet in threes, forming angles of $120^\circ = \arccos(-1/2)$. (III) Equilibrium of vertices: At the vertices, the edges meet four-fold, forming angles of $109.5^\circ = \arccos(-1/3)$. These laws are the necessary and sufficient conditions to maintain the mechanical equilibrium of an ideal foam, and there are also two-dimensional versions of these laws.

So far, our culinary experience with bubbly drinks have led us to discuss foams mainly in the context of air bubbles in liquid. However, given their lightness and texture, foams are actually a pleasure to eat! The Chocolate mousse for desert is one of the most popular examples of edible foams [Fig. 11d]. These edible foams such as mousses and breads are typically solids [286, 296–298] with complex mechanical properties [299]. They are often prepared by solidification of a liquid foam by refrigeration or cooking. Since these foams are solidified before their collapse, they do not need a stabilizing agent. Another interesting point is that air is an important raw material in these edible foams: air contributes greatly to increasing the volume of the product, but it practically doesn't cost anything. On a final note, many other popular deserts are edible foams, these include favorites such as ice cream, meringue, marshmallows, many types of cakes, baked Alaska, etc.

We have mainly discussed foams which are stable for a finite duration of time. There are several interesting examples of dynamic and unstable foams, we show two popular examples in Fig. 12. We know in general that bubbles rise due their buoyancy in a liquid, but in Guinness beer there is a collective downward movement of bubbles, creating a 'cascade of bubble textures'. It has been demonstrated that this bubble texture cascade motion [Fig. 12(a)] arises due to a roll-wave instability of gravity currents [300], a phenomenon that is analogous to the roll-wave instability in liquid films that case water films to slide downhill on rainy days [§IX E]. Furthermore, it has been theoretically shown that these bubble cascades can occur in systems other than the Guinness beer [301].

Another interesting phenomenon is 'beer tapping' – a beer bottle foams up resulting in an overflow when it is tapped from the top [Fig. 12(b)]. The fascinating fluid physics underlying this phenomenon was explained recently [302]. It turns out that when the beer bottle is first hit at the top, a compression wave travels through the bottle. This wave gets rebounded through the liquid as an expansion wave. At the base of the bottle, the compression and expansion waves interact to cause 'mother' bubbles to break up. This is a rapid process resulting in the formation of smaller 'daughter' bubbles, which expand rapidly to create foam that starts to overflow [302].

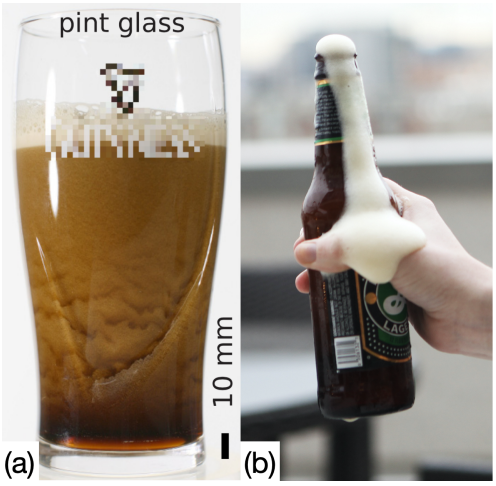

FIG. 12. Examples of dynamic and unstable foaming phenomena: **(a)** Unique foamy textures in stout with nitrogen bubbles. From Watamura *et al.* [301]. **(b)** Foam overflow 'volcano' due to tapping on a beer bottle. Public domain image.

G. Ouzo effect

Ouzo, raki, arak, pastis, and sambuca are popular aperitifs in Southern Europe. They are known for their anise aroma and the remarkable change in turbidity: Clear when pure, they turn milky-white when clear water or ice is added, which has been termed the 'ouzo effect' [303]. The key to this puzzle lies in the chemical composition of the drink, being mostly a mixture of water, alcohol, and essential oils, of which anethole is a prominent part. Anethole (also known as anise camphor) is highly soluble in ethanol but not in water [304], thus an undiluted spirit has a completely clear appearance. Upon the addition of small amounts of water, however, the oils start separating and create an emulsion of fine droplets which act as light scattering centres, resulting in the final cloudiness.

The process is also called louching or the louche effect, and can be regarded as spontaneous emulsification. Such emulsions are highly stable and require little mixing [305]. In these multi-component mixtures, the thermodynamic stability of the emulsion comes from the trapping

between the binodal and spinodal curves in the phase diagram. The ouzo effect has been widely studied to elucidate its mechanisms [303]. However, the microscopic dynamics are still under active investigation. Small-angle neutron scattering studies in Pastis [306] and Limoncello [307] measured the size of the demixing oil droplets to be of the order of a micron, a bit larger than the wavelengths of visible light, giving rise to Mie scattering [§II D]. Sitnikova *et al.* [305] established the mechanism for oil droplets growth to be Ostwald ripening without coalescence and observed the ripening rate to be lower at higher ethanol concentration, with stable droplets reaching an average diameter of 3 microns. Lu *et al.* [308] tried to disentangle the effects of concentration gradients from the extrinsic mixing dynamics by following the nanodroplet formation in a confined planar geometry and observed universal branch structures of the nucleating droplets under the external diffusive field, analogous to the ramification of stream networks in large scale [309, 310], and the enhanced local mobility of colloids driven by the emerging concentration gradient. The ouzo effect can be triggered not only by the addition of water but also by the evaporation of ethanol, e.g. in sessile ouzo droplets [311–313], leading to an astoundingly rich drying dynamics involving multiple phase transitions.

The remarkable stability of the spontaneously formed emulsion gives hope for potential generation of surfactant-free microemulsions without resorting to mechanical stabilisation, for example high-shear stabilisation that is often used in fat-filled milk formulations [314]. Thus, the ouzo effect has been used for the creation of a variety of pseudolatexes, silicone emulsions, and biodegradable polymeric capsules of nanometric size [315]. Nanoprecipitation can also be used for drug delivery and the design of nanocarriers [316]. Particles created using the ouzo effect are kinetically stabilised, and provide an alternative to thermodynamically stabilised micelles formed using surfactants [317].

IV. SOUP STARTER: COMPLEX FLUIDS

Most foods are neither purely liquid nor solid, but rather something in between: they are often viscoelastic or complex materials. This strongly affects how we perceive taste since their flow behaviour is directly linked with mouthfeel, the oral processing and texture of foods [318, 319]. The rheology of complex fluids are also of extreme importance in the food industry, in terms of transport phenomena, production processes, storage, and processing techniques that need to be adopted to the properties of materials at hand [19, 320–322]. Complex fluids are a bit of a soup sandwich, so we begin this section with an introduction to food rheology. Then we get into the thick of it, reviewing the science of food suspensions, emulsions, and the mixing of sauces. Shall we board the gravy train?

A. Food rheology

Viscosity quantifies internal friction in a fluid, and it is often the interplay between the viscosity, elasticity and inertia of a moving fluid that gives rise to complex phenomena seen everywhere. In essence, viscosity relates shear stresses to gradients in flow velocity. That is, for a simple incompressible fluid moving steadily along the x-axis with a velocity field $u_x(y)$ varying along y, the shear stress component σ_{xy} is given by Newton's law of viscosity,

$$\sigma_{xy} = \mu(\partial u_x/\partial y), \tag{28}$$

where the constant of proportionality μ is the *dynamic viscosity* and the second term is the flow gradient. In a general coordinate system, the rate-of-strain tensor can be written as $\mathbf{E} = \left(\boldsymbol{\nabla u} + (\boldsymbol{\nabla u})^T\right)/2$ and the scalar shear rate as $\dot{\gamma} = \sqrt{2\mathbf{E} : \mathbf{E}}$.

The stres field $\boldsymbol{\sigma}$ arising in the fluid gives rise to motion, and the momentum balance is expressed by the Cauchy equation

$$\rho \frac{D\boldsymbol{u}}{Dt} = \boldsymbol{\nabla} \cdot \boldsymbol{\sigma} + \boldsymbol{f}, \tag{29}$$

which is valid for all fluids. However, the stress field in Eq. (29) above can on the rate-of-strain in various ways, depending on the fluid microstructure.

For an isotropic linear viscous fluid, the total stress combines isotropic pressure with shear stresses as in Eq. (28), via

$$\boldsymbol{\sigma} = -p\mathbf{I} + 2\mu\mathbf{E}, \tag{30}$$

where $\mathbf{I}$ is the identity matrix. Inserting this expression into the Cauchy momentum equation (29), we recover the incompressible Navier-Stokes equations [Eq. (2a)]. Specifying the relationship of between the stress $\boldsymbol{\sigma}$ and the flow $\boldsymbol{u}$ (or the tensorial quantities based on this field) defines the particular fluid model. A *Newtonian fluid* is defined by the linear relation (30) between the stress and the shear, when viscosity is independent of the shear rate. Most simple liquids are indeed Newtonian, including water, alcohol, and most thin oils. However, many fluids deviate from this linear relation because of their complex internal structure. Ubiquitous examples are emulsions, suspensions or polymer solutions [323]. Such *non-Newtonian fluids* can feature different types of behaviours, including:

- *Shear-thinning* liquids, whose viscosity decreases with increasing rate of strain (e.g. yoghurt, mustard, ketchup, clotted cream, but also paint);
- *Shear-thickening* liquids, whose viscosity increases with strain rate (e.g. cornstarch in water and solubilised starches in general [324]); see Fig. 13(a).
- *Bingham plastics* or yield-stress materials, which behave as solids at low stresses but start flowing

at high stresses (e.g. toothpaste or mayonnaise); in the latter, rigdes and peaks on the surface show the existence of a critical yield stress above which it flows [325–327]; see Fig. 13c.

- *Rheopectic* fluids, that gradually become more viscous with duration of stress (e.g. whipped cream) or heat (e.g. pancake batter in a frying pan);
- *Thixotropic* fluids [328], that become less viscous over time when agitated (e.g. yoghurt, peanut butter, ketchup, or margarine); this quality is desirable in spreads, which should stay solid but be easy to spread on toast; see Fig. 13d.

These fluids obey the same Cauchy momentum equation, with a different stress tensor $\boldsymbol{\sigma}$ specified by a *constitutive equation* that captures the relevant material properties and relates the stress and stress rate to strain and strain rate. The topic is vast and discussed widely in classic textbooks, also in the context of applicability and structure of different models [329, 330]. Typical rheological experiments, also widely used in food science, involve periodic variations of stress or strain, with a harmonic excitation at a given frequency ω, in which the response of the material is recorded. The latter is subdivided into an in-phase and out-of-phase components. The amplitude of the in-phase component is the shear storage modulus $G'(\omega)$, which provides information about the energy stored in a deformation cycle in the material, which corresponds to its elastic energy. The out-of-phase amplitude $G''(\omega)$ is termed the shear loss modulus and is proportional to the energy dissipated as heat over a period of oscillations, quantifying the viscous nature of the material [331].

Below we briefly discuss the two main classes of models, linear and non-linear constitutive relation, together with the most popular examples of particular materials or applications.

1. *Linear viscoelasticity*

When deformations are small, slow, or slowly varying, it suffices to use the models assuming a linear constitutive law. Within this approximation, stress and strain are related by a Volterra integral equation. It is purely phenomenological and aims only to describe the response of a material. To probe this response, apart from oscillatory rheometry measurements, two typical tests can be run. The creep test consists of measuring a time-dependent strain upon the application of a steady stress. The material starts flowing with a certain delay, which is grasped by this experiment. In linear approximation, doubling the stress doubles the strain. This is observed widely e.g. in processed fruit tissues [333], or in dynamic rheology measurements of honey [334]. A complementary experiment, the stress relaxation test, measures the time-dependent stress resulting from a steady strain. In

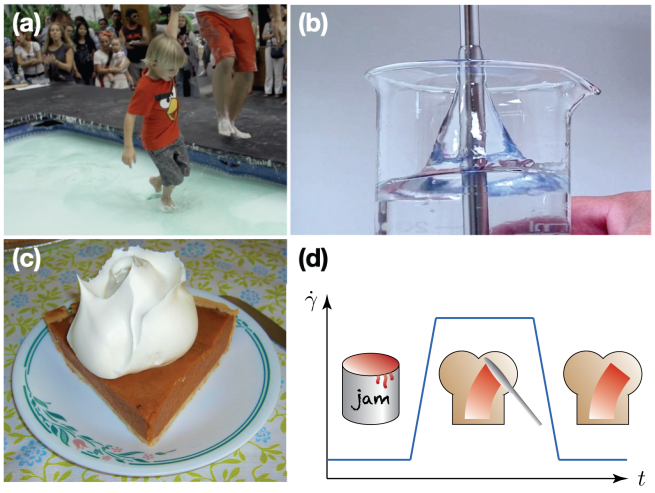

FIG. 13. Examples of complex rheological behaviour of fluids: **(a)** People walking over a swimming pool full of oobleck, a mixture of cornstarch and water. Image courtesy of Ion Furjanic, director of We are KIX [332]. **(b)** The Weissenberg rod climbing effect seen on a 2% solution of high molecular weight polyacrylamide. From Wikimedia Commons, licensed under CC BY 4.0. **(c)** Whipped cream is an example of a Bingham plastic which remains solid in the absence of stresses but can be squeezed out onto a slice of pie like a fluid. From Wikimedia Commons, licensed under CC BY 4.0. **(d)** Thixotropic fluids become thinner with time when they are sheared, and solidify again at rest. Classic examples are paint or sandwich spread.

the range of small deformations, many food products can be aptly described by linear models. Rheology measurements of frankfurters of various composition show a good linear response for strains up to about 3.8% [335]. Stress relaxation and creep-recovery tests on oat grains also show linear behaviour for a range of temperatures and moisture content [336].

Many non-Newtonian fluids are called viscoelastic because they exhibit both viscous (creep) and elastic (relaxation) effects. Linear viscoelastic response can thus be described by ordinary differential equations, which can be rationalised by thinking about their mechanical analogues, called 'spring-dashpot' models. In such models, the fluid response is portrayed by a collection of connected Hookean (elastic) springs and (viscous) dashpots, producing a combined effect together. The springs relate stress σ with strain ϵ linearly, via

$$\sigma = \mathcal{E}\epsilon, \tag{31}$$

with the spring constant $\mathcal{E}$ being an analogue of Young's modulus. The springs models an instantaneous deformation of the material and strain energy stored therein. The creep response is modelled by a Newtonian dashpot, in which stress induces strain rate,

$$\sigma = \eta \frac{\mathrm{d}\epsilon}{\mathrm{d}t}, \tag{32}$$

where η is the viscosity. The ratio of viscosity to stiffness, $\tau = \eta/\mathcal{E}$, will thus measure the response (or relaxation) time of a viscoelastic material. This time can be compared to a typical observation (or process) time, τ_0, to yield the dimensionless Deborah number,

$$\mathrm{De} \equiv \frac{\text{time scale of relaxation}}{\text{time scale of process}} = \frac{\tau}{\tau_0}, \tag{33}$$

which indicates whether at a given observation times the material would behave in a fluid-like manner (at low De) or whether it would exhibit non-Newtonian properties, with an increasingly manifested elasticity at high De. For example, viscoelastic ice cream [337] [see §VI K] should preferably be consumed at high De for practical reasons.

Different combinations of springs and dashpots can be proposed to describe the linear response of a viscoelastic material. The simplest models are the *Maxwell model*, represented by a spring and a dashpot connected in series, and the *Voigt* or *Kelvin model*, in which a spring and a dashpot are connected in parallel. By considering the composite dynamic behaviour, we find the constitutive relation for a Maxwell material as

$$\sigma + \frac{\eta}{\mathcal{E}}\dot{\sigma} = \eta\dot{\epsilon}, \tag{34}$$

while for a Kelvin-Voigt material we obtain

$$\sigma = \mathcal{E}\epsilon + \eta\dot{\epsilon}. \tag{35}$$

These simple models are rather limited. The Maxwell model aptly describes stress relaxation, being the response of a material to a constant strain, for example in moth bean flour dough [338]. However, for constant-stress conditions it predicts a linear increase of strain, which is not seen e.g. in polymers where the strain rate decreases in time; thus it is not a good model for creep processes [330]. The Kelvin-Voigt model, on the other hand, is highly successful at describing creep, e.g. in potato tissues [339], but it is much less accurate in terms of stress relaxation.

The simplest model that accurately grasps both creep and relaxation is the *standard linear solid* (SLS) model, or Zener model, which involves two springs and a dashpot, connected both in series and in parallel. Again, the constitutive equation takes the general form

$$\sigma + \eta f_1(\mathcal{E}_1, \mathcal{E}_2)\dot{\sigma} = f_2(\mathcal{E}_1, \mathcal{E}_2)\epsilon + \eta f_3(\mathcal{E}_1, \mathcal{E}_2)\dot{\epsilon}, \tag{36}$$

with the coefficients dependent on the exact arrangement of the elements. A fluid version of the SLS model is the Jeffreys model. Such models predict the general shape of the strain curve, both at long times and at instantaneous loads but still it is a simplified representation with no direct strategy to model actual materials.

Modifications of the above mentioned models are also available to better account for various phenomena seen in actual fluids. The Burgers model incorporates viscous flow into the SLS model. The Generalised Maxwell Model (GMM) (also called the Wiechert model) involves combinations of Maxwell elements which account for a distribution of relaxation times, present e.g. in materials composed of molecular segments of different lengths. GMM has been successfully used to describe the stress relaxation behaviour for a variety of semi-solid food products, such as agar gel, meat, mozzarella cheese, ripened cheese, and white pan bread [340]. Systems with finer microstructure, such as protein-stabilised oil-in-water emulsions, can also exhibit linear viscoelastic behaviour [341].

2. *Non-linear viscoelasticity*

Some biological fluids can be inherently non-Newtonian. Rheology measurements of yoghurts show that overlapping polymer molecules cause viscoelastic behaviour even at dilute concentrations ($\phi < 10^{-2}$) and a sharp increase in viscosity with concentration [342]. Yoghurts are shear-thinning in addition to being viscoelastic. Shear thinning or thickening cannot be explained using linear constitutive equations, thus more complex models are needed to quantify their behaviour. Non-Newtonian properties manifest themselves particularly in the material properties, which become dynamic quantites, and in particular depend on the shear rate $\dot{\gamma}$. The non-Newtonian (or shear-dependent) viscosity is defined as in eq. (28) but now with $\mu = \mu(\dot{\gamma})$. In the same geometry as before, we also define the *normal stress coefficients* by

$$\sigma_{xx} - \sigma_{yy} = -\Psi_1(\dot{\gamma})\dot{\gamma}^2, \tag{37}$$

$$\sigma_{yy} - \sigma_{zz} = -\Psi_2(\dot{\gamma})\dot{\gamma}^2. \tag{38}$$

Together, μ, Ψ_1, and Ψ_2 are referred to as viscometric functions.

The Weissenberg number is another relevant dimensionless function which quantifies the ratio of elastic to viscous forces. In a simple shear flow, the latter are proportional to the shear stress σ_{xy}, while the former are represented the first normal stress Ψ_1. For a fluid with characteristic relaxation time λ under shear, we write this ratio as

$$\mathrm{Wi} \equiv \frac{\text{elastic forces}}{\text{viscous forces}} = \frac{\sigma_{xx} - \sigma_{yy}}{\sigma_{xy}} = \lambda\dot{\gamma}. \tag{39}$$

Although seemingly akin to De, the Weissenberg number has a different interpretation, because it captures the degree of anisotropy introduced by the deformation, rather than the effect of time-dependent forcing [343]. The two numbers span a phase space interpolating between purely viscous and purely elastic deformations, with both linear (typically moderate De and low Wi) and nonlinear viscoelasticity (at higher Wi) in between.

A first step into the nonlinear territory is the *generalised Newtonian fluid* model, in which the stress depends only on the instantaneous flow, but the viscosity in Eq. (30) is replaced by a shear-dependent function $\mu(\dot{\gamma})$. Its form is usually derived empirically from the available

data. Some common approximations include a *power law fluid* with $\mu(\dot\gamma) = k(\dot\gamma)^{n-1}$, where k and n are fitting parameters. If $n > 1$ the fluid is shear-thickening (dilatant), and if $n < 1$ it is shear thinning. Most fruit and vegetable purees belong to the latter category [344]. Another set of examples are Carreau-Yasuda-Cross models [345–347], which interpolate between the different zero and infinite shear rate viscosities (μ_0 and μ_∞, respectively) by $\mu(\dot\gamma) = \mu_\infty + (\mu_0 - \mu_\infty)[1 + (\lambda\dot\gamma)^a]^{(n-1)/a}$, with fitting parameters λ, a, n. Such models successfully describe e.g. the flow of skim milk concentrate [348] or semisolid *natillas* (Spanish dairy desserts) [349]. An important category are yield fluids, which flow only above some critical stress $\sigma > \sigma_c$. Within those, Bingham models satisfy $\mu(\dot\gamma) = \mu_0 + \sigma_c/\dot\gamma$ [350]. This type of behaviour is seen commonly e.g. in tomato pastes [351]. The Herschel Bulkley models use $\mu(\dot\gamma) = k\dot\sigma^{n-1} + \sigma_c/\dot\gamma$ [352], and have proved useful to aptly describe the rheology of stirred yoghurts [353].

Before we present other popular nonlinear constitutive relations, we introduce a useful mathematical construct appearing therein: the upper-convected (or Oldroyd) time derivative. It describes the rate of change of a tensorial property of a fluid parcel, written in the coordinate system rotating and stretching with the fluid. Typically denoted by a triangle above a tensorial quantity $\mathbf{A}$, it is defined by

$$\overset{\triangledown}{\mathbf{A}} = \frac{D\mathbf{A}}{Dt} - (\nabla\mathbf{v})^T \cdot \mathbf{A} - \mathbf{A} \cdot (\nabla\mathbf{v}), \tag{40}$$

where D/Dt is the material derivative.

The simplest nonlinear model that involves the flow history is the *second-order fluid*. In a Newtonian fluid, the stress tensor (30) is linear in the rate-of-strain tensor $\mathbf{E}$, which in turn is linear in the (typically small) flow velocity gradients. Here, we look at the stress tensor as at an expansion in $\mathbf{E}$ and include also second-order terms, which results in the following stress-strain relationship

$$\boldsymbol{\sigma} = -p\mathbf{I} + 2\mu\mathbf{E} - \Psi_1\overset{\triangledown}{\mathbf{E}} + 4\Psi_2\mathbf{E}\cdot\mathbf{E}, \tag{41}$$

where two new coefficients appear, in addition to viscosity. The first and second normal stress coefficients [331], are here assumed to be constant material properties of the fluid. They describe the anisotropic normal stress response in a viscoelastic fluid. The nonlinearity enters via the last term in the stress tensor. The second-order fluid model accurately describes the flow at high strains and at moderate Deborah numbers, in the region between Newtonian fluids and more complicated nonlinear viscoelastic models.

Another idea to account for nonlinearities consists of modifying the Maxwell model to include nonlinear stress response. The upper-convected Maxwell (UCM) model modifies the stress response while keeping the linear dependence on rate-of-strain via

$$\boldsymbol{\sigma} + \lambda\overset{\triangledown}{\boldsymbol{\sigma}} = 2\mu\mathbf{E}, \tag{42}$$

thus introducing the relaxation time λ. The UCM model predicts some properties of non-Newtonian fluids (such as non-zero first normal stress coefficient) while missing others (no second normal stress coefficient or constant shear viscosity), which is typically a limiting factor in its applicability.

A widely used extension of the UCM model is the *Oldroyd-B model* [354]. The relevant equation of state involves nonlinearities both in the stress and strain parts, and takes the form

$$\boldsymbol{\sigma} + \lambda_1\overset{\triangledown}{\boldsymbol{\sigma}} = 2\mu\left(\mathbf{E} + \lambda_2\overset{\triangledown}{\mathbf{E}}\right), \tag{43}$$

where now λ_1 is interpreted as the relaxation time, while λ_2 governs the retardation time scale. Microscopically, the Oldroyd-B model can be thought of as a fluid filled with elastic dumbbells strained by the flow. This model is popular for its good approximation of viscoelastic behaviour in shear flow. Other constitutive equations have also been proposed to fit the experimental data but the choice of a particular model depends on the character of the problem at hand.

The shear-dependent properties of kitchen matter can be seen e.g. in the context of mixing and whisking. The Weissenberg effect [355] is an illustrative proxy for viscoelasticity. It is seen when a spinning rod is inserted into an elastic fluid, as in Fig. 13(b). Instead of the meniscus curving inwards, the solution is attracted towards the rod and rises up its surface. This is due to normal stresses in the fluid acting as hoop stresses and pushing the fluid towards the rod [356]. When whisking egg whites with a mixer [357], we see the solution rise up close to the mixer shaft, rather than move outwards in a parabolic shape characteristic for Newtonian liquids, described in §II J. The same effect is observed in sweetened condensed milk [358], gelatin [359] or dough [298].

Importantly, the viscosity may also change due to a changing chemical composition under external stimuli such as heat. This complex landscape is particularly important in the kitchen environment, where we often work with thickening agents such as roux or Xanthan gum, gently heat up egg yolks to make Hollandaise sauce, or milk for the béchamel. Composite food products typically respond in a non-Newtonian manner to deformation. Dynamic quantities characterising the rheology of food products are of paramount importance for the process of food processing, in which appropriate length and time scales ought to be chosen for the expected result. Thus there are numerous papers quantifying the rheological response; extending yield-stress of Nutella [360], rheology of chewing gum [361], and rheometry of mayonnaise [362] or salad dressing [363] are but a few examples of a wide current aiming to describe transient effects in the flow of food products [364]. The rheological properties of food are also important for medical conditions including dysphagia [365], where fluid dynamics can help with predicting the ease of swallowing [366].

For a more detailed description of food rheology, we

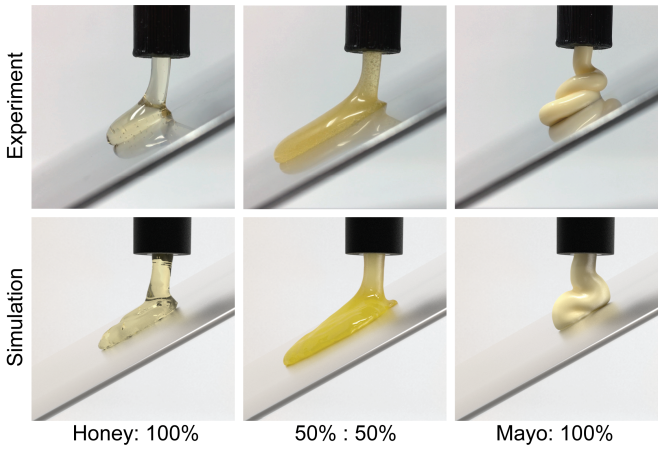

FIG. 14. Blending sauces. Left: pure honey. Middle: 50:50 mixture. Right: pure mayonnaise. Top row: Rheometry experiments of the sauces mixtures flowing down an inclined plane. While honey and mayo move slowly, the mixture runs down fast. Bottom row: The same dynamics simulated with a shear-thinning mixing model and displayed using computer-generated imagery (CGI). Image courtesy of Yonghao Yue.

recommend reading the following books and reviews [19, 320–322], as well as these works on soft matter [20–22, 367–369], and references therein.

B. Mixing up a sauce

When making a sauce, rather counter-intuitive effects can emerge: the combination of two thin liquids can suddenly lead to a thick mixture, or vice versa. Indeed, as discussed in §III C, we saw that an ethanol-water blend has a higher viscosity than both pure liquids. In general, the viscosity μ_{12} of most binary mixtures is not a linear function of their relative composition [370]. Instead, a first approximation is given by the Arrhenius equation,

$$\ln \mu_{12} = x_1 \ln \mu_1 + x_2 \ln \mu_2 \tag{44}$$

where x_i and μ_i are the mole fraction and viscosity of the ith component, respectively. This expression holds for an ideal binary mixture, where the volume of the components is conserved, i.e. the excess volume of mixing is zero. Building on this work, a more accurate description was given Grunberg and Nissan [371] and Oswal and Desai [372], which reads

$$\begin{aligned}\ln \mu_{12} = {} & x_1 \ln \mu_1 + x_2 \ln \mu_2 + \epsilon x_1 x_2 \\ & + K_1 x_1 x_2 (x_1 - x_2) + K_2 x_1 x_2 (x_1 - x_2)^2 ,\end{aligned} \tag{45}$$

where ϵ, K_1, K_2 are empirical parameters that account for molecular interactions. While there is no universal theory that accurately predicts the viscosity of a liquid blend, more extended models have been derived that are important for many industrial applications including food science [373, 374].

In terms of mixing sauces, most ingredients each have different elasto-viscoplastic properties. To describe the material properties of food mixtures, Nagasawa *et al.* [375] considered a wide range of theoretical models and derived a viscosity blending model for shear thinning fluids. Using rheometry experiments, they also tested these models for various sauces including honey, mustard, mayonnaise, ketchup, hot chilli sauce, condensed milk, chocolate syrup, sweet bean sauce, oyster sauce, Japanese pork cutlet sauce, and BBQ sauce. When mixed together, unexpected behaviours can arise: The top row of Fig. 14 shows experimentally that pure honey flows down an inclined slope slowly because of its high viscosity (left) and pure mayonnaise remains stagnant because of its yield stress (right) [327]. However, a 50:50 mixture runs down the slope quickly, with a much lower viscosity μ_{12} than its constituents (middle). In the bottom row, the authors reproduced these surprising dynamics using numerical simulations combined with high-end computer-generated imagery (CGI) techniques.

C. Suspensions

Drinks and foods often take the form of a particle suspension [376], with examples ranging from unfiltered coffee and wine to Turkish pepper paste and Kimchi. The texture and mouth-feel of suspensions depend on their rheology [see §IV A], which is sensitive to the particle size, microstructure and concentration. Dilute suspensions such as coffee and juices, are typically Newtonian fluids, while concentrated suspensions such as pastes and purees typically display non-Newtonian behavior due to both long-ranged hydrodynamic interactions between the particles [see §VI B] and various short-ranged interactions including friction [377, 378]. Indeed, these rheological properties have been studied to optimise food paste 3D printing [379].

The influence of internal structure on macroscopic properties of suspensions has been actively investigated since the birth of statistical physics. Einstein [380] established that the viscosity of a dilute suspension increases by adding solute according to the Einstein viscosity,

$$\mu = \mu_0 \left(1 + \frac{5}{2}\phi\right), \tag{46}$$

where μ_0 is the (dynamic) viscosity of the solvent, and ϕ the volumetric concentration of particles. This relationship which was later developed in the context of other transport coefficients, including the diffusion and sedimentation coefficients of suspended particles, and to account for higher volume fractions and different interactions between the particles [381]. This is reviewed in the context of food suspensions by Genovese *et al.* [382] and Moelants *et al.* [376].

When we grind coffee beans or otherwise create a suspension, the particles are not all of the same size, but instead they follow a size distribution. The width of this

size distribution is called the dispersity, and it can be tuned to control the rheology of a suspension. Notably, the Farris effect [383] explains how the viscosity of a suspension decreases when the dispersity increases; that is, a broader distribution of particle sizes yields a lower viscosity as compared to a narrow distribution of particle sizes. In food science, the Farris effect has been exploited to adjust the rheological properties of edible microgel suspensions such as cheese [384], and it has been used to minimise the apparent viscosity of cooked cassava pastes [385]. Conversely, by narrowing the particle dispersity in coffee and unfiltered wine, it should be possible to enhance the mouthfeel by the opposite mechanism, but we are not aware of any reports on this topic. The Kaye effect is a phenomenon that occurs when a complex fluid is poured onto a flat surface, where a jet suddenly spouts upwards [386]. Many non-Newtonian liquids feature this effect, including shampoo, and recent experiments have explained it by using high-speed microscopy to show that the jet slips on a thin air layer [387–389].

D. Emulsions

An emulsion consists of two (or more) immiscible liquids [390], where droplets of one phase (called the discontinuous or internal phase) are dispersed inside the other fluid (referred to as the continuous or external phase). The most typical pair is water and oil, where the two main classes are water-in-oil (W/O) systems such as margarine, and oil-in-water (O/W) systems such as milk [321].

Indeed, emulsions are ubiquitous in gastronomy and food science [391, 392], with everyday products such as cream, yoghurt, mayonnaise, salad dressing, sauces, spreads, ice cream, dips and desserts [390]. In these examples, precise control over composition, functionality and stability are key requirements for a successful dish, where manipulation techniques, as well as timing, have to be adjusted to achieve the desired effect, thus forming a vast part of modern food science. The physicochemical stability of many emulsions is also affected by their natural components, which often are low-processed or raw, thus heterogeneous and varying in composition.

The process of converting two separate fluids into an emulsion is called homogenization [393] and is industrially realized with high-energy mechanical methods, such as blenders or ultrasonics [394], where strong shear forces break up the dispersed phase into droplets. In the kitchen, we make use of the same capillary breakup mechanism when we vividly shake or stir the oil and water phase, but, as anyone who have tried to make a Hollandaise sauce would painfully know, such mixtures are by design thermodynamically unstable and prone to phase separation, sometimes called a 'broken sauce'.

In the food industry, phase separation is a major hurdle as it can severely degrade the food product and shorten the shelf life, but fortunately stabilizers such as emulsifiers, texture modifiers, ripening inhibitors and weighting agents can be added to keep the system in a metastable state (by creating a free energy barrier), efficiently extending the lifetime to hours, days, months, or even years [395]. Pickering emulsions [396, 397] are stabilised with solid nanoparticles that sit at the drop interface, with promising applications in drug delivery and structured nanomaterials [398, 399], and adsorbed protein molecules stabilise emulsions by lowering the interfacial tension and by forming viscoelastic networks that act as barriers against coalescence [400, 401]. The stabilizing effect of proteins can be readily observed by adding a small amount of mustard to vinaigrette dressing. In addition to be stabilizing, these surface proteins control the complex rheology of emulsions, which is responsible for the appearance and our sensory perception of food products [322]. Salad dressing is a widely studied kitchen emulsion, which has been examined in the context of its complex rheological response [402] and processing [403], stability, and linear viscoelasticity [404].

Due to the enormous surface area of emulsion drops, the overall rheology and stability is controlled by interfacial properties, and in particular, by the surface coverage and structure of adsorbed protein layers [322]. Animal proteins such as whey and casein readily form viscoelastic networks with high surface coverage, leading to excellent emulsion stability, while plant-based proteins such as those from cereals and pulses are less efficient stabilizers, and this is mainly due to their poor solubility in the aqueous phase [405]. While heating can be used to increase the stabilizing abilities by denaturing the proteins [406], such treatment can degrade the taste as well as the texture and the nutritional value of plant based foods. As such, the ability to control the interfacial properties of plant-based emulsions without denaturing the protein is an important goal, and an exciting new direction in food science for vegetarians and vegans [407].

Bulk-based methods such as Dynamic light scattering (DLS) have traditionally been used to characterise food emulsions [395], but they lack optical resolution needed to resolve details of adsorbed particles, proteins and surfactants near individual emulsion drops [408]. Droplet-based microfluidics is a viable alternative to such methods, and is characterized by excellent optical resolution, monodisperse droplet distributions [109], and controllable surface chemistry [408]. In recent years, microfluidics has contributed to new fundamental understanding of surfactant and protein transport in microfluidic food emulsions, with a handful of important publications [27]. Notably, Brosseau *et al.* [409] extracted the adsoption kinetics via so-called microfluidic dynamic interfacial tensiometry (μDIT) by measuring the interfacial deformation as a droplet is passed through a series of expansions. Another approach was adopted by Muijlwijk *et al.* [410], who measured the dynamic interfacial tension (due to surfactant adsoption) during droplet production in a T-junction. Using the same method, they also showed that convection controls the transport of surfac-

tants [411] and proteins [412] during droplet production, resulting in adsorption-limited kinetics, and for proteins, they found that the first interfacial layers form within seconds [413]. Finally, they mixed plant-based protein with animal protein and studied their competitive adsorption to suspended emulsion drops, with potential implications in future hybrid protein products [414].

E. Cheerios effect: capillary floating

Before the mixture about to be cooked is stirred well, we frequently add ingredients by sprinkling or tossing them on a liquid surface. Sometimes they are deliberately added to form the top layer, as some of us do with corn flakes. Interestingly, small objects that are more dense than water may still float at the air-water interface because of surface tension [415]. Moreover, floating objects tend to aggregate at the surface, brought together by capillary forces induced by the presence of a curved meniscus around floating objects. Aptly named the 'cheerios effect' [416], this is seen not only with corn flakes, but also e.g. bread crumbles [417], foams, and generally object that are large enough to create the menisci of considerable size. The mechanism of lateral capillary interaction due to interfacial deformation admits a universal theoretical description for particle sizes ranging from 10^{-9} to 10^{-2} cm [418]. Initially, the interaction of widely spaced particles may be regarded as a two-body problem [419] but eventually multiparticle rafts are formed [420]. The dynamics of these aggregates is more complex, since they may undergo internal redistribution and destabilisation [421]. An interesting example is an active assembly of dozens of fire ants on a water surface [422]. The presence of surface tension allows to sustain deformed surfaces which can support a load of an insect walking on water [244, 423, 424], or a biomimetic water-walking device [425]. Similar behaviour, termed the inverted cheerios effect, is seen when water droplets sit on a soft, deformable substrate, and the induced deformation drives their assembly [426, 427].

By a combination of capillary forces and externally controlled fields, e.g. electromagnetic field, both static and dynamic assembly can be achieved in capillary disks [428, 429]. Capillary forces between spherical particles floating at a liquid-liquid interface have also been quantified to show a qualitatively similar behaviour [430]. Same guiding principles are used in micro-scale for colloidal self-assembly, driven not by gravity but by an anisotropically curved interface [431]. Finally, in active microrheology [432–436], an external force field (usually magnetic or optical) is used to distort surface active or bulk probes in order to extract viscoelastic responses of complex materials, with direct applications in food science [437].

A separate class of interfacial interaction involves the dynamic problem of stone skipping, known in Britain as 'ducks and drakes', where the interfacial properties determine the optimal angle of attack for the most successful rebound and therefore maximal range [438–440]. Moreover, elastic 'stones' have been shown to demonstrate superior skipping ability by assuming hydrodynamically optimal shapes during the collision [441].

V. HOT MAIN COURSE: THERMAL EFFECTS

> Heat not a furnace for your foe so hot, that it do singe yourself. – William Shakespeare

The work 'cooking' refers to the preparation of food in general, but specifically the operations involving temperature and heat such as boiling, frying, baking and poaching, to transform food products into a final dish. Thus, many kitchen flows involve thermal effects which drive them or alter the behaviour of substances involved. Below we highlight a number of such phenomena.

A. Feel the heat: energy transfer

Heat is transported in fluids in a way similar to momentum [§II B]. Fluid parcels are advected with the flow, and additionally exchange heat by conduction. Local variations in temperature can additionally induce density gradients, which can drive macroscale convective motion. Moreover, dissipation of momentum by viscosity acts as a local source of heat, but in most practical situations its contribution is negligible.

The relevant quantity characterising the thermal properties of the fluid is the scalar temperature field, $T(\boldsymbol{r})$. The spread of temperature is described by the heat equation, which for a fluid of density ρ and heat capacity at constant pressure c_p can be written as

$$\rho c_p \frac{DT}{Dt} = k\nabla^2 T + h + Q, \tag{47}$$

where k is the thermal conductivity, governing the diffusive spread of temperature by thermal conduction, h is a source term accounting for local heating (e.g. by chemical or nuclear reactions), and Q is the viscous dissipation term, which for an incompressible fluid takes the form $Q = 2\mu\mathbf{E} : \mathbf{E}$, with $\mathbf{E}$ being the symmetric velocity gradient tensor [see Eq. (30)]. The dissipation, which scales as $\mu U_0/(L_0\rho c_p)$, is typically small compared to other terms, and thus is often neglected. In the absence of local heat sources, the heat equation becomes simply a Fourier's diffusion equation, with the thermal diffusivity $D_T = k/(\rho c_p)$. The dominant (heat) transport mechanism is determined by the (thermal) Péclet number,

$$\mathrm{Pe}_{(T)} \equiv \frac{\text{Diffusion time}}{\text{Convection time}} = \frac{L_0 U_0}{D_{(T)}}, \tag{48}$$

which besides thermal diffusion can equally be used to characterise molecular diffusive transport.

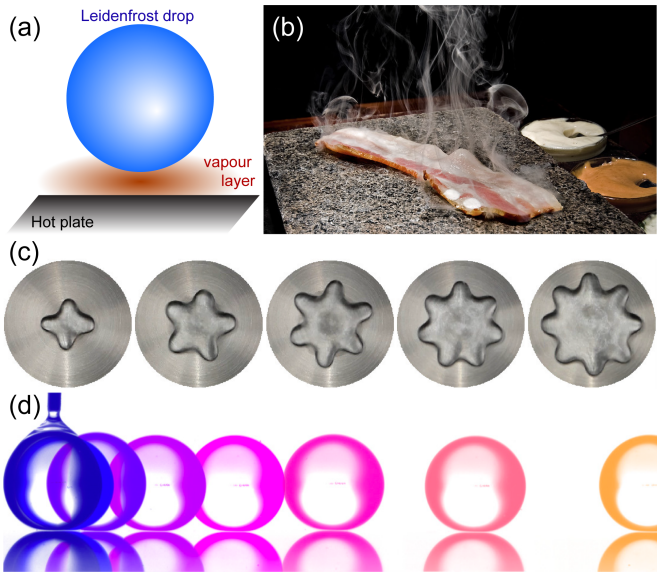

FIG. 15. Leidenfrost effect. **(a)** Diagram of a droplet levitating on a cushion of evaporated vapour above a heated surface. **(b)** The Leidenfrost effect prevents meat from sticking to a hot plate. Artwork entitled 'Bacon Prelude' by Pedro Moura Pinheiro, licensed under CC BY-NC-SA 2.0. **(c)** Star-shaped oscillations of Leidenfrost drops [444] that make characteristic sounds. From Singla and Rivera [445]. **(d)** Time-lapse image of a self-propelled Leidenfrost drop on a reflective wafer heated at 300 °C. From Bouillant *et al.* [446].

The concept of diffusion of heat suffices to explain several kitchen processes. Baking a cake requires the heat to reach the inner parts of the dough but changing either the dimensions of the cake or the amount of batter used alters the baking time in a way that can indeed be predicted from the diffusion equation [442]. Similarly, the problem of perfectly boiling an egg can be quantified in terms of the energy equation [443] to aid many breakfast table discussions.

B. Levitating drops: Leidenfrost effect

When grilling steaks, one way to assess whether the frying pan is hot enough is to sprinkle a handful of water droplets onto it. When the surface temperature slightly exceeds the water boiling point, the droplets become vigorously evaporating, producing a sizzling sound. However, if the pan is left on full heat for a while and becomes considerably hotter, small droplets change their behaviour completely and start levitating above the hot surface without boiling [Fig. 15a,b]. This levitation can help with preventing the meat from sticking [447].

This phenomenon was first known to be observed by a Dutch scientist H. Boerhaave in 1732, and later described in detail by a German doctor Johan Gottlob Leidenfrost in 1756. He provided a record of water poured onto a heated spoon that 'does not adhere to the spoon, as water is accustomed to do, when touching colder iron' [448]. The Leidenfrost effect, as it was later termed, has been studied extensively in the scientific context [449–451], and even became a plot device in Jules Verne's novel *Michel Strogoff* in 1876.

The explanation of this effect boils down to the analysis of heat transfer rate between a hot plate and a droplet. For intermediate excess temperatures above the boiling temperature (between 1°C and ca. 100°C) the droplets undergo either nucleate boiling, with vapour bubbles forming inside, or transition boiling, when they sizzle explosively upon impact on the plate. However, above the Leidenfrost temperature, which for water on a metal plate is approximately 150-180°C, the heat transfer dynamics change when a thin vapour layer is created between the droplet and the plate. This thin cushion both insulates the droplet and prevents it from touching the substrate which would cause nucleation boiling inside the droplet [Fig. 15a]. Due to the competition between evaporation and film draining, the typical thickness of the insulating layer is about 100 µm. Because of this effect, the lifetime of droplets on a substrate can increase by an order of magnitude [452]. Further increase in the substrate temperature naturally decreases the lifetime but the decrease is slow. The minimum temperature required for the Leidenfrost effect to occur on smooth surfaces was characterised recently by Harvey *et al.* [453].

The presence of a thin lubricating vapour layer, which is characterised by a low Reynolds number, makes the droplets highly mobile due to the diminished friction [Fig. 15d]. As soon as a spontaneous instability causes a slight difference in the thickness of the vapour layer, a flow emerges which triggers self-propulsion by rolling motion [454, 455]. The interaction with a structured substrate can also be used to induce directed motion, e.g. across ratcheted grooves [456–458], and the motion may further be controlled with thermal gradients [459]. A video featured on BBC Earth shows how the Leidenfrost effect can be used to make water run uphill [460]. Besides self-propulsion, the energy injected by droplet heating can cause droplet vibration with star-shaped droplet modes [444] that lead to distinct Leidenfrost sounds [445] [Fig. 15c].

The Leidenfrost phenomenon is seen all across the temperature scale and is controlled mainly by the temperature difference between the substrate and the droplet, and surface roughness. Interestingly, the substrate need not be solid: a similar effect is observed with acetone droplets (nail polish remover) on a bath of hot water [461]. More generally, the Leidenfrost state, in which an object hovers on a solid or on a liquid due to the presence of a vapour layer, can be seen in a variety of contexts. For example, it occurs when a block of sublimating solid carbon dioxide (dry ice) is placed on a plate at room temperature [462], which is also termed the *inverse Leidenfrost effect* [463], or when room temperature ethanol droplet falls on a bath of liquid nitrogen [464] and start moving. Furthermore, when two water droplets are placed on a

hot plate, the vapour layer between them prevents their coalescence, which is called the triple Leidenfrost effect [465]. Frequently demonstrated in popular lectures and science fairs, Leidenfrost effect allows a person to quickly dip a wet finger in molten lead or blow out a mouthful of liquid nitrogen without injury [466].

C. Heating and Boiling: Rayleigh-Bénard convection

Let's cook some pasta [467–470]. We place a pot with water on the stove and start heating. Heat from the stove is transferred to the water, first through conduction, and then through natural convection, which we see as characteristic structures called 'plumes' near the bottom wall [Fig. 16]. The fluid layer adjacent to the heated surface becomes unstable [see §III A, RT instability] and starts rising, since it is lighter than the bulk fluid. This fundamental process has been widely studied in many different configurations. One of the most well-studied is the Rayleigh-Bénard Convection (RBC) system, consisting of a fluid layer bound between two horizontal plates, heated from below and cooled from above, as reviewed by Ahlers *et al.* [471], Lohse and Xia [472], Kadanoff [473]. It occurs ubiquitously in natural contexts, including astrophysics [474, 475], geophysics [476, 477]) and in engineering applications such as metallurgy, chemical and nuclear engineering [478, 479].

The key non-dimensional parameters governing natural convection is the Rayleigh number,

$$\mathrm{Ra} \equiv \frac{\text{heat diffusion time}}{\text{heat convection time}} = \frac{g\beta_T \Delta T H^3}{\nu D_T}, \tag{49}$$

and the Prandtl number,

$$\mathrm{Pr} \equiv \frac{\text{momentum diffusivity}}{\text{thermal diffusivity}} = \frac{\nu}{D_T}, \tag{50}$$

where g is gravity, β_T is the coefficient of thermal expansion, ΔT is the temperature difference between the walls, H is the height of the fluid layer, ν is the kinematic viscosity of the fluid, and D_T is the thermal diffusivity of the fluid. Note that the Prandtl number only depends on the inherent properties of the liquid. Most oils have $\mathrm{Pr} \gg 1$, which means that heat diffuses very slowly in oils. Then, depending on the magnitude of Ra, we can identify different regimes of natural convection. The heat transfer through the fluid is solely through conduction till a critical $\mathrm{Ra} \sim 1708$ [482, 483]. Beyond this value of Ra, the convection consists of steady 'laminar' rolls [Fig. 16e]. At $\mathrm{Ra} \sim 10^4$, these convection rolls become unsteady, and beyond $\mathrm{Ra} \sim 10^5$ the convection is characterized as turbulent natural convection [Fig. 16a-d,f].

Now coming back to our water pot, as we continue supplying heat, the temperature will eventually reach the boiling point of the water. At this point, the boiling process begins with vapor bubbles forming in a superheated layer adjacent to the heated surface [484]. In this two-phase system, the vapor bubbles enhance the convective heat transfer in the standard RBC system [485]. This boiling process is so complicated that we currently only have an empirical understanding of the process [484], and theoretical progress has been lacking. However, cutting-edge numerical simulations seem to be a promising direction to model these processes accurately [486]. We put the pasta into the boiling water and allow it to cook for approximately 10 minutes. Once the pasta is cooked, we drain the excess water and serve with a favorite sauce.

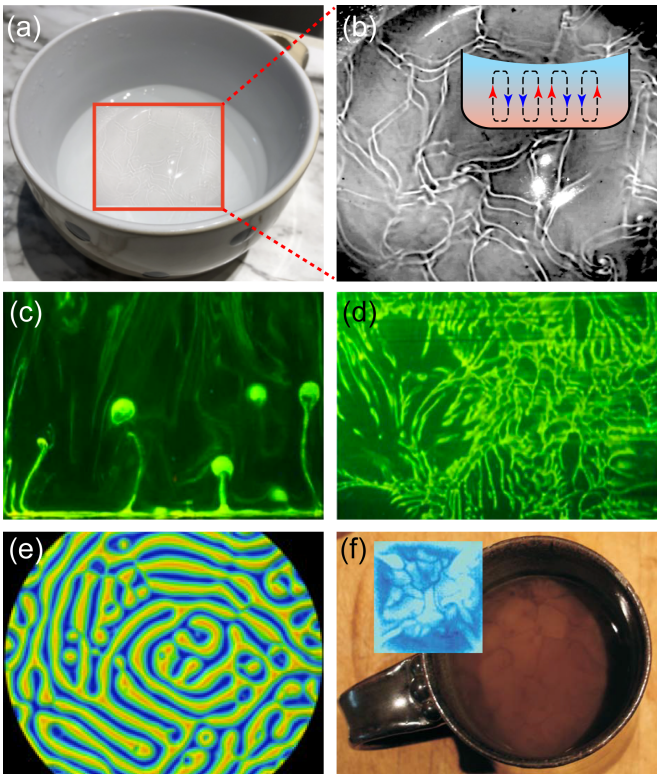

FIG. 16. Rayleigh-Bénard convection. **(a)** Rising plumes in a pot of water heated from below, visible because the refractive index shifts with temperature differences. **(b)** Contrast-enhanced magnification. **(c)** Side-view of mushroom-like plumes in a high-viscosity fluid. The green line at the bottom is the boundary layer. **(d)** Top-view of dendritic line plumes. (c,d) From Prakash *et al.* [477]. **(e)** Temperature field in a simulation of Rayleigh-Bénard convection at $\mathrm{Ra} = 5000$ and $\mathrm{Pr} = 0.7$. From Emran and Schumacher [480]. **(f)** Vortex structures in a coffee cup with milk at the bottom, which gets displaced by cold plumes that sink down from the evaporating interface. Inset: IR thermograph showing convection cells of colder (downwelling) and warmer (upwelling) regions. From Wettlaufer [481].

D. Layered latte: double-diffusive convection

In §V C we discussed Rayleigh-Bénard convection, which occurs because the fluid density depends on tem-

perature. Often the density also depends on a second scalar, like salt or sugar concentration. Importantly, their molecular diffusivity D_S is smaller than the thermal diffusivity D_T. This explains why your tea cools down before the sugar diffuses up, but it can also lead to double-diffusive convection (DDC) that can cause a range of unexpected phenomena, as reviewed initially by Huppert and Turner [487], and more recently by Radko [488] and Garaud [489]. Besides the Rayleigh and the Prandtl numbers [Eqs. (49), (50)], DDC also depends on the Schmidt number,

$$\mathrm{Sc} \equiv \frac{\text{momentum diffusivity}}{\text{molecular diffusivity}} = \frac{\nu}{D_S}, \tag{51}$$

where the ratio $\mathrm{Le} = \mathrm{Sc}/\mathrm{Pr}$ is called the Lewis number.

One surprising DDC phenomenon that is readily observed in the kitchen [490] is called salt fingering, which happens when warmer saltier water rests on colder fresher water of a higher density [491]. Then, in the words of Stern [492], "[the] 'gravitationally stable' stratification ... is actually unstable". If a parcel of warm salty water is perturbed to move down a bit, it loses its heat quicker than its salinity, so it will keep sinking further. Hence, salt fingers (vertical convection cells) spontaneously start growing downwards, accelerated by thermal diffusion, which gives rise to strong mixing. Kerr [493] jokes that one might have a Martini cocktail "fingered, not stirred", which could in fact be quite a spectacle with coloured layers [Fig. 17a]. This mixing effect is likely important for nutrient transport in the ocean and climate change [494, 495]. In astronomy, thermohaline mixing can occur in evolved low-mass stars [496]. DDC can equally feature in porous media [497], which might be relevant for heat and mass transfer in porous materials under microwave heating [498].

Another striking example of DDC is the formation of distinct layers in a caffè latte [499] [Fig. 17b]. To make one, warm a tall glass with 150 ml of milk up to 50 °C, and pour 30 ml of espresso at 50 °C into it. The milk is denser than espresso, so the dynamics will follow an inverted fountain effect [§III A] leading to stratification with a vertical density gradient. Subsequently, a horizontal temperature gradient is established because the glass slowly cools down from the sides. This double gradient leads to stacked convection rolls separated by sharp interfaces, as seen in creaming emulsions [500]. The coffee pouring (injection) velocity sets the initial density gradient, and thus the Rayleigh number, which much exceed a critical value for layers to form [499]. This was investigated further with direct numerical simulations by Chong *et al.* [501], who also discussed the mechanism how the layers merge over time. Besides café au lait, similar stacked layers are observed in the ocean, meters thick and kilometers wide, called thermohaline staircases [502, 503].

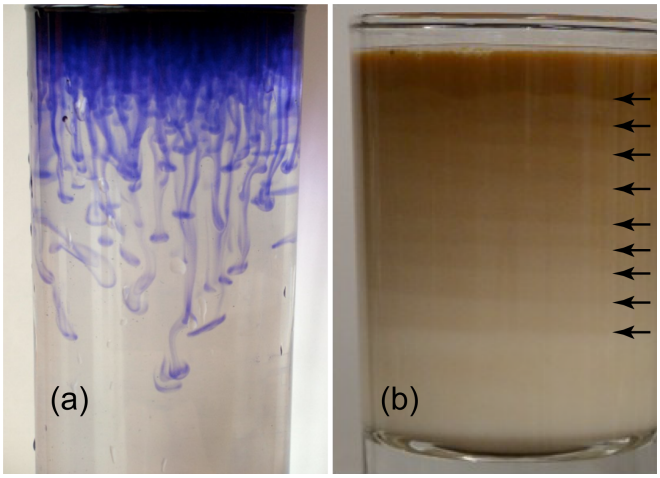

FIG. 17. Double-diffusive convection phenomena. **(a)** A cocktail with blue salt fingers, produced by warmer salty water resting on colder fresh water of a higher density. Image courtesy of Matteo Cantiello (Flatiron Institute). **(b)** Layered caffè latte. Adapted from Xue *et al.* [499]. Black arrows are added to highlight the layer boundaries.

E. Tenderloin: moisture migration

So far, we have described various fluid mechanical phenomena related to drinks or liquids. When cooking solid foods, it is also important to understand moisture migration to achieve a tender result [470]. We will consider the example of meat cooking (e.g. tenderloin), where two important physical aspects include time-dependent protein denaturation and cooking loss (water loss). To reach the desired meat textures, the meat must be cooked at well-defined temperatures to ensure selective protein denaturation [504]. Since our focus here is on fluid dynamics, we will discuss water loss during the heat treatments, which also depends on the temperature [504]. This cooking loss has been described using the Flory-Rehner theory of rubber elasticity [505, 506]. This theory models the transport of liquid moisture due to denaturation and shrinkage when the protein is heated. The moisture transport is due to a shrinking protein matrix, similar to a 'self-squeezing sponge'. It is assumed that the poroelastic theory applies here. Then, this theory describes moisture transport by Darcy's law [see §VII D], where the fluid flow rate is linear with pressure gradient. The pressure is due to the elasticity of the solid matrix of the porous material, an here it is referred to as the 'swelling' pressure, p_{swell}. According to Flory-Rehner theory, the swelling pressure can be decomposed into two components,

$$p_{\mathrm{swell}} = p_{\mathrm{mix}} + p_{\mathrm{el}}, \tag{52}$$

where p_{mix} is the mixing or osmotic pressure, and p_{el} is the pressure due to elastic deformation of the cross-linked polymer gel [323]. In equilibrium, the network pressure opposes the osmotic pressure, and the swelling

pressure is zero. The temperature rise during cooking causes and imbalance between the osmotic pressure and network pressure, leading to the expelling of excess fluid from the meat. Hence, the swelling pressure in meat is proportional to the difference between moisture content and water holding capacity. The gradient of this swelling pressure will drive the liquid moisture flow, and is used in Darcy's Law [Eq. (73)]. This model has been found to agree well with experimental data, proving that the Flory-Rehner theory provides a sound physical basis for the moisture migration in cooking meat [506].

F. Flames, vapors, fire and smoke

Next, we consider the flows generated around the hot cookware, utensils, or hot beverages. There are various heat transfer processes in the kitchen that can give rise to vapors, fumes, fires, and smoke. We of course enjoy the smell of a good dish that is cooking, and unexpected smoke is oftentimes an indicator that something is burning. Hence, in addition to increasing the overall room/kitchen temperature, the vapors/smoke also play an important role in giving us positive or negative feedback on how the cooking is going. Hot utensils transfer heat into the surrounding air setting up buoyancy-driven convection or natural convective flows around them. Figure 18 shows the beautiful flow of vapors and convection around a hot espresso cup [507], and around a hot tea kettle, visualised with Schlieren imaging as reviewed by Settles [216], Settles and Hargather [508]. Such convective flows are present around all heated objects, and one can imagine how different geometries of vessels/cookware can give rise to complicated flows around them.

The kitchen is our safe place to prepare food, but we must remember that it is also a place where several safety hazards exist. At some point in our lives, most of us have forgotten to turn off the kitchen stove and suffered the consequences. When food is overheated, it starts to burn and eventually the temperature gets so high that the carbon content gets converted to soot that give rise to smoke and fumes. Smoke decreases the overall air quality and inhaling it can adversely affect our health [509], especially if the burning becomes intense and the heating is continued. While the dispersion of smoke as a general pollutant in the atmosphere has been studied extensively, smoke in the kitchen has also been the subject of several studies [509, 510]. A critical issue related to this is ventilation, i.e. how well a kitchen is designed to get rid of harmful smoke and fumes. Most modern kitchens feature a ventilation or exhaust 'hood' right above the stove. Both Experimental Fluid Dynamics (EFD) and Computational Fluid Dynamics (CFD) techniques such have been utilized to study the flow through kitchen hoods in order to maximise their performance [511]. Fires in the kitchen are the most dangerous safety hazard [512], and can result in destruction of property and loss of life. Given the importance of minimizing safety hazards in the kitchen, fire engineers rely on fluid dynamics modeling to develop designs for optimum and safe kitchen ventilation [513–515].

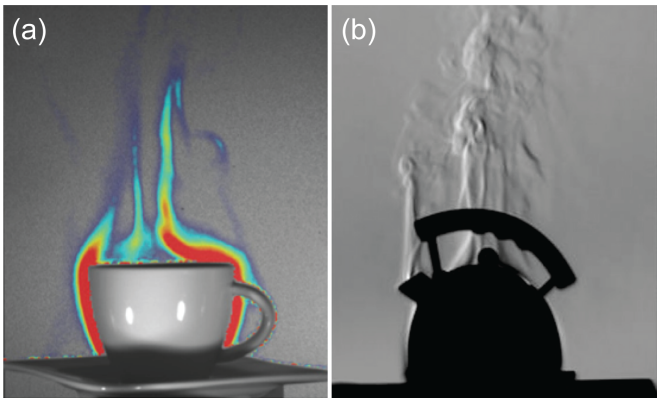

FIG. 18. Buoyancy-driven plumes. **(a)** Flows developing over an espresso cup visualised with schlieren imaging. Colors indicate fluid displacement, where red is the highest, and blue the lowest. From Cai *et al.* [507]. **(b)** Plume around a hot tea kettle captured with schlieren imaging. From Settles and Hargather [508].

G. Melting and freezing

We tend to naturally associate cooking with heat. Boiling, melting, freezing, solidifying, dissolving and crystallizing food products need the external heat stimulus to transform. Thermally driven reconfiguration can happen on a molecular level but more often it is enough to consider phase transitions due to the heating or cooling of a substance.

Melting is an exemplary fundamental process of phase transition. From thawing to cooking, solid substances are transformed into soft matter or liquid products. The sole process of melting and flows induced therein are still of fundamental interest for physicists. The mechanism of heat transfer relies, in the simplest case described in §V A, on the Fourier law, where the heat flux q across a surface is locally proportional to the temperature gradient ∇T. The temperature field thus satisfies the advection-diffusion equation (47), which can then be solved numerically or analytically in specific geometric configurations. Geometry itself inspires questions on how the process of thawing can be exploited to create desired forms, i.e. seen in constantly evolving ice sculptures or in ordinary ice cubes melting in a cocktail. Although the initial shapes of frozen structures may be arbitrary, macroscopic objects such as melting ice cubes and growing stalactites can approach non-intuitive geometric ideals. For the dissolution of non-crystalline objects, a paraboloidal shape was shown to be the geometric attractor [516]. Even the simple melting of icicles is governed by a combination heat transfer from the air, the latent heat of condensation of water vapour, and the net

radiative heat transfer from the environment to the ice [517], which emphasizes the complexity of phase change processes. In kitchen flows, an additional factor is the microstructure of food products, which renders their flow non-Newtonian, and their response to temperature variations non-linear. Even though the flow of molten chocolate in a fountain is aptly described by a power-law fluid [518], the process of melting involves different crystalline phases and is thus highly complex. Subsequent freezing typically leads to a change in structure and appearance, with different physical properties and even taste. The quality of chocolate products, in particular their gloss, their texture and their melting behaviour, depends primarily on two processing steps: the precrystallisation of the chocolate mass and the eventual cooling process [519]. These factors must be considered in confectionery manufacturing and, fundamentally, in the modelling of crystallization and melting kinetics of cocoa butter in chocolate [520].

Butter (plant or animal-based) itself, being a vital product for cooking, responds strongly to external temperature, transiting from completely solid and brittle when taken out from the refrigerator, to pleasantly spreadable at intermediate temperatures, to liquid. This empirical feeling can be related to its viscoelastic characteristics [521, 522], which additionally depend on the substance and on the method of production [523]. Rheology and texture are often the basic characteristics when heating or baking cheese [524], such as in the melting and browning of mozzarella in the oven [525]. The temperature can be also coupled to the nonlinear viscoelastic properties, for instance when considering starch gelatinisation while making gravies and thick sauces [526] or when freezing and thawing a gelatin-filtered consommé [527].

H. Non-stick coatings

Many non-stick pans or cookware are designed to be hydrophobic (water repellent) and oleophobic (oil repellent), which together is called amphiphobic [528, 529]. Waterproof fabrics often use chemical coatings such as polyurethane (PU), polyvinyl chloride (PVC), or fluoropolymers. However, there are many concerns for these materials regarding toxicity and other environmentally damaging effects [530], and to limit their destructive impact, the European Union has announced a ban on such chemicals by 2030 [531]. As such, interest has risen for purely physical coatings that make use of the "lotus effect" [532, 533]. Like leaves of the lotus plant (*Nelumbo* genus), micron-sized structures can be designed that give rise to superhydrophobicity [534–536]. A droplet that impacts these surfaces can bounce off without wetting them [537, 538]. Moreover, decorating sub-millimetric posts with nanotextures can lead to "pancake bouncing", where the contact time of droplets with the surface is significantly reduced [539, 540]. This is important for anti-icing [541] and self-cleaning surfaces [542], with possible applications for airplanes and cars. Remarkably, superamphiphobic coatings can also be made with candle soot [543].

VI. HONEY DESSERT: VISCOUS FLOWS

Viscosity controls both slow and small-scale flows, shaping our notion of 'heavy' or 'thick' substances such as honey [544], oil, gravy, or cream. Moreover, viscous flow theory underlies the behaviour of most composite flowing food products, such as emulsions, suspensions, and particle-laden fluid substances. When you are trying to mix together viscous fluids, you might bear in mind the kinematic reversibility experiment of Taylor [545], showing that the time-reversible driving force will lead to time-reversible particle trajectories in Stokes flow [see Fig. 19a]. When pouring honey or golden syrup on pancakes or toast [Fig. 19b], the apparent coiling of the impinging stream is but one of the many phenomena at the interplay of gravity, viscosity, and surface tension. Finally, the complex shapes of sedimenting clouds of food colouring added to a cocktail can be aptly described using many-body hydrodynamic interactions of Stokesian microparticles [378, 546], as seen in Fig. 19c. Below, we will discuss how the concept from Stokes flow manifest themselves in a myriad of culinary aspects, some of which are highlighted in this section.

A. Flows at low Reynolds number

Viscous liquids are everywhere in the kitchen, and their fluid mechanics can be rather non-intuitive. To understand these flows better, we must determine which of the terms in the Navier-Stokes equations (2) are relevant in different situations. It is helpful to scale the time by a characteristic value T_0, the velocities by the characteristic speed U_0, and distances by the characteristic length L_0. Hence, one can introduce the dimensionless variables

$$\tilde{\boldsymbol{x}} = \boldsymbol{x}/L_0, \qquad \tilde{\boldsymbol{\nabla}} = L_0\boldsymbol{\nabla}, \qquad \tilde{t} = t/T_0,$$
$$\tilde{\boldsymbol{u}} = \boldsymbol{u}/U_0, \qquad \tilde{p} = \frac{p - p_{\mathrm{atm}}}{\mu U_0/L_0}, \qquad \tilde{\boldsymbol{f}} = \frac{\boldsymbol{f}}{\mu U_0/L_0^2}, \quad (53)$$

where p_{atm} is the atmospheric pressure. Then, rewriting Eq. (2a) in terms of these variables yields the non-dimensionalised momentum equation,

$$\mathrm{Re}\left(\frac{1}{\mathrm{St}}\frac{\partial\tilde{\boldsymbol{u}}}{\partial\tilde{t}} + (\tilde{\boldsymbol{u}}\cdot\tilde{\boldsymbol{\nabla}})\tilde{\boldsymbol{u}}\right) = -\tilde{\boldsymbol{\nabla}}\tilde{p} + \tilde{\nabla}^2\tilde{\boldsymbol{u}} + \tilde{\boldsymbol{f}}, \quad (54)$$

where the Reynolds number is $\mathrm{Re} = \rho U_0 L_0/\mu$, as we discussed before in §II D, and the transient Reynolds number is $\mathrm{Re}_T = \frac{\rho L_0^2}{\mu T_0} = \frac{\mathrm{Re}}{\mathrm{St}}$. Here the Stokes number (St) compares the relative importance of transient inertial forces compared to viscous forces.

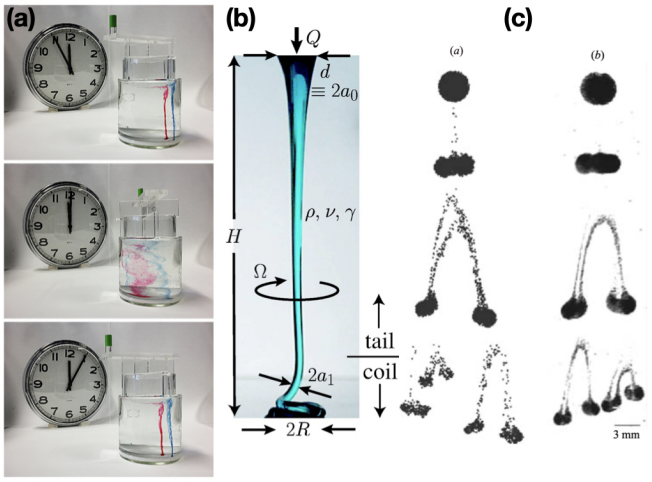

FIG. 19. Examples of Stokes flows relevant to kitchen setting. **(a)** Experimental demonstration of kinematic reversibility in an annular cylindrical space filled with silicone oil. Upon rotating the inner cylinder slowly a number of times and then reversing the forcing, the dyed fluid blobs remain unchanged, thus illustrating the difficulties in mixing viscous fluids. From Wikimedia Commons, licensed under CC BY 2.0. **(b)** Coiling of a liquid rope made of a viscous fluid (corn syrup) demonstrates the complexities of free-surface gravity flows and also of pouring honey on the pancakes. From Ribe *et al.* [547]. **(c)** Snapshots of the falling cloud: (left) in point-particle Stokesian dynamics simulation with 3000 particles and (right) in sedimentation experiments using 70 µm glass beads in silicon oil. From Metzger *et al.* [546].

The Reynolds number is typically very small in viscous fluids, or at small length scales. For example, when humans swim in water with a dynamic viscosity $\mu \approx 0.9\,\mathrm{mPa\,s}$ and density $\rho \approx 10^3\,\mathrm{kg/m^3}$, we find $\mathrm{Re} \sim 10^6$. This means that the fluid inertia is much more important than viscosity. For microbes swimming in the same medium, however, we have $\mathrm{Re} \sim 10^{-5}$, so the viscosity is overwhelmingly dominant [548]. Then, Eqs. (2) reduce to the Stokes equations,

$$0 = -\boldsymbol{\nabla} p + \mu \nabla^2 \boldsymbol{u} + \boldsymbol{f}, \qquad \boldsymbol{\nabla} \cdot \boldsymbol{u} = 0. \tag{55}$$

These equations have several important properties. Firstly, they are linear, which makes them much easier to solve than the Navier-Stokes equations. This also means that, for given set of boundary conditions, there is only one unique solution [549]. Secondly, the Stokes equations do not depend explicitly on time. Viscosity-dominated flows will therefore respond essentially instantaneously to changes in the applied force, pressure, or the boundary conditions. In other words, disturbances to the flow field spread much faster than the flow itself. Thirdly, Eqs. (55) are kinematically reversible, i.e. they are invariant under the simultaneous reversion of the direction of forces and the direction of time. This means that if the forces driving the flow are reversed, the fluid particles retrace their trajectories in time. As a consequence, it is notoriously difficult to mix fluids at low Reynolds number [see §VIII E]. Apart from beautiful demonstrations of mixing and demixing under reversed forcing in famous video experiments by G.I. Taylor [545], this issue bears great significance for microfluidic flows, which are becoming increasingly relevant for food science [see §IV D and §VI J].

B. Fundamental solution of Stokes flow

The fundamental solution to the Stokes equations, the Green's function, is called the Stokeslet. It is the flow $\boldsymbol{u}_S(\boldsymbol{x}, t)$ at position $\boldsymbol{x}$ and time t due to a point force,

$$\boldsymbol{f}(\boldsymbol{x}, \boldsymbol{y}, t) = \delta^3(\boldsymbol{x} - \boldsymbol{y}) \boldsymbol{F}(t), \tag{56}$$

which has time-dependent strength $\boldsymbol{F}(t)$ exerted on the liquid, and the force is located at position $\boldsymbol{y}(t)$. For an unbounded fluid, the boundary condition is $\boldsymbol{u} = 0$ as $|\boldsymbol{x}| \to \infty$. Physically, one could think of this point force as a small particle being dragged through the liquid, such as a sedimenting coffee grain [see §VI C]. The flow generated by this point force is given by

$$\boldsymbol{u}_S(\boldsymbol{x}, t) = \mathcal{J}(\boldsymbol{x} - \boldsymbol{y}(t)) \cdot \boldsymbol{F}(t), \tag{57}$$

where the Oseen tensor $\mathcal{J}_{ij}(\boldsymbol{r})$ has Cartesian components

$$\mathcal{J}_{ij}(\boldsymbol{r}) = \frac{1}{8\pi\mu} \left(\frac{\delta_{ij}}{r} + \frac{r_i r_j}{r^3} \right), \tag{58}$$

with indices $i, j \in \{1, 2, 3\}$, the relative distance is $\boldsymbol{r} = \boldsymbol{x} - \boldsymbol{y}$, and $r = |\boldsymbol{r}|$. There are different ways to derive this tensor, as summarised by Lisicki [550].

This Stokeslet solution is powerful, analogous to Coulomb's law for electric point charges. Like the Stokes equations, it also reveals important properties of viscous flows. First, Eq. (57) shows that the applied force is directly proportional to the flow velocity. As opposed to Newtonian mechanics, where the forces are proportional to acceleration, this reflects Aristotelian mechanics [551], where there is no motion in the absence of forces. Inertia vanishes at low Reynolds number, that is, so the dynamics are overdamped. Second, hydrodynamic interactions are very long ranged. The Stokeslet flow decays as $1/r$ with distance, as opposed to gravitation or electrostatics that both follow inverse-square laws. This has important consequences. For example, in a particle suspension, the motion of one particle will produce a flow that moves other particles, which in turn generate flows that affect the first particle again [see §IV C].

The fundamental solution can also be used to derive the widely celebrated Stokes law,

$$\boldsymbol{F} = -6\pi\mu a \boldsymbol{U}, \tag{59}$$

which describes the viscous drag force exerted on a small sphere of radius a moving with velocity $\boldsymbol{U}$ relative to the

viscous fluid [54, 552]. The flow generated by this finite-sized sphere can be written [see e.g. 553] in terms of the Stokeslet flow as

$$\boldsymbol{u}(\boldsymbol{x},t) = \left(1+\frac{a^2}{6}\nabla^2\right)\boldsymbol{u}_S. \tag{60}$$

$$= \boldsymbol{U}\left(\frac{3a}{4r}+\frac{a^3}{4r^3}\right)+\boldsymbol{r}\frac{\boldsymbol{U}\cdot\boldsymbol{r}}{r^2}\left(\frac{3a}{4r}-\frac{3a^3}{4r^3}\right), \tag{61}$$

where we used Eqs. (57-59) for the second step. One can verify that this expression (61) will satisfy the Stokes equations and the required no-slip condition on the surface of the sphere, $\boldsymbol{u}(r=a)=\boldsymbol{U}$. The significance of Stokes' law can hardly be overemphasized. Dusenbery [554] writes that it is directly connected to at least three Nobel Prizes. Can you name them?

C. Coffee grains in free fall

To optimise our coffee, we may want to assess the size distribution of the coffee grains after grinding. This can be achieved in a simple sedimentation experiment, using the Stokes law [Eq. (59)]. The gravitational force, $\boldsymbol{F}_g = m\boldsymbol{g}$, pulling on a spherical grain of size a is proportional to the mass differential with the surrounding fluid, $m = (\rho_p-\rho)\,\frac{4}{3}\pi a^3$. The same grain is slowed by a viscous drag force, given by Eq. (59). When the drag force balances the gravitational force, the terminal velocity is

$$U_\infty = \frac{2}{9}\frac{a^2\,(\rho_p-\rho)\,g}{\mu}. \tag{62}$$

To measure U_∞ in the kitchen, we can use a mobile phone to videotape individual grains sedimenting. Eq. (62) can be rearranged to solve for the particle size a. Conversely, it is possible to solve for μ if a is known, which is the principle of falling sphere viscometry [555]. Not least, Millikan [556] used a form of Eq. (62) to find the elementary electrical charge. Note that the above equation was developed under several assumptions. In the paragraphs to follow we assess the validity of these.

The first assumption is that the grain sediments at low Reynolds number, given by $\mathrm{Re} = aU_\infty\,(\rho_p-\rho)\,/\mu$. Using Eq. (62), we find that a typical grain of radius $a = 1\,\mathrm{mm}$ sediments at $0.1\,\mathrm{mm/s}$, yielding a Reynolds number just below order unity. We should therefore be cautious when using Stokes' law in this case [557]. In order to obtain the range of Reynolds numbers over which Eq. (62) gives a good approximation, one can turn to experiments. Numerous reports have been published on this topic [558, 559], and it is generally agreed that Eq. (62) gives good estimates up to $\mathrm{Re}\approx 1$ [560].

The sedimenting coffee grain generates a flow field that decays slowly with distance from its center [see §VI B]. Close to the particle, viscous forces dominate, while in the far field the inertial terms dominate. It is the absence of walls that facilitates this shift from viscous to inertial dominance, as walls provide friction to the flow. By accounting for inertial effects, considering an unbounded fluid, Oseen [561] developed the following improved formula for the drag coefficient,

$$C_D = \frac{24}{\mathrm{Re}}\left(1+\frac{3}{16}\mathrm{Re}\right). \tag{63}$$

The first term is the Stokes drag close to the particle, while the second term stems from inertial effects far away from the particle. Oseen's formula agrees fairly well with experiments up to $\mathrm{Re}\approx 10$ [562].

Beyond the Oseen regime, inertial effects in the flow surrounding the particle can no longer be neglected. This causes the nearby fluid streamlines to divert from the particle, causing the flow to separate. Then the pressure drop across the particle is reduced, which leads to a drag reduction. A simple experiment using coffee grains released in air (instead of water) can be performed to observe this behavior. By accounting for inertial effects around a sedimenting sphere, Stewartson [563] found the drag coefficient to be approximately 1.06, which may be compared to the value of 7.2 using Eq. (63) for $Re = 10$. For more details, we refer the interested reader to the excellent review paper on Stokes' law, and its legacy, by Dey *et al.* [562].

Wall effects: We now return to the assessment of the validity of Stokes' law for sedimenting coffee grains in bounded water. In developing Eq. (62), we assumed that the grain falls without influences of walls. O'Neill [564] showed that hydrodynamic contributions due to walls can slow down a sedimenting grain (or a rising bubble) by as much as 5% when the distance to the walls is ten times its size. The degree of retardation increases linearly as the grain gets closer to the vessel walls. Using matched asymptotic expansions, Goldman *et al.* [565] obtained a solution for the drag force acting on a sedimenting sphere moving parallel to a wall,

$$\frac{F_{\parallel \mathrm{W}}}{F_S} = 1-\frac{9}{16}\frac{a}{h}+\frac{1}{8}\left(\frac{a}{h}\right)^3-\frac{45}{256}\left(\frac{a}{h}\right)^4-\frac{1}{16}\left(\frac{a}{h}\right)^5, \tag{64}$$

which is normalized by the Stokes drag force [Eq. (59)]. Thorough experiments have been performed to validate the above result, showing good agreement [566].

For spheres very close to a wall, lubrication effects become important [§VI E], yielding a logarithmic relationship between the force and the distance to the wall [567]. This strong logarithmic dependence can be readily observed when making French press coffee: grains close to the vessel container sediment much slower than grains out in the bulk. Recently, Rad and Moradi [568] revisited this problem in non-Newtonian liquids, which has important biophysical implications.

Collective effects: Our final assessment of Eq. (62) concerns the influence of multiple particles correlated by long-ranged hydrodynamic interactions [see §VI B]. When two spheres sediment side-by-side, they fall slower than in the absence of the other particle, while if they

are separated by a vertical line going through their centers, the opposite is true [377, 378]. In a suspension containing several grains, the influence of other particles always leads to a decrease in sedimentation velocity. This observation is known as hindered settling [569] and is mainly due to an upward flow generated by each particle as it sediments. In a dilute suspension, the hindered settling velocity depends on the particle concentration as $U \approx U_\infty (1 - 6.55\phi)$, as shown by Batchelor [570]. Other effects such as Brownian motion [571] and shape [558] can also affect the sedimentation velocity. Finally, if particles sediment towards a surface covered with moving actuators, a self-cleaning effect can occur where hydrodynamic fluctuations repel the particles, leading to a non-Boltzmannian sedimentation profile [572].

D. Slender body theory

A generalisation of the Stokes law [Eq. (59)] can be derived for a cylinder of length ℓ and radius a. When it moves through the fluid along its major axis, it will experience a viscous drag force

$$F_\parallel \approx \frac{2\pi\mu\ell U}{\ln(\ell/a)}, \tag{65}$$

as predicted by slender-body theory [573, 574]. Because of the structure of the Oseen tensor, $\mathcal{J}_{ij}$ [Eq. (58)], the cylinder will exert a larger force on the fluid when it moves sideways,

$$F_\perp \approx 2F_\parallel. \tag{66}$$

Despite its simplicity, this result lies at the heart of numerous transport processes for viscous fluids. The drag asymmetry for slender filaments enables propulsion of microorganisms: bacteria rotate their helical flagella and exploit the rotation-translation coupling due to their chirality to generate propulsion force [575–577]; ciliates perform coordinated motion of tiny hair-like appendages covering their bodies, creating metachronal waves which transport the fluid along their surfaces [578–580]. Moreover, various experimental designs for artificial swimmers, which tend to mimic their biological archetypes, are based on this hydrodynamic anisotropy [257]. Interestingly, it could be possible to tailor food texture and rheology by microstructured fibers [581].

E. Lubrication theory

In systems where one dimension is significantly smaller than the others, its hydrodynamics can often be described using lubrication theory. This is relevant in many contexts where the fluid is confined between surfaces or forms a thin film on a substrate. The former has industrial applications in fluid bearings, but also in kitchen flows involving squeezing and spreading of viscous fluids in thin layers. The key goal there is to relate the geometry to the resulting pressure distribution. The latter, involving a free surface, is related to the shape evolution of the fluid surface under the action of external forces or in response to substrate patterning. This bears importance for coating and painting, also in the food industry. In shaping these flows, surface tension and substrate wetting properties may become significant.

From a mathematical point of view, lubrication theory builds on the separation of length scales, with the fluid layer thickness h (say, in the direction z locally perpendicular to the substrate) being much smaller than the substrate length scale L (in the direction x along the surface). Then, the leading-order expansion in the small parameter $\varepsilon = h/L$ yields the equations

$$\frac{\partial p}{\partial z} = 0, \qquad \frac{\partial p}{\partial x} = \mu \frac{\partial^2 u_x}{\partial z^2}. \tag{67}$$

This reflects the fact that in the thin gap the pressure changes very little with height above the substrate, and its change along the substrate is related to the flow variation across the gap. In the general three-dimensional case, as described by Reynolds [582] and reviewed by Batchelor [54], Oron *et al.* [583], Szeri [584], this equation is referred to as the Reynolds equation,

$$h\frac{\partial \rho}{\partial t} + \rho w^{ab} = \sum_{i=x,y} \rho u_i^a \partial_i h + \partial_i \left(\frac{\rho h^3}{12\mu} \partial_i p - \frac{\rho h u_i^{ab}}{2} \right), \tag{68}$$

where a, b denote the top and bottom surfaces, respectively, w is the vertical flow velocity, u_i with $i = x, y$ denotes the horizontal velocities, $w^{ab} = w^a - w^b$ and $u_i^{ab} = u_i^a + u_i^b$. This equations may be solved analytically or numerically for a range of different applications.

Indeed, lubrication theory is used ubiquitously. In tribology, it is crucial for reducing wear and friction between bearings [585]. In biology, tree frogs can climb vertical walls using liquid film flows, which has inspired new tire technology [586], and biomimetic materials that adhere under wet conditions [587, 588]. Thin films significantly alter the motion of trapped microorganisms [589], governing their surface accumulation. Note that many biological fluids are viscoelastic, which changes the Reynolds equation (68), but the basic concepts still hold. Using ferrofluids, adhesion can also be made switchable for use smart adaptable materials [590]. Recent developments on the nanoscale physics can improve lubricant design [591]. Additionally, lubrication theory has been used to model air hockey [592] and, in the spirit of kitchen experiments, Reynolds also used it to determine the viscosity of olive oil [582]. Pan lubrication is also an important step in industrial baking [593]. Finally, the lubrication theory can also be used to model hand washing, as explained in §II K.

F. Pot stuck to stove top: Stefan adhesion

If a pot of pasta overboils, a common subsequent problem is that the pan is "stuck" to the surface. This effect does not require any glue or the formation of molecular bonds – it stems from the viscous liquid film that is sandwiched between the objects. Josef Stefan [594] first described this "apparent adhesion", and later Reynolds [582] quantified it with a detailed treatise on lubrication theory [see §VI E].

Making use of the disparity between the radius of the pan, R, and the width of the liquid film, $h \ll R$, one can derive the pressure distribution inside the film described by the Reynolds equations (68). Integrating this expression shows that the force required to lift the pan from the surface, the Stefan adhesion force, is

$$F = \frac{3\pi\mu R^4}{2h^3}\frac{dh}{dt}. \tag{69}$$

This force can be very large for thin films due to the strong dependence on h, making it hard to squeeze a viscous liquid through a narrow gap. For pan radius $R \sim 12$cm, film thickness $h \sim 10\mu$m and separation speed $\frac{dh}{dt} = 1$mm/s, the force is $F \sim 10^6$N, orders of magnitude larger than the weight of the filled pan. Conversely, it is very difficult to bring two surfaces into close contact, as described by squeeze flow theory, with many generalisations for viscoelastic fluids [595].

G. Viscous gravity currents

"Open the front door of a centrally-heated house and a gravity current of cold air immediately flows in." These opening words by Huppert [596] describe many processes in the kitchen: Opening the fridge or the oven door, but also the spreading of oil in a frying pan. To understand how long this spreading takes, we need to determine the evolution of the height profile, $h(\boldsymbol{r}, t)$, which strongly depends on the dynamic viscosity and density of the oil, μ and ρ, gravity, g, and the pouring rate, Q. The presence of inertia makes predictions of the radial spreading velocity difficult. If we instead pour the oil really slowly, at low Reynolds number, assuming that both the oil layer thickness h and the 'jet' radius R_j are small compared to the current R, then we can use a lubrication approximation [see §VI E] to obtain a simplified version of the radial force balance:

$$\frac{\partial h}{\partial t} - \frac{1}{3}\frac{\rho g}{\mu}\frac{1}{r}\frac{\partial}{\partial r}\left(rh^3\frac{\partial h}{\partial r}\right) = 0. \tag{70}$$

By adding a mass conservation equation to Eq. (70), and by introducing a similarity variable, Huppert showed that the radial extent of the evolving puddle, R, is given exactly by:

$$R = 0.715\left(\frac{\rho g Q^3}{3\mu}\right)^{1/8} t^{1/2}. \tag{71}$$

The dominant balance of forces in Huppert's analysis is between a hydrostatic pressure head, that drive the fluid, and viscous stresses, that slow the fluid. Huppert discarded effects of surface tension, γ, and Eq. (71) requires that the Bond number be large, $\mathrm{Bo} = \rho R^2/\gamma \gg 1$. Many geophysical flows are characterized by large Bond numbers, and the scalings by Huppert have seen widespread use for predicting spreading rates of saltwater currents into freshwater, lava flows, and many other geophysical gravity currents [597–599]. The success of these scalings in *miscible* fluids might seem surprising. However, geophysical flows are often characterized by high Péclet numbers [Eq. (48)], such that the transport of momentum outpaces the transport of mass [see §V A]. On the fast time scale of the flow, diffusion does not have sufficient time to blur the interface separating miscible liquids, resulting in the liquids displaying immiscible behavior. Recently, Eq. (71) was found to accurately describe the spreading rate of miscible sessile drops of corn syrup and glycerol in water [600]. Other important contributions to the study of gravity currents include the spreading of a saltwater current under a bath of freshwater [601], spreading hot plumes in cold environments [602], and oil spreading on the sea [603]. These and other works are described in detail in a number of review papers [597, 604] and in the book by Ungarish [605].

Making the perfect crêpe

In the analysis by Huppert [596], the viscosity is treated as a constant. If the pan is heated, however, the spreading problem becomes more complicated as the viscosity must be treated as a non-linear function of time. This situation is typical in many cooking processes. For example, when pouring pancake batter into a hot pan to make a crêpe, the temperature of the spreading batter increases, and this temperature rise is associated with a reduced viscosity. Later in the spreading process, the batter starts to solidify, and the liquid-solid transformation leads to a viscosity *increase*. Since the current continually loses momentum as it spreads, the solidification can arrest the flow long before it extends the entire pan. Conveniently, flow arrest can prevented by swirling the pan, which enhances the spreading rate dramatically. Motivated by the aim of making a perfectly flat and uniform crêpe, Boujo and Sellier [606] recently approached the spreading problem with both time-dependent viscosity and gravity. Armed with numerical tools, they identified different swirling modes and measured the resulting pancake shape. Interestingly, a swirling mode that is naturally adopted in pancake making, namely draining all the batter in one place and then rotating the batter around the perimeter of the pan in one big swirling motion, appeared to optimise the pancake shape. To learn more about the rheology of pancake making and other cooking processes, see §IV A.

H. Viscous fingering

When a less viscous fluid displaces a more viscous one, such as when we inject water into glycerol, then the frontal lip of the current is susceptible to Saffman-Taylor instabilities [607, 608] , causing "viscous fingering" patterns to evolve [609]. Viscous fingers can also be created in the kitchen when mixing water (less viscous) with condensed milk (more viscous) when making a banana pudding, or when a sessile drop of water spread on a layer of honey. The local destabilization of a finger occurs by a splitting of its tip and results in the formation of two branches separated by a fjord, leading to an elaborate pattern formation due to successive tip-splitting [610].

The vast literature on viscous fingering spans from occurrences in biological systems [611, 612] and porous media drainage [613], to methods for mitigation in oil extraction processes [614]. Another example with geophysical relevance includes the report by Snyder and Tait [615], who introduced a miscible current of intermediate density in between two stably stratified liquid layers. They found that the interface is unstable when bounded by more viscous liquids on either side, and that the instability is suppressed when at least one of the two stratified liquids are of higher viscosity. A new and refreshing direction in the field concerns so-called particle induced fingering. Tang *et al.* [616] discovered that particles can cause an otherwise stable front between a viscous liquid such as glycerol displacing a less viscous liquid such as water to develop viscous fingering patterns. The instability arises because of an uneven particle distribution along the perimeter, which leads to local viscosity differences. The evolving front propagates faster in low viscosity regions than in regions of high local viscosity, and it is these differences that allow irregularities at the interface to develop [617].

Viscous fingers can also appear in the context of boundary driven lubrication flows. A drop of treacle or honey squeezed between two glass plates spreads upon the gravitational settling of the top plate into a circular structure with its radius R growing with time as $R(t) \sim t^{1/8}$, in analogy to the viscous gravity flows in §VI G. Upon levering one of the plates, a draining flow arises. The droplet front is unstable and thus produces a network of fingering branches which thin over time as the gap width increases [618].

I. Microbial fluid mechanics

The remarkable properties of the Stokes equations [see §VI A] have pronounced consequences for the life of microscopic swimming organisms, which have to obey these physical limitations [259, 548, 575]. One of these constraints is the scallop theorem, stating that a time-reversible swimming gait cannot lead to a net displacement. In order to achieve propulsion, microorganisms they rely on a variety of mechanisms circumventing kinematic reversibility of flows. Some organisms use helically-shaped flagella [576] or cilia [619], others exploit elasticity to break time-reversibility [620], or use the non-Newtonian properties of the surrounding fluid [621]. Microbes play an role in cuisine in a spectrum of aspects; their presence can improve texture and taste of food, but their growth and development can also cause illness. It is thus crucially important to understand the mechanisms of their growth and locomotion to control their influence on food products and living systems they inhabit. Even in the absence of a bulk fluid phase, aerosols can also transport microscopic passengers, such as bacteria or viruses. Cell motility is particularly important in infectious disease transmission [147], bacterial contamination by upstream swimming [622, 623], and the microbiology of bacterial coexistence [624]. Microbial dynamics are critical in food science, and intricate detector designs lead to sensors capable of detection of harmful microbes. For example, a porous silk microneedle array can be used to sense the presence of *E. coli* in fish fillets [625]. In general, a wide spectrum of potential pathogens stimulates research on diverse biosensors to provide the information necessary for food safety [626].

J. Microfluidics for improved food safety

Food borne pathogens such as *E. coli* and *Salmonella* bacteria cause approximately 420,000 deaths and 600 million illnesses yearly [627]. Such pathogens often originate from bacterial biofilms [628, 629] in food processing plants, and on-site rapid detection is therefore necessary to prevent these harmful bacteria from entering our grocery stores and ending up in foods. The traditional way of detecting pathogens is by cultivating them in petri dishes, but slow bacterial growth limits the usefulness of such 'babysitting' in food plants. This has led to alternatives such as nucleic-acid based methods (including polymerase chain reactions (PCR) [33], which is the primary method to test patients for COVID-19), but extensive training requirements, expensive equipment and labor intensive steps prevent a robust and efficient implementation in food production facilities.

Fortunately, microfluidic-based biosensors can detect or "sense" pathogens on much faster timescales thanks to small volumes and flow-mediated transport, with high-speed imaging enabling real-time monitoring [26, 28, 630]. Biosensors work by measuring an electrical or optical signal induced by a chemical reaction as a target molecule (pathogen) binds to a bioreceptor molecule [631, 632]. The bioreceptors are designed to exactly match the surface elements of the pathogen (these elements are called antigens) like a lock and key fit. Due to their excellent specificity, monoclonal antibodies (mAbs) are the most widely used bioreceptor molecules. Figure 20 shows the working principle a biosensor functionalized with Y-shaped mAbs molecules for detecting *E.coli* [633].

The speed and accuracy of surface-based biosensors de-

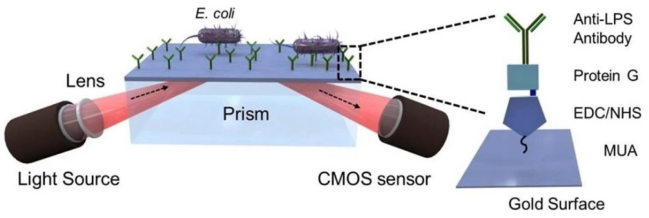

FIG. 20. Working principle of an optofluidic pathogen detector. When *E.coli* bind to Y-shaped mAbs molecules, it induces a shift in refractive index which can be detected by an optical sensor. From Tokel *et al.* [633].

pend on a number of factors where the most important are the pathogen concentration, the number of available binding sites on the sensor, the transport of pathogens from the bulk fluid to the sensor via flow and diffusion, and finally, the kinetics of the binding reaction. Without flow, the sensing time is usually limited by the time it takes for a pathogen or a virus to diffuse to the sensor, which can take several hours in a microchannel due to the low diffusivity of such large particles. However, by leveraging microfluidic flow, the solute transport can be sped up by several orders of magnitude, leading to reaction-limited kinetics. We recommend the pedagogical reviews on transport and reaction kinetics in surface based biosensors by Gervais and Jensen [634], Squires *et al.* [635] and Sathish and Shen [636].

K. Ice creams

Towards the end of the meal or on a hot summer day, ice cream comes to mind naturally. The origins of the creamy taste and crunchy texture are less obvious. The feeling results from the composition and an elaborate process of production. From a chemical point of view, ice cream is an emulsion [see §IV D] made with water, ice, milk fat and protein, sugar and air. The ingredients are mixed together and turned into foam upon the addition of air bubbles. The colloidal emulsion is then frozen to preserve the metastable mixture. The details of the process have been extensively studied within the food science community [637, 638], but also from the physics and general science viewpoint [639, 640]. Special attention has been paid to the colloidal character of the emulsion [641].

An appealing texture and rheology are crucial aspects of ice cream quality. Due to its popularity, ice cream was apparently the first food product to have its extensional viscosity measured, as early as in 1934 [642]. Since then, rheological properties of ice cream have been examined in detail, and various dynamical models have been proposed to account for their behaviour [643]. The breadth of related topics has even inspired an interdisciplinary undergraduate course taught within the physics programme [644].

The production of ice cream involves a flow undergoing a structural and phase transition by a combination of mechanical processing and freezing. The dynamics of ice crystallisation therein are not fully understood. Because an ice cream mix is opaque, *in situ* crystallisation has not been observed and its mechanism is debated [645]. In a typical ice cream freezer, ice is formed on externally cooled walls by surface nucleation and growth, and is then scraped off to the bulk fluid, where secondary nucleation and ripening take place [646]. The number and size of ice crystals formed is also heavily dependent on the mixture composition, and also affects the melting rate and hardness of the final food product [647]. Studying the characteristics of ice cream production leads to the development of novel methods for rapid freezing and thawing of foods [648]. Although the structure of ice cream can be practically controlled for a satisfactory product, a detailed description of the underlying complex growth process is still under development.

In contrast, one sometimes sees 'hot ice cream' that seems to melt upon cooling. This effect can be achieved using methyl cellulose, a thickener that acts in high temperatures to produce a product with surprising, 'opposite' melting properties [649].

VII. COFFEE: GRANULAR MATTER & POROUS MEDIA

The Hungarian probability theorist Alfréd Rényi (1921-1970) once said [650],

> A mathematician is a device for turning coffee into theorems.

In this section we will investigate the fluid dynamics of coffee. We start with the flow of coffee beans and other granular materials, including avalanches, hoppers, and the Brazil nut effect. We then consider brewing coffee using different methods in the context of porous media flows and percolation theory, and we finish with the illustrious coffee ring effect. In the words of Wettlaufer [481], there is a "universe in a cup of coffee".

A. Granular flows and avalanches

Granular materials [651] are found everywhere in the kitchen, including flour, rice, nuts, coffee beans, sugar and salt. Indeed, the food industry processes billions of kilograms of granular material every year [652]. They are composed of discrete, solid particles (grains) that feature across a wide range of sizes. Therefore, the grain diameter D is often denoted on the Krumbein phi scale, $\phi = -\log_2(D/D_0)$, with $D_0 = 1\,\mathrm{mm}$ [653]. For example, $\phi = -6$ and 6 correspond to oranges and powdered sugar, respectively.

Granular matter can have surprising properties [654, 655]. One example is the Janssen effect: The hydrostatic pressure at the bottom of a cylindrical container does

not grow linearly with the filling height of grains, unlike a liquid [see Eq. (1)]. Instead, the pressure saturates exponentially to a value much less than the weight of the grains, because they are partially supported by the vertical silo walls due to friction forces [656]. Another example is that granular matter can behave like solids, liquids, or even gases, depending on the amount of kinetic energy per grain [657–659]. For this reason, granular flows are hard to predict.

A notorious example thereof is avalanche dynamics [660–663]. A pile of grains [Fig. 21a] is held together by 'chains' of frictional and compressive forces [664], but the pile will suddenly collapse if the slope exceeds a maximum angle, θ_m. This sliding will only stop after the slope has reduced below the critical angle of repose, θ_r, of which typical values range between 45° for wheat flour to 25° for whole grains [665]. The angle of repose is important across food industry, from silo roof design to conveyor belt transport [666] and the geology of hillslopes [667] that limits farming. It also sets a fundamental rule for food plating, which in turn affects the perception of taste [668], and the design of food sculptures [Fig. 21b]. In this artwork the grains are sticky, but the weakest links are still susceptible to avalanche dynamics. From a fundamental point of view, avalanche dynamics exhibits self-organized critical (SOC) behaviour for rice grains with a large aspect ratio, as shown by Frette *et al.* [662]. Moreover, Einav and Guillard [669] used a column of puffed rice to investigate the crumbling of a brittle porous medium by fluid flow. These 'ricequake' experiments may give insight how to prevent the collapse of rockfill dams, sinkholes, and ice shelves. Needless to say, avalanches can be extremely dangerous, also in food science such as entrapment in grain storage facilities [670]. Thankfully there are helpful rescue strategies in case of grain entrapment [671].

Sometimes it is desirable to make granular matter flow faster. This can often be achieved with granulation [672], where a powder or small grains are made to clump together. Perhaps counter-intuitively, these aggregates can flow more easily. This has many important examples in the kitchen, such as granulated sugar: Compared to powdered sugar, granulated sugar has a smaller angle of repose and considerably better flow characteristics [673] because the larger grains are less cohesive and more easily fluidised [674]. Moreover, it is much easier to compactify granulated materials than powders, which is of vital importance for making tablets in the pharmaceutical and food industry [675]. Food for thought when you next sweeten your coffee.

B. Hoppers: grains flowing through an orifice

An important quantity across food science is how quickly a granular material can pass through an orifice [679]. Chefs experience this daily when dispensing spices or grains from a hopper. The flow rate Q is given empirically by the Beverloo law,

$$Q = C(\mu, \theta)\rho_b\sqrt{g}(D - kd)^{3/2}, \tag{72}$$

where the constant C depends on the friction coefficient μ and the hopper angle *theta*, where ρ_b is the grain bulk density, D is the neck width, d is the grain diameter, and the parameter $k \approx \mathcal{O}(1)$. This scaling relation can be explained partially by dimensional analysis and hourglass theory [680], but the foundations of the Beverloo law are still under active investigation, as discussed recently by Alonso-Marroquin and Mora [681]. This problem is hard to solve because the grains behave both like a liquid and a solid near the opening [682]. This is the result of jamming [683, 684], where the effective viscosity increases dramatically above a critical particle density, so the flowing grains suddenly form a rigid arch or vault [677], as shown in Fig. 21c,d. This clogging becomes exponentially unlikely as the opening size is increased, so all hoppers have a non-zero probability to clog [685]. Clogging is particularly common in grain hoppers [686] and microfluidic devices [687], but also sheep herds and pedestrian crowds moving through a bottleneck [688]. Jamming is equally

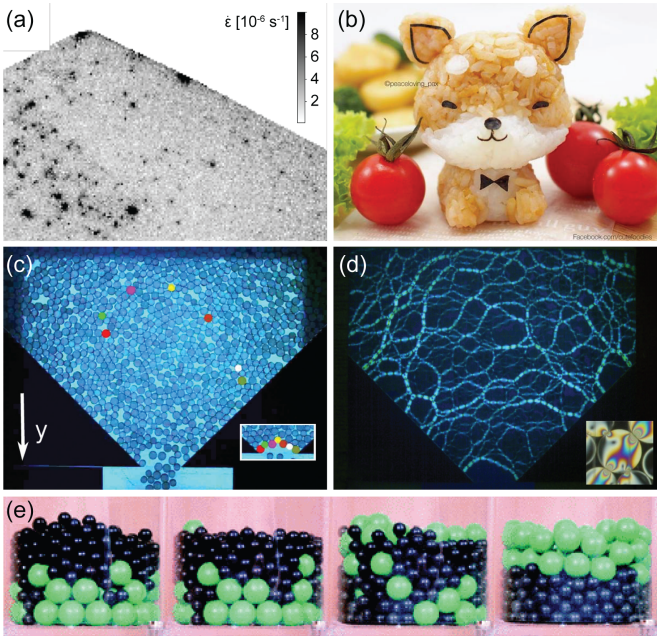

FIG. 21. Granular matter. **(a)** In a pile of grains, the motion is quantified by the rate of strain $\dot{\varepsilon}$ using spatially-resolved diffusing wave spectroscopy (DWS). From Deshpande *et al.* [667]. **(b)** Rice sculpture by doctor and food artist Nawaporn Pax Piewpun [676]. **(c)** The velocity field of grains flowing in a 2D hopper is measured by direct particle tracking. The seven particles that are marked in colour form a jamming arch, shown in the inset. **(d)** Force chains in a jammed state, visualised by photoelastic particles that show intensity fringes under stress, highlighted in the inset. From Tang and Behringer [677]. **(e)** The Brazil nut effect, with 8 mm black glass beads and 15 mm green polypropylene beads. Evolution in time from left to right. From Breu *et al.* [678].

essential for food processing [689], for biological tissue development [690] and for food structuring [691].

The non-linear nature of jamming can lead to surprising consequences. For example, the observed flow rate does not depend on the filling height of the hopper [Eq. (72)]. This was assumed to be due to the Janssen effect [§VII A], but Aguirre *et al.* [656] showed that the grain flow rate remains constant even if the pressure at the orifice decreases during discharge, and that different flow rates can be achieved with the same pressure. More counterintuitively, inserting an obstacle just above the outlet of a silo can in fact help with clogging reduction [692]. Not least, 'the sands of time run faster near the end', which is caused by a self-generated pumping of fluid through the packing [693]. You may want to take this into account for your kitchen timer. By varying the softness of the grains, Tao *et al.* [694] showed that clogging occurs more often for stiffer particles, and that clogging arches are larger for particles with larger frictional interactions. Understanding jamming dynamics can help with the design of clog-free particle separation devices [695].

C. Brazil nut effect

When you repeatedly shake a box of cereal mix, the larger (and heavier) grains often rise to the top. This phenomenon was called the 'Brazil nut effect' after the seminal work by Rosato *et al.* [696], also known as granular segregation [652, 697, 698]. One explanation is buoyancy, but the effect can happen even when the larger grains are denser than the smaller ones. A second contributing factor is called percolation (not to be confused with §VII D), where smaller grains fall into the gaps below the larger grains during shaking. However, a container shape can be designed where the larger grains move downwards [699]. This was explained by a third effect called 'granular convection', where the shaking leads to a flow pattern of grains moving upward along the walls and downward in the middle of the container [699]. Soon after, granular convection was imaged directly using Magnetic Resonance Imaging (MRI) [700, 701] and extensive computer simulations [702]. However, the scientific trail was mixed up again by the discovery of the 'reverse Brazil nut effect' by Shinbrot and Muzzio [703], verified experimentally by Breu *et al.* [678]. Here larger but lighter particles can sink in a shaken bed of smaller grains, which cannot be explained by granular convection alone, nor by percolation nor buoyancy. Furthermore, Möbius *et al.* [704] showed that particle segregation depends on the interstitial air between the grains, and depends non-monotonically on the density. Huerta and Ruiz-Suárez [705] then found that there are two distinct regimes: At low vibration frequencies, inertia and convection drive segregation, where inertia (cf. convection) dominates when the relative density is greater (cf. less) than one. At high frequencies, segregation occurs due to buoyancy (or sinkage) because the granular bed is fluidised and convection is suppressed.

Interestingly, granular convection can occur even in very densely packed shaken containers, on the brink of jamming, where unexpected dynamic structures can arise under geometrical restrictions [706]. Murdoch *et al.* [707] studied granular convection in microgravity during parabolic flights, revealing that gravity tunes the frictional particle-particle and particle-wall interactions, which have been proposed to drive secondary flow structures. Recently, D'Ortona and Thomas [708] discovered that a self-induced Rayleigh-Taylor instability [see §III A 4] can occur in segregating granular flows, where particles continuously mix and separate when flowing down inclines.

Granular separation is of vital importance in the food industry. It might be convenient if grains need to be sorted, but the effect is often undesirable when we require an even grain mixture. This is especially problematic when the product must be delivered within a narrow particle-size distribution or with specific compositions of active ingredients [652]. However, most food storage facilities (heaps or silos) and processing units (chutes or rotating tumblers) are prone to grain segregation [709]. Researchers are learning how to prevent separation, but this is hard because it strongly depends on details of the flow kinematics. One technique is to add small amounts of liquid to make the grains more cohesive [710], but at the cost of reduced food longevity due to rot. Another strategy is to use modulation of the feeding flow rate onto heaps [711]. The Brazil nut effect might also be suppressed using a system with cyclical shearing, where grains remain mixed or segregate slowly [712]. There are also new developments in machine vision systems for food grain quality evaluation [713]. Granular flows are often hard to image with opaque particles, but powerful techniques to measure the 3D dynamics is using MRI [700], Positron Emission Particle Tracking (PEPT) [714] or X-ray Computed Tomography (CT) [715].

In the kitchen, the Brazil nut effect may occur too when stir-frying. Chefs often toss the ingredients into the air repeatedly, fluidising the grains, to mix them evenly and to avoid burning them at very high temperatures. Ko and Hu [716] recently described the physics of tossing fried rice. There is also an interesting connection with the physics of popcorn [717]

D. Brewing coffee: porous media flows

Henry Darcy (1803-1858) was a French hydrologist who studied the drinking water supply system of Dijon, a city also known for its mustard. In an appendix of his famous publication [720], he describes experiments on water flowing through a bed of sand. From the results he obtained Darcy's law, an empirical expression for the average velocity $\boldsymbol{q}$ of the liquid moving through the bed. It was refined by Muskat [721], and can be written as

$$\boldsymbol{q} = -\mathcal{K}(\boldsymbol{\nabla} p - \rho \boldsymbol{g})/\mu, \tag{73}$$

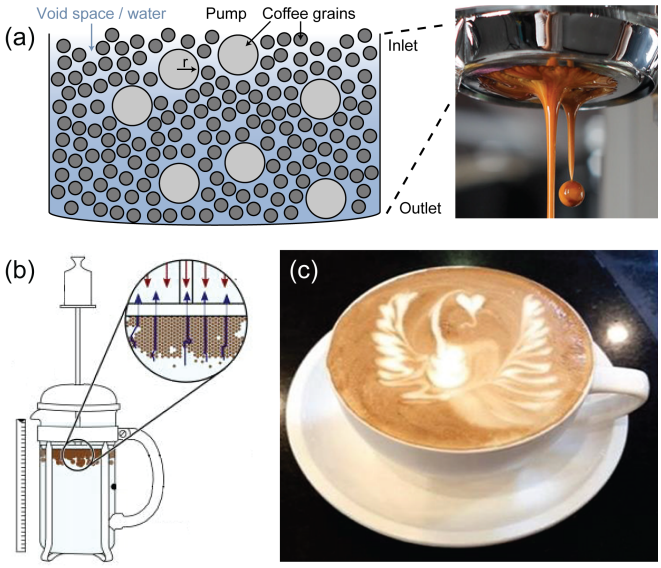

FIG. 22. Coffee brewing. **(a)** Schematic of percolation in an espresso machine basket. A pressure differential pushes water down through the pore spaces. Image courtesy of Christopher H. Hendon. Inset: Espresso drops by photographer theferdi, licensed under CC BY-NC-SA 2.0. **(b)** Diagram of a French press. The water moves up around the coffee grounds (blue arrows) by applying a constant gravitational force on the plunger (red arrows). From Wadsworth *et al.* [718]. **(c)** A cappuccino with latte art in the shape of a phoenix. From Hsu and Chen [719].

where $\mathcal{K}$ is a tensor that describes the permeability of the material in different directions, sometimes replaced by a constant k for isotropic materials. Note that the local velocity in the pores is $\boldsymbol{u} = \boldsymbol{q}/\phi$, where $\phi \in [0, 1]$ is called the porosity. Darcy's law can indeed be derived theoretically [722], and it is integral to many industrial processes in food science, such as sand filtration and antimicrobial water treatment [723, 724]. Moreover, it can be applied to a much broader class of porous media flows [725–727], which are found everywhere in gastronomy: Examples include percolation in a salad spinner, drizzle cake, squeezing a sponge, and not least, making coffee [728, 729].

For espresso brewing [see e.g. 730], one can use the first term in Darcy's law for pressure-driven flow [Fig. 22a], while drip coffee [see e.g. 731] can be described using the second term for gravity-driven flow in Eq. (73). In both cases, the permeability $\mathcal{K}$ can be changed by tamping the grounds or adjusting the grain size, in order to tune the flow rate and thus the extraction time [732]. Another particularly well-studied method of making coffee is using the Italian 'moka' pot [see Fig. 1c]. Its sophisticated design was patented by Alfonso Bialetti (1888-1970) [733]. Gianino [734] used a moka pot to measure the flow rate through a bed of grains and applied Darcy's law to measure its permeability. Later, Navarini *et al.* [50] improved this method by accounting for the decreasing permeability as aromatic substances dissolve into water. In a third study, King [735] investigated the effect of packing and coffee grain temperature on the permeability. Percolation in a moka pot was visualised beautifully by looking through the metal using neutron imaging [736].

Most studies on coffee extraction showcase some direct applications of Darcy's law under idealized conditions, but they do not attempt a description beyond the Darcy regime [737]. For instance, they ignore the initial stage of percolation, when the water invades the (initially dry) coffee grain matrix. This process can be described with percolation theory [738], where the pores between the coffee particles can be considered as a random network of microscopic flow channels [727]. If the coffee is coarsely ground or tamped lightly, the many open microchannels (bonds) allow the water to find a connecting path through the coffee. Then this process is first characterised by capillary wetting [739] [§II G], after which Darcy's law becomes applicable. For intermediate tamping, as the permeability $\mathcal{K}$ decreases, we approach the percolation threshold. Then the extraction time will significantly increase, which can result in over-extraction [740]. Finally, if the coffee is tamped too strongly or too finely ground, the water cannot find a path between the grounds. Then, either there is nothing to drink, or the pressure builds up until we see hydraulic fracturing [741]. In that case, large flow channels suddenly crack open that bypass the microchannels [742]. This 'fracking' can give the coffee a bad taste because it leads to an uneven extraction. Symptoms that your espresso is fractured are liquid spraying through the bottom of the basket, irregular flow, and a cracked coffee cake. Percolation theory has many other applications, including predictions for forest fires, disease spreading, and communication in biology [743, 744].

Coffee can be made in many ways, each involving different fluid mechanics. Here we only mention a few preparation methods, with some recent results: To make an espresso, it is important to note that coffee beans are often prone to variations in quality. Even if the theory is perfect, the ingredients are not. To overcome this, Cameron *et al.* [745] offer advice to systematically improve espresso brewing by proposing a set of guidelines towards a uniform extraction yield. Interestingly, they also found that the smallest grains do not give the highest yield as they tend to clump together and form aggregates [see granulation in §VII A]. For drip brew coffee it is common to use a precise temperature-controlled kettle, but Batali *et al.* [746] surprisingly found that the brew temperature may not have quite so much impact on the sensory profile at fixed brew strength and extraction. Considering the French press, Wadsworth *et al.* [718] recently determined the force required to operate the plunger [Fig. 22b]. They recommend using a maximum force of 32 N to complete the pressing action in 50 s, using 54 g of coffee grounds for 1 l of boiling water. Looking at cold brew coffee, Cordoba *et al.* [747] recently evaluated the extraction time and flavour characteristics, and Rao and Fuller [748] investigated its acidity and an-

tioxidant activity. Finally, Greek and Turkish coffee rely on the sedimentation of fine particles, which we discuss in §VI C.

After having made the perfect cup, it can be decorated with latte art [Fig. 22c]. Indeed, Hsu and Chen [719] showed that coffee tastes sweeter with latte art, which they related to brainwave activity using electroencephalography (EEG). The fluid mechanics of pouring steamed milk foam into the denser coffee can be described as an inverted fountain [see §III A], which depends on the jet diameter and the pouring height via the Froude number [Eq. (19)]. Large fountains lead to more mixing and brown foam, while gentle pouring gives white foam. After much practice, these colours can be combined in rapid succession to make exquisite patterns, including a heart and the phoenix [749]. Some people prefer their coffee without milk, but with a thin layer of espresso crema [750]. Undesirably, this coffee foam can agglomerate along the perimeter. This effect can often be suppressed by heating the cup beforehand since it is caused by Bénard-Maragoni convection, which we discuss in the next section.

E. Coffee ring effect

When the last sip of coffee or wine is left overnight, it dries out creating a stain with a brighter interior and much darker borders, where most residues are deposited, see Fig. 23. The coffee ring effect, as it has been termed, can be observed in almost any kitchen mixture containing small particles. As explained by Deegan *et al.* [754], the coffee ring effect results from the drying dynamics of a droplet, combined with the pinning of its contact line with the substrate [755, 756]. As the solvent evaporates, the outflow of matter decreases the thickness of the droplet at every point. If the contact line was not pinned, the droplet would shrink. This additional constraint, together with the surface tension requirement to keep the contact angle fixed [see §II G], induces an outward flow from the interior to replenish the evaporated liquid at the borders. This flow transports the sediment, which is then deposited at the outer ring, leaving the lower-concentration interior.

Instead of a solid particle suspension, the coffee ring effect also emerges if the dissolved component is another liquid. In that case, the edge of the puddle remaining after a volatile solvent evaporates forms either "fingers" or spherical "pearls", or some combination of the two [757]. Understanding the underpinning dynamics of coffee ring formations remain an active research topic. An example of the many excellent publications in recent years is the study by Moore *et al.* [758] on the effects of diffusion of solute from the pinned contact line to the bulk of the drop on the pattern formation.

Interestingly, by adding some alcohol to the drop to make it more volatile, the coffee ring effect can be suppressed by consequential Marangoni flows from the contact line to the drop's interior [759]. These flows are induced by a surface tension gradient along the surface of the drop [see §III B], which is in turn caused by nonuniform cooling as the droplet evaporates, because the surface tension increases as the temperature decreases. This is referred to as Bénard-Marangoni convection. The deposition pattern then depends on the strength of the relative magnitude of thermocapillary stresses to viscous ones, as expressed by the dimensionless Marangoni number, Ma, as defined in Eq. (23) with $\Delta\gamma = (\partial\gamma/\partial T)\Delta T$. For large Ma, the particles end up in the center, for intermediate Ma, they are deposited evenly along the substrate, while for small Ma, the coffee ring ring effect is fully recovered. Therefore, by tuning Ma, for example through tuning the alcohol percentage in the coffee, it is in principle possible to control the deposition pattern. Moreover, the coffee-ring effect can be suppressed by shape-dependent capillary interactions [760, 761].

The applications of the coffee-ring effect and the drying of thin colloidal films in general go far beyond kitchen experiments [756, 762]. For example, it is the basis of

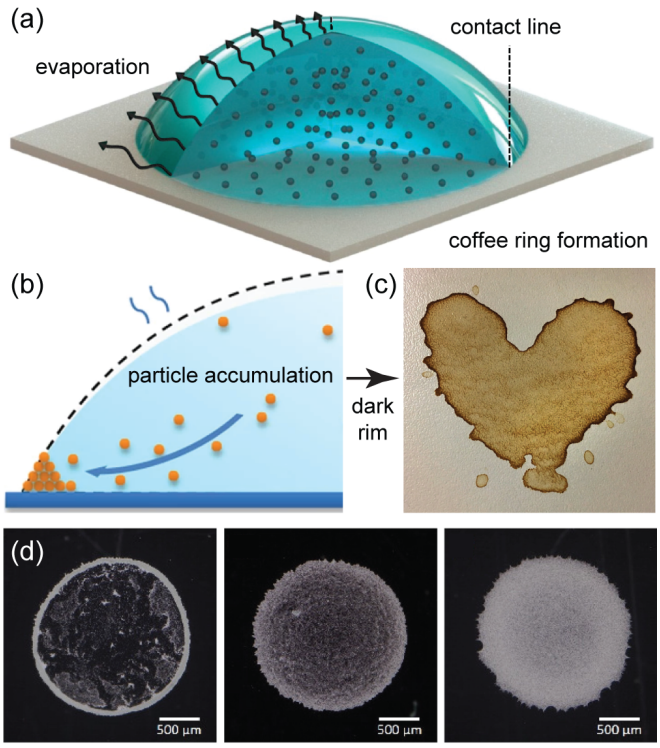

FIG. 23. Coffee ring effect. **(a)** Schematic of an evaporating droplet containing a suspension of microparticles. Stronger evaporation near the contact line drives an internal flow to the outer edge. From Jafari Kang *et al.* [751]. **(b)** A dark rim is formed by particles that accumulate at the pinned contact line. From Li *et al.* [752]. **(c)** Example of a heart-shaped coffee ring. Image by Robert Couse-Baker, licenced under CC BY 2.0. **(d)** Suppressing the coffee ring effect by adding cellulose nanofibers (CNF) to a drop of 0.1 wt% colloidal particles. From left to right: CNF concentration of 0, 0.01, 0.1 wt%. From Ooi *et al.* [753].

Controlled Evaporative Self-Assembly (CESA), which is used to create functional surfaces with controllable features [763]. The coffee-ring effect can also be used for controlled inkjetting of a conductive pattern of silver nanoparticles [764], and particle deposition on surfaces could be controlled further by light-directed patterning by evaporative optical Marangoni assembly [765]. Moreover, the effect can be used for nanochromatography to separate particles such as proteins, micro-organisms, and mammalian cells with a separation resolution on the order of 100 nm [766]. Interestingly, the growth dynamics of coffee rings are altered when active particles such as motile bacteria move around in the evaporating droplet [767–770], and bacterial suspensions can feature acive depinning dynamics. Hence, in the spirit of frugal science, it might be possible to exploit the coffee ring effect to detect antimicrobial resistance [771].

VIII. TEMPEST IN A TEACUP: NON-LINEAR FLOWS, TURBULENCE AND MIXING

What is turbulence? This intriguing question has fascinated fluid mechanicians throughout history. Leonardo da Vinci already eluded to two important properties of turbulence [772]: The generation at large scales, and the destruction due to viscosity at the smallest scales. The many scales of motion in turbulence is arguably its main signature; for example, a volcanic plume spans over several kilometers, with eddies all the way down to the Kolmogorov microscales [773]. As the turbulent structures break up, energy is transferred from large whirls to smaller ones. The poem by Richardson [774] beautifully describes this energy cascade:

> *Big whirls have little whirls*
> *That heed on their velocity,*
> *And little whirls have littler whirls*
> *And so on to viscosity.*

The consequences of turbulence are numerous in our lives of gluttony. It gives us the characteristic sound of a kettle whistle, it helps with mixing milk into our tea, and it gives us some frictional losses when biking home from the restaurant. In this section, we will catch a whiff of turbulence in the kitchen.

A. Tea leaf paradox

Before diving into chaotic realms, we consider the surprising effects that the non-linearity of the Navier-Stokes equations [Eq. (2)] can bear in laminar flow. One such surprises is the "tea leaf paradox". Biological tissues tend to be denser than water [775], thus soaked tea leaves will sink to the bottom of a cup. When the water is stirred around in circles, the leaves are expected to move towards the edge of the cup because of centrifugal action. The opposite happens, however: The leaves always migrate to the center of the cup, as seen in Fig. 24a. Thomson [776] first recognised that the solution of this paradox stems from 'friction on the bottom'. Later, Einstein [777] gave a detailed description of the tea leaf experiment itself, in order to explain the erosion of riverbanks. A d etailed theoretical treatment was provided later by Greenspan and Howard [778].

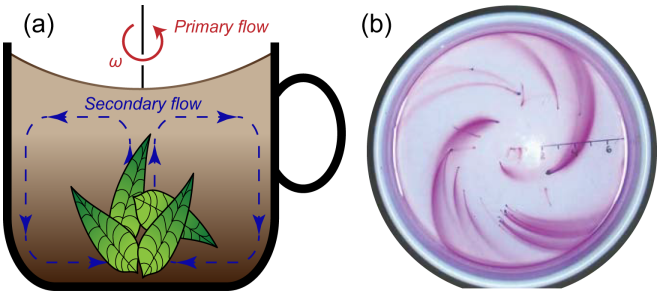

FIG. 24. Tea leaf effect due to secondary flows. **(a)** Illustration. After stirring the tea, the rotating liquid (primary flow) slowly comes to a halt because of friction with the walls (spin-down). This friction also induces a toroidal recirculation (secondary flow) directed outwards at the top and inwards at the bottom, which causes the leaves to collect in the center. **(b)** Spiral dye streaks due to secondary flows in a cake pan. Instead of slowing down, the liquid is rotated increasingly faster (spin-up), so the secondary flow is reversed, such that the dye spirals outwards at the bottom of the cake pan. From Heavers and Dapp [779].

The paradox is resolved with fluid mechanics, as follows: As the liquid rotates in the cup, the first approximation of the fluid flow is just a solid-body rotation. Specifically, we have $\boldsymbol{u} = \boldsymbol{\Omega} \times \boldsymbol{r}$ with a uniform angular velocity $\boldsymbol{\Omega}$. On the fluid acts a centrifugal force, $\boldsymbol{F}_c \propto \boldsymbol{\Omega} \times (\boldsymbol{\Omega} \times \boldsymbol{r})$. If Ω is constant in space, then this force does not modify the flow. However, frictional drag with the cup walls slows the fluid down in the boundary layer. In particular, near the bottom surface the angular velocity $\boldsymbol{\Omega}(\boldsymbol{r})$ and thus the centrifugal force will be less than near the top water-air interface. Consequently, an in-up-out-down recirculation emerges [Fig. 24a] as the liquid slowly stops spinning. Interestingly, this recirculation can also be reversed [Fig. 24b], when the liquid is rotated increasingly faster (spin-up) from rest [778, 780].

The tea leaf effect has many applications. In the kitchen, it can be applied conveniently when poaching eggs [779, 781]: Before cracking the egg into the pot, the hot water can be gyred to keep the egg whites together at the center of the pot. But be quick, because the flow ceases after a time

$$\tau_E \sim \sqrt{\frac{H^2}{\nu\Omega}}, \tag{74}$$

called the Ekman time [778, 782], in terms of the kinematic viscosity ν and H is the height of the liquid layer, the depth. The same technique is also used to separate out trub during beer brewing [783], and to separate blood

cells from plasma in microfluidics [784]. Also in geophysical flows, the same in-up-out-down circulation is seen in tornadoes [785]. In modern additive manufacturing (AM) technologies, the Ekman time sets a limit to how quickly objects can be 3D printed [786].

B. Secondary flows

When discussing the tea leaf paradox, we saw that frictional drag with the surfaces induces a flow structure on top of the initial rigid body motion. More generally, it is a very powerful concept to understand fluid flows in terms of a 'primary flow', guessed from simplified or basic physical principles, and a 'secondary flow', a correction due to high-order effects such as obstacles in the main flow. Care must be taken with such superpositions, since the Navier-Stokes equations are non-linear, but often perturbation methods can be followed [787].

Another classic example of a secondary flow is the emergence of Dean vortices in a curved pipe [788]. Starting from a straight Poiseuille flow [see §II C], the vortices can be explained using a perturbation method accounting for centrifugal forces [789, 790]. The relative strength of the secondary flow is determined by the balance between inertial and centrifugal forces with respect to viscous forces, which is given by the Dean number,

$$\mathrm{De} = \mathrm{Re}\sqrt{R_p/R_c}, \tag{75}$$

where Re is the Reynolds number [Eq. (5)], R_p is the radius of the pipe, and R_c its radius of curvature. For small Dean numbers the flow is unidirectional, for intermediate values Dean vortices emerge, and for large De the flow turns turbulent [791]. This is directly applicable to separating particles by size using inertia [792]. These vortices also emerge naturally in straight channels when two stratified fluid layers such as air and water flow through them [793], which is associated with huge pressure losses in (food) industrial pipelines. On the flip side, Dean vortices may be used along with UV-C to inactivate microoganisms in fruit juices [794].

Similar calculations can be performed to study secondary flows in turbomachinery compressors and turbines [795], and oceanic and atmospheric currents with Ekman layers [782, 796, 797]. Ekman layers are associated with transport of biomaterials in the ocean through so-called Ekman transport processes. The secondary flow pattern of Ekman transport can lead to upwelling and downwelling of algae. A thorough understanding of the underpinning mechanisms is crucial to mitigate the devastating implications of harmful algal blooms. Secondary flows can also contribute to bridge scour [798], by the removal of sediment such as sand and gravel from around bridge abutments or piers, leading to one of the major causes of bridge failure around the world.

C. Turbulent jets emanating from tea kettles

When the water in the tea kettle boils, a turbulent jet of steam emerges from the spout with a conical profile [Fig. 25a]. To describe the dynamics of a turbulent jet, it is useful to decompose the velocities into an average and a fluctuating component. This averaging procedure is named after its inventor, Osborne Reynolds (1842-1912), and is written as $u_i = \bar{u_i} + u_i'$ with $i=\{x, y\}$ for the velocity components in two dimensions [799]. By Reynolds averaging we arrive at the famous equation for the conservation of momentum in turbulent flow,

$$\frac{\partial \bar{u_i}}{\partial t} + \bar{u_j}\frac{\partial \bar{u_i}}{\partial x_j} + \overline{u_j'\frac{\partial u_i'}{\partial x_j}} = -\frac{1}{\rho}\frac{\partial \bar{p}}{\partial x_i} + \nu\frac{\partial^2 \bar{u_i}}{\partial x_j^2}, \tag{76}$$

using Einstein notation. The third term is an apparent stress due to turbulent fluctuations, and the remaining ones are the averaged transport terms in the Navier-Stokes equation [see §II B], where the last (viscous stress) term can be neglected in inertia-dominated flows. Interestingly, the flux of momentum remains constant beyond a certain distance from the spout [560]. To maintain its momentum, the jet must continually entrain ambient air. This is why blowing on a finger burnt by a hot kettle has a cooling effect.

Moreover, fluid jets tend to follow a convex surface, rather than being scattered off, which is called the Coanda effect [800]. This is sometimes demonstrated by extinguishing a candle by blowing around a tin can. Similarly, when a steam kettle jet curves around another pot, it can pose an unexpected safety hazard. An interesting application is robotic food processing using Coanda grippers [801]. The Coanda effect should not be confused with the teapot effect [802–804], where a liquid follows a curved surface like a teapot spout [Fig. 25b], because this flow is dominated by surface tension and wetting [§II G]. While the teapot effect can cause a mess when pouring too slowly, it can be advantageous for coating or making complex shapes [805], perhaps in novel culinary decorations.

Other examples of turbulent jets include the stripes produced by air crafts. According to one study [806], this warms the planet even more than the carbon emitted by the jet engines, but fortunately it seems these effects can be mitigated by avoiding certain altitudes [807]. In any event, when flying it is best to steer clear off plumes, such as those emanating from smoke stacks or volcanoes. As part of a safety assessment, we can use the predictions by Taylor [808] for the shape and final height of such plumes. Taylor's theory is valid across many length scales: It could equally be used to estimate the shape of a plume rising from a cup of coffee [Fig. 18].

D. Sound generation by kitchen flows

The tea kettle we just discussed can make a pleasant whistle sound [809, 810]. As described by Lord Rayleigh

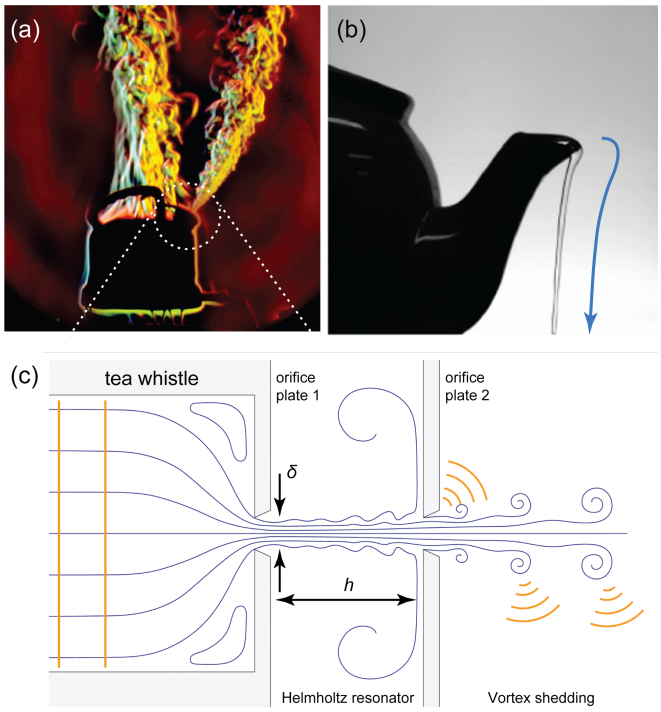

FIG. 25. Tea time. **(a)** A turbulent jet emanating from a tea kettle. Image courtesy of Gary S. Settles. **(b)** The teapot effect, showing a liquid stream following the curved surface of the spout (blue arrow). Pouring any slower will make the liquid stick to the pot entirely. From Scheichl *et al.* [804]. **(c)** Diagram of a tea kettle whistle. The steam passes through two orifice plates from left to right. From Henrywood and Agarwal [809].

[811], sound is carried by pressure waves that propagate according to the wave equation,

$$\frac{\partial^2 p}{\partial x^2} - \frac{1}{c^2}\frac{\partial^2 p}{\partial t} = 0, \tag{77}$$

where the speed sound $c \sim 343\,\mathrm{m/s}$ in air. Sir Isaac Newton (1642-1726) was the first known to measure the speed of sound, as reported in his book on classical mechanics *Principia* [812]. Since then many creative attempts to measure this quantity have been reported, including the accurate experiments by the Reverend William Derham (1657-1735) involving a telescope and gunshots [813]. According to Lord Rayleigh [814], the parameters determining the sound generation of a whistle are a characteristic length scale, L_0, the frequency, f_0, the fluid (steam) viscosity, ν, and the steam jet velocity, U_0. They form two dimensionless groups, namely the Strouhal number,

$$\mathrm{St} = \frac{\text{Time scale of background flow}}{\text{Time scale of oscillating flow}} = \frac{f_0 L_0}{U_0}, \tag{78}$$

and the Reynolds number [Eq. (5)]. Henrywood and Agarwal [809] found that for a typical tea kettle with two orifice plates [Fig. 25c], the frequency giving rise to the sound generation is sensitive to the jet diameter, δ, and not the plate separation distance, so L_0 is replaced with δ. Furthermore, the same authors found that the whistle's behaviour is divided into two regions: For $\mathrm{Re}_\delta \lesssim 2000$, the whistle operates like a Helmholtz resonator, with an approximately constant frequency (pitch). However, above a critical Reynolds number, $\mathrm{Re}_\delta \gtrsim 2000$, the whistle's tone is determined by vortex shedding [815], with a frequency that increases with U_0 at an approximately constant $\mathrm{St}_\delta \approx 0.2$. Vortex shedding also occurs for cables or tall buildings in strong wind, which can be destructive if the aerodynamic driving frequency resonates with the structural eigenmodes [816]. To prevent damage from happening, newer buildings are designed to have several eigenfrequencies to effectively dissipate the energy, or to have roughness elements, as perfected by the glass sponge *Euplectella aspergillum* [817]. The sound of the tea kettle whistle might inspire you to whistle for yourself while stirring your tea [§VIII A]. The physiology of mouth whistling was discussed by Wilson *et al.* [818], Azola *et al.* [819], Shadle [820].

Plink. plink. plink. Another kitchen sound is the maddening noise of a leaky tap [821, 822]. The paradox how a single drop impacting on a liquid surface can be so loud, compared to a more energetic continuous stream, is still not fully understood. Franz [823] already discussed that the droplet can entrain air bubbles, which oscillate to make sound at a frequency $f = (1/2\pi a)\sqrt{3\gamma p_0/\rho}$ given by Minnaert [824], where a is the bubble radius, γ is the ratio of specific heats of air, and p_0 is the pressure outside the bubble. However, not every drop makes a sound. Longuet-Higgins [825] and Oguz and Prosperetti [826] developed the first detailed analytical models to explain this in terms of the Froude number [Eq. (13)] and the Weber number [Eq. (14)] given the droplet radius and impact velocity. The sound volume is set by the wave amplitude, but how does sound generated underwater cross the water-air interface? Prosperetti and Oguz [827] reviewed the underwater noise of rain, and Leighton [828] discusses whether goldfish can hear their owners talking. Looking at the dripping tap, Phillips *et al.* [829] tested previous theories by comparing sound recordings with direct high-speed camera imaging. They write that the airborne sound field is not simply the underwater field propagating through the water-air interface, but that the oscillating bubble induces oscillations of the water surface itself, which could explain the surprisingly strong airborne sound. Plink.

It is impossible to cook without making noise, often to the extend of breaking the sound barrier. Indeed, we already mentioned the supersonic 'pop' made by cracking open a Champagne bottle [§III E]. Similarly, supersonic shock waves can be generated by snapping a tea towel [830, 831]. Dropping an object in a filled kitchen sink can also create a supersonic air jet [832]. By investigating the popping sound of a bursting soap bubble, Bussonnière *et al.* [833] found a way to acoustically measure the forces that drive fast capillary flows. Not least, numerous situations in food science involve hydrodynamic

cavitation [834, 835], which can produce flashes of light called sonoluminescence [836, 837] with internal temperatures reaching thousands of degrees Kelvin [838].

The hot chocolate effect [839] occurs when heating a cup of cold milk in the microwave, mixing in cocoa powder, and tapping the bottom with a spoon: The sound pitch initially descends by nearly three octaves, comparable to the vocal range of an operatic soprano, after which the pitch gradually rises again. This happens because air is less soluble in hot liquids, so it becomes supersaturated with heating, and adding a fine powder provides nucleation sources for fine bubbles. Air is more compressible than water, which lowers the speed of sound, and thus the pitch. The same musical scales are heard when opening a fresh beer [840], which is supersaturated with CO_2 [§III E]. The hot chocolate effect was visualised directly by Trávníček *et al.* [841].

E. Making macarons: chaotic advection

A milk droplet with diffusivity $D \sim 10^{-9}\,\mathrm{m}^2/\mathrm{s}$ takes a long time to mix in a cup of coffee in the absence of fluid motion, typically $\tau = L_0^2/D$, so days, and slower than the diffusion of heat [§V D]. However, stirring reduces the mixing time dramatically, down to seconds, as turbulent eddies stretch the drop into thin filaments so diffusion can act efficiently [842]. Moreover, hydrodynamic instabilities [§III A] can lead to turbulence, which enhances the mixing rate by maximizing the exposed surface area and the concentration gradient between adjacent fluids [199]. However, turbulence does not occur in viscous fluids at low Reynolds numbers [§II D]. Here, mixing can be achieved by stretching and folding lamelles of one fluid into another through 'chaotic advection' [843–845].

A culinary example of chaotic advection is making macarons, where a viscous batter must be mixed gently to maintain its foam structure [846]. The choice of stirring protocol has a dramatic impact on the mixing rate: If we move a rod back and forth, we see no mixing at all because of the scallop theorem [548]. Thus, we must break time-reversal symmetry, so we change our strategy and stir in circular patterns instead. Now the fluid does mix, but slowly, because it is stretched only linearly. Next, we stir in figure-of-eight patterns [847] [see Fig. 26a], which speeds up the mixing rate dramatically as this strategy yields exponential stretching [848]. This can also be achieved by rotating two rods, at the same speed but in opposite directions, as in commercial egg beaters [849].

A particularly efficient mixing protocol is the 'blinking vortex' [843], where two rotors alternately spin in the same direction. For the first half period, the first rod rotates while the other one is stationary, then vice versa. A task that could perhaps be performed by a cooking robot [850]. This canonical and time-periodic blinking vortex is used ubiquitously in chaotic mixing theory to compare the effectiveness of different mixing protocols [851].

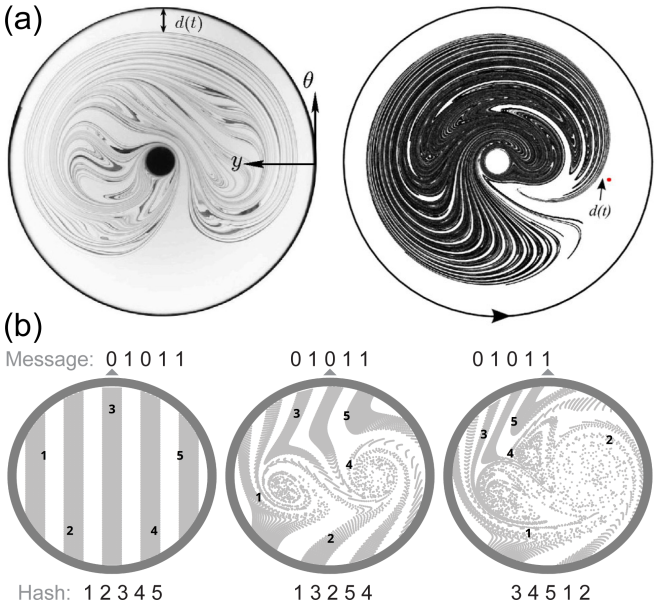

FIG. 26. Chaotic stirring protocols can be used for a broad range of applications, from making macarons to cryptography. **(a)** Experiment (left) and simulation (right) of the figure-of-eight stirring protocol used to mix a blob of dye in sugar syrup. From Thiffeault *et al.* [847]. **(b)** Chaotic advection used to create a digital message hashing function. Image courtesy of William Gilpin.

Similarly, the Arnold-Beltrami-Childress (ABC) flow is often considered the archetypal flow for many studies on chaotic advection in 3D [845]. Besides expedient cooking, chaotic advection has numerous applications in other disciplines [852]. For example, Gilpin [853] used a blinking vortex model to create digital hash functions with potential applications in cryptography [Fig. 26b].

By adding another pair of counter-rotating rods, for example by using two eggbeaters, one obtains the famous 'four-roll mill'. This concept was invented by Taylor [854] to study the formation of emulsions [§IV D]. Oil drops immersed in golden syrup (ideal for baking) were placed at the center of the mill, in a stagnation-point flow, which elongates them. The drops split when the viscous stresses on their surface exceed the stabilising surface tension, as described by the capillary number,

$$\mathrm{Ca} \equiv \frac{\text{viscous stresses}}{\text{surface tension}} = \frac{\mu U_0}{\gamma}, \tag{79}$$

where the characteristic velocity, $U_0 = \dot{\gamma} L_0$, can be written as the local shear rate times the droplet size. The four-roll mill laid the basis for studies of droplet breakup and stability, but fluctuating stagnation points made practical implementation difficult. To alleviate this issue, Bentley and Leal [855] implemented an image-based feedback loop that controlled the speed of each roller independently. Using their invention, the same group [856] validated theoretical limits for drop deformation [857, 858] and paired their experiments with theory for

studying drop dynamics [859]. The flow fields generated by the automated four-roll mill also pioneered polymer elongational rheometry [860, 861]. More recently, Hudson *et al.* [862] introduced the microfluidic analogue of the four-roll mill. This device been used extensively to characterise the material properties of biomaterials and single cells by extensional rheometry [863], and in applications of stagnation point flows in microfluidics have been extended to include substrate patterning [864–866] and the trapping of cells by hydrodynamic confinements, allowing new developments in analytical chemistry and in life sciences [867].

F. Sweetening tea with honey: mixing at low Re and high Pe

Returning to the mixing of two liquids, we now make a cup of tea sweetened with a drop of honey. By pure dissolution, a viscous drop mixes slowly with the tea, but stirring can help us again. However, since the drop is very viscous, turbulent eddies cannot stretch the drop into thin filaments, as was the case with much less viscous milk drops [see §VIII E]. Instead, the sharp flow velocity gradients around the drop increase the mass transfer by maintaining a correspondingly sharp concentration gradient [868].

We seek an estimate of the mixing time. We consider a honey drop of size $L_0 \sim 1\,\mathrm{mm}$ and diffusivity $D \sim 10^{-10}\,\mathrm{m}^2/\mathrm{s}$ in water [869]. We also assume a very viscous honey drop, so the mass transport is dominated by advection due to large Schmidt numbers [Eq. (51)]. Using a stirring speed of $U_0 \sim 1\,\mathrm{mm/s}$, the Péclet number [Eq. (48)] is large, $\mathrm{Pe} \sim 10^4$, but the flow close to the drop is still laminar at an intermediate Reynolds number, $\mathrm{Re} \lesssim 1$. Then, as the drop dissolves, a diffusion layer develops between the pure phases. Acrivos and Goddard [870] showed that, in the low Reynolds number and high Péclet number limit, this diffusion layer has thickness

$$\delta \sim L_0 \mathrm{Pe}^{-1/3}. \tag{80}$$

In our case, at high Pe, the boundary layer is rather thin, $L_0/\delta \sim 20$. By substituting δ for L_0 in the expression for the diffusion time, $\tau_D \sim L_0^2/D$, following Mossige *et al.* [871], we obtain a typical mixing time

$$\tau_{\mathrm{mix}} \sim (L_0^2/D)\mathrm{Pe}^{-2/3}. \tag{81}$$

By inspecting this expression, we can immediately appreciate the dramatic effect of fluid flow: It can reduce the mixing time by a factor of a thousand or more. Putting in the numbers, it takes $\sim 22\,\mathrm{s}$ to stir the viscous honey droplets (or sugar grains) into our tea. This approximation can be improved by accounting for open streamlines and inertial effects [872, 873].

Instead of stirring, we can also let the honey drop sediment down. If it is sufficiently small, it will have be spherical and sediment at low Reynolds number [§VI C].

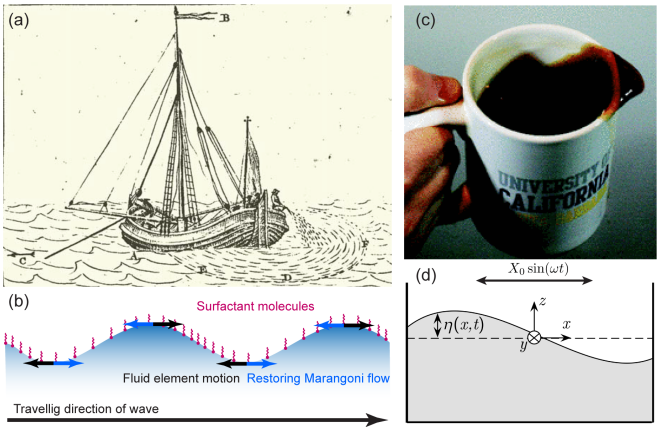

FIG. 27. Waves and splashes. **(a)** Protecting a ship by calming the waves with oil. The Dutch fisheman Isak Kalisvaar reported to have conducted this experiment, in a letter to Frans van Lelyveld in 1776, after his ship got into a violent storm. From Mertens [876]. **(b)** Diagram of capillary wave dampening by surfactants. **(c)** Representative image of coffee spilling. From Mayer and Krechetnikov [877]. **(d)** Schematic of sloshing dynamics in an oscillated container. From Sauret *et al.* [878].

When we substitute the terminal velocity U_∞ [Eq. (62)] for U_0 in Eq. (81), we obtain a characteristic time scale of mixing for the sinking drop,

$$\tau_{\mathrm{mix,\ sink}} \sim \left(\frac{\mu^2}{(\Delta\rho g)^2 D}\right)^{1/3}. \tag{82}$$

This timescale also applies to the inverted system of a water drop rising in another viscous, miscible liquid like corn syrup [871].

IX. WASHING THE DISHES: INTERFACIAL FLOWS

Even the best restaurant cannot perform without its dish washers. This job is somewhat strenuous and boring, but much alleviated by the mesmerizing colors of soap bubbles and the startling wave dynamics. Fun, you might think, but interfacial phenomena have led to exceptional scientific discoveries ranging from cell biology to nanotechnology [see e.g. 874, 875]. In this penultimate section, we will pop the bubble of some old misconceptions and catch the wave of the latest developments concerning interfacial flows.

A. Greasy galleys smooth the waves

Benjamin Franklin (1706-1790) noticed a remarkable phenomenon during one of his journeys at sea, sailing in a fleet of 96 ships. *"I observed the wakes of two of the ships to be remarkably smooth, while all the others*

were ruffled by the wind, which blew fresh" [879]. Being puzzled with the differing appearance, Franklin at last pointed it out to the captain, and asked him the meaning of it. The captain's answer may come as a surprise: *"The cooks, says he, have, I suppose, been just emptying their greasy water."* The calming effect of oil on water was common knowledge to seamen at the time, and had indeed been described since ancient Greeks. However, legends circulated about a ship that miraculously survived a storm by taming it with olive oil [Fig. 27a], so Franklin decided to initiate a series of systematic experiments [879]. The amusing details of these stories, and the scientific interest that emerged since, are described eloquently by Mertens [876] and Tanford [880].

While the dampening of surface waves was known for millennia, its precise cause was a mystery until recently, as described by Henderson and Miles [881], Nicolas and Vega [882], Behroozi *et al.* [883], Kidambi [884] and references therein. Franklin thought that the oil film stopped the wind from catching the water, but more than a century passed before more progress was made. In her kitchen, Agnes Pockels performed pioneering experiments on the surface tension of oil films [see §IX C]. We now know that this surface tension increases when the oil film is stretched thin, for example by the wind. Because of the Marangoni effect [see §III B], the resulting gradients in surface tension then induce flows that oppose the film deformation, thus dampening the surface waves [Fig. 27b]. This interfacial restoring force is referred to as the Gibbs surface elasticity, or the Marangoni elasticity [885], which is a multiphase flow effect that occurs in many other applications, as reviewed extensively by Brennen [164].

B. Splashing and sloshing

No culinary achievement happens without a little mess left behind, be it an accidental spill, or the usual drop of wine from the cook's glass on the kitchen table [see §VII E]. The question of sloshing, why liquids spill out of a container under acceleration, has received prior attention in the context of space vehicles and ballistics: Depending on the size of the container, and the type of agitation, large-scale oscillations of the encased fluid can be enhanced to the point of spilling [886, 887]. In the academic context, it is known to everyone trying to walk to seminars with their coffee cup [Fig. 27c]. It turns out that spilling results from a combination of excess acceleration for a given coffee level when we start walking, and a complex enhancement of vibrations present in the range of common coffee cups sizes [877]. With some relief came the realisation that beer does not slosh so easily, since the presence of even a few layers of foam bubbles on the free surface introduces strong damping of surface oscillations [878].

We generally want to avoid or control splashing or spreading, especially when mixing and pouring liquids. The impact and breakdown of droplets on a solid or liquid surface is mainly controlled by the Reynolds number [Eq. (5)] and the Weber number [Eq. (14)]. Another important factor determining the splashing behaviour is the type of substrate, which regulates the contact angle dynamics of impinging droplets [888]. The elasticity of the substrate also plays an important role [620], as soft solids noticeably reduce or eliminate splashing. Estimates and experiments show that the droplet kinetic energy needed to splash on a very soft substrate can be almost twice as large as in a rigid case [889]. Droplet spreading and recoil can result in a number of complex fluid dynamics phenomena, when the elongating and stretching drops form jets and sheets which further destabilise into smaller droplets via the Rayleigh-Plateau instability [§II H]. The possible outcomes of a collision of a droplet with a solid substrate involve deposition, a fervent splash, so-called corona splash in which the liquid forms a circular layer which detaches from the wall, and retraction in which the droplet can de-stabilise and break up or rebound (partially or entirely) [537, 539, 890]. The process is controlled by the wettability of the surface, the parameters of the droplet, and its impact speed.

Before a stream separates into impacting droplets, liquid jets are frequently seen and used in the kitchen [106]. When plating a gourmet meal, the way sauces are spread on a plate is carefully engineered to achieve a variety of shapes and textures. The same questions appear when glazing a cake, where various edible jets and streams are placed on surfaces in a skillful way that manages buckling instabilities in such elongated filaments to produce the desired visual effect. In art, the understanding of hydrodynamics was crucial to Jackson Pollock, for one, who used a stick to drizzle paint on his canvas in a variety of ways [99]. The complex fluid dynamics behind different painting effects has only recently been analysed and reviewed by Herczyński *et al.* [891] and Zenit [892].

C. Dishwashing and soap film dynamics

The interference patterns on soap bubbles have fascinated physicists for centuries [894], which has resulted in pioneering discoveries in optics, statistical mechanics, and in fluid mechanics by Newton [895], Plateau [896], and De Gennes *et al.* [84]. An even more remarkable story is how the self-taught chemist Agnes Pockels (1862-1935) was inspired to study surface tension while doing the dishes. Women were not allowed to enter universities, so she did not have a scientific training and could not publish her work in scientific journals [897]. Ten years after her first experiments, she was encouraged to write a letter explaining her findings to Lord Rayleigh, who then forwarded it to Nature [898]. Along with her subsequent papers [899–902], all in top-level journals, she contributed to establishing the field of surface science. Without formal training and without access to a lab, Pockels also used simple kitchen tools to develop the precursor

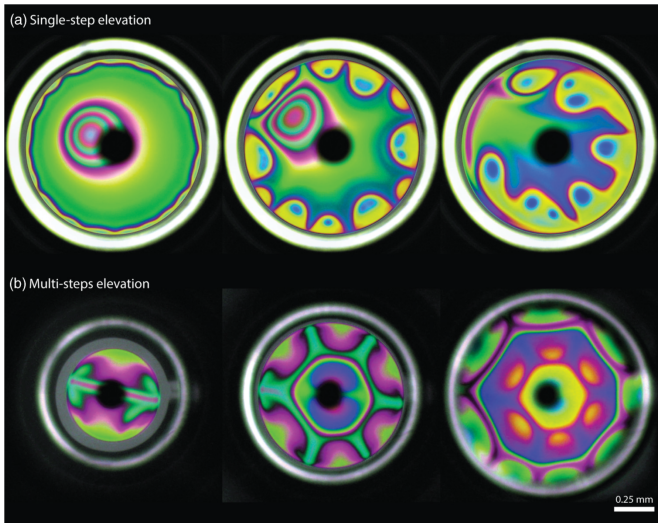

FIG. 28. Thin-film interferograms showing the evolution of surfactant driven flows in soap bubbles. **Top:** When the soap bubble is brought through an air-liquid interface in one single step, an unstable dimple forms at the apex. The dimple is quickly washed away by surfactant plumes rising from the periphery. **Bottom:** When the bubble is instead elevated in multiple, small steps, controllable Marangoni instabilities can be utilized to stabilise the bubble and to prolong its life span. From Bhamla and Fuller [893].

to the now widely celebrated Langmuir trough, which is now used widely to measure the surface pressure of soap molecules and other surfactants upon compression [903].

Soap bubbles are comprised of a thin aqueous film that is sandwiched between two surfactant layer, where each color corresponds to a different film thickness. This film starts to drain immediately due to gravity [893]. In turn, this drainage causes a small deficit in soap concentration at the bubble apex and the formation of a small dimple [Fig. 28, top left panel]. This gradient in surfactant concentration sets up a Marangoni flow towards the apex. By replenishing interfacial material, these flows stabilise the bubble against rupture. However, these Marangoni flows are short-lived and are quickly destroyed by chaotic flows which do not stabilise the bubble [Fig. 28, top right panel]. A simple trick can solve this issue. Bhamla *et al.* [904] showed that by elevating the soap bubble in multiple small steps through a soap solution (instead of in one huge step), it is possible to induce a cascade of Marangoni instabilities. Each Marangoni instability arrests the previous one, and this prevents chaotic flows from developing. This method produces beautiful flow patterns, as displayed in the bottom panel in Fig. 28.

The rate of draining depends on the viscosity of the soap film: Adding glycerol, a natural ingredient in soap, effectively extends the life span of a bubble. Adding corn syrup or honey does the same job, but it might not help to clean your dishes. However, it *will* help to make giant soap bubbles. By retarding film drainage and by reducing the evaporation rate, a bubble stabilized by viscosity has sufficient time to grow before it eventually pops. Another approach was taken by Frazier *et al.* [905]. They appreciated the central role of viscoelasticity in stabilizing thin liquid films, and utilized polyethylene glycol (PEG), a long-chained polymer commonly found in hand sanitizers, to create bubbles with surface areas close to $100\,\mathrm{m}^2$, the area of a badminton field.

To conclude this section, we note that modern video games use computer-generated imagery (CGI) techniques coupled to mathematical models that vary the soap film thickness to render bubbles realistically [906]. Moreover, the nature of the boundary between water and oil is crucial to many nanometre-scale assembly processes, including biological functions such as protein folding and liquid-liquid phase separation [907, 908].

D. Ripples and waves

Whenever an interface between two fluids is disturbed, ripples and waves emerge and propagate along the surface [also see §III A]. When a group of waves moves across a pond, we see waves of different wave lengths λ propagating at different speeds and, importantly, groups of waves travelling at different speeds than the crests and troughs of individual sinusoidal perturbations. The reason for this is the dispersity of water waves, that is the dependence of the wave propagation speed on the wavelength, with longer waves generally travelling faster. For a wave of frequency ω, the relationship between the *wave speed* c and the wavenumber k is $c = \omega/k$, where the dependence of the frequency $\omega = \omega(k)$ on the wavenumber is called the *dispersion relation*. In a wave packet, where each crests travels at the speed c, the velocity of travel of the whole group is $c_\mathrm{g} = \mathrm{d}\omega/\mathrm{d}k$ and is called the *group velocity*.

On deep water, where the dispersion relation reads $\omega^2 = gk$, the wave speed $c = \sqrt{g/k}$ is twice as large as the group propagation speed, which is the reason why in a travelling wave packet individual crests will seem to continuously appear at the back of the packet, propagate through it towards the front, and eventually vanish there. Deep water here means that the depth of the layer is much larger than the wavelength, $\lambda = 2\pi/k$, in which case the dispersion relation above is obtained from the assumption of a potential flow with a linearised boundary condition at the free surface, which is appropriate when the wave amplitude is small compared to the wavelength [135]. Such waves are referred to as *gravity waves*.

However, in many small-scale flows, the surface tension forces at the interface cannot be neglected. Accounting for them leads to a dispersion relation for *capillary-gravity waves*, $\omega^2 = gk + \gamma k^3/\rho$, where the importance of the surface tension parameter is measured by the dimensionless number $\mathrm{S} = \gamma k^2/\rho g$.

For very short waves, the capillary term dominates, so $\mathrm{S} \ll 1$ and the dispersion relation simplifies to $\omega^2 = \sigma k^3/\rho$. Such waves are termed *capillary waves*, and for

water typical cross-over wavelength when S = 1 is about 1.7 cm. Notably, for capillary waves, the group velocity exceeds the wave (or phase) velocity ($c_g = 3c/2$) and so crests move backwards in propagating wave packet. In most small-scale kitchen flows surface tension has a pronounced effect on the appearance and propagation of waves. Such are the waves created by a dripping faucet in a filled sink.

Moreover, in various food science circumstances we might have to do with waves of wavelength comparable to the depth of the vessel in which they propagate. For such *shallow-water waves* the propagation speed depends on the local depth with larger speeds at deeper water. In particular, for gravity waves the dispersion relation becomes in this case $\omega^2 = gk \tanh kh$, with h being the water depth. This again holds for wavelengths small compared to h. The general case is much more complex and nonlinear in nature, yet the linear wave theory is often enough to grasp the dominant behaviour. We considered here only free-surface flows but the reasoning is easily generalised to any fluid-fluid interface [909].

E. Rinsing flows: thin film instabilities

Thin fluid films are a remarkable example of a kitchen flow which has already received a considerable attention exactly in this context. The stability of falling films was the subject of investigation of a father-son team of the Kapitza family, led by the elder Nobel prize winner Pyotr Leonidovich Kapitza, in the 1940s [910]. After World War II, Kapitza was removed from all his positions, including the directorship of his own Institute for Physical Problems, for refusing to work on nuclear weapons. He was ordered to stay at his country house and, deprived of advanced equipment, devised experiments to work on there, including a famous set of experiments on falling films of liquid [911]. Kapitza and Kapitza [912] were the first to experimentally investigate traveling waves on the free surface of a liquid film falling down a smooth plate. The emerging Kapitza instability takes form of roll waves [913], and evolves from a two-dimensional disturbance (i.e., invariant in the spanwise direction) into a fully developed three-dimensional flow [914]. Since the early works of Kapitza, the dynamics of waves in viscous films over the flat substrates were reviewed extensively [583, 598, 915]. We often encounter such waves after a rainfall, on an inclined asphalt road, or even in flowing mud [916]. Film and rivulet flows at solid surfaces bear importance for gas exchange also in industrial applications, including distillation columns [917]. In the kitchen context, they emerge predominantly in rinsing flows or spreading flows, where the thin film dynamics may be governed either by capillarity or external diving, such as gravity, or centrifugal forces [918]. We discussed viscous spreading in §VI G, thus here we focus purely on waving instability.

The phenomenon of roll waves formation is governed by two dimensionless parameters: the Reynolds number describing the flow character, and the Kapitza number

$$\mathrm{Ka} = \frac{\text{surface tension}}{\text{inertial forces}} = \frac{\sigma}{\rho g^{1/3} \nu^{1/4}}, \tag{83}$$

where g is the gravitational acceleration driving the flow. In the context of thin films flows down an inclined slope, the formation of roll waves can also be discussed in terms of the Froude number Fr , defined in Eq. (13) in §II I. For moderate Reynolds numbers, the value of Fr ≈ 2 marks the onset of instability in the thin film flow equations [919]. However, Benjamin has shown in his seminal paper [920] that such flow is unstable for all values of Re, but the rates of amplification of unstable waves become very small when Re is made fairly small, while their wavelengths tend to increase greatly. He proposed a criterion that for an observable instability of flow down a slope with inclination angle β the critical Reynolds number is $\mathrm{Re} = \frac{5}{6} \cot \beta$, as later corroborated by Yih [921].

F. Dynamics of falling and rising drops

1. *Immiscible drops*

The literature describing buoyant immiscible drops is vast, and we try not to give a comprehensive review here; for that, we refer the reader to the many excellent reviews and books previously published, see e.g. Harper [922] and Leal [868]. Nonetheless, due to its central position in the field of fluid dynamics and its omnipresence in the kitchen, we mention a few seminal works regarding freely suspended drops.

When a drop of water is released in cooking oil, it starts to fall immediately due to gravity. During its descent, surface traction from the outer liquid mobilise the fluid-fluid interface and the degree of surface mobility is given by the viscosity ratio between the ambient and drop fluid, $\hat{\mu}/\mu$. For very viscous drops translating through low viscosity liquids (such as a drop of oil rising through water, $\hat{\mu}/\mu \to 0$), the small surface traction is insufficient to mobilise the interface: this results in the drop translating at the velocity of a rigid Stokes' sphere of the same size and volume. The opposite mobility limit is reached when the viscosity ratio is reversed such that $\hat{\mu}/\mu \to \infty$): the interface is then expected to be completely mobile, which causes a vortex ring to develop within the drop. A completely mobile interface is not able to resist viscous stresses, and this leads to the terminal drop velocity being one and a half times as high as that of a Stokes' sphere of the same size and density. The solution to the flow field within a translating, rigid drop at low Reynolds number was worked out simultaneously and independently by the French mathematician Jacques Salomon Hadamard (1865-1963) [923] and the Polish physicist and mathematician Witold Rybczynski (1881-1949) [924] as early as in 1911.

In reality, most small droplets rise or descend at velocities that lie between the theoretical prediction by Hadamard and Rybczynski and the Stokes prediction for rigid spheres [290], and this is true even in pure liquids with no surfactants added [Fig. 29a,b]. The terminal velocity generally depends strongly on size as reported by Bond [925], who found small water droplets to descend through castor oil at only 1.16 times the Stokes' velocity, while drops exceeding a critical radius of about 0.6 cm descended at 1.4 times the Stokes' velocity. To explain the sudden jump in velocity with drop size, Bond and Newton [926] postulated that a ratio of buoyancy to surface tension determines the mobility of the interface. Boussinesq [927] instead suggested that an increased viscosity at the drop's surface is responsible for slowing the drop. However, without experimental evidence of the flow field within the drop, it is impossible to judge the correctness of these models.

Aiming to obtain a better description, Savic [928] published photographic evidence of the flow streamlines inside water droplets descending through castor oils. Savic [928] visualizations show that the streamline patterns of drops exceeding 1 cm in radius are almost indistinguishable from the Hadamard-Rybczynski-solution and that the terminal velocities for large drops are in good agreement with theory as well. However, for smaller drops, the vortex rings are shifted forward, and this occurs as a stagnant cap emerges in the rear of the drop. As the drop size is further reduced, the stagnant region covers a larger and larger portion until it envelops the entire drop, with the result of the drop sedimenting as a Stokes sphere.

To explain his observations, Savic [928] proposed that the interface is immobilized by *surface active* molecules, which are in turn de-stabilized by viscous stresses from the outer fluid. For the smallest drops, the viscous stress is insufficient to distort the surface layer: this leads to a complete immobilization. However, as the drop size increases, the shear stress increases as well, and this leads to a gradual removal of the surface layer until the Hadamard-Rybczynski-theory is fully recovered for the largest drops.

Savic [928] developed a theory to calculate the drag of a drop from the degree of surface coverage, which he extracts from the flow visualizations. He also attempted to calculate the critical drop size of the transition between a mobile and an immobile no-slip boundary, however the transition occurred at larger radii than predicted, and he suggests this discrepancy to be due to a finite solubility between water and castor oil not accounted for in the theoretical model. Later, Davis and Acrivos [929] improved Savic's analysis to obtain better agreement with experiments, and Sadhal and Johnson [930] extended these results to obtain an exact solution of the drag force on the drop for a given surface coverage. For a droplet sedimenting at a given rate, Sadhal and Johnson [930] also obtained an analytical expression for the total amount of surfactant adsorbed to the interface. However, the solution to the internal flow field and the corresponding sedimentation rate for a drop of a given size remains an open question.

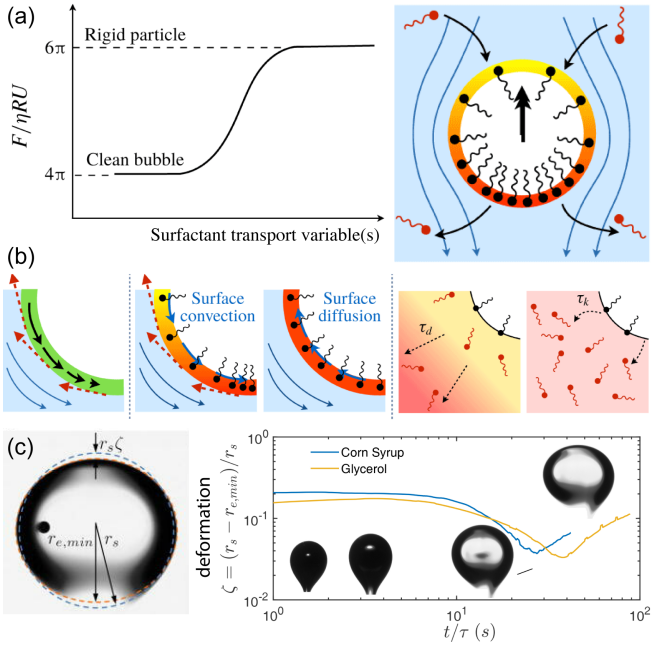

FIG. 29. Interfacial phenomena in rising bubbles and drops. **(a)** The drag force on a rising bubble is affected by 'hidden' surfactant transport variables **(b)** including (i) Interfacial viscosity can resist the surface flow. (ii) Surfactant concentration gradients generate Marangoni stresses. (iii) Marangoni forces weakened by surface diffusion against the gradient. (iv) Diffusive transport of surfactants in the bulk. (v) Adsorption and desorption kinetics of soluble surfactants. (a-b) From Manikantan and Squires [290]. **(c)** Water drops ascending through corn syrup and glycerol undergo shape transformations from prolate to oblate spheroids. The travel time t is rescaled by the characteristic mixing time τ from Eq. (81). From Mossige *et al.* [871].

2. *Miscible drops*

As compared to immiscible drops covered in the last section, transport problems involving miscible drops have enjoyed far less attention, which is surprising given their omnipresence in our daily lives and their rich dynamics. In section §VIII F we looked at how fluid motion can accelerate the mixing rate between a viscous drop and its surroundings in the low Reynolds number case. In this section, we discuss how finite inertia may influence the shape of falling drops, and we discuss the stabilizing effects of transient tensions between miscible liquids.

When a miscible drop descends in another liquid, it changes shape in response to the viscous drag acting on it, and when it reaches a critical velocity, inertial effects also start to play a role. A simple way to visualise the effect of inertia on the drop shape is to produce a drop

of food dye in air and let it fall into a glass of water. Upon impact with the water surface, the central part of the drop gets accelerated upward in a Rayleigh-Taylor instability, and this causes the drop to evolve into an open torus. For drops made of honey or corn syrup, this shape transformation is delayed by the high viscosity, but on a long time scale, even the most viscous drop deform into oblate spheroids or donuts.

Kojima *et al.* [931] developed a theory to explain the shape transitions of miscible drops and validated their theory against experiments of corn syrup drops falling through diluted corn syrup solutions. When the drop is created in air, immediately above a water surface, they showed that the descending drop does not experience inertia in the early stages of its descent: In this case, it is solely deformed by viscous traction forces, causing the drop to develop into an oblate spheroid. However, by pairing theory with experiments, Kojima *et al.* [931] showed that later in the drop's descent, inertia does play a key role in its shape evolution, and this causes the drop to develop into an open torus. The fact that inertia is relevant at long time scales is intuitive; however, they also had to incorporate a small, but finite tension across the miscible interface to fully explain the material deformation. The inverted system concerning water drops ascending through corn syrup was recently examined by Mossige *et al.* [871] [Fig. 29c].

The tension existing between miscible liquids is not a surface tension as defined in the classical sense between *immiscible* phases [see §II F]. Instead, it is caused by sharp gradients in composition between the pure phases by giving rise to so-called Korteweg stresses [932] that mimic the effect of a surface tension. These tensions are typically at least two orders of magnitude smaller than in immiscible systems (for example, 0.43 mN/m between glycerol and water [933] as compared to 73 mN/m between water and air) and diminish in time as diffusion smears out the miscible interface; as a result, they are inherently difficult to measure and usually neglected. However, in many situations including miscible displacements in capillary tubes [934] and in Hele-Shaw geometries [935], effective interfacial tensions must be accounted for to accurately describe a deforming, miscible interface, and theoretical and experimental evidence for this is given in Refs. [936–941]. Non-equilibrium stresses are not only of academic interest, but can be tuned to control the morphology of miscible interfaces in modern industrial processes. Notably, Brouzet *et al.* [942] utilized transient tensions to align nanofibrils in microfluidic flow focusing geometries, with implications in the paper production industry and in the development of new, sustainable alternatives to plastics, and Wylock *et al.* [943] used it to control gravitational instabilities in carbon sequestration plants.

X. DISCUSSION

A. Summary

In this Review, we have presented a overview of culinary fluid mechanics and other currents in food science. Starting from ancient times, the connection between cooking and fluid mechanics has led to innovations that benefit both. We have explored how this connection grows stronger every day, to the frontier of modern research and gastronomy. Culinary fluid mechanics brings people together from across society, from chefs to food scientists, physicists and chemical engineers, medical and nutrition specialists, and students in any discipline. To make this article accessible to this broad audience, we started our discussion with an overview of kitchen sink fundamentals [§II], where we summarised the basics of fluid mechanics in the context of food science. Starting the meal with drinks [§III], we reviewed hydrodynamic instabilities in cocktails, Marangoni flows, bubble effervescence and culinary foams. Getting into the thick of it with a soup for starters [§IV], we discussed the rheological properties of viscoelastic food, non-linear sauces, suspensions and emulsions. Moving on to a hot main course [§V], we analysed the role of heat in cooking, including the Leidenfrost effect, Rayleigh-Bénard convection, double-diffusive convection, flames and smoke. Going for a sticky desert [§VI], we described flows at low Reynolds numbers, from Stokes' law to lubrication theory, viscous gravity currents, ice cream and microbial fluid dynamics. Eager for a postprandial espresso [§VII], we examined the physics of granular matter and porous media flows, different brewing methods, and the coffee ring effect. Thirsty for another cup of tea [§VIII], we delineated the tea leaf paradox and other non-linear flows, succeeded by turbulence and chaos. Finally, when doing the dishes [§IX], we explore interfacial phenomena including the Gibbs surface elasticity, soap film dynamics, waves and jets, miscible drops and roll wave instabilities. Quite a bit to digest, but a place worth coming back to.

B. Learning from kitchen experiments

Humans are naturally curious. From an infant age, we explore by actively interacting with our surroundings [944]. Through touch, smell and taste, we learn about the natural world. Becoming a scientist starts with asking questions like "what?", "why?" or "how?".

In physics education, we try to answer these questions the by comparing observations with theoretical descriptions. Traditionally, this knowledge is transferred from teacher to students through in-class lecturing and instructor-made assignments [945], but this linear learning protocol is not necessarily compatible with curiosity-driven exploration and observation [946]. As a result, students often feel alien to the physics topics taught in class [39] and lose the natural intuition and curiosity that

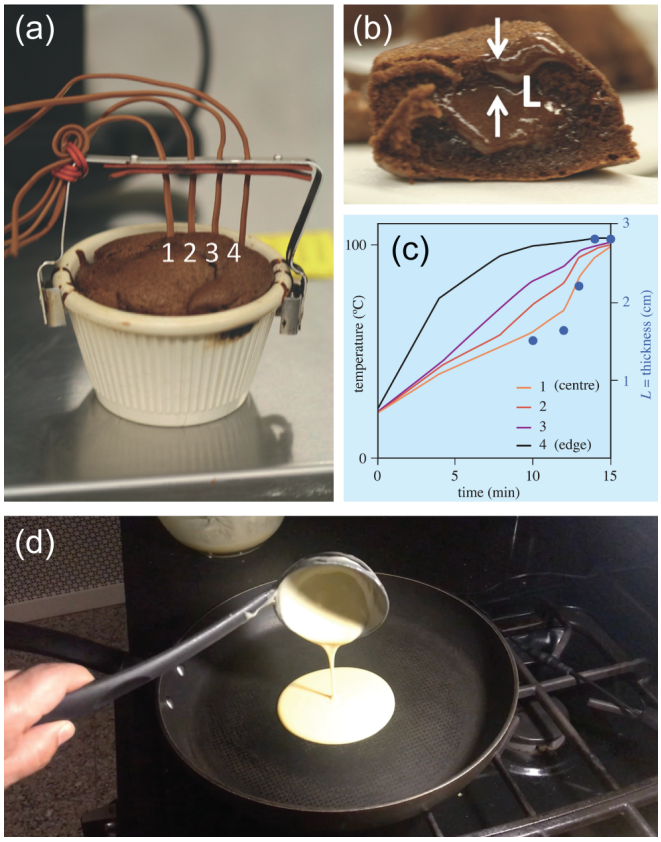

FIG. 30. Kitchen-based learning is an affordable and accessible strategy to foster curiosity and intuition for a wide range of physics topics. **(a-c)** In a science class accessible to non-science majors, cake making was used to demonstrate heat transfer and elasticity. From Rowat *et al.* [39]. (a) Thermocouples are used to measure the rise in temperature at different points inside a molten chocolate cake as it bakes in an oven. (b) The thickness of the solid crust of the cake L increases over time. (c) Results of experiments. **(d)** Students pour pancake batter to learn about viscous gravity currents. They used cell phones to video-record the spreading rate and fit their data into a theoretical model to back-calculate the viscosity. Image courtesy of Roberto Zenit.

is so important for learning [947, 948]. Inevitably, physics has a reputation for being difficult and abstract and with little relevance to students' daily lives, and this disconnect is largely responsible for the relatively poor recruitment to science and education disciplines in higher education [949]. To address this issue, it is vitally important to develop effective teaching strategies that fosters both intuition, engagement and curiosity. This is best achieved through an hands-on active learning strategy [950, 951], without creating the perception of learning by ineffective engagement [952], where experiments that relate to our daily lives have a prominent role.

The kitchen is an accessible learning environment where simple physics experiments can be performed at home with humble ingredients; For example, Benjamin [40] showed that students in elementary physics education can learn about surface tension, mixing and gravity by studying Rayleigh-Taylor instabilities [see §III A] in their own kitchen. The simple experimental design allowed for a high degree of flexibility and were designed in such a way that they could be performed either individually, or in groups to foster collective accomplishment and collaborative learning. As compared to experiments conducted in school laboratories, kitchen experiments have a higher potential for engagement as we encounter them every single day, and since they require very little equipment. They offer a low-cost 'frugal science' alternative that is less susceptible to budget cuts, and more accessible to students from underrepresented socioeconomic backgrounds [953, 954].

Affordable and accessible kitchen experiments can also be utilized to develop intuition for advanced mathematical concepts. Notably, a famous class at Harvard and UCLA teaches general physics concepts such as heat transfer and phase transformations to non-science majors through the lens of cooking [Fig. 30a-c] [39]. In this popular course, top chefs give weekly seminars for further engagement. Kitchen experiments can also be used to learn about more specialized topics in fluid mechanics; For example, take-home experiments such as measuring the flow rate from a hose and estimating the density and the viscosity of household fluids has been used to enhance learning in an introductory fluid mechanics class [955]. In addition, the kitchen can be a gateway to learn about the intrinsic fluid properties that govern these flows. Notably, in a special session on Kitchen Flows at the 73rd Annual Meeting of the APS Division of Fluid Dynamics (APS-DFD), Zenit *et al.* [956] demonstrated how pancake-making can be used to teach students about fluid viscosity. Instead of extracting the viscosity from a classical sedimenting-sphere experiment [555], which is less common in our daily lives, the students were asked to pour pancake batter and other viscous fluids like honey and syrup into frying pans and measure the spreading rate [Fig. 30d]. By fitting their data to a theoretical prediction [596], which is described in §VI G, the students were able to back-calculate the viscosity. Such *in-situ* kitchen measurements can be used for numerous other scientific concepts, as discussed throughout this Review, thereby creating direct links between physics and everyday experiences.

In addition, many canonical flows can be generated with simple kitchen tools, including the circular hydraulic jumps [see §II I], and Poiseuille flows [§II C], which can be used to validate theoretical predictions taught in class as a means to develop intuition for advanced mathematical concepts. Finally, to further accelerate the learning in fluid mechanics, e-learning tools can be implemented [957] such as the extremely extensive Multimedia Fluid Mechanics Online [958].

From these examples, it is evident that easy-to-do kitchen experiments can be implemented for enhanced learning and engagement across all ages. They are highly scalable, and can even can be taught on an online plat-

form to make learning available for large groups of students, including students who can not afford enrollment in an educational program. Therefore, kitchen-based learning represents a viable strategy to increase the number of competent scientists and engineers in the world, which is necessary to address immediate threats to humankind and ensure a sustainable future [959].

C. Curiosity-driven research

As well as being a vehicle for accessible and affordable science education, culinary fluid mechanics is a hotspot for curiosity-driven research [960]. Indeed, Agnes Pockels found inspiration for her breakthrough discoveries in surface science and hydrodynamic instabilities from dish washing [§IX]. Valuable data can be extracted relatively quickly from a kitchen-based laboratory, in the spirit of a 'Friday afternoon experiment' [961]. A minimum of investments of time, training and equipment are needed, which makes this field approachable not only to experimentalists, but also to theorists and researchers in other fields. Since many kitchen flows can be described by scaling theories and other analytical techniques, they can serve to validate theoretical models in fluid mechanics and materials science [469]. As such, kitchen experiments are attractive to theorists, and by lowering the activation barrier to start a new experiment, they can be combined with mathematical models to solve a large class of problems in science and in engineering. Curiosity-driven learning is foundational to human cognition [962], and sometimes the best discoveries are made in a few hours.

Perhaps the most influential fluid mechanician of all time, Sir. G. I. Taylor, was known for his special ability to make groundbreaking discoveries from humble ingredients and to design simple experiments that could be described theoretically [963]. Instead of following the hypes in science and 'going with the flow', Taylor was merely driven by his own interest and curiosity, without thinking about specific applications. Outstanding contributions in fundamental science always find useful applications, which is immediately evident when we look at the enormous implication of Taylor's contributions to science and engineering. However, today's funding schemes often require that research should preferentially address a particular problem and have immediate impact [964], which leaves little room for curiosity-driven research and scientific investigations for its own sake [965]. But, since curiosity is a prerequisite for exploration and discovery, the scientific philosophy of Taylor and his predecessors could serve as inspiration for the modern physicist.

D. Conclusion

Culinary fluid mechanics is the study of everything that flows in the food supply chain, covering a wide range of surprising phenomena that can be harnessed for the benefit of gastronomy, food science, and for our planet as a whole. This field naturally connects practical technologies with basic research, just how fluid mechanics once started. Culinary flows are accessible to experimentalists and theorists alike: Their intuitive geometry and well-defined conditions are suitable for mathematical modelling, while the relatively low equipment costs reduces the activation energy for pilot investigations, thus catalysing curiosity-driven education [§X B] and research [§X C].

Where 'kitchen flow' papers may initially have been considered occasional or incidental, their breath and depth now constitute a rapidly growing field. A field that this Review can cover only partially because it is so interconnected. Yet, culinary fluid mechanics is unified by a number of well-defined research directions and goals. Firstly, it aims to establish a sustainable and fair global food supply. Secondly, it has the potential to develop reliable food technologies with a strong fundamental backbone. Thirdly, it can facilitate new discoveries far beyond gastronomy by making science and engineering more accessible. Finally, it can advise policy makers on important decisions for our future generations, such as the announced EU ban on PFAS non-stick coatings by 2030 [531] and help the reduction of climate change [966, 967]. To achieve these goals, scientists from related fields must become even more interconnected.

Indeed, as we discussed, culinary fluid mechanics directly links to other disciplines across the sciences, from molecular gastronomy to biological tissue mechanics and rheology. Furthermore, it has extensive engineering applications ranging from the stream engine to 3D printing and nanotechnology. Not least, there are immediate connections with food safety, microbiology and medicine. However, unlike many fields in science, kitchen flows create a bond with people who couldn't have a scientific training. People who want to learn more, and people who want to contribute themselves. People like Agnes writing to Lord Rayleigh. So much talent is lost in this world full of inequality, and we have a responsibility to make science more inclusive and accessible to people from under-represented backgrounds. Through science communication, through education, and through research itself. We hope that more scientists will stand up to this challenge.

ACKNOWLEDGEMENTS

Comments or suggestions on this arXiv submission are most welcome. Please contact us, and we will try to incorporate them. A.J.T.M.M. acknowledges funding from the United States Department of Agriculture (USDA-NIFA AFRI grants 2020-67017-30776 and 2020-67015-32330).

[1] Mays, L., ed., *Ancient water technologies* (Springer, 2010).

[2] Kurti, N. and This-Benckhard, H., The kitchen as a lab, Scientific American **270**, 120–123 (1994).

[3] Drazin, P., Fluid mechanics, Phys. Educ. **22**, 350 (1987).

[4] This, H., *Molecular gastronomy: exploring the science of flavor* (Columbia University Press, 2006).

[5] Barham, P., Skibsted, L. H., Bredie, W. L. P., Bom Frøst, M., Møller, P., Risbo, J., Snitkjær, P., and Mortensen, L. M., Molecular gastronomy: a new emerging scientific discipline, Chem. Rev. **110**, 2313–2365 (2010).

[6] Myhrvold, N., Young, C., and Bilet, M., *Modernist cuisine*, 7th ed. (The Cooking Lab, 2021).

[7] Borkenhagen, C., Evidence-based creativity: Working between art and science in the field of fine dining, Soc. Stud. Sci. **47**, 630–654 (2017).

[8] McGee, H., *On Food and Cooking: The Science and Lore of the Kitchen* (Scribner, 2007).

[9] López-Alt, J. K., *The Food Lab: Better Home Cooking Through Science* (W.W. Norton, 2015).

[10] Escoffier, G. A., *Le Guide Culinaire: Aide-Mémoire de Cuisine Pratique* (Editions Flammarion, 1903) translated as The Complete Guide to the Art of Modern Cookery.

[11] Trubek, A. B., *Haute cuisine: How the French invented the culinary profession* (University of Pennsylvania Press, 2000).

[12] Kurti, N. and Kurti, G., *But the crackling is superb: an anthology on food and drink by Fellows and Foreign Members of the Royal Society* (Adam Hilger Publishers, Philadelphia, 1988).

[13] Donald, A. M., Food for thought, Nat. Mater. **3**, 579–581 (2004).

[14] Mezzenga, R., Schurtenberger, P., Burbidge, A., and Michel, M., Understanding foods as soft materials, Nat. Mater. **4**, 729–740 (2005).

[15] Fennema, O. R., *Fennema's food chemistry*, 5th ed., edited by S. Damodaran and K. L. Parkin (CRC press, 2017).

[16] Capozzi, F. and Bordoni, A., Foodomics: a new comprehensive approach to food and nutrition, Genes & Nutr. **8**, 1–4 (2013).

[17] Heldman, D. R., Lund, D. B., and Sabliov, C., *Handbook of food engineering* (CRC press, 2018).

[18] Doyle, M. P., Diez-Gonzalez, F., and Hill, C., *Food microbiology: fundamentals and frontiers* (John Wiley & Sons, 2019).

[19] Ahmed, J., Ptaszek, P., and Basu, S., *Advances in food rheology and its applications* (Woodhead Publishing, 2016).

[20] Vilgis, T. A., Soft matter food physics: The physics of food and cooking, Rep. Progr. Phys. **78**, 124602 (2015).

[21] Assenza, S. and Mezzenga, R., Soft condensed matter physics of foods and macronutrients, Nat. Rev. Phys. **1**, 551–566 (2019).

[22] Pedersen, M. T. and Vilgis, T. A., Soft matter physics meets the culinary arts: From polymers to jellyfish, Int. J. Gastr. Food Sci. **16**, 100135 (2019).

[23] Foegeding, E. A., Food biophysics of protein gels: A challenge of nano and macroscopic proportions, Food Biophys. **1**, 41–50 (2006).

[24] Nelson, P. C., *Biological Physics: Energy, Information, Life*, 2nd ed. (Chiliagon Science, 2020).

[25] Knorr, D., Froehling, A., Jaeger, H., Reineke, K., Schlueter, O., and Schoessler, K., Emerging technologies in food processing, Annu. Rev. Food Sci. Tech. **2**, 203–235 (2011).

[26] Skurtys, O. and Aguilera, J. M., Applications of microfluidic devices in food engineering, Food Biophys. **3**, 1–15 (2008).

[27] Gunes, D. Z., Microfluidics for food science and engineering, Curr. Opin. Food Sci. **21**, 57–65 (2018).

[28] He, S., Joseph, N., Feng, S., Jellicoe, M., and Raston, C. L., Application of microfluidic technology in food processing, Food Funct. **11**, 5726–5737 (2020).

[29] Welti-Chanes, J. and Velez-Ruiz, J. F., eds., *Transport phenomena in food processing* (CRC press, 2016).

[30] Gould, G. W., ed., *New methods of food preservation* (Springer, Boston, MA, 2012).

[31] Amit, S. K., Uddin, M. M., Rahman, R., Islam, S. R., and Khan, M. S., A review on mechanisms and commercial aspects of food preservation and processing, Agricult. Food Secur. **6**, 1–22 (2017).

[32] Donald, A. M., Understanding starch structure and functionality, in *Starch in food: Structure, function and applications*, edited by A.-C. Eliasson, M. Sjöö, and L. Nilsson (Woodhead Publishing, 2017) 2nd ed., pp. 156–184.

[33] Kant, K., Shahbazi, M.-A., Dave, V. P., Ngo, T. A., Chidambara, V. A., Than, L. Q., Bang, D. D., and Wolff, A., Microfluidic devices for sample preparation and rapid detection of foodborne pathogens, Biotechnology advances **36**, 1003–1024 (2018).

[34] Bajpai, V. K., Kamle, M., Shukla, S., Mahato, D. K., Chandra, P., Hwang, S. K., Kumar, P., Huh, Y. S., and Han, Y.-K., Prospects of using nanotechnology for food preservation, safety, and security, J. Food Drug Analys. **26**, 1201–1214 (2018).

[35] Ozilgen, M., *Handbook of food process modeling and statistical quality control* (CRC Press, 2011).

[36] Neethirajan, S., Kobayashi, I., Nakajima, M., Wu, D., Nandagopal, S., and Lin, F., Microfluidics for food, agriculture and biosystems industries, Lab Chip **11**, 1574–1586 (2011).

[37] Drndić, M., 20 years of solid-state nanopores, Nat. Rev. Phys. , 1–1 (2021).

[38] American Physical Society Press Office,, Lab closed? Head to the kitchen (2020).

[39] Rowat, A. C., Sinha, N. N., Sörensen, P. M., Campàs, O., Castells, P., Rosenberg, D., Brenner, M. P., and Weitz, D. A., The kitchen as a physics classroom, Phys. Educ. **49**, 512 (2014).

[40] Benjamin, R. F., Rayleigh-Taylor instability–Fascinating gateway to the study of fluid dynamics, Phys. Teach. **37**, 332–336 (1999).

[41] Vieyra, R. E., Vieyra, C., and Macchia, S., Kitchen physics: Lessons in fluid pressure and error analysis, Phys. Teach. **55**, 87–90 (2017).

[42] Glessmer, M. S., How to teach motivating and hands-on laboratory and field courses in a virtual setting, Oceanography **33**, 130–132 (2020).

[43] Schmidt, S. J., Bohn, D. M., Rasmussen, A. J., and Sutherland, E. A., Using food science demonstrations to engage students of all ages in science, technology, engineering, and mathematics (stem), J. Food Sci. Educ. **11**, 16–22 (2012).

[44] Piergiovanni, P. and Goundie, D., Modernist cuisine as an introduction to chemical engineering, Chem. Eng. Educ. **53**, 80–80 (2019).

[45] Giles, S., Jackson, C., and Stephen, N., Barriers to fieldwork in undergraduate geoscience degrees, Nat. Rev. Earth Environ. **1**, 77–78 (2020).

[46] Ogborn, J., Soft matter: food for thought, Phys. Educ. **39**, 45 (2004).

[47] Miles, D. T. and Bachman, J. K., Science of food and cooking: a non-science majors course, J. Chem. Educ. **86**, 311 (2009).

[48] Brenner, M., Sörensen, P., and Weitz, D. A., *Science and Cooking: Physics Meets Food, From Homemade to Haute Cuisine* (W.W. Norton Books, 2020).

[49] Vulić, H., Doračić, D., Hobbs, R., and Lang, J., The Vinkovci treasure of late Roman silver plate: preliminary report, J. Roman Archaeol. **30**, 127–150 (2017).

[50] Navarini, L., Nobile, E., Pinto, F., Scheri, A., and Suggi-Liverani, F., Experimental investigation of steam pressure coffee extraction in a stove-top coffee maker, Appl. Thermal Eng. **29**, 998–1004 (2009).

[51] Barrass, B. and Derrett, D. R., *Ship stability for masters and mates* (Elsevier, 2011).

[52] Lautrup, B., *Physics of Continuous Matter: Exotic and Everyday Phenomena in the Macroscopic World* (CRC Press, 2011).

[53] Batchelor, G. K., Heat convection and buoyancy effects in fluids, Quart. J. Roy. Meteorol. Soc. **80**, 339–358 (1954).

[54] Batchelor, G. K., *An introduction to fluid dynamics* (Cambridge University Press, 2000).

[55] Lindén, J., Upside down glass of water experiment revisited, Phys. Educ. **55**, 055023 (2020).

[56] Marshall, J., Clarke, S., Escott, C., and Pados, B. F., Assessing the flow rate of different bottles and teats for neonates with feeding difficulties: An Australian context, J. Neonatal Nursing **27**, 285–290 (2021).

[57] Woodcroft, B., ed., *The Pneumatics of Hero of Alexandria: From the Original Greek* (Taylor, Walton and Maberly, 1851).

[58] Dickinson, H. W., Joseph Bramah and his inventions, Trans. Newcomen Soc. **22**, 169–186 (1941).

[59] Carlson, J. A., Jaffe, A., and Wiles, A., eds., *The millennium prize problems* (Clay Mathematics Institute, American Mathematical Society, 2006).

[60] Sutera, S. P. and Skalak, R., The history of Poiseuille's law, Annu. Rev. Fluid Mech. **25**, 1–20 (1993).

[61] Stokes, G. G., On the theories of the internal friction of fluids in motion, and of the equilibrium and motion of elastic solids, Trans. Cambridge Phil. Soc. **8**, 75–129 (1880).

[62] Tabeling, P., *Introduction to microfluidics* (Oxford University Press, 2005).

[63] Bruus, H., *Theoretical Microfluidics*, Vol. 18 (Oxford university press Oxford, 2008).

[64] Squires, T. M. and Quake, S. R., Microfluidics: Fluid physics at the nanoliter scale, Rev. Mod. Phys. **77**, 977–1026 (2005).

[65] Kirby, B. J., *Micro- and Nanoscale Fluid Mechanics: Transport in Microfluidic Devices* (Cambridge University Press, 2010).

[66] Reynolds, O., An experimental investigation of the circumstances which determine whether the motion of water shall be direct or sinuous, and of the law of resistance in parallel channels, Phil. Trans. Roy. Soc. Lond. **35**, 84–99 (1883).

[67] Thomsen, V., Estimating Reynolds number in the kitchen sink, Phys. Teach. **31**, 410–410 (1993).

[68] Heavers, R. M. and Medeiros, M. G., Laminar and turbulent flow in a glass tube, Phys. Teach. **28**, 297–299 (1990).

[69] Schlichting, H. and Gersten, K., *Boundary-layer theory* (Springer-Verlag, Berlin, Heidelberg, 2017).

[70] Chizner, M. A., Cardiac auscultation: rediscovering the lost art, Curr. Prob. Cardiol. **33**, 326–408 (2008).

[71] Stein, P. D. and Sabbah, H. N., Turbulent blood flow in the ascending aorta of humans with normal and diseased aortic valves, Circul. Res. **39**, 58–65 (1976).

[72] Marsden, A. L., Optimization in cardiovascular modeling, Annu. Rev. Fluid Mech. **46**, 519–546 (2014).

[73] Seo, J. H., Bakhshaee, H., Garreau, G., Zhu, C., Andreou, A., Thompson, W. R., and Mittal, R., A method for the computational modeling of the physics of heart murmurs, J. Comp. Phys. **336**, 546–568 (2017).

[74] Grotberg, J. B., Respiratory fluid mechanics and transport processes, Annu. Rev. Biomed. Eng. **3**, 421–457 (2001).

[75] Kleinstreuer, C. and Zhang, Z., Airflow and particle transport in the human respiratory system, Annu. Rev. Fluid Mech. **42**, 301–334 (2010).

[76] Bohadana, A., Izbicki, G., and Kraman, S. S., Fundamentals of lung auscultation, New Engl. J. Med. **370**, 744–751 (2014).

[77] Anderson Jr, J. D., *Fundamentals of aerodynamics*, 6th ed. (McGraw-Hill, 2017).

[78] Ribéreau-Gayon, P., Glories, Y., Maujean, A., and Dubourdieu, D., *Handbook of Enology, Volume 2: The Chemistry of Wine-Stabilization and Treatments*, Vol. 2 (John Wiley & Sons, 2006).

[79] Balboa-Lagunero, T., Arroyo, T., Cabellos, J. M., and Aznar, M., Sensory and olfactometric profiles of red wines after natural and forced oxidation processes, Am. J. Enol. Viticult. **62**, 527–535 (2011).

[80] Pasteur, L., *Études sur le vin: ses maladies, causes qui les provoquent, procédés nouveaux pour le conserver et pour le vieillir* (Simon Raçou et Comp., Paris, 1873).

[81] Davis, S., Gray, J. O., and Caldwell, D. G., An end effector based on the Bernoulli principle for handling sliced fruit and vegetables, Robot. Comp.-Int. Manuf. **24**, 249–257 (2008).

[82] Petterson, A., Ohlsson, T., Caldwell, D. G., Davis, S., Gray, J. O., and Dodd, T. J., A Bernoulli principle gripper for handling of planar and 3D (food) products, Indust. Robot **37**, 518–526 (2010).

[83] Rowlinson, J. S. and Widom, B., *Molecular Theory of Capillarity*, Dover Books on Chemistry (Dover, 2013).

[84] De Gennes, P.-G., Brochard-Wyart, F., Quéré, D., *et al.*, *Capillarity and wetting phenomena: drops, bubbles, pearls, waves*, Vol. 336 (Springer, 2004).

[85] Marchand, A., Weijs, J. H., Snoeijer, J. H., and Andreotti, B., Why is surface tension a force parallel to

the interface?, Am. J. Phys. **79**, 999–1008 (2011).
[86] Berry, J. D., Neeson, M. J., Dagastine, R. R., Chan, D. Y. C., and Tabor, R. F., Measurement of surface and interfacial tension using pendant drop tensiometry, J. Colloid Interf. Sci. **454**, 226–237 (2015).
[87] Kundan, A., Plawsky, J. L., Wayner, P. C., Chao, D. F., Sicker, R. J., Motil, B. J., Lorik, T., Chestney, L., Eustace, J., and Zoldak, J., Thermocapillary phenomena and performance limitations of a wickless heat pipe in microgravity, Phys. Rev. Lett. **114**, 146105 (2015).
[88] Hadfield, C., Wringing out a water soaked washcloth in space - Canadian space agency science HD video, `https://www.youtube.com/watch?v=KFPvdNbftOY` (2013), last accessed: 8-May-2020.
[89] Goy, N.-A., Denis, Z., Lavaud, M., Grolleau, A., Dufour, N., Deblais, A., and Delabre, U., Surface tension measurements with a smartphone, Phys. Teach. **55**, 498–499 (2017).
[90] Bonn, D., Eggers, J., Indekeu, J., Meunier, J., and Rolley, E., Wetting and spreading, Rev. Mod. Phys. **81**, 739–805 (2009).
[91] Tadmor, R., Line energy and the relation between advancing, receding, and Young contact angles, Langmuir **20**, 7659–7664 (2004).
[92] Jasper, W. J. and Anand, N., A generalized variational approach for predicting contact angles of sessile nanodroplets on both flat and curved surfaces, J. Mol. Liq. **281**, 196–203 (2019).
[93] Jurin, J., An account of some experiments shown before the Royal Society; with an enquiry into the cause of the ascent and suspension of water in capillary tubes, Phil. Trans. Roy. Soc. Lond. **30**, 739–747 (1718).
[94] Jensen, K. H., Berg-Sørensen, K., Bruus, H., Holbrook, N. M., Liesche, J., Schulz, A., Zwieniecki, M. A., and Bohr, T., Sap flow and sugar transport in plants, Rev. Mod. Phys. **88**, 035007 (2016).
[95] Katifori, E., The transport network of a leaf, Compt. Rend. Phys. **19**, 244–252 (2018).
[96] Redon, C., Brochard-Wyart, F., and Rondelez, F., Dynamics of dewetting, Phys. Rev. Lett. **66**, 715–718 (1991).
[97] Reiter, G., Dewetting of thin polymer films, Phys. Rev. Lett. **68**, 75–78 (1992).
[98] Herminghaus, S., Jacobs, K., Mecke, K., Bischof, J., Fery, A., Ibn-Elhaj, M., and Schlagowski, S., Spinodal dewetting in liquid crystal and liquid metal films, Science **282**, 916–919 (1998).
[99] Palacios, B., Rosario, A., Wilhelmus, M. M., Zetina, S., and Zenit, R., Pollock avoided hydrodynamic instabilities to paint with his dripping technique, PLoS ONE **14**, 1–16 (2019).
[100] Thompson, C. V., Solid-state dewetting of thin films, Annu. Rev. Mater. Res. **42**, 399–434 (2012).
[101] Burton, L. J., Cheng, N., Vega, C., Andrés, J., and Bush, J. W. M., Biomimicry and the culinary arts, Bioinspir. Biomim. **8**, 044003 (2013).
[102] Plateau, J. A. F., *Statique expérimentale et théorique des liquides soumis aux seules forces moléculaires* (Gauthier-Villars, 1873).
[103] Lord Rayleigh,, On the capillary phenomena of jets, Proc. Roy. Soc. Lond. **29**, 71–97 (1879).
[104] Wheeler, A. P. S., Physics on tap, Phys. Educ. **47**, 403–408 (2012).
[105] Bohr, N. and Ramsay, W., Determination of the surface-tension of water by the method of jet vibration, Phil. Trans. Roy. Soc. A **209**, 281–317 (1909).
[106] Eggers, J. and Villermaux, E., Physics of liquid jets, Rep. Progr. Phys. **71**, 036601 (2008).
[107] Eggers, J., Nonlinear dynamics and breakup of free-surface flows, Rev. Mod. Phys. **69**, 865–930 (1997).
[108] Martin, G. D., Hoath, S. D., and Hutchings, I. M., Inkjet printing - the physics of manipulating liquid jets and drops, J. Phys. Conference Series **105**, 012001 (2008).
[109] Anna, S. L., Droplets and bubbles in microfluidic devices, Annu. Rev. Fluid Mech. **48**, 285–309 (2016).
[110] Jung, S., Pinch-off dynamics to elucidate animal lapping, Phys. Rev. Fluids **6**, 073102 (2021).
[111] Smith, N. M., Ebrahimi, H., Ghosh, R., and Dickerson, A. K., High-speed microjets issue from bursting oil gland reservoirs of citrus fruit, Proc. Natl. Acad. Sci. U.S.A. **115**, E5887–E5895 (2018).
[112] Martens, E. A., Watanabe, S., and Bohr, T., Model for polygonal hydraulic jumps, Phys. Rev. E **85**, 036316 (2012).
[113] Hager, W. H., *Energy dissipators and hydraulic jump*, Vol. 8 (Springer, 2013).
[114] Lord Rayleigh,, On the theory of long waves and bores, Proc. Roy. Soc. A **90**, 324–328 (1914).
[115] Watson, E. J., The radial spread of a liquid jet over a horizontal plane, J. Fluid Mech. **20**, 481–499 (1964).
[116] Olsson, R. G. and Turkdogan, E. T., Radial spread of a liquid stream on a horizontal plate, Nature **211**, 813–816 (1966).
[117] Bush, J. W. M. and Aristoff, J. M., The influence of surface tension on the circular hydraulic jump, J. Fluid Mech. **489**, 229–238 (2003).
[118] Mathur, M., DasGupta, R., Selvi, N. R., John, N. S., Kulkarni, G. U., and Govindarajan, R., Gravity-free hydraulic jumps and metal femtoliter cups, Phys. Rev. Lett. **98**, 164502 (2007).
[119] Bhagat, R. K., Jha, N., Linden, P., and Wilson, D. I., On the origin of the circular hydraulic jump in a thin liquid film, J. Fluid Mech. **851**, R5 (2018).
[120] Duchesne, A., Andersen, A., and Bohr, T., Surface tension and the origin of the circular hydraulic jump in a thin liquid film, Phys. Rev. Fluids **4**, 084001 (2019).
[121] Bohr, T. and Scheichl, B., Surface tension and energy conservation in a moving fluid, Phys. Rev. Fluids **6**, L052001 (2021).
[122] Bhagat, R. K. and Linden, P. F., The circular capillary jump, J. Fluid Mech. **896**, A25 (2020).
[123] Walker, T. W., Hsu, T. T., Frank, C. W., and Fuller, G. G., Role of shear-thinning on the dynamics of rinsing flow by an impinging jet, Phys. Fluids **24**, 093102 (2012).
[124] Walker, T. W., Hsu, T. T., Fitzgibbon, S., Frank, C. W., Mui, D. S., Zhu, J., Mendiratta, A., and Fuller, G. G., Enhanced particle removal using viscoelastic fluids, J. Rheol. **58**, 63–88 (2014).
[125] Hsu, T. T., Walker, T. W., Frank, C. W., and Fuller, G. G., Instabilities and elastic recoil of the two-fluid circular hydraulic jump, Exp. Fluids **55**, 1645 (2014).
[126] Ellegaard, C., Hansen, A. E., Haaning, A., Hansen, K., Marcussen, A., Bohr, T., Hansen, J. L., and Watanabe, S., Creating corners in kitchen sinks, Nature **392**, 767–768 (1998).

[127] Ellegaard, C., Hansen, A. E., Haaning, A., Hansen, K., Marcussen, A., Bohr, T., Hansen, J. L., and Watanabe, S., Cover illustration: Polygonal hydraulic jumps, Nonlinearity **12**, 1–7 (1999).

[128] Bush, J. W. M., Aristoff, J. M., and Hosoi, A. E., An experimental investigation of the stability of the circular hydraulic jump, J. Fluid Mech. **558**, 33–52 (2006).

[129] Nichols, T. E. and Bostwick, J. B., Geometry of polygonal hydraulic jumps and the role of hysteresis, Phys. Rev. Fluids **5**, 044005 (2020).

[130] Dressaire, E., Courbin, L., Crest, J., and Stone, H. A., Thin-film fluid flows over microdecorated surfaces: Observation of polygonal hydraulic jumps, Phys. Rev. Lett. **102**, 194503 (2009).

[131] Knorr, W., The geometry of burning-mirrors in antiquity, Isis **74**, 53–73 (1983).

[132] Hickson, P., Pfrommer, T., Cabanac, R., Crotts, A., Johnson, B., De Lapparent, V., Lanzetta, K. M., Gromoll, S., Mulrooney, M. K., Sivanandam, S., *et al.*, The large zenith telescope: A 6 m liquid-mirror telescope, Publ. Astro. Soc. Pacific **119**, 444 (2007).

[133] Wilson, R. N., *Reflecting telescope optics I: basic design theory and its historical development* (Springer, 2007).

[134] Price, H., Lu¨ pfert, E., Kearney, D., Zarza, E., Cohen, G., Gee, R., and Mahoney, R., Advances in parabolic trough solar power technology, J. Sol. Energy Eng. **124**, 109–125 (2002).

[135] Acheson, D. J., *Elementary Fluid Dynamics* (Clarendon Press, 1990).

[136] Lubarda, V. A., The shape of a liquid surface in a uniformly rotating cylinder in the presence of surface tension, Acta Mechanica **224**, 1365–1382 (2013).

[137] Jansson, T. R. N., Haspang, M. P., Jensen, K. H., Hersen, P., and Bohr, T., Polygons on a rotating fluid surface, Phys. Rev. Lett. **96**, 174502 (2006).

[138] Bergmann, R., Tophøj, L., Homan, T. A. M., Hersen, P., Andersen, A., and Bohr, T., Polygon formation and surface flow on a rotating fluid surface, J. Fluid Mech. **679**, 415 (2011).

[139] Andersen, A., Bohr, T., Stenum, B., Rasmussen, J. J., and Lautrup, B., Anatomy of a bathtub vortex, Phys. Rev. Lett. **91**, 104502 (2003).

[140] Smith, E., Out damned spot: the Lady Macbeth handwashing scene that became a Coronavirus meme, Penguin Articles (2020).

[141] Handwashing Liaison Group,, Hand washing: a modest measure—with big effects, British Med. J. **318**, 686 (1999).

[142] Todd, E. C., Michaels, B. S., Smith, D., Greig, J. D., and Bartleson, C. A., Outbreaks where food workers have been implicated in the spread of foodborne disease. Part 9. Washing and drying of hands to reduce microbial contamination, J. Food Protect. **73**, 1937–1955 (2010).

[143] Chin, A., Chu, J., Perera, M., Hui, K., Yen, H.-L., Chan, M., Peiris, M., and Poon, L., Stability of SARS-CoV-2 in different environmental conditions, Lancet Microbe **1**, E10 (2020).

[144] Poon, W. C. K., Brown, A. T., Direito, S. O. L., Hodgson, D. J. M., Le Nagard, L., Lips, A., MacPhee, C. E., Marenduzzo, D., Royer, J. R., Silva, A. F., *et al.*, Soft matter science and the COVID-19 pandemic, Soft Matter **16**, 8310–8324 (2020).

[145] Bar-On, Y. M., Flamholz, A., Phillips, R., and Milo, R., Science forum: SARS-CoV-2 (COVID-19) by the numbers, eLife **9**, e57309 (2020).

[146] Dancer, S. J., Revising Nightingale's legacy, J. Hosp. Infect. **105**, 344–345 (2020).

[147] Mittal, R., Ni, R., and Seo, J.-H., The flow physics of COVID-19, J. Fluid Mech. **894**, 1–14 (2020).

[148] Rotter, M. L., 150 years of hand disinfection-Semmelweis' heritage, Hyg. Med. **22**, 332–339 (1997).

[149] Hammond, P. S., Will we ever wash our hands of lubrication theory?, Phys. Fluids **33**, 081908 (2021).

[150] Gammon, J. and Hunt, J., COVID-19 and hand hygiene: the vital importance of hand drying, British J. Nursing **29**, 1003–1006 (2020).

[151] Lopes, M. C. and Bonaccurso, E., Evaporation control of sessile water drops by soft viscoelastic surfaces, Soft Matter **8**, 7875–7881 (2012).

[152] Gerber, J., Lendenmann, T., Eghlidi, H., Schutzius, T. M., and Poulikakos, D., Wetting transitions in droplet drying on soft materials, Nat. Commun. **10**, 1–10 (2019).

[153] Huang, C., Ma, W., and Stack, S., The hygienic efficacy of different hand-drying methods: a review of the evidence, Mayo Clinic Proc. **87**, 791–798 (2012).

[154] Reynolds, K. A., Sexton, J. D., Norman, A., and McClelland, D. J., Comparison of electric hand dryers and paper towels for hand hygiene: a critical review of the literature, J. Appl. Microbiol. **130**, 25–39 (2020).

[155] Best, E. L., Parnell, P., and Wilcox, M. H., Microbiological comparison of hand-drying methods: the potential for contamination of the environment, user, and bystander, J. Hospit. Infect. **88**, 199–206 (2014).

[156] Kang, Y.-j. and Frank, J. F., Biological aerosols: a review of airborne contamination and its measurement in dairy processing plants, J. Food Protect. **52**, 512–524 (1989).

[157] Walters, R. M., Mao, G., Gunn, E. T., and Hornby, S., Cleansing formulations that respect skin barrier integrity, Dermatol. Res. Pract. **2012**, 495917 (2012).

[158] Cerda, E. and Mahadevan, L., Geometry and physics of wrinkling, Phys. Rev. Lett. **90**, 074302 (2003).

[159] Aharoni, H., Todorova, D. V., Albarrán, O., Goehring, L., Kamien, R. D., and Katifori, E., The smectic order of wrinkles, Nat. Commun. **8**, 1–7 (2017).

[160] Proksch, E., Berardesca, E., Misery, L., Engblom, J., and Bouwstra, J., Dry skin management: practical approach in light of latest research on skin structure and function, J. Dermatol. Treat. **31**, 716–722 (2020).

[161] Dussaud, A. D., Adler, P. M., and Lips, A., Liquid transport in the networked microchannels of the skin surface, Langmuir **19**, 7341–7345 (2003).

[162] Das, C. and Olmsted, P. D., The physics of stratum corneum lipid membranes, Phil. Trans. Roy. Soc. A **374**, 20150126 (2016).

[163] Brooks, N., Cates, M., Clegg, P., Lips, A., Poon, W., and Seddon, J., Soft interfacial materials: from fundamentals to formulation, Phil. Trans. Roy. Soc. A **374**, 20150135 (2016).

[164] Brennen, C. E., *Fundamentals of multiphase flow* (Cambridge University Press, 2005).

[165] Michaelides, E., Crowe, C. T., and Schwarzkopf, J. D., *Multiphase flow handbook*, 2nd ed. (CRC Press, 2016).

[166] Ouimet, M., Bartending guide: Specific gravity chart (2015), last accessed: 15-Jul-2021.

[167] Mahrt, L., Stably stratified atmospheric boundary layers, Annu. Rev. Fluid Mech. **46**, 23–45 (2014).

[168] Li, G., Cheng, L., Zhu, J., Trenberth, K. E., Mann, M. E., and Abraham, J. P., Increasing ocean stratification over the past half-century, Nat. Climate Change **10**, 1116–1123 (2020).

[169] Grimshaw, R., ed., *Environmental stratified flows* (Springer, 2002).

[170] Pedlosky, J., *Geophysical fluid dynamics* (Springer-Verlag, 1987).

[171] Turner, J. S., Jets and plumes with negative or reversing buoyancy, J. Fluid Mech. **26**, 779–792 (1966).

[172] Hunt, G. R. and Burridge, H. C., Fountains in industry and nature, Annu. Rev. Fluid Mech. **47**, 195–220 (2015).

[173] Xue, N., Khodaparast, S., and Stone, H. A., Fountain mixing in a filling box at low Reynolds numbers, Phys. Rev. Fluids **4**, 024501 (2019).

[174] Wood, I. R. F. and Simpson, J. E., Jumps in layered miscible fluids, J. Fluid Mech. **140**, 329–342 (1984).

[175] Thorpe, S. A. and Li, L., Turbulent hydraulic jumps in a stratified shear flow. Part 2, J. Fluid Mech. **758**, 94–120 (2014).

[176] Baines, P. G., Internal hydraulic jumps in two-layer systems, J. Fluid Mech. **787**, 1–15 (2016).

[177] Ungarish, M. and Hogg, A. J., Models of internal jumps and the fronts of gravity currents: unifying two-layer theories and deriving new results, J. Fluid Mech. **846**, 654–685 (2018).

[178] Ogden, K. A. and Helfrich, K., Internal hydraulic jumps in two-layer flows with increasing upstream shear, Phys. Rev. Fluids **5**, 074803 (2020).

[179] Dhar, M., Ray, S., Das, G., and Das, P. K., Internal hydraulic jump in plane Poiseuille two-layer flow: theoretical, numerical and experimental study, J. Fluid Mech. **912**, A45 (2021).

[180] Yoshikawa, H. N. and Wesfreid, J. E., Oscillatory Kelvin–Helmholtz instability. Part 2. An experiment in fluids with a large viscosity contrast, J. Fluid Mech. **675**, 249–267 (2011).

[181] Benjamin, T. B., Internal waves of permanent form in fluids of great depth, J. Fluid Mech. **29**, 559–592 (1967).

[182] Helfrich, K. R. and Melville, W. K., Long nonlinear internal waves, Annu. Rev. Fluid Mech. **38**, 395–425 (2006).

[183] Vallis, G. K., *Atmospheric and oceanic fluid dynamics* (Cambridge University Press, 2017).

[184] Garrett, C. and Munk, W., Internal waves in the ocean, Annu. Rev. Fluid Mech. **11**, 339–369 (1979).

[185] Lamb, D. and Verlinde, J., *Physics and chemistry of clouds* (Cambridge University Press, 2011).

[186] Lord Kelvin,, Hydrokinetic solutions and observations, Philos. Mag. **42**, 362–377 (1871).

[187] Drazin, P. G. and Reid, W. H., *Hydrodynamic stability* (Cambridge University Press, 2010).

[188] Yan, Z., Sun, L., Xiao, J., and Lan, Y., The profile of an oil-water interface in a spin-up rotating cylindrical vessel, Am. J. Phys. **85**, 271–276 (2017).

[189] Peltier, W. R. and Caulfield, C. P., Mixing efficiency in stratified shear flows, Annu. Rev. Fluid Mech. **35**, 135–167 (2003).

[190] Thorpe, S. A., Experiments on the instability of stratified shear flows: immiscible fluids, J. Fluid Mech. **39**, 25–48 (1969).

[191] Drazin, P. G., Kelvin–Helmholtz instability of finite amplitude, J. Fluid Mech. **42**, 321–335 (1970).

[192] Qin, H., Zhang, R., Glasser, A. S., and Xiao, J., Kelvin-Helmholtz instability is the result of parity-time symmetry breaking, Phys. Plasmas **26**, 032102 (2019).

[193] Foullon, C., Verwichte, E., Nakariakov, V. M., Nykyri, K., and Farrugia, C. J., Magnetic Kelvin-Helmholtz instability at the sun, Astrophys. J. Lett. **729**, L8 (2011).

[194] Bodo, G., Mignone, A., and Rosner, R., Kelvin-Helmholtz instability for relativistic fluids, Phys. Rev. E **70**, 036304 (2004).

[195] Blaauwgeers, R., Eltsov, V. B., Eska, G., Finne, A. P., Haley, R. P., Krusius, M., Ruohio, J. J., Skrbek, L., and Volovik, G. E., Shear flow and Kelvin-Helmholtz instability in superfluids, Phys. Rev. Lett. **89**, 155301 (2002).

[196] Lord Rayleigh,, Investigation of the character of the equilibrium of an incompressible heavy fluid of variable density, Proc. Lond. Math. Soc. **s1-14**, 170–177 (1882).

[197] Taylor, G. I., The instability of liquid surfaces when accelerated in a direction perpendicular to their planes. I, Proc. Roy. Soc. A **201**, 192–196 (1950).

[198] Lewis, D. J., The instability of liquid surfaces when accelerated in a direction perpendicular to their planes. II, Proc. Roy. Soc. A **202**, 81–96 (1950).

[199] Chandrasekhar, S., *Hydrodynamic and hydromagnetic stability* (Dover Publications, New York, 1961).

[200] Kuranz, C. C., Park, H.-S., Huntington, C. M., Miles, A. R., Remington, B. A., Plewa, T., Trantham, M., Robey, H., Shvarts, D., Shimony, A., *et al.*, How high energy fluxes may affect Rayleigh–Taylor instability growth in young supernova remnants, Nat. Commun. **9**, 1–6 (2018).

[201] Abarzhi, S. I., Bhowmick, A. K., Naveh, A., Pandian, A., Swisher, N. C., Stellingwerf, R. F., and Arnett, W. D., Supernova, nuclear synthesis, fluid instabilities, and interfacial mixing, Proc. Natl. Acad. Sci. U.S.A. **116**, 18184–18192 (2019).

[202] Andrews, M. J. and Dalziel, S. B., Small Atwood number Rayleigh–Taylor experiments, Phil. Trans. Roy. Soc. A **368**, 1663–1679 (2010).

[203] Boffetta, G. and Mazzino, A., Incompressible Rayleigh–Taylor turbulence, Annu. Rev. Fluid Mech. **49**, 119–143 (2017).

[204] Dehaeck, S., Wylock, C., and Colinet, P., Evaporating cocktails, Phys. Fluids **21**, 091108 (2009).

[205] Kreis, T., Digital holographic interference-phase measurement using the Fourier-transform method, J. Opt. Soc. America A **3**, 847–855 (1986).

[206] Mossige, E. J., Chandran Suja, V., Islamov, M., Wheeler, S., and Fuller, G. G., Evaporation-induced Rayleigh-Taylor instabilities in polymer solutions, Phil. Trans. Roy. Soc. A **378**, 20190533 (2020).

[207] Dukler, Y., Ji, H., Falcon, C., and Bertozzi, A. L., Theory for undercompressive shocks in tears of wine, Phys. Rev. Fluids **5**, 034002 (2020).

[208] Marangoni, C., Ueber die Ausbreitung der Tropfen einer Flüssigkeit auf der Oberfläche einer anderen, Ann. Phys. (Berlin) **219**, 337–354 (1871).

[209] Levich, V. G. and Krylov, V. S., Surface-tension-driven phenomena, Annu. Rev. Fluid Mech. **1**, 293–316 (1969).

[210] Halpern, D. and Grotberg, J. B., Dynamics and transport of a localized soluble surfactant on a thin film, J. Fluid Mech. **237**, 1–11 (1992).

[211] Lee, K. S. and Starov, V. M., Spreading of surfactant solutions over thin aqueous layers: Influence of solubility

and micelles disintegration, J. Colloid Interf. Sci. **314**, 631–642 (2007).
[212] Roché, M., Li, Z., Griffiths, I. M., Le Roux, S., Cantat, I., Saint-Jalmes, A., and Stone, H. A., Marangoni flow of soluble amphiphiles, Phys. Rev. Lett. **112**, 208302 (2014).
[213] Kim, H., Muller, K., Shardt, O., Afkhami, S., and Stone, H. A., Solutal Marangoni flows of miscible liquids drive transport without surface contamination, Nat. Phys. **13**, 1105–1110 (2017).
[214] Thomson, J., On certain curious motions observable at the surfaces of wine and other alcoholic liquors, Philos. Mag. **10**, 330–333 (1855).
[215] Fournier, J. B. and Cazabat, A. M., Tears of wine, Europhys. Lett. **20**, 517 (1992).
[216] Settles, G. S., *Schlieren and shadowgraph techniques: visualizing phenomena in transparent media* (Springer, 2001).
[217] Vuilleumier, R., Ego, V., Neltner, L., and Cazabat, A. M., Tears of wine: the stationary state, Langmuir **11**, 4117–4121 (1995).
[218] Hosoi, A. E. and Bush, J. W. M., Evaporative instabilities in climbing films, J. Fluid Mech. **442**, 217 (2001).
[219] Fanton, X. and Cazabat, A. M., Spreading and instabilities induced by a solutal Marangoni effect, Langmuir **14**, 2554–2561 (1998).
[220] Venerus, D. C. and Simavilla, D. N., Tears of wine: New insights on an old phenomenon, Sci. Rep. **5**, 16162 (2015).
[221] Nikolov, A., Wasan, D., and Lee, J., Tears of wine: The dance of the droplets, Adv. Colloid Interf. Sci. **256**, 94–100 (2018).
[222] Sur, J., Bertozzi, A. L., and Behringer, R. P., Reverse undercompressive shock structures in driven thin film flow, Phys. Rev. Lett. **90**, 126105 (2003).
[223] Münch, A., Pinch-off transition in Marangoni-driven thin films, Phys. Rev. Lett. **91**, 016105 (2003).
[224] Williams, S. J., Brown, M. J., and Carrithers, A. D., Whiskey webs: Microscale "fingerprints" of bourbon whiskey, Phys. Rev. Fluids **4**, 100511 (2019).
[225] Velasco, C., Jones, R., King, S., and Spence, C., Assessing the influence of the multisensory environment on the whisky drinking experience, Flavour **2**, 23 (2013).
[226] Maclean, C., *Malt Whisky* (Octopus, 2020).
[227] Miller, G. H., *Whisky Science: A Condensed Distillation*, 1st ed. (Springer International, 2019).
[228] Russell, I., Bamforth, C., and Stewart, G., *Whisky: technology, production and marketing* (Elsevier, 2014).
[229] MacLean, C., Whisky university - what about the legs - viscimetry?, `https://www.youtube.com/watch?v=_OwVN6mGHhA` (2010), last accessed: 8-Oct-2020.
[230] Mosedale, J. R., Effects of oak wood on the maturation of alcoholic beverages with particular reference to whisky, Forestry: Int. J. Forest Res. **68**, 203–230 (1995).
[231] Hlavác, P. and Božiková, M., Influence of storing and temperature on rheologic and thermophysical properties of whisky samples, J. Central Eur. Agricult. **14**, 291–304 (2013).
[232] Davidson, J. A., Foam stability as an historic measure of the alcohol concentration in distilled alcoholic beverages, J. Colloid Interf. Sci. **81**, 540–542 (1981).
[233] MacLean, C., The Scotch malt whisky society (SMWS) masterclass: What beading can tell us, `https://www.youtube.com/watch?v=x_WDNHyfsOQ` (2018), last accessed: 8-Oct-2020.
[234] Smith, G. D., *A to Z of Whisky* (Neil Wilson Publishing, 2011).
[235] Karlsson, B. C. and Friedman, R., Dilution of whisky–the molecular perspective, Sci. Rep. **7**, 1–9 (2017).
[236] Harwood, W. S., Parker, M. N., and Drake, M., Influence of ethanol concentration on sensory perception of rums using temporal check-all-that-apply, J. Sensory Stud. **35**, e12546 (2020).
[237] Dizechi, M. and Marschall, E., Viscosity of some binary and ternary liquid mixtures, J. Chem. Eng. Data **27**, 358–363 (1982).
[238] Carrithers, A. D., Brown, M. J., Rashed, M. Z., Islam, S., Velev, O. D., and Williams, S. J., Multiscale self-assembly of distinctive weblike structures from evaporated drops of dilute American whiskeys, ACS Nano **14**, 5417–5425 (2020).
[239] Williams, S. J., Whiskey webs: Fingerprints of evaporated bourbon, Phys. Today **74**, 62–63 (2021).
[240] Kim, H., Boulogne, F., Um, E., Jacobi, I., Button, E., and Stone, H. A., Controlled uniform coating from the interplay of Marangoni flows and surface-adsorbed macromolecules, Phys. Rev. Lett. **116**, 124501 (2016).
[241] Yakhno, T., Sanin, A., Yakhno, V., Kazakov, V., Pakhomov, A., Guguchkina, T., and Markovsky, M., Drying drop technology in wine and hard drinks quality control, in *Food Control and Biosecurity* (Elsevier, 2018) pp. 451–480.
[242] Keller, J. B., Surface tension force on a partly submerged body, Phys. Fluids **10**, 3009–3010 (1998).
[243] Wasin, M., Marangoni effect, `https://www.youtube.com/watch?v=y6RSGzxEjVM` (2017), last accessed: 5-May-2020.
[244] Bush, J. W. M. and Hu, D. L., Walking on water: biolocomotion at the interface, Annu. Rev. Fluid Mech. **38**, 339–369 (2006).
[245] Renney, C., Brewer, A., and Mooibroek, T. J., Easy demonstration of the Marangoni effect by prolonged and directional motion: "Soap Boat 2.0", J. Chem. Educ. **90**, 1353–1357 (2013).
[246] Kohira, M. I., Hayashima, Y., Nagayama, M., and Nakata, S., Synchronized self-motion of two camphor boats, Langmuir **17**, 7124–7129 (2001).
[247] Burton, L. J., Cheng, N., and Bush, J. W. M., The cocktail boat, Integr. Comp. Biol. **54**, 969–973 (2014).
[248] Schmidt-Nielsen, K. and Randall, D. J., *Animal Physiology: Adaptation and Environment* (Cambridge University Press, 1997).
[249] Maass, C. C., Krüger, C., Herminghaus, S., and Bahr, C., Swimming droplets, Annu. Rev. Cond. Matt. Phys. **7**, 171–193 (2016).
[250] Jin, C., Chen, Y., Maass, C. C., and Mathijssen, A. J. T. M., Collective entrainment and confinement amplify transport by schooling microswimmers, Phys. Rev. Lett. **127**, 088006 (2021).
[251] Dietrich, K., Jaensson, N., Buttinoni, I., Volpe, G., and Isa, L., Microscale Marangoni surfers, Phys. Rev. Lett. **125**, 098001 (2020).
[252] Timm, M. L., Kang, S. J., Rothstein, J. P., and Masoud, H., A remotely controlled Marangoni surfer, Bioinsp. Biomim. **16**, 066014 (2021).
[253] Anderson, J. L., Colloid transport by interfacial forces, Annu. Rev. Fluid Mech. **21**, 61–99 (1989).

[254] Howse, J. R., Jones, R. A. L., Ryan, A. J., Gough, T., Vafabakhsh, R., and Golestanian, R., Self-motile colloidal particles: From directed propulsion to random walk, Phys. Rev. Lett. **99**, 048102 (2007).

[255] Koch, D. L. and Subramanian, G., Collective hydrodynamics of swimming microorganisms: living fluids, Annu. Rev. Fluid Mech. **43**, 637–659 (2011).

[256] Marchetti, M. C., Joanny, J. F., Ramaswamy, S., Liverpool, T. B., Prost, J., Rao, M., and Simha, R. A., Hydrodynamics of soft active matter, Rev. Mod. Phys. **85**, 1143–1189 (2013).

[257] Bechinger, C., Di Leonardo, R., Löwen, H., Reichhardt, C., Volpe, G., and Volpe, G., Active particles in complex and crowded environments, Rev. Mod. Phys. **88**, 045006 (2016).

[258] Cates, M. E. and Tailleur, J., Motility-induced phase separation, Annu. Rev. Cond. Mat. Phys. **6**, 219 (2015).

[259] Elgeti, J., Winkler, R. G., and Gompper, G., Physics of microswimmers – Single particle motion and collective behavior: A review, Rep. Progr. Phys. **78**, 056601 (2015).

[260] Zöttl, A. and Stark, H., Emergent behavior in active colloids, J. Phys. Cond. Mat. **28**, 253001 (2016).

[261] Weber, C. A., Zwicker, D., Jülicher, F., and Lee, C. F., Physics of active emulsions, Rep. Progr. Phys. **82**, 064601 (2019).

[262] Anderson, J. L., Transport mechanisms of biological colloids, Annal. New York Acad. Sci. **469**, 166 (1986).

[263] Needleman, D. and Dogic, Z., Active matter at the interface between materials science and cell biology, Nat. Rev. Mater. **2**, 17048 (2017).

[264] Keiser, L., Bense, H., Colinet, P., Bico, J., and Reyssat, E., Marangoni bursting: Evaporation-induced emulsification of binary mixtures on a liquid layer, Phys. Rev. Lett. **118**, 074504 (2017).

[265] Liger-Belair, G., Polidori, G., and Jeandet, P., Recent advances in the science of champagne bubbles, Chem. Soc. Rev. **37**, 2490–2511 (2008).

[266] Planinsic, G., Fizziology, Phys. Educ. **39**, 65 (2004).

[267] Polidori, G., Jeandet, P., and Liger-Belair, G., Bubbles and flow patterns in Champagne: Is the fizz just for show, or does it add to the taste of sparkling wines?, American Sci. **97**, 294–301 (2009).

[268] Chandrashekar, J., Yarmolinsky, D., von Buchholtz, L., Oka, Y., Sly, W., Ryba, N. J., and Zuker, C. S., The taste of carbonation, Science **326**, 443–445 (2009).

[269] Zenit, R. and Rodríguez-Rodríguez, J., The fluid mechanics of bubbly drinks, Physics Today **71**, 44 (2018).

[270] Mathai, V., Lohse, D., and Sun, C., Bubbly and buoyant particle–laden turbulent flows, Annu. Rev. Cond. Matt. Phys. **11**, 529–559 (2020).

[271] Rage, G., Atasi, O., Wilhelmus, M. M., Hernández-Sánchez, J. F., Haut, B., Scheid, B., Legendre, D., and Zenit, R., Bubbles determine the amount of alcohol in Mezcal, Sci. Rep. **10**, 1–16 (2020).

[272] Liger-Belair, G., Cordier, D., and Georges, R., Underexpanded supersonic CO_2 freezing jets during champagne cork popping, Sci. Adv. **5**, eaav5528 (2019).

[273] Lubetkin, S. and Blackwell, M., The nucleation of bubbles in supersaturated solutions, J. Colloid Interf. Sci. **126**, 610–615 (1988).

[274] Poujol, M., Wunenburger, R., Ollivier, F. m. c., Antkowiak, A., and Pierre, J., Sound of effervescence, Phys. Rev. Fluids **6**, 013604 (2021).

[275] Beaumont, F., Liger-Belair, G., and Polidori, G., Unveiling self-organized two-dimensional (2D) convective cells in champagne glasses, J. Food Eng. **188**, 58–65 (2016).

[276] Ford, I. J., Statistical mechanics of nucleation: a review, Proc. Inst. Mech. Eng. C **218**, 883–899 (2004).

[277] Jones, S. F., Evans, G. M., and Galvin, K. P., The cycle of bubble production from a gas cavity in a supersaturated solution, Adv. Colloid Interf. Sci. **80**, 51–84 (1999).

[278] Polidori, G., Beaumont, F., Jeandet, P., and Liger-Belair, G., Artificial bubble nucleation in engraved champagne glasses, J. Visualiz. **11**, 279 (2008).

[279] Liger-Belair, G., Vignes-Adler, M., Voisin, C., Robillard, B., and Jeandet, P., Kinetics of gas discharging in a glass of champagne: The role of nucleation sites, Langmuir **18**, 1294–1301 (2002).

[280] Liger-Belair, G., Parmentier, M., and Jeandet, P., Modeling the kinetics of bubble nucleation in champagne and carbonated beverages, J. Phys. Chem. B **110**, 21145–21151 (2006).

[281] Beaumont, F., Liger-Belair, G., and Polidori, G., Flow analysis from PIV in engraved champagne tasting glasses: flute versus coupe, Exp. Fluids **56**, 1–6 (2015).

[282] Dijkstra, H. A., On the structure of cellular solutions in Rayleigh–Bénard–Marangoni flows in small-aspect-ratio containers, J. Fluid Mech. **243**, 73–102 (1992).

[283] Beaumont, F., Liger-Belair, G., and Polidori, G., Computational Fluid Dynamics (CFD) as a tool for investigating self-organized ascending bubble-driven flow patterns in Champagne glasses, Foods **9**, 972 (2020).

[284] Liger-Belair, G., Cilindre, C., Gougeon, R. D., Lucio, M., Gebefügi, I., Jeandet, P., and Schmitt-Kopplin, P., Unraveling different chemical fingerprints between a champagne wine and its aerosols, Proc. Natl. Acad. Sci. U.S.A. **106**, 16545–16549 (2009).

[285] Ghabache, E., Liger-Belair, G., Antkowiak, A., and Séon, T., Evaporation of droplets in a Champagne wine aerosol, Sci. Rep. **6**, 1–10 (2016).

[286] Cantat, I., Cohen-Addad, S., Elias, F., Graner, F., Höhler, R., Pitois, O., Rouyer, F., and Saint-Jalmes, A., *Foams: structure and dynamics* (Oxford University Press, 2013).

[287] Weaire, D. and Hutzler, S., *The Physics of Foams* (Clarendon Press, 2001).

[288] Kraynik, A. M., Foam flows, Annu. Rev. Fluid Mech. **20**, 325–357 (1988).

[289] Weaire, D., Hutzler, S., Cox, S., Kern, N., Alonso, M. D., and Drenckhan, W., The fluid dynamics of foams, J. Phys. Cond. Mat. **15**, S65–S73 (2002).

[290] Manikantan, H. and Squires, T. M., Surfactant dynamics: hidden variables controlling fluid flows, J. Fluid Mech. **892**, P1 (2020).

[291] Janiaud, E. and Graner, F., Foam in a two-dimensional Couette shear: a local measurement of bubble deformation, J. Fluid Mech. **532**, 243–267 (2005).

[292] Durian, D. J., Foam mechanics at the bubble scale, Phys. Rev. Lett. **75**, 4780–4783 (1995).

[293] Durian, D. J., Weitz, D. A., and Pine, D. J., Scaling behavior in shaving cream, Phys. Rev. A **44**, R7902–R7905 (1991).

[294] Prakash, V. N., Tagawa, Y., Calzavarini, E., Mercado, J. M., Toschi, F., Lohse, D., and Sun, C., How gravity and size affect the acceleration statistics of bubbles in

turbulence, New J. Phys. **14**, 105017 (2012).
[295] Almgren, F. J. and Taylor, J. E., The geometry of soap films and soap bubbles, Scientific American **235**, 82–93 (1976).
[296] Haedelt, J., Beckett, S., and Niranjan, K., Bubble-included chocolate: Relating structure with sensory response, J. Food Sci. **72**, E138–E142 (2007).
[297] Kraynik, A. M., Neilsen, M. K., Reinelt, D. A., and Warren, W. E., Foam micromechanics, in *Foams and emulsions*, edited by J. Sadoc and R. N. (Springer, 1999) pp. 259–286.
[298] Janssen, F., Wouters, A. G., Meeus, Y., Moldenaers, P., Vermant, J., and Delcour, J. A., The role of non-starch polysaccharides in determining the air-water interfacial properties of wheat, rye, and oat dough liquor constituents, Food Hydrocolloids **105**, 105771 (2020).
[299] Robin, F., Engmann, J., Pineau, N., Chanvrier, H., Bovet, N., and Della Valle, G., Extrusion, structure and mechanical properties of complex starchy foams, J. Food Eng. **98**, 19–27 (2010).
[300] Watamura, T., Iwatsubo, F., Sugiyama, K., Yamamoto, K., Yotsumoto, Y., and Shiono, T., Bubble cascade in Guinness beer is caused by gravity current instability, Sci. Rep. **9**, 1–9 (2019).
[301] Watamura, T., Sugiyama, K., Yotsumoto, Y., Suzuki, M., and Wakabayashi, H., Bubble cascade may form not only in stout beers, Phys. Rev. E **103**, 063103 (2021).
[302] Rodríguez-Rodríguez, J., Casado-Chacón, A., and Fuster, D., Physics of beer tapping, Phys. Rev. Lett. **113**, 214501 (2014).
[303] Vitale, S. A. and Katz, J. L., Liquid droplet dispersions formed by homogeneous liquid- liquid nucleation:'the ouzo effect', Langmuir **19**, 4105–4110 (2003).
[304] Ashurst, P. R., *Food flavorings* (Springer, 2012).
[305] Sitnikova, N. L., Sprik, R., Wegdam, G., and Eiser, E., Spontaneously formed trans-anethol/water/alcohol emulsions: mechanism of formation and stability, Langmuir **21**, 7083–7089 (2005).
[306] Grillo, I., Small-angle neutron scattering study of a world-wide known emulsion: Le Pastis, Coll. Surf. A: Physicochem. Eng. Asp. **225**, 153–160 (2003).
[307] Chiappisi, L. and Grillo, I., Looking into limoncello: the structure of the Italian liquor revealed by small-angle neutron scattering, ACS Omega **3**, 15407–15415 (2018).
[308] Lu, Z., Schaarsberg, M. H. K., Zhu, X., Yeo, L. Y., Lohse, D., and Zhang, X., Universal nanodroplet branches from confining the ouzo effect, Proc. Natl. Acad. Sci. U.S.A. **114**, 10332–10337 (2017).
[309] Devauchelle, O., Petroff, A. P., Seybold, H. F., and Rothman, D. H., Ramification of stream networks, Proc. Natl. Acad. Sci. U.S.A. **109**, 20832–20836 (2012).
[310] Cohen, Y., Devauchelle, O., Seybold, H. F., Yi, R. S., Szymczak, P., and Rothman, D. H., Path selection in the growth of rivers, Proc. Natl. Acad. Sci. U.S.A. **112**, 14132–14137 (2015).
[311] Tan, H., Diddens, C., Lv, P., Kuerten, J. G. M., Zhang, X., and Lohse, D., Evaporation-triggered microdroplet nucleation and the four life phases of an evaporating ouzo drop, Proc. Natl. Acad. Sci. U.S.A. **113**, 8642–8647 (2016).
[312] Diddens, C., Tan, H., Lv, P., Versluis, M., Kuerten, J. G. M., Zhang, X., and Lohse, D., Evaporating pure, binary and ternary droplets: thermal effects and axial symmetry breaking, J. Fluid Mech. **823**, 470–497 (2017).
[313] Tan, H., Diddens, C., Versluis, M., Butt, H.-J., Lohse, D., and Zhang, X., Self-wrapping of an ouzo drop induced by evaporation on a superamphiphobic surface, Soft Matter **13**, 2749–2759 (2017).
[314] O'Sullivan, J. J., Drapala, K. P., Kelly, A. L., and O'Mahony, J. A., The use of inline high-shear rotor-stator mixing for preparation of high-solids milk protein-stabilised oil-in-water emulsions with different protein: fat ratios, J. Food Eng. **222**, 218–225 (2018).
[315] Ganachaud, F. and Katz, J. L., Nanoparticles and nanocapsules created using the ouzo effect: Spontaneous emulsification as an alternative to ultrasonic and high-shear devices, ChemPhysChem **6**, 209–216 (2005).
[316] Lepeltier, E., Bourgaux, C., and Couvreur, P., Nanoprecipitation and the 'ouzo effect': Application to drug delivery devices, Adv. Drug Deliv. Rev. **71**, 86–97 (2014).
[317] Almoustafa, H. A., Alshawsh, M. A., and Chik, Z., Technical aspects of preparing PEG-PLGA nanoparticles as carrier for chemotherapeutic agents by nanoprecipitation method, Int. J. Pharm. **533**, 275–284 (2017).
[318] Stokes, J. R., Boehm, M. W., and Baier, S. K., Oral processing, texture and mouthfeel: From rheology to tribology and beyond, Curr. Opin. Colloid Interf. Sci. **18**, 349–359 (2013).
[319] Sahin, S. and Sumnu, S. G., *Physical Properties of Foods*, Food Science Text Series (Springer, 2006).
[320] Borwankar, R. P. and Shoemaker, C. F., eds., *Rheology of foods* (Elsevier, 1992).
[321] Brummer, R., *Rheology essentials of cosmetic and food emulsions* (Springer, 2006).
[322] Fischer, P. and Windhab, E. J., Rheology of food materials, Curr. Opin. Colloid Interf. Sci. **16**, 36–40 (2011).
[323] Vilgis, T. A., Polymer theory: path integrals and scaling, Phys. Rep. **336**, 167–254 (2000).
[324] Dintzis, F. R., Shear-thickening behavior and shear-induced structure in gently solubilized starches, Cereal chemistry **v. 73**, pp. 638–643–1996 v.73 no.5 (1996).
[325] Figoni, P. I. and Shoemaker, C. F., Characterization of time dependent flow properties of mayonnaise under steady shear, J. Texture Studies **14**, 431–442 (1983).
[326] Goshawk, J., Binding, D., Kell, D., and Goodacre, R., Rheological phenomena occurring during the shearing flow of mayonnaise, J. Rheol. **42**, 1537–1553 (1998).
[327] Balmforth, N. J., Frigaard, I. A., and Ovarlez, G., Yielding to stress: recent developments in viscoplastic fluid mechanics, Annu. Rev. Fluid Mech. **46**, 121–146 (2014).
[328] Larson, R. G. and Wei, Y., A review of thixotropy and its rheological modeling, J. Rheol. **63**, 477–501 (2019).
[329] Macosko, C. W., *Rheology: Principles, Measurements, and Applications* (Wiley-VCR, 1994).
[330] McCrum, N. G., Buckley, C. P., and Bucknall, C. B., *Principles of Polymer Engineering* (Oxford University Press, 1988).
[331] Bird, R. B., Armstrong, R. C., and Hassager, O., *Dynamics of Polymeric Liquids, Volume 1: Fluid Mechanics* (Wiley, 1987).
[332] We are KIX,, Can you walk on water? (2014), video available at `https://www.youtube.com/watch?v=dts-LIdwK0O`. Last accessed: 20-Nov-2021.
[333] Alzamora, S. M., Viollaz, P. E., Martínez, V. Y., Nieto, A. B., and Salvatori, D., Exploring the linear viscoelastic properties structure relationship in processed fruit tissues, in *Food Engineering: Integrated*

Approaches, edited by G. F. Gutiérrez-López, G. V. Barbosa-Cánovas, J. Welti-Chanes, and E. Parada-Arias (Springer, New York, 2008) pp. 155–181.
[334] B. Yoo,, Effect of temperature on dynamic rheology of Korean honeys, J. Food Eng. **65**, 459–463 (2004).
[335] Skinner, G. E. and Rao, V. N. M., Linear viscoelastic behavior of frankfurters, J. Texture Stud. **17**, 421–432 (1986).
[336] Zhao, N., Li, B., Zhu, Y., Li, D., and Wang, L., Viscoelastic analysis of oat grain within linear viscoelastic region by using dynamic mechanical analyzer, Int. J. Food Eng. **16**, 20180350 (2020).
[337] Bolliger, S., Wildmoser, H., Goff, H. D., and Tharp, B. W., Relationships between ice cream mix viscoelasticity and ice crystal growth in ice cream, Int. Dairy J. **10**, 791–797 (2000).
[338] Bhattacharya, S., Stress relaxation behaviour of moth bean flour dough: Product characteristics and suitability of model, J. Food Eng. **97**, 539–546 (2010).
[339] Alvarez, M. D., Canet, W., Cuesta, F., and Lamua, M., Viscoelastic characterization of solid foods from creep compliance data: application to potato tissues, Z. Lebensm. Unters. Forsch. **207**, 356–362 (1998).
[340] Del Nobile, M., Chillo, S., Mentana, A., and Baiano, A., Use of the generalized maxwell model for describing the stress relaxation behavior of solid-like foods, J. Food Eng. **78**, 978–983 (2007).
[341] Ruiz-Márquez, D., Partal, P., Franco, J. M., and Gallegos, C., Linear viscoelastic behaviour of oil-in-water food emulsions stabilised by tuna-protein isolates, Food Sci. Tech. Int. **19**, 3–10 (2013).
[342] Benezech, T. and Maingonnat, J., Characterization of the rheological properties of yoghurt—a review, J. Food Eng. **21**, 447–472 (1994).
[343] Poole, R. J., The Deborah and Weissenberg numbers, Rheol. Bull **53**, 32–39 (2012).
[344] Krokida, M. K., Maroulis, Z. B., and Saravacos, G. D., Rheological properties of fluid fruit and vegetable puree products: Compilation of literature data, Int. J. Food Prop. **4**, 179–200 (2001).
[345] Carreau, P. J., Rheological equations from molecular network theories, Trans. Soc. Rheol. **16**, 99–127 (1972).
[346] Yasuda, K., Armstrong, R. C., and Cohen, R. E., Shear flow properties of concentrated solutions of linear and star branched polystyrenes, Rheol. Acta **20**, 163–178 (1981).
[347] Cross, M. M., Rheology of non-Newtonian fluids: A new flow equation for pseudoplastic systems, J. Colloid Sci. **20**, 417–437 (1965).
[348] Karlsson, A., Ipsen, R., Schrader, K., and Ardö, Y., Relationship between physical properties of casein micelles and rheology of skim milk concentrate, J. Dairy Sci. **88**, 3784–3797 (2005).
[349] Tárrega, A., Durán, L., and Costell, E., Rheological characterization of semisolid dairy desserts. effect of temperature, Food Hydrocolloids **19**, 133–139 (2005).
[350] Bingham, E. C., *Fluidity and Plasticity* (McGraw-Hill, 1922).
[351] Rao, M. A. and Cooley, H. J., Rheological behavior of tomato pastes in steady and dynamic shear, J. Texture Stud. **23**, 415–425 (1992).
[352] Herschel, W. H. and Bulkley, R., Konsistenzmessungen von Gummi-Benzollösungen, Kolloid-Zeitschrift **39**, 291–300 (1926).
[353] Ramaswamy, H. S. and Basak, S., Rheology of stirred yogurts, J. Texture Stud. **22**, 231–241 (1991).
[354] Oldroyd, J. G. and Wilson, A. H., On the formulation of rheological equations of state, Proc. Roy. Soc. A **200**, 523–541 (1950).
[355] Freeman, S. M. and Weissenberg, K., Some new rheological phenomena and their significance for the constitution of materials, Nature **162**, 320–323 (1948).
[356] Muller, H. G., Weissenberg effect in the thick white of the hen's egg, Nature **189**, 213–214 (1961).
[357] Walker, J., The amateur scientist, Scientific American **239**, 186–197 (1978).
[358] Reiner, M., Scott Blair, G. W., and Hawley, H. B., The Weissenberg effect in sweetened condensed milk, J. Soc. Chem. Ind. **68**, 327–328 (1949).
[359] Wiegand, J. H., Demonstrating the Weissenberg effect with gelatin, J. Chem. Educ. **40**, 475 (1963).
[360] Nelson, A. Z., Bras, R. E., Liu, J., and Ewoldt, R. H., Extending yield-stress fluid paradigms, J. Rheol. **62**, 357–369 (2018).
[361] Martinetti, L., Mannion, A. M., Voje, W. E., Xie, R., Ewoldt, R. H., Morgret, L. D., Bates, F. S., and Macosko, C. W., A critical gel fluid with high extensibility: The rheology of chewing gum, J. Rheol. **58**, 821–838 (2014).
[362] Campanella, O. H. and Peleg, M., Analysis of the transient flow of mayonnaise in a coaxial viscometer, J. Rheol. **31**, 439–452 (1987).
[363] Elliott, J. H. and Ganz, A. J., Salad dressings—preliminary rheological characterization1, J. Texture Stud. **8**, 359–371 (1977).
[364] Kokini, J. L. and Dickie, A., An attempt to identify and model transient viscoelastic flow in foods, J. Texture Stud. **12**, 539–557 (1981).
[365] Nita, S. P., Murith, M., Chisholm, H., and Engmann, J., Matching the rheological properties of videofluoroscopic contrast agents and thickened liquid prescriptions, Dysphagia **28**, 245–252 (2013).
[366] Marconati, M., Engmann, J., Burbidge, A., Mathieu, V., Souchon, I., and Ramaioli, M., A review of the approaches to predict the ease of swallowing and post-swallow residues, Trends Food Sci. Tech. **86**, 281–297 (2019).
[367] Piazza, R., *Soft matter: the stuff that dreams are made of* (Springer, 2011).
[368] Ubbink, J., Burbidge, A., and Mezzenga, R., Food structure and functionality: a soft matter perspective, Soft Matter **4**, 1569–1581 (2008).
[369] McLeish, T., *Soft Matter: A Very Short Introduction* (Oxford University Press, 2020).
[370] Bingham, E. C., The viscosity of binary mixtures, J. Phys. Chem. **18**, 157–165 (1914).
[371] Grunberg, L. and Nissan, A. H., Mixture law for viscosity, Nature **164**, 799–800 (1949).
[372] Oswal, S. L. and Desai, H. S., Studies of viscosity and excess molar volume of binary mixtures, Fluid Phase Equilibria **149**, 359–376 (1998).
[373] Zhmud, B., Viscosity blending equations, Lube Mag. **121**, 24–9 (2014).
[374] Schikarski, T., Peukert, W., and Avila, M., Direct numerical simulation of water–ethanol flows in a T-mixer, Chem. Eng. J. **324**, 168–181 (2017).
[375] Nagasawa, K., Suzuki, T., Seto, R., Okada, M., and Yue, Y., Mixing sauces: a viscosity blending model

for shear thinning fluids, ACM Trans. Graph. **38**, 1–17 (2019).
[376] Moelants, K. R. N., Cardinaels, R., Van Buggenhout, S., Van Loey, A. M., Moldenaers, P., and Hendrickx, M. E., A review on the relationships between processing, food structure, and rheological properties of plant-tissue-based food suspensions, Compreh. Rev. Food Sci. Food Saf. **13**, 241–260 (2014).
[377] Guazzelli, E. and Morris, J. F., *A physical introduction to suspension dynamics* (Cambridge University Press, 2011).
[378] Zenit, R. and Feng, J. J., Hydrodynamic interactions among bubbles, drops, and particles in non-Newtonian liquids, Annu. Rev. Fluid Mech. **50**, 505–534 (2018).
[379] Zhu, S., Stieger, M. A., van der Goot, A. J., and Schutyser, M. A. I., Extrusion-based 3D printing of food pastes: Correlating rheological properties with printing behaviour, Innov. Food Sci. Emerg. Tech. **58**, 102214 (2019).
[380] Einstein, A., Eine neue Bestimmung der Moleküldimensionen, Ann. Phys. (Berlin) **324**, 289–306 (1906).
[381] Guazzelli, E., Morris, J. F., and Pic, S., *A Physical Introduction to Suspension Dynamics*, Cambridge Texts in Applied Mathematics (Cambridge University Press, 2011).
[382] Genovese, D. B., Lozano, J. E., and Rao, M. A., The rheology of colloidal and noncolloidal food dispersions, J. Food Sci. **72**, R11–R20 (2007).
[383] Farris, R. J., Prediction of the viscosity of multimodal suspensions from unimodal viscosity data, Transa. Soc. Rheol. **12**, 281–301 (1968).
[384] Hahn, C., Nöbel, S., Maisch, R., Rösingh, W., Weiss, J., and Hinrichs, J., Adjusting rheological properties of concentrated microgel suspensions by particle size distribution, Food Hydrocolloids **49**, 183–191 (2015).
[385] Ojijo, N. K. O. and Shimoni, E., Minimization of cassava paste flow properties using the 'farris effect', LWT - Food Science and Technology **41**, 51 – 57 (2008).
[386] Kaye, A., A bouncing liquid stream, Nature **197**, 1001–1002 (1963).
[387] Versluis, M., Blom, C., van der Meer, D., van der Weele, K., and Lohse, D., Leaping shampoo and the stable Kaye effect, J. Stat. Mech. **2006**, P07007 (2006).
[388] Lee, S., Li, E. Q., Marston, J. O., Bonito, A., and Thoroddsen, S. T., Leaping shampoo glides on a lubricating air layer, Phys. Rev. E **87**, 061001 (2013).
[389] King, J. R. C. and Lind, S. J., The Kaye effect: New experiments and a mechanistic explanation, J. Non-Newtonian Fluid Mech. **273**, 104165 (2019).
[390] McClements, D. J., *Food emulsions: principles, practices, and techniques*, 3rd ed. (CRC press, 2015).
[391] Dickinson, E., Food emulsions and foams: Stabilization by particles, Curr. Opin. Colloid Interf. Sci. **15**, 40–49 (2010).
[392] Berton-Carabin, C. C., Sagis, L., and Schroën, K., Formation, structure, and functionality of interfacial layers in food emulsions, Annu. Rev. Food Sci. Tech. **9**, 551–587 (2018).
[393] Håkansson, A., Emulsion formation by homogenization: Current understanding and future perspectives, Annu. Rev. Food Sci. Tech. **10**, 239–258 (2019).
[394] Kentish, S., Wooster, T. J., Ashokkumar, M., Balachandran, S., Mawson, R., and Simons, L., The use of ultrasonics for nanoemulsion preparation, Innov. Food Sci. Emerg. Tech. **9**, 170–175 (2008).
[395] Friberg, S., Larsson, K., and Sjöblom, J., *Food emulsions*, 4th ed. (CRC Press, 2003).
[396] Pickering, S. U., Emulsions, J. Chem. Soc. Trans. **91**, 2001–2021 (1907).
[397] Ramsden, W., Separation of solids in the surface-layers of solutions and 'suspensions' (observations on surface-membranes, bubbles, emulsions, and mechanical coagulation).—Preliminary account, Proc. Roy. Soc. Lond. **72**, 156–164 (1904).
[398] Chevalier, Y. and Bolzinger, M.-A., Emulsions stabilized with solid nanoparticles: Pickering emulsions, Colloids Surf. A **439**, 23–34 (2013).
[399] Zanini, M., Marschelke, C., Anachkov, S. E., Marini, E., Synytska, A., and Isa, L., Universal emulsion stabilization from the arrested adsorption of rough particles at liquid-liquid interfaces, Nat. Commun. **8**, 1–9 (2017).
[400] McClements, D. J., Protein-stabilized emulsions, Curr. Opin. Colloid Interf. Sci. **9**, 305–313 (2004).
[401] Tcholakova, S., Denkov, N. D., Ivanov, I. B., and Campbell, B., Coalescence stability of emulsions containing globular milk proteins, Adv. Colloid Interf. Sci. **123**, 259–293 (2006).
[402] Barnes, H. A., Rheology of emulsions—a review, Colloids Surf. A **91**, 89–95 (1994).
[403] Franco, J. M., Guerrero, A., and Gallegos, C., Rheology and processing of salad dressing emulsions, Rheol. Acta **34**, 513–524 (1995).
[404] Franco, J. M., Berjano, M., and Gallegos, C., Linear viscoelasticity of salad dressing emulsions, *J. Agric. Food Chem.*, J. Agric. Food Chem. **45**, 713–719 (1997).
[405] Fischer, P., Personal conversation (2021).
[406] Amagliani, L. and Schmitt, C., Globular plant protein aggregates for stabilization of food foams and emulsions, Trends Food Sci. Tech. **67**, 248–259 (2017).
[407] Liu, J., Zhou, H., Tan, Y., Mundo, J. L. M., and McClements, D. J., Comparison of plant-based emulsifier performance in water-in-oil-in-water emulsions: Soy protein isolate, pectin and gum Arabic, J. Food Eng. **307**, 110625 (2021).
[408] Bremond, N. and Bibette, J., Exploring emulsion science with microfluidics, Soft Matter **8**, 10549–10559 (2012).
[409] Brosseau, Q., Vrignon, J., and Baret, J.-C., Microfluidic dynamic interfacial tensiometry (μDIT), Soft Matter **10**, 3066–3076 (2014).
[410] Muijlwijk, K., Hinderink, E., Ershov, D., Berton-Carabin, C., and Schroën, K., Interfacial tension measured at high expansion rates and within milliseconds using microfluidics, J. Colloid Interf. Sci. **470**, 71–79 (2016).
[411] Hinderink, E. B. A., de Ruiter, J., de Leeuw, J., Schroën, K., Sagis, L. M. C., and Berton-Carabin, C. C., Early film formation in protein-stabilised emulsions: Insights from a microfluidic approach, Food Hydrocolloids **118**, 106785 (2021).
[412] Muijlwijk, K., Huang, W., Vuist, J.-E., Berton-Carabin, C., and Schroën, K., Convective mass transport dominates surfactant adsorption in a microfluidic Y-junction, Soft Matter **12**, 9025–9029 (2016).
[413] Wang, K., Zhang, L., Zhang, W., and Luo, G., Mass-transfer-controlled dynamic interfacial tension in microfluidic emulsification processes, Langmuir **32**, 3174–

3185 (2016).
[414] Hinderink, E. B. A., Sagis, L., Schroën, K., and Berton-Carabin, C. C., Sequential adsorption and interfacial displacement in emulsions stabilized with plant-dairy protein blends, J. Colloid Interf. Sci. **583**, 704–713 (2021).
[415] Vella, D., Floating versus sinking, Annu. Rev. Fluid Mech. **47**, 115–135 (2015).
[416] Vella, D. and Mahadevan, L., The cheerios effect, Am. J. Phys. **73**, 817–825 (2005).
[417] Singh, P. and Joseph, D. D., Fluid dynamics of floating particles, J. Fluid Mech. **530**, 31–80 (2005).
[418] Kralchevsky, P. A. and Nagayama, K., Capillary interactions between particles bound to interfaces, liquid films and biomembranes, Adv. Colloid Interf. Sci. **85**, 145–192 (2000).
[419] Paunov, V., Kralchevsky, P., Denkov, N., and Nagayama, K., Lateral capillary forces between floating submillimeter particles, J. Colloid Interf. Sci. **157**, 100–112 (1993).
[420] Lagarde, A., Josserand, C., and Protière, S., The capillary interaction between pairs of granular rafts, Soft Matter **15**, 5695–5702 (2019).
[421] Abkarian, M., Protière, S., Aristoff, J. M., and Stone, H. A., Gravity-induced encapsulation of liquids by destabilization of granular rafts, Nat. Commun. **4**, 1895 (2013).
[422] Mlot, N. J., Tovey, C. A., and Hu, D. L., Fire ants self-assemble into waterproof rafts to survive floods, Proc. Natl. Acad. Sci. U.S.A. **108**, 7669–7673 (2011).
[423] Gao, X. and Jiang, L., Water-repellent legs of water striders, Nature **432**, 36–36 (2004).
[424] Childress, S., Walking on water, J. Fluid Mech. **644**, 1–4 (2010).
[425] Hu, D. L., Prakash, M., Chan, B., and Bush, J. W. M., Water-walking devices, in *Animal Locomotion* (Springer, 2010) pp. 131–140.
[426] Karpitschka, S., Pandey, A., Lubbers, L. A., Weijs, J. H., Botto, L., Das, S., Andreotti, B., and Snoeijer, J. H., Liquid drops attract or repel by the inverted Cheerios effect, Proc. Natl. Acad. Sci. U.S.A. **113**, 7403–7407 (2016).
[427] Pandey, A., Karpitschka, S., Lubbers, L. A., Weijs, J. H., Botto, L., Das, S., Andreotti, B., and Snoeijer, J. H., Dynamical theory of the inverted cheerios effect, Soft Matter **13**, 6000–6010 (2017).
[428] Wang, W., Giltinan, J., Zakharchenko, S., and Sitti, M., Dynamic and programmable self-assembly of microrafts at the air-water interface, Sci. Adv. **3**, e1602522 (2017).
[429] Koens, L., Wang, W., Sitti, M., and Lauga, E., The near and far of a pair of magnetic capillary disks, Soft Matter **15**, 1497–1507 (2019).
[430] Vassileva, N. D., van den Ende, D., Mugele, F., and Mellema, J., Capillary forces between spherical particles floating at a liquid-liquid interface, *Langmuir*, Langmuir **21**, 11190–11200 (2005).
[431] Ershov, D., Sprakel, J., Appel, J., Stuart, M. A. C., and van der Gucht, J., Capillarity-induced ordering of spherical colloids on an interface with anisotropic curvature, Proc. Natl. Acad. Sci. U.S.A. **110**, 9220–9224 (2013).
[432] Furst, E. M. and Squires, T. M., *Microrheology* (Oxford University Press, 2017).
[433] Squires, T. M. and Mason, T. G., Fluid mechanics of microrheology, Annu. Rev. Fluid Mech. **42**, 413–438 (2010).
[434] MacKintosh, F. C. and Schmidt, C. F., Microrheology, Curr. Opin. Colloid Interf. Sci. **4**, 300–307 (1999).
[435] Mizuno, D., Head, D. A., MacKintosh, F. C., and Schmidt, C. F., Active and passive microrheology in equilibrium and nonequilibrium systems, Macromolec. **41**, 7194–7202 (2008).
[436] Zia, R. N., Active and passive microrheology: theory and simulation, Annu. Rev. Fluid Mech. **50**, 371–405 (2018).
[437] Yang, N., Lv, R., Jia, J., Nishinari, K., and Fang, Y., Application of microrheology in food science, Annu. Rev. Food Sci. Tech. **8**, 493–521 (2017).
[438] Lorenz, R. D., *Spinning flight: dynamics of frisbees, boomerangs, samaras, and skipping stones* (Springer-Verlag New York, 2006).
[439] Clanet, C., Hersen, F., and Bocquet, L., Secrets of successful stone-skipping, Nature **427**, 29–29 (2004).
[440] Hewitt, I. J., Balmforth, N. J., and McElwaine, J. N., Continual skipping on water, J. Fluid Mech. **669**, 328–353 (2011).
[441] Belden, J., Hurd, R. C., Jandron, M. A., Bower, A. F., and Truscott, T. T., Elastic spheres can walk on water, Nat. Commun. **7**, 1–10 (2016).
[442] Olszewski, E. A., From baking a cake to solving the diffusion equation, Am. J. Phys. **74**, 502–509 (2006).
[443] Roura, P., Fort, J., and Saurina, J., How long does it take to boil an egg? A simple approach to the energy transfer equation, Eur. J. Phys. **21**, 95 (2000).
[444] Ma, X., Liétor-Santos, J.-J., and Burton, J. C., Star-shaped oscillations of Leidenfrost drops, Phys. Rev. Fluids **2**, 031602 (2017).
[445] Singla, T. and Rivera, M., Sounds of Leidenfrost drops, Phys. Rev. Fluids **5**, 113604 (2020).
[446] Bouillant, A., Mouterde, T., Bourrianne, P., Clanet, C., and Quéré, D., Symmetry breaking in Leidenfrost flows, Phys. Rev. Fluids **3**, 100502 (2018).
[447] Herwig, H., *Ach, so ist das!* (Springer, Wiesbaden, 2018).
[448] Leidenfrost, J. G., *De aquae communis nonnullis qualitatibus tractatus* (Ovenius, 1756).
[449] Curzon, F. L., The Leidenfrost phenomenon, Am. J. Phys. **46**, 825–828 (1978).
[450] Thimbleby, H., The Leidenfrost phenomenon, Phys. Educ. **24**, 300 (1989).
[451] Quéré, D., Leidenfrost dynamics, Annu. Rev. Fluid Mech. **45**, 197–215 (2013).
[452] Biance, A.-L., Clanet, C., and Quéré, D., Leidenfrost drops, Phys. Fluids **15**, 1632–1637 (2003).
[453] Harvey, D., Harper, J. M., and Burton, J. C., Minimum Leidenfrost temperature on smooth surfaces, Phys. Rev. Lett. **127**, 104501 (2021).
[454] Bouillant, A., Mouterde, T., Bourrianne, P., Lagarde, A., Clanet, C., and Quéré, D., Leidenfrost wheels, Nat. Phys. **14**, 1188–1192 (2018).
[455] Leon, V. J. and Varanasi, K. K., Self-propulsion of boiling droplets on thin heated oil films, Phys. Rev. Lett. **127**, 074502 (2021).
[456] Linke, H., Alemán, B. J., Melling, L. D., Taormina, M. J., Francis, M. J., Dow-Hygelund, C. C., Narayanan, V., Taylor, R. P., and Stout, A., Self-propelled Leidenfrost droplets, Phys. Rev. Lett. **96**, 154502 (2006).

[457] Jia, Z.-h., Chen, M.-y., and Zhu, H.-t., Reversible self-propelled Leidenfrost droplets on ratchet surfaces, Appl. Phys. Lett. **110**, 091603 (2017).

[458] Würger, A., Leidenfrost gas ratchets driven by thermal creep, Phys. Rev. Lett. **107**, 164502 (2011).

[459] Sobac, B., Rednikov, A., Dorbolo, S., and Colinet, P., Self-propelled Leidenfrost drops on a thermal gradient: A theoretical study, Phys. Fluids **29**, 082101 (2017).

[460] BBC Earth Unplugged,, Water flows uphill! Leidenfrost effect, `https://www.youtube.com/watch?v=hIXFxP_6m7I` (2013), last accessed: 25-May-2020.

[461] Janssens, S. D., Koizumi, S., and Fried, E., Behavior of self-propelled acetone droplets in a Leidenfrost state on liquid substrates, Phys. Fluids **29**, 032103 (2017).

[462] Lagubeau, G., Le Merrer, M., Clanet, C., and Quéré, D., Leidenfrost on a ratchet, Nat. Phys. **7**, 395–398 (2011).

[463] Hall, R. S., Board, S. J., Clare, A. J., Duffey, R. B., Playle, T. S., and Poole, D. H., Inverse Leidenfrost phenomenon, Nature **224**, 266–267 (1969).

[464] Gauthier, A., Diddens, C., Proville, R., Lohse, D., and van der Meer, D., Self-propulsion of inverse Leidenfrost drops on a cryogenic bath, Proc. Natl. Acad. Sci. U.S.A. **116**, 1174–1179 (2019).

[465] Pacheco-Vázquez, F., Ledesma-Alonso, R., Palacio-Rangel, J. L., and Moreau, F., Triple Leidenfrost effect: Preventing coalescence of drops on a hot plate, Phys. Rev. Lett. **127**, 204501 (2021).

[466] Walker, J., Boiling and the Leidenfrost effect, Fundament. Phys. , 1–4 (2010).

[467] Audoly, B. and Neukirch, S., Fragmentation of rods by cascading cracks: Why spaghetti does not break in half, Phys. Rev. Lett. **95**, 095505 (2005).

[468] Heisser, R. H., Patil, V. P., Stoop, N., Villermaux, E., and Dunkel, J., Controlling fracture cascades through twisting and quenching, Proc. Natl. Acad. Sci. U.S.A. **115**, 8665–8670 (2018).

[469] Tao, Y., Lee, Y.-C., Liu, H., Zhang, X., Cui, J., Mondoa, C., Babaei, M., Santillan, J., Wang, G., Luo, D., Liu, D., Yang, H., Do, Y., Sun, L., Wang, W., Zhang, T., and Yao, L., Morphing pasta and beyond, Sci. Adv. **7**, eabf4098 (2021).

[470] Hwang, J., Ha, J., Siu, R., Kim, Y. S., and Tawfick, S., Swelling, softening and elastocapillary adhesion of cooked pasta, arXiv , 2201.09621 (2022).

[471] Ahlers, G., Grossmann, S., and Lohse, D., Heat transfer and large scale dynamics in turbulent Rayleigh-Bénard convection, Rev. Mod. Phys. **81**, 503–537 (2009).

[472] Lohse, D. and Xia, K.-Q., Small-scale properties of turbulent Rayleigh-Bénard convection, Annu. Rev. Fluid Mech. **42**, 335–364 (2010).

[473] Kadanoff, L. P., Turbulent heat flow: Structures and scaling, Physics Today **54**, 34–39 (2001).

[474] Moore, D. R. and Weiss, N. O., Two-dimensional Rayleigh-Bénard convection, J. Fluid Mech. **58**, 289–312 (1973).

[475] Cattaneo, F., Emonet, T., and Weiss, N., On the interaction between convection and magnetic fields, Astrophys. J. **588**, 1183–1198 (2003).

[476] Mckenzie, D. P., Roberts, J. M., and Weiss, N. O., Convection in the earth's mantle: towards a numerical simulation, J. Fluid Mech. **62**, 465–538 (1974).

[477] Prakash, V. N., Sreenivas, K., and Arakeri, J. H., The role of viscosity contrast on plume structure in laboratory modeling of mantle convection, Chem. Eng. Sci. **158**, 245–256 (2017).

[478] Brent, A. D., Voller, V. R., and Reid, K. J., Enthalpy-porosity technique for modeling convection-diffusion phase change: Application to the melting of a pure metal, Numer. Heat Transf. **13**, 297–318 (1988).

[479] Zhong, J.-Q., Patterson, M. D., and Wettlaufer, J. S., Streaks to rings to vortex grids: Generic patterns in transient convective spin up of an evaporating fluid, Phys. Rev. Lett. **105**, 044504 (2010).

[480] Emran, M. S. and Schumacher, J., Large-scale mean patterns in turbulent convection, J. Fluid Mech. **776**, 96–108 (2015).

[481] Wettlaufer, J. S., The universe in a cup of coffee, Phys. Today **64**, 66–67 (2011).

[482] Krishnamurti, R., On the transition to turbulent convection. Part 1. The transition from two- to three-dimensional flow, J. Fluid Mech. **42**, 295–307 (1970).

[483] Krishnamurti, R., On the transition to turbulent convection. Part 2. The transition to time-dependent flow, J. Fluid Mech. **42**, 309–320 (1970).

[484] Dhir, V. K., Boiling heat transfer, Annu. Rev. Fluid Mech. **30**, 365–401 (1998).

[485] Lakkaraju, R., Stevens, R. J. A. M., Oresta, P., Verzicco, R., Lohse, D., and Prosperetti, A., Heat transport in bubbling turbulent convection, Proc. Natl. Acad. Sci. U.S.A. **110**, 9237–9242 (2013).

[486] Dhir, V. K., Mechanistic prediction of nucleate boiling heat transfer–achievable or a hopeless task?, J. Heat Transf. **128**, 1–12 (2005).

[487] Huppert, H. E. and Turner, J. S., Double-diffusive convection, J. Fluid Mech. **106**, 299–329 (1981).

[488] Radko, T., *Double-diffusive convection* (Cambridge University Press, 2013).

[489] Garaud, P., Double-diffusive convection at low Prandtl number, Annu. Rev. Fluid Mech. **50**, 275–298 (2018).

[490] Heavers, R. M. and Colucci, L. A., Sugar fingers and double-diffusive convection, J. Chem. Educ. **86**, 1326 (2009).

[491] Yang, Y., Verzicco, R., and Lohse, D., From convection rolls to finger convection in double-diffusive turbulence, Proc. Natl. Acad. Sci. U.S.A. **113**, 69–73 (2016).

[492] Stern, M. E., The "salt-fountain" and thermohaline convection, Tellus **12**, 172–175 (1960).

[493] Kerr, R. A., Salt fingers mix the sea, Science **295**, 1821–1821 (2002).

[494] Johnson, G. C. and Kearney, K. A., Ocean climate change fingerprints attenuated by salt fingering?, Geophys. Res. Lett. **36**, L21603 (2009).

[495] Fernández-Castro, B., Mouriño-Carballido, B., Marañón, E., Chouciño, P., Gago, J., Ramírez, T., Vidal, M., Bode, A., Blasco, D., Royer, S.-J., *et al.*, Importance of salt fingering for new nitrogen supply in the oligotrophic ocean, Nat. Commun. **6**, 1–10 (2015).

[496] Cantiello, M. and Langer, N., Thermohaline mixing in evolved low-mass stars, Astron. Astrophys. **521**, A9 (2010).

[497] Griffiths, R. W., Layered double-diffusive convection in porous media, J. Fluid Mech. **102**, 221–248 (1981).

[498] Dinčov, D., Parrott, K. A., and Pericleous, K., Heat and mass transfer in two-phase porous materials under intensive microwave heating, J. Food Eng. **65**, 403–412 (2004).

[499] Xue, N., Khodaparast, S., Zhu, L., Nunes, J. K., Kim, H., and Stone, H. A., Laboratory layered latte, Nat.

Commun. **8**, 1960 (2017).
[500] Mueth, D. M., Crocker, J. C., Esipov, S. E., and Grier, D. G., Origin of stratification in creaming emulsions, Phys. Rev. Lett. **77**, 578 (1996).
[501] Chong, K. L., Yang, R., Wang, Q., Verzicco, R., and Lohse, D., Café latte: spontaneous layer formation in laterally cooled double diffusive convection, J. Fluid Mech. **900**, R6 (2020).
[502] Tait, R. I. and Howe, M. R., Thermohaline staircase, Nature **231**, 178–179 (1971).
[503] Yang, Y., Chen, W., Verzicco, R., and Lohse, D., Multiple states and transport properties of double-diffusive convection turbulence, Proc. Natl. Acad. Sci. U.S.A. **117**, 14676–14681 (2020).
[504] Zielbauer, B. I., Franz, J., Viezens, B., and Vilgis, T. A., Physical aspects of meat cooking: time dependent thermal protein denaturation and water loss, Food Biophys. **11**, 34–42 (2016).
[505] Vilgis, T. A., Flory theory of polymeric fractals-intersection, saturation and condensation, Physica A **153**, 341–354 (1988).
[506] Van der Sman, R. G. M., Moisture transport during cooking of meat: An analysis based on Flory–Rehner theory, Meat Sci. **76**, 730–738 (2007).
[507] Cai, S., Wang, Z., Fuest, F., Jeon, Y. J., Gray, C., and Karniadakis, G. E., Flow over an espresso cup: inferring 3-D velocity and pressure fields from tomographic background oriented Schlieren via physics-informed neural networks, J. Fluid Mech. **915**, A102 (2021).
[508] Settles, G. S. and Hargather, M. J., A review of recent developments in schlieren and shadowgraph techniques, Measur. Sci. Tech. **28**, 042001 (2017).
[509] Comstock, G. W., Meyer, M. B., Helsing, K. J., and Tockman, M. S., Respiratory effects of household exposures to tobacco smoke and gas cooking, American Rev. Respir. Dis. **124**, 143–148 (1981).
[510] Rogge, W. F., Hildemann, L. M., Mazurek, M. A., Cass, G. R., and Simoneit, B. R. T., Sources of fine organic aerosol. 1. Charbroilers and meat cooking operations, Environ. Sci. Tech. **25**, 1112–1125 (1991).
[511] Chen, W., Li, J., Wang, C., Dai, X., and Liu, J., 2D-PIV measurement of range hood-driven flow in a domestic kitchen, Energy and Buildings **177**, 64–76 (2018).
[512] Gao, Y., Liu, Q. K., Chow, W. K., and Wu, M., Analytical and experimental study on multiple fire sources in a kitchen, Fire Saf. J. **63**, 101–112 (2014).
[513] Yeoh, G. H. and Yuen, K. K., *Computational fluid dynamics in fire engineering: theory, modelling and practice* (Butterworth-Heinemann, 2009).
[514] Norton, T., Tiwari, B., and Sun, D.-W., Computational fluid dynamics in the design and analysis of thermal processes: a review of recent advances, Criti. Rev. Food Sci. Nutrit. **53**, 251–275 (2013).
[515] Chen, Z., Xin, J., and Liu, P., Air quality and thermal comfort analysis of kitchen environment with CFD simulation and experimental calibration, Build. Environ. **172**, 106691 (2020).
[516] Nakouzi, E., Goldstein, R. E., and Steinbock, O., Do dissolving objects converge to a universal shape?, *Langmuir*, Langmuir **31**, 4145–4150 (2015).
[517] Neufeld, J. A., Goldstein, R. E., and Worster, M. G., On the mechanisms of icicle evolution, J. Fluid Mech. **647**, 287–308 (2010).
[518] Townsend, A. K. and Wilson, H. J., The fluid dynamics of the chocolate fountain, Eur. J. Phys. **37**, 015803 (2015).
[519] Mehrle, Y. E., *Solidification and contraction of confectionery systems in rapid cooling processing* (ETH Zürich, 2007).
[520] Le Révérend, B. J. D., Fryer, P. J., and Bakalis, S., Modelling crystallization and melting kinetics of cocoa butter in chocolate and application to confectionery manufacturing, Soft Matter **5**, 891–902 (2009).
[521] Hayashi, H., Viscoelasticity of butter, in *Developments in Food Engineering: Proceedings of the 6th International Congress on Engineering and Food*, edited by T. Yano, R. Matsuno, and K. Nakamura (Springer US, Boston, MA, 1994) pp. 75–77.
[522] Landfeld, A., Novotna, P., Strohalm, J., Houska, M., and Kyhos, K., Viscosity of cocoa butter, Int. J. Food Propert. **3**, 165–169 (2000).
[523] Shukla, A., Bhaskar, A. R., Rizvi, S. S. H., and Mulvaney, S. J., Physicochemical and rheological properties of butter made from supercritically fractionated milk fat, J. Dairy Sci. **77**, 45–54 (1994).
[524] Lucey, J., Johnson, M., and Horne, D., Invited review: Perspectives on the basis of the rheology and texture properties of cheese, J. Dairy Sci. **86**, 2725–2743 (2003).
[525] Rudan, M. A. and Barbano, D. M., A model of mozzarella cheese melting and browning during pizza baking, J. Dairy Sci. **81**, 2312–2319 (1998).
[526] Ratnayake, W. S. and Jackson, D. S., Starch gelatinization, in *Advances in Food and Nutrition Research*, Vol. 55 (Academic Press, 2008) pp. 221–268.
[527] Lahne, J. B. and Schmidt, S. J., Gelatin-filtered consommé: A practical demonstration of the freezing and thawing processes, J. Food Sci. Educ. **9**, 53–58 (2010).
[528] Williams, J. T., ed., *Waterproof and water repellent textiles and clothing* (Woodhead Publishing, 2018).
[529] Tehrani-Bagha, A. R., Waterproof breathable layers–a review, Adv. Colloid Interf. Sci. **268**, 114–135 (2019).
[530] Sajid, M. and Ilyas, M., PTFE-coated non-stick cookware and toxicity concerns: a perspective, Environ. Sci. Pollut. Res. **24**, 23436–23440 (2017).
[531] European Commission,, Poly- and perfluoroalkyl substances (PFAS) (2020), SWD(2020) 249 final.
[532] Marmur, A., The lotus effect: superhydrophobicity and metastability, Langmuir **20**, 3517–3519 (2004).
[533] Barthlott, W., Mail, M., Bhushan, B., and Koch, K., Plant surfaces: structures and functions for biomimetic innovations, Nano-Micro Lett. **9**, 23 (2017).
[534] Feng, L., Li, S., Li, Y., Li, H., Zhang, L., Zhai, J., Song, Y., Liu, B., Jiang, L., and Zhu, D., Super-hydrophobic surfaces: from natural to artificial, Adv. Mater. **14**, 1857–1860 (2002).
[535] Lafuma, A. and Quéré, D., Superhydrophobic states, Nat. Mater. **2**, 457–460 (2003).
[536] Dupuis, A. and Yeomans, J. M., Modeling droplets on superhydrophobic surfaces: equilibrium states and transitions, Langmuir **21**, 2624–2629 (2005).
[537] Richard, D., Clanet, C., and Quéré, D., Contact time of a bouncing drop, Nature **417**, 811–811 (2002).
[538] Reyssat, M., Yeomans, J. M., and Quéré, D., Impalement of fakir drops, Europhys. Lett. **81**, 26006 (2007).
[539] Liu, Y., Moevius, L., Xu, X., Qian, T., Yeomans, J. M., and Wang, Z., Pancake bouncing on superhydrophobic surfaces, Nat. Phys. **10**, 515–519 (2014).

[540] Liu, Y., Andrew, M., Li, J., Yeomans, J. M., and Wang, Z., Symmetry breaking in drop bouncing on curved surfaces, Nat. Commun. **6**, 1–8 (2015).

[541] Mishchenko, L., Hatton, B., Bahadur, V., Taylor, J. A., Krupenkin, T., and Aizenberg, J., Design of ice-free nanostructured surfaces based on repulsion of impacting water droplets, ACS nano **4**, 7699–7707 (2010).

[542] Blossey, R., Self-cleaning surfaces—virtual realities, Nat. Mater. **2**, 301–306 (2003).

[543] Deng, X., Mammen, L., Butt, H.-J., and Vollmer, D., Candle soot as a template for a transparent robust superamphiphobic coating, Science **335**, 67–70 (2012).

[544] Wray, A. W. and Cimpeanu, R., Reduced-order modelling of thick inertial flows around rotating cylinders, J. Fluid Mech. **898**, A1–33 (2020).

[545] Taylor, G. I., *Low-Reynolds-number flows* (National Committee for Fluid Mechanics Films, 1967) last accessed: 16-Dec-2020.

[546] Metzger, B., Nicolas, M., and Guazzelli, E., Falling clouds of particles in viscous fluids, J. Fluid Mech. **580**, 283–301 (2007).

[547] Ribe, N. M., Habibi, M., and Bonn, D., Stability of liquid rope coiling, Phys. Fluids **18**, 084102 (2006).

[548] Purcell, E. M., Life at low Reynolds number, Am. J. Phys. **45**, 3–11 (1977).

[549] Kim, S. and Karrila, S. J., *Microhydrodynamics: principles and selected applications* (Butterworth-Heinemann, 1991).

[550] Lisicki, M., Four approaches to hydrodynamic Green's functions–the Oseen tensors, arXiv , 1312.6231 (2013).

[551] Van Leeuwen, J., *The Aristotelian mechanics: text and diagrams*, Vol. 316 (Springer, 2016).

[552] Stokes, G. G., On the effect of the internal friction of fluids on the motion of pendulums, in *Mathematical and Physical Papers*, Cambridge Library Collection - Mathematics, Vol. 3 (Cambridge University Press, 1851) p. 1–10.

[553] Yeomans, J. M., Pushkin, D. O., and Shum, H., An introduction to the hydrodynamics of swimming microorganisms, Eur. Phys. J. Spec. Top. **223**, 1771–1785 (2014).

[554] Dusenbery, D. B., *Living at micro scale: the unexpected physics of being small* (Harvard University Press, 2009).

[555] Sutterby, J. L., Falling sphere viscometry. I. Wall and inertial corrections to Stokes' law in long tubes, Trans. Soc. Rheol. **17**, 559–573 (1973).

[556] Millikan, R. A., On the elementary electrical charge and the Avogadro constant, Phys. Rev. **2**, 109 (1913).

[557] Arnold, H. D., Limitations imposed by slip and inertia terms upon Stokes's law for the motion of spheres through liquids, Phys. Rev. (Series I) **32**, 233 (1911).

[558] Ruby, W., Settling velocities of gravel, sand and silt particles, American . Sci. **25**, 325–338 (1933).

[559] Flemmer, R. L. C. and Banks, C. L., On the drag coefficient of a sphere, Powder Techn. **48**, 217–221 (1986).

[560] Guyon, E., Hulin, J.-P., Petit, L., Mitescu, C. D., *et al.*, *Physical hydrodynamics* (Oxford University Press, 2001).

[561] Oseen, C. W., Über die Stokes'sche Formel und über eine verwandte Aufgabe in der Hydrodynamik, Arkiv för Matematik, Astronomi och Fysik **6**, 1–20 (1910), paper 29.

[562] Dey, S., Zeeshan Ali, S., and Padhi, E., Terminal fall velocity: the legacy of Stokes from the perspective of fluvial hydraulics, Proc. Roy. Soc. A **475**, 20190277 (2019).

[563] Stewartson, K., On the steady flow past a sphere at high Reynolds number using Oseen's approximation, Philosoph. Mag. **1**, 345–354 (1956).

[564] O'Neill, M. E., A slow motion of viscous liquid caused by a slowly moving solid sphere, Mathematika **11**, 67–74 (1964).

[565] Goldman, A. J., Cox, R. G., and Brenner, H., Slow viscous motion of a sphere parallel to a plane wall—I Motion through a quiescent fluid, Chemical engineering science **22**, 637–651 (1967).

[566] Brown, P. P. and Lawler, D. F., Sphere drag and settling velocity revisited, J. Environ. Eng. **129**, 222–231 (2003).

[567] Cichocki, B. and Jones, R. B., Image representation of a spherical particle near a hard wall, Physica A **258**, 273–302 (1998).

[568] Rad, V. F. and Moradi, A.-R., Flat wall proximity effect on micro-particle sedimentation in non-Newtonian fluids, Sci. Rep. **10**, 1–9 (2020).

[569] Richardson, J. F. and Zaki, W. N., Sedimentation and fluidisation: Part I, Chem. Eng. Res. Design **75**, S82–S100 (1997).

[570] Batchelor, G. K., Sedimentation in a dilute dispersion of spheres, J. Fluid Mech. **52**, 245–268 (1972).

[571] Lin, C.-Y., Zhou, W., Hu, C.-T., Yang, F., and Lee, S., Brownian motion and Einstein relation for migration of coffee particles in coffee suspensions, J. Sci. Food Agricult. **99**, 3950–3956 (2019).

[572] Guzmán-Lastra, F., Löwen, H., and Mathijssen, A. J. T. M., Active carpets drive non-equilibrium diffusion and enhanced molecular fluxes, Nat. Commun. **12**, 1–15 (2021).

[573] Batchelor, G. K., Slender-body theory for particles of arbitrary cross-section in Stokes flow, J. Fluid. Mech. **44**, 419–440 (1970).

[574] Cox, R. G., The motion of long slender bodies in a viscous fluid Part 1. General theory, J. Fluid. Mech. **44**, 791–810 (1970).

[575] Lauga, E., *The Fluid Dynamics of Cell Motility*, Cambridge Texts in Applied Mathematics (Cambridge University Press, 2020).

[576] Lauga, E. and Powers, T. R., The hydrodynamics of swimming microorganisms, Rep. Progr. Phys. **72**, 096601 (2009).

[577] Gilpin, W., Bull, M. S., and Prakash, M., The multiscale physics of cilia and flagella, Nat. Rev. Phys. **2**, 74–88 (2020).

[578] Elgeti, J. and Gompper, G., Emergence of metachronal waves in cilia arrays, Proc. Natl. Acad. Sci. U.S.A. **110**, 4470–4475 (2013).

[579] Gilpin, W., Prakash, V. N., and Prakash, M., Vortex arrays and ciliary tangles underlie the feeding–swimming trade-off in starfish larvae, Nat. Phys. **13**, 380–386 (2017).

[580] Ramirez-San Juan, G. R., Mathijssen, A. J. T. M., He, M., Jan, L., Marshall, W., and Prakash, M., Multi-scale spatial heterogeneity enhances particle clearance in airway ciliary arrays, Nat. Phys. **16**, 958–964 (2020).

[581] Sordo, F., Janecek, E.-R., Qu, Y., Michaud, V., Stellacci, F., Engmann, J., Wooster, T. J., and Sorin, F., Microstructured fibers for the production of food, Adv. Mater. **31**, 1807282 (2019).

[582] Reynolds, O., On the theory of lubrication and its application to Mr. Beauchamp tower's experiments, including an experimental determination of the viscosity of olive oil, Phil. Trans. Roy. Soc. Lond. **177**, 157–234 (1886).

[583] Oron, A., Davis, S. H., and Bankoff, S. G., Long-scale evolution of thin liquid films, Rev. Mod. Phys. **69**, 931–980 (1997).

[584] Szeri, A. Z., *Fluid film lubrication* (Cambridge University Press, 2010).

[585] Khonsari, M. M. and Booser, E. R., *Applied tribology: bearing design and lubrication* (John Wiley & Sons, 2017).

[586] Barnes, W. J. P., Tree frogs and tire technology, Tire Technol. Int. **99**, 42–47 (1999).

[587] Barnes, W. J. P., Biomimetic solutions to sticky problems, Science **318**, 203–204 (2007).

[588] Meng, F., Liu, Q., Wang, X., Tan, D., Xue, L., and Barnes, W. J. P., Tree frog adhesion biomimetics: opportunities for the development of new, smart adhesives that adhere under wet conditions, Phil. Trans. Roy. Soc. A **377**, 20190131 (2019).

[589] Mathijssen, A. J. T. M., Doostmohammadi, A., Yeomans, J. M., and Shendruk, T. N., Hydrodynamics of micro-swimmers in films, J. Fluid Mech. **806**, 35–70 (2016).

[590] Wang, W., Timonen, J. V., Carlson, A., Drotlef, D.-M., Zhang, C. T., Kolle, S., Grinthal, A., Wong, T.-S., Hatton, B., Kang, S. H., *et al.*, Multifunctional ferrofluid-infused surfaces with reconfigurable multiscale topography, Nature **559**, 77–82 (2018).

[591] Xu, R.-G. and Leng, Y., Squeezing and stick–slip friction behaviors of lubricants in boundary lubrication, Proc. Natl. Acad. Sci. U.S.A. **115**, 6560–6565 (2018).

[592] Weidman, P. D. and Sprague, M. A., Steady and unsteady modelling of the float height of a rotating air hockey disk, J. Fluid Mech. **778**, 39–59 (2015).

[593] De La Cruz Garcia, C., Sánchez Moragas, G., and Nordqvist, D., Food contact materials, in *Food Safety Management. A Practical Guide for the Food Industry*, edited by Y. Motarjemi and H. Lelievelt (Academic Press, Elsevier, 2014).

[594] Josef Stefan,, Versuche über die scheinbare adhäsion, Sitz. Kais. Akad. Wiss. Math. Nat. Wien **69**, 713–735 (1874).

[595] Engmann, J., Servais, C., and Burbidge, A. S., Squeeze flow theory and applications to rheometry: A review, J. Non-Newtonian Fluid Mech. **132**, 1–27 (2005).

[596] Huppert, H. E., The propagation of two-dimensional and axisymmetric viscous gravity currents over a rigid horizontal surface, J. Fluid Mech. **121**, 43–58 (1982).

[597] Huppert, H. E., Gravity currents: a personal perspective, J. Fluid Mech. **554**, 299–322 (2006).

[598] Craster, R. V. and Matar, O. K., Dynamics and stability of thin liquid films, Rev. Mod. Phys. **81**, 1131 (2009).

[599] Meiburg, E. and Kneller, B., Turbidity currents and their deposits, Annu. Rev. Fluid Mech. **42**, 135–156 (2010).

[600] Walls, D. J., Meiburg, E., and Fuller, G. G., The shape evolution of liquid droplets in miscible environments, J. Fluid Mech. **852**, 422–452 (2018).

[601] Didden, N. and Maxworthy, T., The viscous spreading of plane and axisymmetric gravity currents, J. Fluid Mech. **121**, 27–42 (1982).

[602] Britter, R. E., The spread of a negatively buoyant plume in a calm environment, Atmos. Environ. (1967) **13**, 1241–1247 (1979).

[603] Hoult, D. P., Oil spreading on the sea, Annu. Rev. Fluid Mech. **4**, 341–368 (1972).

[604] Simpson, J. E., Gravity currents in the laboratory, atmosphere, and ocean, Annu. Rev. Fluid Mech. **14**, 213–234 (1982).

[605] Ungarish, M., *An introduction to gravity currents and intrusions* (CRC press, 2009).

[606] Boujo, E. and Sellier, M., Pancake making and surface coating: Optimal control of a gravity-driven liquid film, Phys. Rev. Fluids **4**, 064802 (2019).

[607] Saffman, P. G. and Taylor, G. I., The penetration of a fluid into a porous medium or Hele-Shaw cell containing a more viscous liquid, Proc. Roy. Soc. A **245**, 312–329 (1958).

[608] Hill, S., Channeling in packed columns, Chem. Eng. Sci. **1**, 247–253 (1952).

[609] Homsy, G. M., Viscous fingering in porous media, Annu. Rev. Fluid Mech. **19**, 271–311 (1987).

[610] Lajeunesse, E. and Couder, Y., On the tip-splitting instability of viscous fingers, J. Fluid Mech. **419**, 125–149 (2000).

[611] Mather, W., Mondragón-Palomino, O., Danino, T., Hasty, J., and Tsimring, L. S., Streaming instability in growing cell populations, Phys. Rev. Lett. **104**, 208101 (2010).

[612] Yang, A., Tang, W. S., Si, T., and Tang, J. X., Influence of physical effects on the swarming motility of *Pseudomonas aeruginosa*, Biophys. J. **112**, 1462–1471 (2017).

[613] Moura, M., Måløy, K. J., Flekkøy, E. G., and Toussaint, R., Verification of a dynamic scaling for the pair correlation function during the slow drainage of a porous medium, Phys. Rev. Lett. **119**, 154503 (2017).

[614] Yuan, Q., Zhou, X., Wang, J., Zeng, F., Knorr, K. D., and Imran, M., Control of viscous fingering and mixing in miscible displacements with time-dependent rates, AIChE J. **65**, 360–371 (2019).

[615] Snyder, D. and Tait, S., A flow-front instability in viscous gravity currents, J. Fluid Mech. **369**, 1–21 (1998).

[616] Tang, H., Grivas, W., Homentcovschi, D., Geer, J., and Singler, T., Stability considerations associated with the meniscoid particle band at advancing interfaces in Hele-Shaw suspension flows, Phys. Rev. Lett. **85**, 2112 (2000).

[617] Xu, F., Kim, J., and Lee, S., Particle-induced viscous fingering, J. Non-Newtonian Fluid Mech. **238**, 92–99 (2016).

[618] Moffatt, H. K., Guest, H., and Huppert, H. E., Spreading or contraction of viscous drops between plates: single, multiple or annular drops, J. Fluid Mech. **925**, A26 (2021).

[619] Brennen, C. and Winet, H., Fluid mechanics of propulsion by cilia and flagella, Annu. Rev. Fluid Mech. **9**, 339–398 (1977).

[620] Vella, D., Buffering by buckling as a route for elastic deformation, Nat. Rev. Phys. **1**, 425–436 (2019).

[621] Lauga, E., Life around the scallop theorem, Soft Matter **7**, 3060–3065 (2011).

[622] Mathijssen, A. J. T. M., Shendruk, T. N., Yeomans, J. M., and Doostmohammadi, A., Upstream swimming in microbiological flows, Phys. Rev. Lett. **116**, 028104

(2016).
[623] Mathijssen, A. J. T. M., Figueroa-Morales, N., Junot, G., Clément, E., Lindner, A., and Zöttl, A., Oscillatory surface rheotaxis of swimming *E. coli* bacteria, Nat. Comm. **10**, 1–12 (2019).
[624] Gude, S., Pinçe, E., Taute, K. M., Seinen, A.-B., Shimizu, T. S., and Tans, S. J., Bacterial coexistence driven by motility and spatial competition, Nature **578**, 588–592 (2020).
[625] Kim, D., Cao, Y., Mariappan, D., Bono Jr, M. S., Hart, A. J., and Marelli, B., A microneedle technology for sampling and sensing bacteria in the food supply chain, Adv. Func. Mater. **31**, 2005370 (2021).
[626] Ali, A. A., Altemimi, A. B., Alhelfi, N., and Ibrahim, S. A., Application of biosensors for detection of pathogenic food bacteria: A review, Biosensors **10**, 58 (2020).
[627] World Health Organization,, WHO estimates of the global burden of foodborne diseases: foodborne disease burden epidemiology reference group 2007-2015 (2015).
[628] Vidakovic, L., Singh, P. K., Hartmann, R., Nadell, C. D., and Drescher, K., Dynamic biofilm architecture confers individual and collective mechanisms of viral protection, Nat. Microbiol. **3**, 26–31 (2018).
[629] Mathijssen, A. J. T. M., Guzmán-Lastra, F., Kaiser, A., and Löwen, H., Nutrient transport driven by microbial active carpets, Phys. Rev. Lett. **121**, 248101 (2018).
[630] Mairhofer, J., Roppert, K., and Ertl, P., Microfluidic systems for pathogen sensing: a review, Sensors **9**, 4804–4823 (2009).
[631] Karunakaran, C., Rajkumar, R., and Bhargava, K., Introduction to biosensors, Biosens. Bioelect. , 1–68 (2015).
[632] Van Dorst, B., Mehta, J., Bekaert, K., Rouah-Martin, E., De Coen, W., Dubruel, P., Blust, R., and Robbens, J., Recent advances in recognition elements of food and environmental biosensors: a review, Biosens. Bioelect. **26**, 1178–1194 (2010).
[633] Tokel, O., Yildiz, U. H., Inci, F., Durmus, N. G., Ekiz, O. O., Turker, B., Cetin, C., Rao, S., Sridhar, K., Natarajan, N., *et al.*, Portable microfluidic integrated plasmonic platform for pathogen detection, Sci. Rep. **5**, 1–9 (2015).
[634] Gervais, T. and Jensen, K. F., Mass transport and surface reactions in microfluidic systems, Chem. Eng. Sci. **61**, 1102–1121 (2006).
[635] Squires, T. M., Messinger, R. J., and Manalis, S. R., Making it stick: convection, reaction and diffusion in surface-based biosensors, Nat. Biotech. **26**, 417–426 (2008).
[636] Sathish, S. and Shen, A. Q., Toward the development of rapid, specific, and sensitive microfluidic sensors: A comprehensive device blueprint, JACS Au , 1c00318 (2021).
[637] Goff, H. D. and Hartel, R. W., *Ice Cream*, SpringerLink : Bücher (Springer US, 2013).
[638] Arbuckle, W. S., *Ice Cream* (Springer, Boston, MA, 2013).
[639] Clarke, C., The physics of ice cream, Phys. Educ. **38**, 248–253 (2003).
[640] Clarke, C., *The Science of Ice Cream* (Royal Society of Chemistry, 2015).
[641] Goff, H., Colloidal aspects of ice cream—a review, Int. Dairy J. **7**, 363–373 (1997).
[642] Leighton, A., Leviton, A., and Williams, O. E., The apparent viscosity of ice cream: I. The sagging beam method of measurement. II. Factors to be controlled. III. The effects of milkfat, gelatin and homogenization temperature, J. Dairy Sci. **17**, 639–650 (1934).
[643] Martin, P. J., Odic, K. N., Russell, A. B., Burns, I. W., and Wilson, D. I., Rheology of commercial and model ice creams, Appl. Rheol. **18**, 12913–1–12913–11 (2008).
[644] Trout, J. J. and Jacobsen, T., The science of ice cream, an undergraduate, interdisciplinary, general education course taught in the physics program, Phys. Educ. **55**, 015009 (2019).
[645] Cook, K. L. K. and Hartel, R. W., Mechanisms of ice crystallization in ice cream production, Compr. Rev. Food Sci. Food Safety **9**, 213–222 (2010).
[646] Hartel, R. W., Ice crystallization during the manufacture of ice cream, Trends Food Sci. Tech. **7**, 315–321 (1996).
[647] Muse, M. and Hartel, R., Ice cream structural elements that affect melting rate and hardness, J. Dairy Sci. **87**, 1–10 (2004).
[648] Li, B. and Sun, D.-W., Novel methods for rapid freezing and thawing of foods - a review, J. Food Eng. **54**, 175–182 (2002).
[649] The Master Chef,, Hot Ice Cream! (2021), last accessed: 23-June-2021.
[650] Suzuki, J., *A history of mathematics* (Prentice-Hall, New Jersey, 2002).
[651] de Gennes, P. G., Granular matter: a tentative view, Rev. Mod. Phys. **71**, S374–S382 (1999).
[652] Gray, J. M. N. T., Particle segregation in dense granular flows, Annu. Rev. Fluid Mech. **50**, 407–433 (2018).
[653] Krumbein, W. C., Size frequency distributions of sediments, J. Sedim. Res. **4**, 65–77 (1934).
[654] Herminghaus, S., Dynamics of wet granular matter, Adv. Phys. **54**, 221–261 (2005).
[655] Mehta, A., *Granular Matter: an interdisciplinary approach* (Springer-Verlag, 2012).
[656] Aguirre, M. A., Grande, J. G., Calvo, A., Pugnaloni, L. A., and Géminard, J.-C., Pressure independence of granular flow through an aperture, Phys. Rev. Lett. **104**, 238002 (2010).
[657] Lun, C. K. K., Savage, S. B., Jeffrey, D. J., and Chepurniy, N., Kinetic theories for granular flow: inelastic particles in Couette flow and slightly inelastic particles in a general flowfield, J. Fluid Mech. **140**, 223–256 (1984).
[658] Jaeger, H. M., Nagel, S. R., and Behringer, R. P., Granular solids, liquids, and gases, Rev. Mod. Phys. **68**, 1259–1273 (1996).
[659] Forterre, Y. and Pouliquen, O., Flows of dense granular media, Annu. Rev. Fluid Mech. **40**, 1–24 (2008).
[660] Nagel, S. R., Instabilities in a sandpile, Rev. Mod. Phys. **64**, 321–325 (1992).
[661] Paczuski, M., Maslov, S., and Bak, P., Avalanche dynamics in evolution, growth, and depinning models, Phys. Rev. E **53**, 414–443 (1996).
[662] Frette, V., Christensen, K., Malthe-Sørenssen, A., Feder, J., Jøssang, T., and Meakin, P., Avalanche dynamics in a pile of rice, Nature **379**, 49–52 (1996).
[663] Hunt, M. L. and Vriend, N. M., Booming sand dunes, Annu. Rev. Earth Planet. Sci. **38**, 281–301 (2010).
[664] Mueth, D. M., Jaeger, H. M., and Nagel, S. R., Force distribution in a granular medium, Phys. Rev. E **57**,

3164–3169 (1998).
[665] Al-Hashemi, H. M. B. and Al-Amoudi, O. S. B., A review on the angle of repose of granular materials, Powder Tech. **330**, 397–417 (2018).
[666] De-Song, B., Xun-Sheng, Z., Guang-Lei, X., Zheng-Quan, P., Xiao-Wei, T., and Kun-Quan, L., Critical phenomenon of granular flow on a conveyor belt, Phys. Rev. E **67**, 062301 (2003).
[667] Deshpande, N., Furbish, D., Arratia, P., and Jerolmack, D., The perpetual fragility of creeping hillslopes, Nat. Commun. **12**, 3909 (2021).
[668] Zellner, D. A., Siemers, E., Teran, V., Conroy, R., Lankford, M., Agrafiotis, A., Ambrose, L., and Locher, P., Neatness counts. How plating affects liking for the taste of food, Appetite **57**, 642–648 (2011).
[669] Einav, I. and Guillard, F., Tracking time with rice-quakes in partially soaked brittle porous media, Sci. Adv. **4**, eaat6961 (2018).
[670] Issa, S. F., Field, W. E., Schwab, C. V., Issa, F. S., and Nauman, E. A., Contributing causes of injury or death in grain entrapment, engulfment, and extrication, J. Agromed. **22**, 159–169 (2017).
[671] Roberts, M. J., Deboy, G. R., Field, W. ., and Maier, D. E., Summary of prior grain entrapment rescue strategies, J. Agri. Safety Health **17**, 303–325 (2011).
[672] Cuq, B., Mandato, S., Jeantet, R., Saleh, K., and Ruiz, T., Agglomeration/granulation in food powder production, in *Handbook of food powders* (Elsevier, 2013) pp. 150–177.
[673] Teunou, E., Fitzpatrick, J. J., and Synnott, E. C., Characterisation of food powder flowability, J. Food Eng. **39**, 31–37 (1999).
[674] Krantz, M., Zhang, H., and Zhu, J., Characterization of powder flow: Static and dynamic testing, Powder Tech. **194**, 239–245 (2009).
[675] Kristensen, H. G. and Schaefer, T., Granulation: A review on pharmaceutical wet-granulation, Drug Devel. Indust. Pharm. **13**, 803–872 (1987).
[676] Nawaporn Pax Piewpun,, Personal blog of food artist Nawaporn Pax Piewpun, a.k.a. Peaceloving Pax, `https://www.facebook.com/cutefoodies` (2021), last accessed: 3-Oct-2021.
[677] Tang, J. and Behringer, R. P., How granular materials jam in a hopper, Chaos **21**, 041107 (2011).
[678] Breu, A. P. J., Ensner, H. M., Kruelle, C. A., and Rehberg, I., Reversing the Brazil-nut effect: Competition between percolation and condensation, Phys. Rev. Lett. **90**, 014302 (2003).
[679] Beverloo, W. A., Leniger, H. A., and Van de Velde, J., The flow of granular solids through orifices, Chem. Eng. Sci. **15**, 260–269 (1961).
[680] Nedderman, R. M., *Statics and kinematics of granular materials* (Cambridge University Press, 2005).
[681] Alonso-Marroquin, F. and Mora, P., Beverloo law for hopper flow derived from self-similar profiles, Granular Matt. **23**, 1–8 (2021).
[682] Zuriguel, I., Invited review: Clogging of granular materials in bottlenecks, Papers Phys. **6**, 060014 (2014).
[683] Liu, A. J. and Nagel, S. R., Jamming is not just cool any more, Nature **396**, 21–22 (1998).
[684] Liu, A. J. and Nagel, S. R., The jamming transition and the marginally jammed solid, Annu. Rev. Condens. Matter Phys. **1**, 347–369 (2010).
[685] Thomas, C. C. and Durian, D. J., Fraction of clogging configurations sampled by granular hopper flow, Phys. Rev. Lett. **114**, 178001 (2015).
[686] To, K., Lai, P.-Y., and Pak, H. K., Jamming of granular flow in a two-dimensional hopper, Phys. Rev. Lett. **86**, 71–74 (2001).
[687] Dressaire, E. and Sauret, A., Clogging of microfluidic systems, Soft Matter **13**, 37–48 (2017).
[688] Zuriguel, I., Parisi, D. R., Hidalgo, R. C., Lozano, C., Janda, A., Gago, P. A., Peralta, J. P., Ferrer, L. M., Pugnaloni, L. A., Clément, E., *et al.*, Clogging transition of many-particle systems flowing through bottlenecks, Sci. Rep. **4**, 1–8 (2014).
[689] Barker, G. C., Granular and jammed food materials, in *Food Microstructures* (Elsevier, 2013) pp. 325–335.
[690] Lawson-Keister, E. and Manning, M. L., Jamming and arrest of cell motion in biological tissues, Curr. Opin. Cell Biol. **72**, 146–155 (2021).
[691] Van der Sman, R. G. M., Soft matter approaches to food structuring, Adv. Colloid Interf. Sci. **176**, 18–30 (2012).
[692] Zuriguel, I., Janda, A., Garcimartín, A., Lozano, C., Arévalo, R., and Maza, D., Silo clogging reduction by the presence of an obstacle, Phys. Rev. Lett. **107**, 278001 (2011).
[693] Koivisto, J. and Durian, D. J., The sands of time run faster near the end, Nat. Commun. **8**, 1–6 (2017).
[694] Tao, R., Wilson, M., and Weeks, E. R., Soft particle clogging in two-dimensional hoppers, Phys. Rev. E **104**, 044909 (2021).
[695] Mossige, E. J., Jensen, A., and Mielnik, M. M., Separation and concentration without clogging using a high-throughput tunable filter, Phys. Rev. Applied **9**, 054007 (2018).
[696] Rosato, A., Strandburg, K. J., Prinz, F., and Swendsen, R. H., Why the Brazil nuts are on top: Size segregation of particulate matter by shaking, Phys. Rev. Lett. **58**, 1038–1040 (1987).
[697] Ottino, J. M. and Khakhar, D. V., Mixing and segregation of granular materials, Annu. Rev. Fluid Mech. **32**, 55–91 (2000).
[698] Kudrolli, A., Size separation in vibrated granular matter, Rep. Progr. Phys. **67**, 209 (2004).
[699] Knight, J. B., Jaeger, H. M., and Nagel, S. R., Vibration-induced size separation in granular media: The convection connection, Phys. Rev. Lett. **70**, 3728–3731 (1993).
[700] Ehrichs, E. E., Jaeger, H. M., Karczmar, G. S., Knight, J. B., Kuperman, V. Y., and Nagel, S. R., Granular convection observed by magnetic resonance imaging, Science **267**, 1632–1634 (1995).
[701] Knight, J. B., Ehrichs, E. E., Kuperman, V. Y., Flint, J. K., Jaeger, H. M., and Nagel, S. R., Experimental study of granular convection, Phys. Rev. E **54**, 5726–5738 (1996).
[702] Gallas, J. A., Herrmann, H. J., Pöschel, T., and Sokołowski, S., Molecular dynamics simulation of size segregation in three dimensions, J. Stat. Phys. **82**, 443–450 (1996).
[703] Shinbrot, T. and Muzzio, F. J., Reverse buoyancy in shaken granular beds, Phys. Rev. Lett. **81**, 4365–4368 (1998).
[704] Möbius, M. E., Lauderdale, B. E., Nagel, S. R., and Jaeger, H. M., Size separation of granular particles, Nature **414**, 270–270 (2001).

[705] Huerta, D. A. and Ruiz-Suárez, J. C., Vibration-induced granular segregation: A phenomenon driven by three mechanisms, Phys. Rev. Lett. **92**, 114301 (2004).

[706] Rietz, F. and Stannarius, R., On the brink of jamming: Granular convection in densely filled containers, Phys. Rev. Lett. **100**, 078002 (2008).

[707] Murdoch, N., Rozitis, B., Nordstrom, K., Green, S. F., Michel, P., de Lophem, T.-L., and Losert, W., Granular convection in microgravity, Phys. Rev. Lett. **110**, 018307 (2013).

[708] D'Ortona, U. and Thomas, N., Self-induced Rayleigh-Taylor instability in segregating dry granular flows, Phys. Rev. Lett. **124**, 178001 (2020).

[709] Baxter, J., Tüzün, U., Heyes, D., Hayati, I., and Fredlund, P., Stratification in poured granular heaps, Nature **391**, 136–136 (1998).

[710] Li, H. and McCarthy, J. J., Controlling cohesive particle mixing and segregation, Phys. Rev. Lett. **90**, 184301 (2003).

[711] Xiao, H., McDonald, D., Fan, Y., Umbanhowar, P. B., Ottino, J. M., and Lueptow, R. M., Controlling granular segregation using modulated flow, Powder technology **312**, 360–368 (2017).

[712] Harrington, M., Weijs, J. H., and Losert, W., Suppression and emergence of granular segregation under cyclic shear, Phys. Rev. Lett. **111**, 078001 (2013).

[713] Vithu, P. and Moses, J. A., Machine vision system for food grain quality evaluation: A review, Trends Food Sci. Tech. **56**, 13–20 (2016).

[714] Windows-Yule, C. R. K., Seville, J. P. K., Ingram, A., and Parker, D. J., Positron emission particle tracking of granular flows, Annu. Rev. Chem. Biomol. Eng. **11**, 367–396 (2020).

[715] Gajjar, P., Johnson, C. G., Carr, J., Chrispeels, K., Gray, J. M. N. T., and Withers, P. J., Size segregation of irregular granular materials captured by time-resolved 3D imaging, Sci. Rep. **11**, 1–6 (2021).

[716] Ko, H. and Hu, D. L., The physics of tossing fried rice, J. R. Soc. Interface **17**, 20190622 (2020).

[717] Virot, E. and Ponomarenko, A., Popcorn: critical temperature, jump and sound, J. R. Soc. Interface **12**, 20141247 (2015).

[718] Wadsworth, F. B., Vossen, C. E. J., Heap, M. J., Kushnir, A., Farquharson, J. I., Schmid, D., Dingwell, D. B., Belohlavek, L., Huebsch, M., Carbillet, L., and Kendrick, J. E., The force required to operate the plunger on a French press, Am. J. Phys. **89**, 769–775 (2021).

[719] Hsu, L. and Chen, Y.-J., Does coffee taste better with latte art? A neuroscientific perspective, British Food J. **123**, 1931–1946 (2021).

[720] Darcy, H., *Les fontaines publiques de la ville de Dijon: exposition et application...* (Victor Dalmont, 1856).

[721] Muskat, M., *The flow of homogeneous fluids through porous media* (McGraw-Hill, New York, 1938).

[722] Whitaker, S., Flow in porous media I: A theoretical derivation of Darcy's law, Transp. Porous Media **1**, 3–25 (1986).

[723] Yang, H., Min, X., Xu, S., Bender, J., and Wang, Y., Development of effective and fast-flow ceramic porous media for point-of-use water treatment: Effect of pore size distribution, ACS Sustain. Chem. Eng. **8**, 2531–2539 (2020).

[724] Hills, B. P., Arnould, L., Bossu, C., and Ridge, Y. P., Microstructural factors controlling the survival of foodborne pathogens in porous media, Int. J. Food Microbiol. **66**, 163–173 (2001).

[725] Philip, J. R., Flow in porous media, Annu. Rev. Fluid Mech. **2**, 177–204 (1970).

[726] Bear, J., *Dynamics of fluids in porous media* (Dover Publications, New York, 2013).

[727] Blunt, M. J., Flow in porous media — pore-network models and multiphase flow, Curr. Opin. Colloid Interf. Sci. **6**, 197–207 (2001).

[728] Thurston, R., Morris, J., and Steiman, S., *Coffee: A Comprehensive Guide to the Bean, the Beverage, and the Industry* (Rowman & Littlefield, 2013).

[729] Egger, S. and Orr, R. A., *The Home Barista: How to Bring Out the Best in Every Coffee Bean* (The Experiment, 2016).

[730] Giacomini, J., Khamitova, G., Maponi, P., Vittori, S., and Fioretti, L., Water flow and transport in porous media for in-silico espresso coffee, Int. J. Multiph. Flow **126**, 103252 (2020).

[731] Angeloni, G., Guerrini, L., Masella, P., Innocenti, M., Bellumori, M., and Parenti, A., Characterization and comparison of cold brew and cold drip coffee extraction methods, J. Sci. Food Agric. **99**, 391–399 (2019).

[732] Corrochano, B. R., Melrose, J. R., Bentley, A. C., Fryer, P. J., and Bakalis, S., A new methodology to estimate the steady-state permeability of roast and ground coffee in packed beds, J. Food Eng. **150**, 106–116 (2015).

[733] Binder, P. and Scheidle, C. B., The moka pot: Thoughts and experiments, Phys. Educ. **55**, 065024 (2020).

[734] Gianino, C., Experimental analysis of the Italian coffee pot "moka", Am. J. Phys. **75**, 43–47 (2007).

[735] King, W. D., The physics of a stove-top espresso machine, Am. J. Phys. **76**, 558–565 (2008).

[736] Kaestner, A., Neutron movie of coffee making, `https://www.youtube.com/watch?v=VESMU7JfVHU` (2012), last accessed: 16-April-2020.

[737] Fasano, A., Talamucci, F., and Petracco, M., The espresso coffee problem, in *Complex Flows in Industrial Processes*, edited by A. Fasano (Birkhäuser Boston, Boston, MA, 2000) pp. 241–280.

[738] Stauffer, D., *Introduction to Percolation Theory*, 2nd ed. (Taylor & Francis, 2018).

[739] Singh, K., Jung, M., Brinkmann, M., and Seemann, R., Capillary-dominated fluid displacement in porous media, Annu. Rev. Fluid Mech. **51**, 429–449 (2019).

[740] Severini, C., Derossi, A., Ricci, I., Fiore, A. G., and Caporizzi, R., How much caffeine in coffee cup? Effects of processing operations, extraction methods and variables, in *The Question of Caffeine* (InTech, 2017) pp. 45–85.

[741] Adler, P. M., Thovert, J.-F., and Mourzenko, V. V., *Fractured porous media* (Oxford University Press, 2013).

[742] Berre, I., Doster, F., and Keilegavlen, E., Flow in fractured porous media: a review of conceptual models and discretization approaches, Transp. Porous Media **130**, 215–236 (2019).

[743] Sahimi, M., *Applications of percolation theory* (Taylor & Francis, 2014).

[744] Mathijssen, A. J. T. M., Culver, J., Bhamla, M. S., and Prakash, M., Collective intercellular communication through ultra-fast hydrodynamic trigger waves, Nature **571**, 560–565 (2019).

[745] Cameron, M. I., Morisco, D., Hofstetter, D., Uman, E., Wilkinson, J., Kennedy, Z. C., Fontenot, S. A., Lee, W. T., Hendon, C. H., and Foster, J. M., Systematically improving espresso: Insights from mathematical modeling and experiment, Matter **2**, 631–648 (2020).

[746] Batali, M. E., Ristenpart, W. D., and Guinard, J.-X., Brew temperature, at fixed brew strength and extraction, has little impact on the sensory profile of drip brew coffee, Sci. Rep. **10**, 1–14 (2020).

[747] Cordoba, N., Pataquiva, L., Osorio, C., Moreno, F. L. M., and Ruiz, R. Y., Effect of grinding, extraction time and type of coffee on the physicochemical and flavour characteristics of cold brew coffee, Sci. Rep. **9**, 1–12 (2019).

[748] Rao, N. Z. and Fuller, M., Acidity and antioxidant activity of cold brew coffee, Sci. Rep. **8**, 1–9 (2018).

[749] Bez, I., Latte art guide (2021), last Accessed: 2021-10-27.

[750] Illy, E. and Navarini, L., Neglected food bubbles: the espresso coffee foam, Food Biophys. **6**, 335–348 (2011).

[751] Jafari Kang, S., Vandadi, V., Felske, J. D., and Masoud, H., Alternative mechanism for coffee-ring deposition based on active role of free surface, Phys. Rev. E **94**, 063104 (2016).

[752] Li, Y., Yang, Q., Li, M., and Song, Y., Rate-dependent interface capture beyond the coffee-ring effect, Sci. Rep. **6**, 1–8 (2016).

[753] Ooi, Y., Hanasaki, I., Mizumura, D., and Matsuda, Y., Suppressing the coffee-ring effect of colloidal droplets by dispersed cellulose nanofibers, Sci. Tech. Adv. Mater. **18**, 316–324 (2017).

[754] Deegan, R. D., Bakajin, O., Dupont, T. F., Huber, G., Nagel, S. R., and Witten, T. A., Capillary flow as the cause of ring stains from dried liquid drops, Nature **389**, 827–829 (1997).

[755] Marín, A. G., Gelderblom, H., Lohse, D., and Snoeijer, J. H., Order-to-disorder transition in ring-shaped colloidal stains, Phys. Rev. Lett. **107**, 085502 (2011).

[756] Mampallil, D. and Eral, H. B., A review on suppression and utilization of the coffee-ring effect, Adv. Coll. Interf. Sci. **252**, 38 – 54 (2018).

[757] Mouat, A. P., Wood, C. E., Pye, J. E., and Burton, J. C., Tuning contact line dynamics and deposition patterns in volatile liquid mixtures, Phys. Rev. Lett. **124**, 064502 (2020).

[758] Moore, M. R., Vella, D., and Oliver, J. M., The nascent coffee ring: how solute diffusion counters advection, J. Fluid Mech. **920**, A54 (2021).

[759] Hu, H. and Larson, R. G., Marangoni effect reverses coffee-ring depositions, J. Phys. Chem. B **110**, 7090–7094 (2006).

[760] Yunker, P. J., Still, T., Lohr, M. A., and Yodh, A. G., Suppression of the coffee-ring effect by shape-dependent capillary interactions, Nature **476**, 308–311 (2011).

[761] Yunker, P. J., Lohr, M. A., Still, T., Borodin, A., Durian, D. J., and Yodh, A. G., Effects of particle shape on growth dynamics at edges of evaporating drops of colloidal suspensions, Phys. Rev. Lett. **110**, 035501 (2013).

[762] Routh, A. F., Drying of thin colloidal films, Rep. Progr. Phys. **76**, 046603 (2013).

[763] Han, W. and Lin, Z., Learning from "coffee rings": Ordered structures enabled by controlled evaporative self-assembly, Angew. Chem. Int. Ed. **51**, 1534–1546 (2012).

[764] Zhang, Z., Zhang, X., Xin, Z., Deng, M., Wen, Y., and Song, Y., Controlled inkjetting of a conductive pattern of silver nanoparticles based on the coffee-ring effect, Adv. Mater. **25**, 6714–6718 (2013).

[765] Varanakkottu, S. N., Anyfantakis, M., Morel, M., Rudiuk, S., and Baigl, D., Light-directed particle patterning by evaporative optical Marangoni assembly, Nano Lett. **16**, 644–650 (2016).

[766] Wong, T.-S., Chen, T.-H., Shen, X., and Ho, C.-M., Nanochromatography driven by the coffee ring effect, Analyt. Chem. **83**, 1871–1873 (2011).

[767] Nellimoottil, T. T., Rao, P. N., Ghosh, S. S., and Chattopadhyay, A., Evaporation-induced patterns from droplets containing motile and nonmotile bacteria, Langmuir **23**, 8655–8658 (2007).

[768] Sempels, W., De Dier, R., Mizuno, H., Hofkens, J., and Vermant, J., Auto-production of biosurfactants reverses the coffee ring effect in a bacterial system, Nat. Commun. **4**, 1–8 (2013).

[769] Hennes, M., Tailleur, J., Charron, G., and Daerr, A., Active depinning of bacterial droplets: The collective surfing of *Bacillus subtilis*, Proc. Natl. Acad. Sci. U.S.A. **114**, 5958–5963 (2017).

[770] Andac, T., Weigmann, P., Velu, S. K., Pinçe, E., Volpe, G., Volpe, G., and Callegari, A., Active matter alters the growth dynamics of coffee rings, Soft Matter **15**, 1488–1496 (2019).

[771] Kang, Y. K., Ryu, J. S., Lee, J., Chung, H. J., *et al.*, Simple visualized readout of suppressed coffee ring patterns for rapid and isothermal genetic testing of antibacterial resistance, Biosens. Bioelect. **168**, 112566 (2020).

[772] Marusic, I. and Broomhall, S., Leonardo da Vinci and fluid mechanics, Annu. Rev. Fluid Mech. **53**, 1–25 (2021).

[773] Kolmogorov, A. N., The local structure of turbulence in incompressible viscous fluid for very large Reynolds numbers, Cr Acad. Sci. URSS **30**, 301–305 (1941).

[774] Richardson, L. F., *Weather prediction by numerical process* (Cambridge University Press, 2007).

[775] Aoyagi, H., Yokoi, H., and Tanaka, H., Measurement of fresh and dry densities of suspended plant cells and estimation of their water content, J. Ferment. Bioengng. **73**, 490–496 (1992).

[776] Thomson, J., Bakerian lecture - On the grand currents of atmospheric circulation, Phil. Trans. Roy. Soc. A , 653–684 (1892).

[777] Einstein, A., The cause of the formation of meanders in the courses of rivers and of the so-called Baer's law, Naturwissenschaften **14**, 223–224 (1926).

[778] Greenspan, H. P. and Howard, L. N., On a time-dependent motion of a rotating fluid, J. Fluid Mech. **17**, 385–404 (1963).

[779] Heavers, R. M. and Dapp, R. M., The Ekman layer and why tea leaves go to the center of the cup, Phys. Teach. **48**, 96–100 (2010).

[780] Baker Jr, D. J., Demonstrations of fluid flow in a rotating system II: The 'spin-up' problem, Am. J. Phys. **36**, 980–986 (1968).

[781] Moore, G. S. M., Swirling tea leaves: problem and solution, Phys. Educ. **24**, 358 (1989).

[782] Ekman, V. W., Beiträge zur theorie der meeresströmungen, Ann. Hydrogr. Mar. Meteorol. **34**, 527–540 (1906).

[783] Bamforth, C., *Beer: tap into the art and science of brewing* (Oxford University Press, 2009).

[784] Arifin, D. R., Yeo, L. Y., and Friend, J. R., Microfluidic blood plasma separation via bulk electrohydrodynamic flows, Biomicrofluid. **1**, 014103 (2007).

[785] Rotunno, R., The fluid dynamics of tornadoes, Annu. Rev. Fluid Mech. **45**, 59–84 (2013).

[786] Kelly, B. E., Bhattacharya, I., Heidari, H., Shusteff, M., Spadaccini, C. M., and Taylor, H. K., Volumetric additive manufacturing via tomographic reconstruction, Science **363**, 1075–1079 (2019).

[787] Van Dyke, M., *Perturbation methods in fluid mechanics*, 2nd ed. (The Parabolic Press, Stanford, 1975).

[788] Dean, W. R., Note on the motion of fluid in a curved pipe, Phil. Mag. **4**, 208–223 (1927).

[789] Germano, M., The Dean equations extended to a helical pipe flow, J. Fluid Mech. **203**, 289–305 (1989).

[790] Boshier, F. A. T. and Mestel, A. J., Extended series solutions and bifurcations of the Dean equations, J. Fluid Mech. **739**, 179–195 (2014).

[791] Kalpakli, A., Örlü, R., and Alfredsson, P. H., Dean vortices in turbulent flows: rocking or rolling?, J. Visualiz. **15**, 37–38 (2012).

[792] Di Carlo, D., Inertial microfluidics, Lab Chip **9**, 3038–3046 (2009).

[793] Vollestad, P., Angheluta, L., and Jensen, A., Experimental study of secondary flows above rough and flat interfaces in horizontal gas-liquid pipe flow, Int. J. Multiph. Flow **125**, 103235 (2020).

[794] Müller, A., Stahl, M. R., Graef, V., Franz, C. M., and Huch, M., UV-C treatment of juices to inactivate microorganisms using Dean vortex technology, J. Food Eng. **107**, 268–275 (2011).

[795] Langston, L. S., Secondary flows in axial turbines—a review, Annal. New York Acad. Sci. **934**, 11–26 (2001).

[796] Eliassen, A., Vilhelm Bjerknes and his students, Annu. Rev. Fluid Mech. **14**, 1–12 (1982).

[797] Garratt, J. R., The atmospheric boundary layer, Earth-Sci. Rev. **37**, 89–134 (1994).

[798] Wang, C., Yu, X., and Liang, F., A review of bridge scour: mechanism, estimation, monitoring and countermeasures, Natural Hazards **87**, 1881–1906 (2017).

[799] White, F. M. and Corfield, I., *Viscous fluid flow*, 3rd ed. (McGraw-Hill New York, 2006).

[800] Barros, D., Borée, J., Noack, B. R., Spohn, A., and Ruiz, T., Bluff body drag manipulation using pulsed jets and Coanda effect, J. Fluid Mech. **805**, 422–459 (2016).

[801] Lien, T. and Davis, P., A novel gripper for limp materials based on lateral Coanda ejectors, CIRP Annals **57**, 33–36 (2008).

[802] López-Arias, T., Gratton, L. M., Bon, S., and Oss, S., Back of the spoon: Outlook of Coanda effect, Phys. Teach. **47**, 508–512 (2009).

[803] Duez, C., Ybert, C., Clanet, C., and Bocquet, L., Wetting controls separation of inertial flows from solid surfaces, Phys. Rev. Lett. **104**, 084503 (2010).

[804] Scheichl, B., Bowles, R., and Pasias, G., Developed liquid film passing a smoothed and wedge-shaped trailing edge: small-scale analysis and the 'teapot effect' at large Reynolds numbers, J. Fluid Mech. **926**, A25 (2021).

[805] Jambon-Puillet, E., Bouwhuis, W., Snoeijer, J. H., and Bonn, D., Liquid Helix: How capillary jets adhere to vertical cylinders, Phys. Rev. Lett. **122**, 184501 (2019).

[806] Burkhardt, U. and Kärcher, B., Global radiative forcing from contrail cirrus, Nat. Clim. Change **1**, 54–58 (2011).

[807] Teoh, R., Schumann, U., Majumdar, A., and Stettler, M. E., Mitigating the climate forcing of aircraft contrails by small-scale diversions and technology adoption, Environ. Sci. Tech. **54**, 2941–2950 (2020).

[808] Taylor, G. I., *Dynamics of a mass of hot gas rising in air*, Vol. 919 (Technical Information Division, Oak Ridge Operations, 1946).

[809] Henrywood, R. H. and Agarwal, A., The aeroacoustics of a steam kettle, Phys. Fluids **25**, 107101 (2013).

[810] Chanaud, R. C., Aerodynamic whistles, Scientific American **222**, 40–47 (1970).

[811] Lord Rayleigh,, *The theory of sound*, Vol. 1 (Cambridge University Press, 1877).

[812] Newton, I., *Mathematical Principles of Natural Philosophy* (Flame Tree Collections, 2020) Philosophiae naturalis principia mathematica, originally published in 1687.

[813] Murdin, P., *Full meridian of glory: perilous adventures in the competition to measure the Earth* (Springer, 2009).

[814] Lord Rayleigh,, *The theory of sound*, Vol. 2 (Cambridge University Press, 1877).

[815] Bearman, P. W., Vortex shedding from oscillating bluff bodies, Annu. Rev. Fluid Mech. **16**, 195–222 (1984).

[816] Irwin, P. A., Vortices and tall buildings: A recipe for resonance, Phys. Today **63**, 68–69 (2010).

[817] Fernandes, M. C., Saadat, M., Cauchy-Dubois, P., Inamura, C., Sirota, T., Milliron, G., Haj-Hariri, H., Bertoldi, K., and Weaver, J. C., Mechanical and hydrodynamic analyses of helical strake-like ridges in a glass sponge, J. R. Soc. Interface **18**, 20210559 (2021).

[818] Wilson, T. A., Beavers, G. S., DeCoster, M. A., Holger, D. K., and Regenfuss, M. D., Experiments on the fluid mechanics of whistling, J. Acoust. Soc. America **50**, 366–372 (1971).

[819] Azola, A., Palmer, J., Mulheren, R., Hofer, R., Fischmeister, F., and Fitch, W. T., The physiology of oral whistling: a combined radiographic and MRI analysis, J. Appl. Physiol. **124**, 34–39 (2018).

[820] Shadle, C. H., Experiments on the acoustics of whistling, Phys. Teach. **21**, 148–154 (1983).

[821] Leighton, T., *The acoustic bubble* (Academic press, 2012).

[822] Speirs, N. B., Pan, Z., Belden, J., and Truscott, T. T., The water entry of multi-droplet streams and jets, J. Fluid Mech. **844**, 1084–1111 (2018).

[823] Franz, G. J., Splashes as sources of sound in liquids, J. Acoust. Soc. America **31**, 1080–1096 (1959).

[824] Minnaert, M., On musical air-bubbles and the sounds of running water, Philos. Mag. **16**, 235–248 (1933).

[825] Longuet-Higgins, M. S., An analytic model of sound production by raindrops, J. Fluid Mech. **214**, 395–410 (1990).

[826] Oguz, H. N. and Prosperetti, A., Bubble entrainment by the impact of drops on liquid surfaces, J. Fluid Mech. **219**, 143–179 (1990).

[827] Prosperetti, A. and Oguz, H. N., The impact of drops on liquid surfaces and the underwater noise of rain, Annu. Rev. Fluid Mech. **25**, 577–602 (1993).

[828] Leighton, T. G., How can humans, in air, hear sound generated underwater (and can goldfish hear their own-

ers talking)?, J. Acoust. Soc. America **131**, 2539–2542 (2012).
[829] Phillips, S., Agarwal, A., and Jordan, P., The sound produced by a dripping tap is driven by resonant oscillations of an entrapped air bubble, Sci. Rep. **8**, 1–12 (2018).
[830] Bernstein, B., Hall, D. A., and Trent, H. M., On the dynamics of a bull whip, J. Acoust. Soc. America **30**, 1112–1115 (1958).
[831] Lee, N., Allen, S., Smith, E., and Winters, L. M., Does the tip of a snapped towel travel faster than sound?, Phys. Teach. **31**, 376–77 (1993).
[832] Gekle, S., Peters, I. R., Gordillo, J. M., van der Meer, D., and Lohse, D., Supersonic air flow due to solid-liquid impact, Phys. Rev. Lett. **104**, 024501 (2010).
[833] Bussonnière, A., Antkowiak, A., Ollivier, F., Baudoin, M., and Wunenburger, R., Acoustic sensing of forces driving fast capillary flows, Phys. Rev. Lett. **124**, 084502 (2020).
[834] Albanese, L., Ciriminna, R., Meneguzzo, F., and Pagliaro, M., Beer-brewing powered by controlled hydrodynamic cavitation: Theory and real-scale experiments, J. Cleaner Production **142**, 1457–1470 (2017).
[835] Albanese, L., Ciriminna, R., Meneguzzo, F., and Pagliaro, M., Gluten reduction in beer by hydrodynamic cavitation assisted brewing of barley malts, LWT Food Sci. Tech. **82**, 342–353 (2017).
[836] Jarman, P. D. and Taylor, K. J., Light emission from cavitating water, British J. Appl. Phys. **15**, 321 (1964).
[837] Patek, S. N., Korff, W., and Caldwell, R. L., Deadly strike mechanism of a mantis shrimp, Nature **428**, 819–820 (2004).
[838] McNamara, W. B., Didenko, Y. T., and Suslick, K. S., Sonoluminescence temperatures during multi-bubble cavitation, Nature **401**, 772–775 (1999).
[839] Crawford, F. S., The hot chocolate effect, Am. J. Phys. **50**, 398–404 (1982).
[840] Crawford, F. S., Hot water, fresh beer, and salt, Am. J. Phys. **58**, 1033–1036 (1990).
[841] Trávníček, Z., Fedorchenko, A., Pavelka, M., and Hrubỳ, J., Visualization of the hot chocolate sound effect by spectrograms, J. Sound Vibr. **331**, 5387–5392 (2012).
[842] Dimotakis, P. E., Turbulent mixing, Annu. Rev. Fluid Mech. **37**, 329–356 (2005).
[843] Aref, H., Stirring by chaotic advection, J. Fluid Mech. **143**, 1–21 (1984).
[844] Ottino, J. M., *The kinematics of mixing: stretching, chaos, and transport* (Cambridge University Press, 1989).
[845] Arnold, V. I. and Khesin, B. A., *Topological methods in hydrodynamics*, Vol. 125 (Springer-Verlag, New York, 1998).
[846] Özer, Ç. and Ağan, C., The influence of aging egg on foaming properties of different meringue types, J. Culin. Sci. Tech. , 1–10 (2020).
[847] Thiffeault, J.-L., Gouillart, E., and Dauchot, O., Moving walls accelerate mixing, Phys. Rev. E **84**, 036313 (2011).
[848] Meunier, P. and Villermaux, E., How vortices mix, J. Fluid Mech. **476**, 213–222 (2003).
[849] Franjione, J. G., Ottino, J. M., and Smith, F. T., Symmetry concepts for the geometric analysis of mixing flows, Phil. Trans. Roy. Soc. Lond. A **338**, 301–323 (1992).
[850] Bollini, M., Tellex, S., Thompson, T., Roy, N., and Rus, D., Interpreting and executing recipes with a cooking robot, in *Experimental Robotics* (Springer, 2013) pp. 481–495.
[851] Aref, H., Blake, J. R., Budišić, M., Cardoso, S. S. S., Cartwright, J. H. E., Clercx, H. J. H., El Omari, K., Feudel, U., Golestanian, R., Gouillart, E., van Heijst, G. F., Krasnopolskaya, T. S., Le Guer, Y., MacKay, R. S., Meleshko, V. V., Metcalfe, G., Mezić, I., de Moura, A. P. S., Piro, O., Speetjens, M. F. M., Sturman, R., Thiffeault, J.-L., and Tuval, I., Frontiers of chaotic advection, Rev. Mod. Phys. **89**, 025007 (2017).
[852] Stroock, A. D., Dertinger, S. K., Ajdari, A., Mezić, I., Stone, H. A., and Whitesides, G. M., Chaotic mixer for microchannels, Science **295**, 647–651 (2002).
[853] Gilpin, W., Cryptographic hashing using chaotic hydrodynamics, Proc. Natl. Acad. Sci. U.S.A. **115**, 4869–4874 (2018).
[854] Taylor, G. I., The formation of emulsions in definable fields of flow, Proc. Roy. Soc. A **146**, 501–523 (1934).
[855] Bentley, B. J. and Leal, L. G., A computer-controlled four-roll mill for investigations of particle and drop dynamics in two-dimensional linear shear flows, J. Fluid Mech. **167**, 219–240 (1986).
[856] Bentley, B. J. and Leal, L. G., An experimental investigation of drop deformation and breakup in steady, two-dimensional linear flows, J. Fluid Mech. **167**, 241–283 (1986).
[857] Barthes-Biesel, D. and Acrivos, A., Deformation and burst of a liquid droplet freely suspended in a linear shear field, J. Fluid Mech. **61**, 1–22 (1973).
[858] Hinch, E. J. and Acrivos, A., Steady long slender droplets in two-dimensional straining motion, J. Fluid Mech **91**, 401 (1979).
[859] Stone, H. A. and Leal, L. G., The influence of initial deformation on drop breakup in subcritical time-dependent flows at low Reynolds numbers, J. Fluid Mech. **206**, 223–263 (1989).
[860] Fuller, G. G. and Leal, L. G., Flow birefringence of dilute polymer solutions in two-dimensional flows, Rheol. Acta **19**, 580–600 (1980).
[861] Fuller, G. G. and Leal, L. G., Flow birefringence of concentrated polymer solutions in two-dimensional flows, J. Polymer Sci. **19**, 557–587 (1981).
[862] Hudson, S. D., Phelan Jr, F. R., Handler, M. D., Cabral, J. T., Migler, K. B., and Amis, E. J., Microfluidic analog of the four-roll mill, Appl. Phys. Lett. **85**, 335–337 (2004).
[863] Haward, S. J., Microfluidic extensional rheometry using stagnation point flow, Biomicrofluidics **10**, 043401 (2016).
[864] Perrault, C. M., Qasaimeh, M. A., and Juncker, D., The microfluidic probe: operation and use for localized surface processing, J. Vis. Exp. , e1418 (2009).
[865] Juncker, D., Schmid, H., and Delamarche, E., Multipurpose microfluidic probe, Nat. Mater. **4**, 622–628 (2005).
[866] Safavieh, M., Qasaimeh, M. A., Vakil, A., Juncker, D., and Gervais, T., Two-aperture microfluidic probes as flow dipoles: Theory and applications, Sci. Rep. **5**, 1–16 (2015).
[867] Brimmo, A. T. and Qasaimeh, M. A., Stagnation point flows in analytical chemistry and life sciences, RSC Adv.

7, 51206–51232 (2017).
[868] Leal, L. G., *Advanced transport phenomena: fluid mechanics and convective transport processes* (Cambridge University Press, 2007).
[869] Fan, L. T. and Tseng, J. T., Apparent diffusivity in honey-water system, J. Food Sci. **32**, 633–636 (1967).
[870] Acrivos, A. and Goddard, J. D., Asymptotic expansions for laminar forced-convection heat and mass transfer, J. Fluid Mech. **23**, 273–291 (1965).
[871] Mossige, E. J., Chandran Suja, V., Walls, D. J., and Fuller, G. G., Dynamics of freely suspended drops translating through miscible environments, Phys. Fluids **33**, 033106 (2021).
[872] Krishnamurthy, D. and Subramanian, G., Heat or mass transport from drops in shearing flows. part 1. the open-streamline regime, J. Fluid Mech. **850**, 439–483 (2018).
[873] Krishnamurthy, D. and Subramanian, G., Heat or mass transport from drops in shearing flows. Part 2. Inertial effects on transport, J. Fluid Mech. **850**, 484–524 (2018).
[874] Rosen, M. J. and Kunjappu, J. T., *Surfactants and interfacial phenomena* (John Wiley & Sons, 2012).
[875] Myers, D., *Surfactant science and technology*, 4th ed. (John Wiley & Sons, 2020).
[876] Mertens, J., Oil on troubled waters: Benjamin Franklin and the honor of Dutch seamen, Physics Today **59**, 36 (2006).
[877] Mayer, H. C. and Krechetnikov, R., Walking with coffee: Why does it spill?, Phys. Rev. E **85**, 046117 (2012).
[878] Sauret, A., Boulogne, F., Cappello, J., Dressaire, E., and Stone, H. A., Damping of liquid sloshing by foams, Phys. Fluids **27**, 022103 (2015).
[879] Franklin, B. and Brownrigg, W., Of the stilling of waves by means of oil, Phil. Trans. Roy. Soc. , 445–460 (1774).
[880] Tanford, C., *Ben Franklin stilled the waves* (Oxford University Press, 2004).
[881] Henderson, D. M. and Miles, J. W., Surface-wave damping in a circular cylinder with a fixed contact line, J. Fluid Mech. **275**, 285–299 (1994).
[882] Nicolas, J. A. and Vega, J. M., A note on the effect of surface contamination in water wave damping, J. Fluid Mech. **410**, 367–373 (2000).
[883] Behroozi, P., Cordray, K., Griffin, W., and Behroozi, F., The calming effect of oil on water, Am. J. Phys. **75**, 407–414 (2007).
[884] Kidambi, R., Damping of surface waves in a brimful circular cylinder with a contaminated free surface, Fluid Dyn. Res. **43**, 035504 (2011).
[885] Kim, I. and Mandre, S., Marangoni elasticity of flowing soap films, Phys. Rev. Fluids **2**, 082001(R) (2017).
[886] Ibrahim, R. A., *Liquid sloshing dynamics: theory and applications* (Cambridge University Press, 2005).
[887] Herczyński, A. and Weidman, P. D., Experiments on the periodic oscillation of free containers driven by liquid sloshing, J. Fluid Mech. **693**, 216–242 (2012).
[888] Quetzeri-Santiago, M. A., Yokoi, K., Castrejón-Pita, A. A., and Castrejón-Pita, J. R., Role of the dynamic contact angle on splashing, Phys. Rev. Lett. **122**, 228001 (2019).
[889] Howland, C. J., Antkowiak, A., Castrejón-Pita, J. R., Howison, S. D., Oliver, J. M., Style, R. W., and Castrejón-Pita, A. A., It's harder to splash on soft solids, Phys. Rev. Lett. **117**, 184502 (2016).
[890] Richard, D. and Quéré, D., Bouncing water drops, Europhys. Lett. **50**, 769–775 (2000).
[891] Herczyński, A., Chernuschi, C., and Mahadevan, L., Painting with drops, jets, and sheets, Physics Today **64**, 31 (2011).
[892] Zenit, R., Some fluid mechanical aspects of artistic painting, Phys. Rev. Fluids **4**, 110507 (2019).
[893] Bhamla, M. S. and Fuller, G. G., Placing Marangoni instabilities under arrest, Phys. Rev. Fluids **1**, 050506 (2016).
[894] Patsyk, A., Sivan, U., Segev, M., and Bandres, M. A., Observation of branched flow of light, Nature **583**, 60–65 (2020).
[895] Newton, I., *Opticks, or, a treatise of the reflections, refractions, inflections & colours of light* (Dover, 2012) originally published in 1704.
[896] Plateau, J., Experimental and theoretical statics of liquids subject to molecular forces only, Gauthier-Villars, Paris **1** (1873).
[897] Byers, N. and Williams, G., *Out of the Shadows: Contributions of Twentieth-Century Women to Physics* (Cambridge University Press, 2006).
[898] Lord Rayleigh,, Surface tension, Nature **43**, 437–439 (1891), translation of letter by Agnes Pockels.
[899] Pockels, A., On the relative contamination of the water-surface by equal quantities of different substances, Nature **46**, 418–419 (1892).
[900] Pockels, A., Relations between the surface-tension and relative contamination of water surfaces, Nature **48**, 152–154 (1893).
[901] Pockels, A., On the spreading of oil upon water, Nature **50**, 223–224 (1894).
[902] Pockels, A., The measurement of surface tension with the balance, Science **64**, 304–304 (1926).
[903] Fuller, G. G. and Vermant, J., Complex fluid-fluid interfaces: rheology and structure, Annu. Rev. Chem. Biomolec. Eng. **3**, 519–543 (2012).
[904] Bhamla, M. S., Chai, C., Alvarez-Valenzuela, M. A., Tajuelo, J., and Fuller, G. G., Interfacial mechanisms for stability of surfactant-laden films, PloS one **12**, e0175753 (2017).
[905] Frazier, S., Jiang, X., and Burton, J. C., How to make a giant bubble, Phys. Rev. Fluids **5**, 013304 (2020).
[906] Ishida, S., Synak, P., Narita, F., Hachisuka, T., and Wojtan, C., A model for soap film dynamics with evolving thickness, ACM Trans. Graph. **39**, 31–1 (2020).
[907] Chandler, D., Oil on troubled waters, Nature **445**, 831–832 (2007).
[908] Hyman, A. A., Weber, C. A., and Jülicher, F., Liquid-liquid phase separation in biology, Annu. Rev. Cell Develop. Biol. **30**, 39–58 (2014).
[909] Lamb, H., *Hydrodynamics*, 6th ed. (Cambridge University Press, 1993) originally published in 1892.
[910] Kapitza, P. L. and Kapitza, S. P., Wave flow of thin layers of a viscous fluid. I-III, Zhurnal Eksperimental'noi i Teoreticheskoi Fiziki **18** (1948).
[911] Kalliadasis, S., Ruyer-Quil, C., Scheid, B., and Velarde, M. G., *Falling Liquid Films* (Springer, 2012).
[912] Kapitza, P. L. and Kapitza, S. P., Wave flow of thin layers of a viscous fluid, in *Collected Papers of P.L. Kapitza*, edited by D. Ter Haar (Pergamon, 1965) pp. 662–709.
[913] Balmforth, N. J. and Mandre, S., Dynamics of roll waves, J. Fluid Mech. **514**, 1–33 (2004).

[914] Liu, J., Schneider, J. B., and Gollub, J. P., Three-dimensional instabilities of film flows, Phys. Fluids **7**, 55–67 (1995).

[915] Chang, H., Wave evolution on a falling film, Annu. Rev. Fluid Mech. **26**, 103–136 (1994).

[916] Balmforth, N. J. and Liu, J. J., Roll waves in mud, J. Fluid Mech. **519**, 33–54 (2004).

[917] De Santos, J. M., Melli, T. R., and Scriven, L. E., Mechanics of gas-liquid flow in packed-bed contactors, Annu. Rev. Fluid Mech. **23**, 233–260 (1991).

[918] Walls, D. J., Ylitalo, A. S., Mui, D. S. L., Frostad, J. M., and Fuller, G. G., Spreading of rinsing liquids across a horizontal rotating substrate, Phys. Rev. Fluids **4**, 084102 (2019).

[919] Barker, B., Johnson, M. A., Noble, P., Rodrigues, L. M., and Zumbrun, K., Note on the stability of viscous roll waves, Compt. Rend. Mécan. **345**, 125–129 (2017).

[920] Benjamin, T. B., Wave formation in laminar flow down an inclined plane, J. Fluid Mech. **2**, 554–573 (1957).

[921] Yih, C.-S., Stability of liquid flow down an inclined plane, Phys. Fluids **6**, 321–334 (1963).

[922] Harper, J. F., The motion of bubbles and drops through liquids, in *Advances in Applied Mechanics*, Vol. 12 (Elsevier, 1972) pp. 59–129.

[923] Hadamard, J. S., Mouvement permanent lent d'une sphère liquid et visqueuse dans un liquide visqueux, CR Hebd. Seances Acad. Sci. Paris **152**, 1735–1738 (1911).

[924] Rybczynski, W., Über die fortschreitende Bewegung einer flussigen Kugel in einem zahen Medium, Bull. Acad. Sci. Cracovie A **1**, 40–46 (1911).

[925] Bond, W. N., Bubbles and drops and Stokes' law, Philos. Mag. **4**, 889–898 (1927).

[926] Bond, W. N. and Newton, D. A., Bubbles, drops, and Stokes' law II, Philos. Mag. **5**, 794–800 (1928).

[927] Boussinesq, M. J., Sur l'existence d'une viscosité superficielle, dans la mince couche de transition séparant un liquide d'un autre fluide contigu, Ann. Chim. Phys **29**, 349–357 (1913).

[928] Savic, P., *Circulation and distortion of liquid drops falling through a viscous medium*, Tech. Rep. (National Research Laboratories, 1953).

[929] Davis, R. E. and Acrivos, A., The influence of surfactants on the creeping motion of bubbles, Chemical Engineering Science **21**, 681–685 (1966).

[930] Sadhal, S. S. and Johnson, R. E., Stokes flow past bubbles and drops partially coated with thin films. Part 1. Stagnant cap of surfactant film–exact solution, J. Fluid. Mech. **126**, 237–250 (1983).

[931] Kojima, M., Hinch, E. J., and Acrivos, A., The formation and expansion of a toroidal drop moving in a viscous fluid, Phys. Fluids **27**, 19–32 (1984).

[932] Joseph, D. D., Huang, A., and Hu, H. H., Non-solenoidal velocity effects and Korteweg stresses in simple mixtures of incompressible liquids, Physica D **97**, 104–125 (1996).

[933] Petitjeans, P. and Maxworthy, T., Miscible displacements in capillary tubes. Part 1. Experiments, J. Fluid. Mech. **326**, 37–56 (1996).

[934] Chen, C. and Meiburg, E., Miscible displacements in capillary tubes: Influence of Korteweg stresses and divergence effects, Phys. Fluids **14**, 2052–2058 (2002).

[935] Chen, C.-Y., Huang, C.-W., Gadêlha, H., and Miranda, J. A., Radial viscous fingering in miscible Hele-Shaw flows: A numerical study, Phys. Rev. E **78**, 016306 (2008).

[936] Pojman, J. A., Whitmore, C., Liveri, M. L. T., Lombardo, R., Marszalek, J., Parker, R., and Zoltowski, B., Evidence for the existence of an effective interfacial tension between miscible fluids: Isobutyric acid/water and 1-butanol/water in a spinning-drop tensiometer, Langmuir **22**, 2569–2577 (2006).

[937] Zoltowski, B., Chekanov, Y., Masere, J., Pojman, J. A., and Volpert, V., Evidence for the existence of an effective interfacial tension between miscible fluids. Part 2. Dodecyl acrylate/poly(dodecyl acrylate) in a spinning drop tensiometer, Langmuir **23**, 5522–5531 (2007).

[938] Lacaze, L., Guenoun, P., Beysens, D., Delsanti, M., Petitjeans, P., and Kurowski, P., Transient surface tension in miscible liquids, Phys. Rev. E **82**, 041606 (2010).

[939] Joseph, D. D., Fluid dynamics of two miscible liquids with diffusion and gradient stresses, Eur. J. Mech. B Fluids **9**, 565–596 (1990).

[940] Joseph, D. D. and Renardy, Y., *Fundamentals of two-fluid dynamics* (Springer, 2013).

[941] Davis, H. T., A theory of tension at a miscible displacement front, in *Numerical Simulation in Oil Recovery*, edited by M. Wheeler (Springer, 1988).

[942] Brouzet, C., Lefranc, T., Söderberg, L. D., Lundell, F., *et al.*, Effective interfacial tension in flow-focusing of colloidal dispersions: 3-D numerical simulations and experiments, J. Fluid. Mech. **876**, 1052–1076 (2019).

[943] Wylock, C., Rednikov, A., Haut, B., and Colinet, P., Nonmonotonic Rayleigh-Taylor instabilities driven by gas–liquid CO_2 chemisorption, J. Phys. Chem. B **118**, 11323–11329 (2014).

[944] Lindholm, M., Promoting curiosity?, Science & Education **27**, 987–1002 (2018).

[945] Cagiltay, N. E., Yildirim, S., and Aksu, M., Students' preferences on Web-based instruction: Linear or nonlinear, J. Educ. Technol. Soc. **9**, 122–136 (2006).

[946] Kallick, B. and Zmuda, A., *Students at the center: Personalized learning with habits of mind* (ASCD, 2017).

[947] Jirout, J. J., Vitiello, V. E., and Zumbrunn, S. K., Curiosity in schools, in *The new science of curiosity*, edited by G. Gordon (Nova, 2018) pp. 243–266.

[948] Gruber, M. J., Valji, A., and Ranganath, C., Curiosity and learning: A neuroscientific perspective, in *The Cambridge Handbook of Motivation and Learning* (Cambridge University Press, 2019) p. 397–417.

[949] Tobias, S. and Birrer, F. A., Who will study physics, and why?, Eur. J. Phys. **20**, 365 (1999).

[950] Freeman, S., Eddy, S. L., McDonough, M., Smith, M. K., Okoroafor, N., Jordt, H., and Wenderoth, M. P., Active learning increases student performance in science, engineering, and mathematics, Proc. Natl. Acad. Sci. U.S.A. **111**, 8410–8415 (2014).

[951] Deslauriers, L., Schelew, E., and Wieman, C., Improved learning in a large-enrollment physics class, Science **332**, 862–864 (2011).

[952] Deslauriers, L., McCarty, L. S., Miller, K., Callaghan, K., and Kestin, G., Measuring actual learning versus feeling of learning in response to being actively engaged in the classroom, Proc. Natl. Acad. Sci. U.S.A. **116**, 19251–19257 (2019).

[953] Whitesides, G. M., The frugal way, The Economist **17** (2011).

[954] Byagathvalli, G., Challita, E. J., and Bhamla, M. S., Frugal science powered by curiosity, Indust. Eng. Chem.

Res. **60**, 15874–15884 (2021).
[955] Kaye, N. B., Teaching fluid mechanics: In-class activities to enhance student understanding (2021), last Accessed: 2021-11-04.
[956] Zenit, R., Kumar, A. H., Mansingka, A., Powers, T., Ravisankar, M., Sollenberger, A., and Tieze, P., Make a pancake: Learn about viscosity (2020), 73rd Annual Meeting of the APS Division of Fluid Dynamics.
[957] Rahman, A., A blended learning approach to teach fluid mechanics in engineering, Eur. J. Eng. Educ. **42**, 252–259 (2017).
[958] Homsy, G. M., *Multimedia Fluid Mechanics Online* (Cambridge University Press, 2019).
[959] Sheppard, S. D., Macatangay, K., Colby, A., and Sullivan, W. M., *Educating Engineers: Designing for the Future of the Field* (Jossey-Bass, 2008).
[960] Agar, J., 2016 wilkins–bernal–medawar lecture: The curious history of curiosity-driven research, Roy. Soc. J. Hist. Sci. **71**, 409–429 (2017).
[961] Smith, D., Play: The path to discovery or my Friday afternoon experiment (2015), last accessed: 21-Nov-2021.
[962] Ten, A., Kaushik, P., Oudeyer, P.-Y., and Gottlieb, J., Humans monitor learning progress in curiosity-driven exploration, Nat. Commun. **12**, 1–10 (2021).
[963] Batchelor, G. K., *The life and legacy of G.I. Taylor* (Cambridge University Press, 1996).
[964] Amon, A., A case for more curiosity-driven basic research, Molec. Biol. Cell **26**, 3690–3691 (2015).
[965] Woxenius, J., The consequences of the extended gap between curiosity-driven and impact-driven research, Transp. Rev. **35**, 401–403 (2015).
[966] Dauxois, T., Peacock, T., Bauer, P., Caulfield, C. P., Cenedese, C., Gorlé, C., Haller, G., Ivey, G. N., Linden, P. F., Meiburg, E., Pinardi, N., Vriend, N. M., and Woods, A. W., Confronting grand challenges in environmental fluid mechanics, Phys. Rev. Fluids **6**, 020501 (2021).
[967] IPCC,, *Climate Change 2021: The Physical Science Basis. Contribution of Working Group I to the Sixth Assessment Report of the Intergovernmental Panel on Climate Change*, edited by V. Masson-Delmotte, P. Zhai, A. Pirani, S. L. Connors, C. Péan, S. Berger, N. Caud, Y. Chen, L. Goldfarb, M. I. Gomis, M. Huang, K. Leitzell, E. Lonnoy, J. B. R. Matthews, T. K. Maycock, T. Waterfield, O. Yelekci, R. Yu, and B. Zhou (Cambridge University Press, 2021) in press.